Characterization of growth, apoptosis, and differentiation of CHO and human erythroleukemic K562 cells exposed to dexrazoxane, and the selection of a dexrazoxane-resistant K562 cell line

BY

MICHAEL E. ABRAM

A Thesis
Submitted to the Faculty of Graduate Studies
in Partial Fulfillment of the Requirements
for the Degree of

MASTER OF SCIENCE

Faculty of Pharmacy
University of Manitoba
Winnipeg, Manitoba

THE UNIVERSITY OF MANITOBA

FACULTY OF GRADUATE STUDIES

*****

COPYRIGHT PERMISSION PAGE

Characterization of growth, apoptosis, and differentiation of CHO and human erythroleukemic K562 cells exposed to dexrazoxane, and the selection of a dexrazoxane-resistant K562 cell line

BY

Michael E. Abram

A Thesis/Practicum submitted to the Faculty of Graduate Studies of The University of Manitoba in partial fulfillment of the requirements of the degree of Master of Science

Abstract

The bisdioxopiperazines including dexrazoxane are strong catalytic inhibitors of DNA topoisomerase II. The aim of the following study was to examine the *in vitro* effects of dexrazoxane on the growth, cytotoxicity, morphology, cell cycle progression, and where applicable induction of apoptosis and differentiation of Chinese hamster ovary (CHO), and human erythroleukemic K562 cell lines. Finally, a dexrazoxane-resistant strain of K562 cells was selected and characterized for cross-resistance towards other bisdioxopiperazines and antineoplastic agents. Daily exposure to dexrazoxane inhibited growth of both CHO and K562 cell lines, while permitting a significant increase in cell size. Cell cycle analysis revealed that these cells were highly polyploid (up to 32 N DNA content). Confocal, electron, and fluorescence microscopy revealed mulitlobed nuclei, and together with the presence of multiple centrosomes suggested continued cell cycling in the absence of cytokinesis. Mean protein and DNA content increased 3.8- and 5.4-fold respectively in CHO cells after 120 hr, and only marginally in K562 cells. Delayed apoptosis was observed only in K562 cells as seen by an increase of sub-diploid apoptotic bodies, condensed and/or fragmented fluorescent stained chromatin, and agarose gel electrophoretic DNA laddering. Dexrazoxane induced erythroid-like differentiation in K562 cells, as measured by increased hemoglobin content and glycophorin A staining. Dexrazoxane-resistant K562/DZ1 cells (~126-fold), were highly cross-resistant towards ICRF-154 and ICRF-193, as well as against doxorubicin (2.4-fold) and etoposide (4-fold). Thus, the prevention of cytokinesis does not necessarily preclude continued cell cycling. The ability of the bisdioxopiperazines to induce differentiation and apoptosis suggests that these compounds may be useful in treating some types of leukemia.

Acknowledgements

I would like to sincerely like thank Dr. Hasinoff for allowing me the opportunity of a lifetime - for in the privilege of studying at the graduate level I was allowed the chance to prove myself, not only to that of others but more importantly to myself. Under his guidance the previous few years I feel that I have come along way from the scientist I once was. With a keen attention to detail, and a daily interest in the workings of everyone in the lab, I cannot help but wonder where I would be now if things had been different.

I would like to also thank my family and all of my friends here and abroad for the continuous support of me, and my aspirations for the future. I would like to especially thank my mom for her relentless emotional support during my times of solitude, homesickness and longing for the future.

Additionally, I would like to thank all those who contributed to the following studies: Dr. Gaik-Lean Chee for her initial discoveries, Dr. Ed Byard and Erwin Huebner for their expertise in fluorescence microscopy, Dr. Victor Ferrans for his assistance in electron and confocal microscopy, Dr. Ed Rector for his assistance in flow cytometry, and Dr. Frank Burczynski for the intermittent use of his laminar flow hood and swinging-bucket centrifuge.

Finally, I would like to thank and acknowledge the financial support of the Medical Research Council of Canada, and as well the Faculty of Pharmacy at the University of Manitoba for their acceptance into the program and various degrees of support.

Table of Contents

Chapter 2 Characterization of the effects of dexrazoxane on morphological, structural, and cell cycle properties of Chinese hamster ovary cells, and related cell lines.

List of Abbreviations

α-MEM	Dulbecco's alpha minimum essential medium
anti-CD41	anti-gpIIb/IIIa-PE conjugated mAb
anti-GlyA	anti-glycophorin A-FITC conjugated mAb
bcr-abl	break point cluster region-Abelson tyrosine kinase
CHO	Chinese hamster ovary cells
CML	chronic myelogenous leukemia
ddH_2O	distilled water purified by reverse osmosis
DIC	differential interference contrast
DMEM	Dulbecco's modified eagle medium
DMSO	dimethyl sulfoxide
DOX	doxorubicin
DNase	deoxyribonuclease
DZR	dexrazoxane-resistant Chinese hamster ovary cells
EDTA	ethylenediaminetetraacetic acid
FALS	forward angle light scatter
FCS	fetal calf serum
FITC	fluorescein-isothiocyanate
gpIIb/IIIa	platelet/megakaryocyte glycoprotein IIb/IIIa (CD41)
Hb	hemoglobin
K562	human erythroleukemic cell line
mAb	monoclonal antibody
MCD	mean cell diameter

MCV	mean cell volume
MTS	(3-(4,5-dimethyl-thiazol-2-yl)-5-(3-carboxymethoxyphenyl)-2-(4-sulfophenyl)-2H-tetrazolium)
MTT	(3-(4,5-dimethylythiazol-2-yl)-2,5-diphenyltetrazolium bromide)
NEC	necrotic
90°LS	90° (side angle) light scatter
NVA	non-viable apoptotic
PBS	phosphate buffered saline
PE	phycoerythrin
PI	propidium iodide
RBC	red blood cells
RNase	ribonuclease
UV	ultraviolet
VA	viable apoptotic
VNA	viable non-apoptotic
WC	Window count
WN	Window number

List of Figures

List of Tables

Chapter 1 Introduction.

1.1 Iron-based oxygen free radical tissue damage

Oxygen-derived free radicals commonly target membranes, nucleic acids, and proteins and have been implicated to play a significant role in various diseases and toxicities through the induction of oxidative stress [1,2]. Although oxygen radicals are produced naturally in biological systems their excessive production in response to drug metabolism or other forms of insult can overwhelm antioxidant protective systems resulting in an oxidative stress [3], intrinsically characteristic of: ischemic damage following myocardial infarction, drug toxicities, inflammatory-immune and radiation injury, as well as Parkinson's, Alzheimer's, and Crohn's disease [4-7].

Hydrogen peroxide, superoxide, and hydroxyl radicals are the three most common, naturally produced oxygen species capable of damaging biological systems. Superoxide ($O_2^{\bullet -}$) can be produced by several biological reactions including: the respiratory electron transport chain of the mitochondria, by heme proteins, or the action of such oxidative enzymes as xanthine and aldehyde oxidases, as well as indoleamine and tryptophan deoxygenases [3]. Hydrogen peroxide is produced by the dismutation of superoxide and is further reduced to hydroxyl radicals in the following simplified sequence of reactions:

$2O_2^{\bullet -} + 2H^+ \rightarrow H_2O_2 + O_2$	(hydrogen peroxide formation)	{1}
$O_2^{\bullet -} + Fe^{3+} \rightarrow Fe^{2+} + O_2$	(reduction of Fe^{3+})	{2}
$Fe^{2+} + H_2O_2 \rightarrow Fe^{3+} + OH^{\bullet} + OH^-$	(Fenton reaction)	{3}

The highly reactive hydroxyl radical can cause membrane cell damage via the initiation of lipid peroxidation chain reactions, consequently affecting the intracellular

levels of such important ions as calcium and iron. Lipid peroxidation begins with the removal of an allylic hydrogen from an unsaturated fatty acid (LH), as follows [3]:

$$LH + OH^{\bullet} \rightarrow L^{\bullet} + H_2O \quad \{4\}$$
$$L^{\bullet} + O_2 \rightarrow LOO^{\bullet} \quad \{5\}$$
$$LOO^{\bullet} + LH \rightarrow LOOH + L^{\bullet} \quad \{6\}$$

1.1.1 Doxorubicin and the oxygen free radical mechanism of anthracycline-induced cardiotoxicity

Doxorubicin (Adriamycin®) and other anthracyclines are limited as useful antitumor agents in the treatment of a variety of cancers [8] due to their potentially fatal cumulative dose-limiting cardiotoxicity [6] and the expression of such side effects as myelosuppression, nausea, and alopecia [9]. As a consequence, the maximum recommended cumulative dose of doxorubicin is 550 mg/m^2 [8]. Current evidence has suggested that the cardiotoxic effects of doxorubicin which include congestive heart failure [10], as well as reduced cardiac output and venous congestion can be attributed to iron-based oxygen free radical-induced oxidative stress [6,11-13]. Heart muscle tissue is commonly most affected by the action of doxorubicin [14-16] due to a relatively low level of antioxidant protective enzymes [3,13,17] such as superoxide dismutase, catalase, and glutathione peroxidase which are normally able to protect other vital organs by diminishing accentuated levels of oxygen radicals through a series of biological reactions [18].

The potency of doxorubicin can be attributed to its site-specific effects on various cellular systems essential for survival resulting in DNA damage, lipid peroxidation, and the inactivation of the mitochondrial electron transport chain [19,20]. The highly reactive

and potentially cytotoxic oxygen free radical species which are responsible for these effects are generated through a one electron redox cycling of doxorubicin in a free or Fe^{3+}-complexed form. Uncomplexed free doxorubicin (DOX) and other anthracyclines can redox cycle through the reduction to a semiquinone radical (reaction 7) [21]. This reaction is accomplished by the transfer of an electron to doxorubicin by one of several enzymes including xanthine oxidase, cytochrome P-450 reductase, and NADH dehydrogenase [21]. Aerobic reoxidation of the doxorubicin semiquinone ($DOX^{\bullet -}$) back to doxorubicin transfers its electron to O_2 to produce superoxide (equation 8). Oxidative damage is subsequently mediated by the production of hydrogen peroxide and the extremely reactive hydroxyl radical through equations 1 and 3.

$$DOX + e^- \rightarrow DOX^{\bullet -} \quad \{7\}$$
$$DOX^{\bullet -} + O_2 \rightarrow DOX + O_2^- \quad \{8\}$$

Redox cycling can also occur through the stable Fe^{3+}-doxorubicin complex which is formed in a 3:1 ratio of anthracycline:Fe^{3+} [6]. The Fe^{3+}-doxorubicin complex may be able to initiate oxygen-radical lipid peroxidation through its site-specific targeting of the cardiolipin-rich inner mitochondrial membrane [22]. The Fe^{3+}-doxorubicin complex is reduced to the Fe^{2+}-doxorubicin complex by superoxide (equation 9) or by the doxorubicin semiquinone radical (equation 10) [23].

$$Fe^{3+}\text{-}(DOX)_3 + O_2^{\bullet -} \rightarrow Fe^{2+}\text{-}(DOX)_3 + O_2 \quad \{9\}$$
$$Fe^{3+}\text{-}(DOX)_3 + DOX^{\bullet -} \rightarrow Fe^{2+}\text{-}(DOX)_3 + DOX \quad \{10\}$$

In the presence of oxygen the Fe^{3+}-doxorubicin complex is regenerated producing superoxide (equation 11) and subsequently hydrogen peroxide (equation 1) as well as the

hydroxyl radical through the oxidation of other forms of the Fe^{2+}-doxorubicin complex (equation 12).

$$Fe^{2+}\text{-}(DOX)_3 + O_2 \rightarrow Fe^{3+}\text{-}(DOX)_3 + O_2^{\bullet -} \quad \{11\}$$
$$Fe^{2+}\text{-}(DOX)_3 + H_2O_2 \rightarrow Fe^{3+}\text{-}(DOX)_3 + OH^- + OH^{\bullet} \quad \{12\}$$

1.1.2 Protection against anthracycline cardiotoxicity with the antioxidant dexrazoxane

The current development of antioxidant drugs has been prompted by iron-dependent oxygen free radical cardiotoxicity of anthracyclines such as doxorubicin, as discussed above. Ideally, adequate protection of susceptible organs to free radical damage would consequently enable the administration of higher dosages of antitumor anthracyclines without compromising the integrity of healthy cells, particularly in the heart. Although many biological compounds including ascorbic acid (vitamin C), glutathione, α-tocopherol (vitamin E), β-carotene, and uric acid [24,25] have been shown to be effective antioxidants it is unlikely that they would be powerful enough to counteract the effects of antitumor therapy and myocardial injury.

Currently the cardiotoxic effects of doxorubicin administered to women with metastatic breast cancer is reduced by a clinically effective agent, known as dexrazoxane (ICRF-187, Zinecard®, or Cardioxane®) [14,26-28]. Dexrazoxane is the (+)-(*S*)-enantiomer of racemic ICRF-159, which in addition to other bisdioxopiperazine analogs (Fig. 1.1) were originally synthesized as potential antitumor [29] and antimetastatic agents [30]. However, when co-administered with doxorubicin to prevent oxygen-mediated free radical damage, the antitumor activity of doxorubicin is unaffected [31,32]. As a result

this permits significantly higher cumulative doses of doxorubicin to be administered [26,33].

Dexrazoxane, in its native form is a non-polar uncharged compound able to transverse the cell membrane [34]. Once in the cell, dexrazoxane undergoes a slow ring-opening hydrolysis through enzymatic or non-enzymatic routes to its active metal ion binding form, ADR-925 (D in Fig. 1.2) via one ring opened intermediate forms, B and C (Fig. 1.2). In the liver and kidney under non-saturating conditions the one ring opening hydrolysis is catalyzed by dihydropyrimidine amidohydrolase (DHPase, EC 3.5.2.2) [35,36]. This is followed by a base-catalyzed second ring opening hydrolysis, which is otherwise responsible for complete hydrolysis once the drug reaches its putative site of action, the heart. Under physiological conditions (pH 7.4 and 37°C), dexrazoxane disappears with a half-time of 9.3 hr, and ADR-925 accumulates with a half-time of 23 hr [37,38].

The hydrolysis reaction of dexrazoxane effectively transforms it from the status of a prodrug to that the active metal-chelating drug ADR-925, structurally similar to EDTA (Fig. 1.1) [39]. However, unlike the polar compound EDTA dexrazoxane may have access to metal ions both intracellularly and extracellularly as it freely passively diffuses back and forth across cell membranes before hydrolysis [40,41]. As the hydrolysis product of dexrazoxane, ADR-925 is a strong chelator of Fe^{3+} and Cu^{2+}, and has a much lower affinity for Ca^{2+} and Mg^{2+} than does EDTA [39]. Cardioprotection against doxorubicin-induced iron-based oxygen free radical damage [42] likely occurs through the ability of ADR-925 to strongly chelate free iron [39], or to quickly and effectively remove iron from its complex with doxorubicin [40,43].

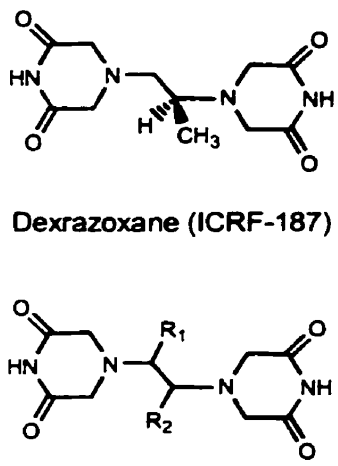

Dexrazoxane (ICRF-187)

ICRF-154 $R_1 = R_2 = H$
ICRF-159 $R_1 = H$, $R_2 = CH_3$ (racemic)
ICRF-187 $R_1 = H$, $R_2 = CH_3$ ((S(-(+))
ICRF-186 $R_1 = H$, $R_2 = CH_3$ ((R(-(-))
ICRF-192 $R_1 = H$, $R_2 = C_2H_5$ (racemic)
ICRF-193 $R_1 = R_2 = CH_3$ (meso)
ICRF-201 $R_1 = R_2 = C_2H_5$ (meso)
ICRF-202 $R_1 = CH_3$, $R_2 = C_2H_5$ (erythro)
ICRF-215 $R_1 = CH_3$, $R_2 = C_3H_7$ (erythro)
ICRF-220 $R_1 = CH_3$, $R_2 = CH_2OCH_3$ (erythro)

Fig. 1.1. Structure of dexrazoxane (ICRF-187) and other bisdioxopiperazine analogs.

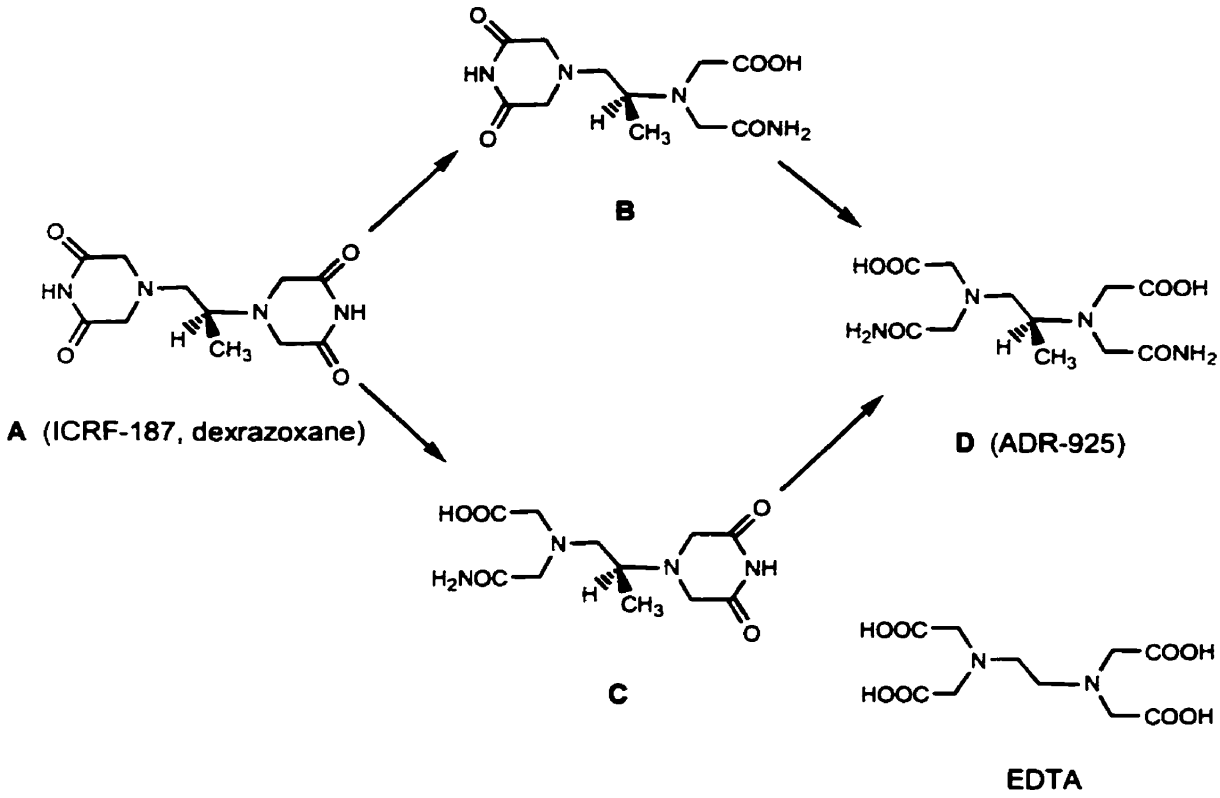

Fig. 1.2. Reaction scheme for the hydrolysis of dexrazoxane.

1.2 Chemotherapeutic targeting of DNA topoisomerase II

The human genome is comprised of billions of DNA base pairs encompassing 46 chromosomes [44] whereby the cellular functions of this genetic material is significantly influenced by such topological relationships as over/underwinding, knotting, or tangling. In order to manage this overwhelming amount of DNA, eukaryotic cells have evolved to contain a class of enzymes known as topoisomerases, capable of relieving torsional strain in DNA double helices without the expense of exorbitant amounts of energy. During many essential processes of DNA metabolism the free rotation of one strand around the other with the separation of the double helix is limited in part due to the length of DNA as well as its anchorage to nuclear matrix regions [45]. Consequently, topoisomerases play an important role during DNA replication, RNA transcription, recombination, as well as in the segregation and condensation of chromosomes during mitosis [46-49]. Beyond their essential physiological functions, topoisomerases have become of key interest as cellular targets for some of the most clinically active and cytotoxic anticancer agents used in the treatment of human malignancies [44,50].

1.2.1 Types of topoisomerase and their mechanism of action

Within eukaryotes, the most characterized classes of topoisomerases are referred to as type I or type II topoisomerases. Type I topoisomerases are monomeric in their active form, and without the expense of energy can alter DNA topology by passing a single strand of DNA through a transient single-stranded nick made in the opposing strand [50-52]. As a result, these enzymes which are constitutively expressed throughout the cell cycle [53] permit a controlled rotation or swivel of over- and underwinding of the double

helix to alter superhelical densities [51,54]. In contrast, type II topoisomerases are homodimeric and act by making a transient double-stranded break in the DNA duplex and passing a separate double-stranded molecule through the break, followed by resealing [46,54]. The catalytic cycle of topoisomerase II activity may be regarded as an ATP-dependent protein clamp model [55,56] consisting of several steps catalyzing the transfer of a DNA phosphodiester bond to tyrosine residue 804 [57] via a transesterification reaction (Fig. 1.3). These steps include: enzyme-DNA binding at nodes (crossovers) in DNA (G or gap segment) [58]; conformational change concomitant with the binding of ATP and second duplex DNA (T or transport segment); pre-strand passage breakage-religation equilibrium via an intermediate enzyme-DNA complex; double-stranded DNA passage; post-strand passage breakage-religation equilibrium; ATP hydrolysis/enzyme turnover, regenerating its active conformation [46,50]. As a consequence of its action topoisomerase II not only modulates over- and underwinding but also relaxes positive and negative supercoiled double-stranded DNA, catenates and decatenates circular DNA, and is a major nuclear component of interphase cells, as well as a major polypeptide of the chromosome scaffold in mitotic cells [50]. Finally, there exist two isoforms of topoisomerase II, α and β. Topoisomerase β is expressed at constant low level [59] whereas topoisomerase α is expressed differentially over the cell cycle peaking in activity at G2/M [50,53,59,60], and is the more sensitive isoform to antineoplastic agents [50].

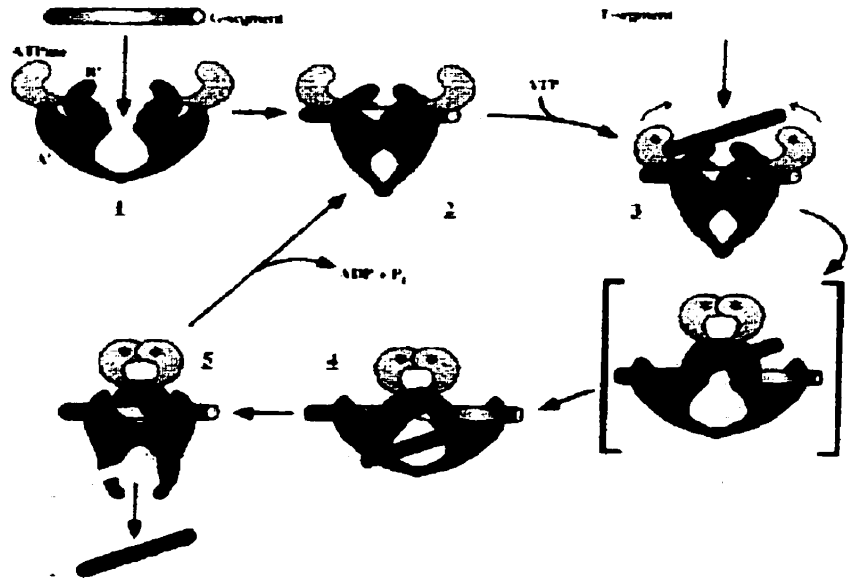

Fig. 1.1. The catalytic cycle of topoisomerase II activity. [46]

1.2.2 Molecular interaction between drugs and topoisomerase II

Topoisomerase-targeted drugs are capable of killing cancer cells in a unique and insidious fashion whereby the inhibition of this essential enzyme forms the basis for therapeutic intervention in a variety of cancers. Topoisomerase II inhibition can be classified into two mechanistically distinct classes, as explained in the following sections.

1.2.2.1 Cleavable complex-forming topoisomerase II poisons

This particular class of classical topoisomerase II inhibitors consists of intercalative and non-intercalative agents which include such clinically effective antineoplastic agents as the anthracyclines (doxorubicin and daunorubicin), epipodophyllotoxins (etoposide and teniposide), and *m*-amsacrine [50,61,62]. Initially, it was believed that such agents as the

anthracyclines were cytotoxic by virtue of their ability to intercalate between DNA base pairs, thus affecting replication by interfering with the spatial arrangement of DNA and sterically hindering nuclear protein formation [61,63]. While this remains true, these and other agents are now thought to be cytotoxic primarily through their ability to interact with topoisomerase II [50,64]. Specifically, these inhibitors stabilize, and increase the concentration of covalent topoisomerase II-cleaved DNA complexes that are requisite intermediates in the catalytic cycle of topoisomerase II. Therefore, instead of destroying the ability of topoisomerase II to mediate its essential cellular functions these drugs rather subvert the enzyme into a potent physiological toxin [50,54].

Since topoisomerase II cleaves DNA in a sequential manner, stabilized topoisomerase II-DNA complexes are detected as protein-linked DNA single- or double-stranded DNA breaks in the genetic material of treated cells. Although the initial nucleic acid breaks present in these complexes are transient in nature [50] they are converted into more permanent breaks when replication complexes (DNA polymerase and helicase enzymes) attempt to transverse the covalently-bound topoisomerase II roadblock [44,50,54,65]. The presence of these breaks alone can greatly stimulate nucleic acid recombination and mutation events, as well as lead to the formation of various chromosomal abnormalities, and the triggering of cell death by apoptosis [50].

Higher levels of topoisomerase II expression are generally correlated with an enhanced sensitivity to the cleavable complex-forming topoisomerase II inhibitors [50,66]. This is particularly evident in rapidly proliferating cells and in fast growing neoplastic tissues [50]. Although the stabilization of covalent complexes between topoisomerase II and DNA may be a precursor to cell death [66], cytotoxicity is not simply due to

topoisomerase II inhibition. If enzyme inhibition was simply the mechanism of damage then the supposition of higher enzyme levels relative to increased resistance would remain true. Instead it is believed that the formation of the cleavable-complex initiates a chain of events and cellular responses causing enzyme-mediated DNA damage which cannot be repaired. Such events may be comprised of replication fork blockage [67], interference with poly(ADP-ribosylation) [68], G2 arrest, and apoptosis [69].

1.2.2.2 Non-cleavable complex-forming, catalytic inhibitors of topoisomerase II

Inhibitors of this class have been reported to mediate an inhibition of the catalytic activity of topoisomerase II without stabilizing the topoisomerase II-DNA covalent complex, and without leading to the formation of DNA strand breakage. These drugs which include merbarone [70], fostriecin [71], suramin [72], aclarubicin [73], and the bisdioxopiperazines [74-77] are structurally diverse and do not necessarily share the same binding site, although they do appear to affect the ATP binding domain of topoisomerase II. The bisdioxopiperazines appear to inhibit topoisomerase II catalytically by blocking the entrance of DNA into the cavity of the enzyme. In particular, these agents induce a conformational change in topoisomerase II that results in the enzyme becoming trapped in an inactive closed clamp form, prior to the formation of the intermediate cleavable complex [76,78]. As a result, the stabilization of the closed clamp form causes an inhibition of the intrinsic ATPase activity of topoisomerase II and prevents recycling of the enzyme [79].

While it remains true that the bisdioxopiperazines, particularly dexrazoxane are capable of reducing anthracycline cytotoxicity through the intracellular chelation of crucial

metals, their topoisomerase II inhibitory mode of action may be equally if not more fundamental in its current clinical usage. Additionally, some potential may still exist for their usage in antitumor [80,81] and/or antimetastatic treatment regimens [14]. In fact, dexrazoxane and ICRF-159 have been shown to effectively inhibit to varying degrees the division of malignant and non-malignant cells, although a complete tumor regression has never been seen [14,82]. Furthermore, ICRF-159 has demonstrated antimetastatic activity in such models as Lewis lung carcinoma and sarcoma 180, attributable to its ability to prevent tumor cell dissemination [14,83].

Although the bisdioxopiperazines are in general less cytotoxic than the cleavable complex-forming topoisomerase II inhibitors, their cytotoxic activity has been correlated with their ability to inhibit the catalytic activity of topoisomerase II [75]. This particular mode of topoisomerase II inhibition has generated some interest into whether the bisdioxopiperazines can antagonize the cytotoxicity of cleavable complex-forming drugs. It is presumed that co-administration with dexrazoxane would lock topoisomerase II into its closed clamp form [78] thus preventing the formation of an anthracycline-induced stabilized topoisomerase II-DNA complex. Previous studies have shown that the bisdioxopierazines are capable of reducing protein-DNA cross-links and preventing induced strand breaks by etoposide, amsacrine, daunorubicin, and doxorubicin [77,79,81], as well as reducing the growth inhibitory cytotoxic effects of daunorubicin, doxorubicin [14,81,84] and etoposide [77,81]. Ultimately the use of such catalytic inhibitors to antagonize anthracycline-mediated growth inhibition would depend on such factors as schedule of administration, drug concentration, topoisomerase II levels, and tumor types [84]. In fact, the exertion of synergistic or antagonistic effects on cell survival with two

opposing types of topoisomerase II inhibitors, ICRF-193 and etoposide has been shown to depend directly on the treatment schedule and drug concentration [82,85]. Furthermore, the activity of dexrazoxane is inversely proportional to topoisomerase II level, as demonstrated by an increased effectiveness in inhibiting etoposide-mediated topoisomerase II-DNA covalent complexes in a cell line with reduced topoisomerase II protein levels [79].

1.3 Research conducted in this thesis

The areas of research and studies conducted over the course of this thesis are based in part on the mechanistic inhibition of topoisomerase II conferred by dexrazoxane. Specifically, the long term molecular, mechanistic and morphological effects of dexrazoxane on various cell lines was investigated and/or discussed. While there exists some overlap between chapters in terms of the protocols and methods employed, the inherent studies are very different if not evolutionary, as explained further in subsequent chapter introductory sections. In Chapter 2 the effects of dexrazoxane on cell growth, cell cycling, and mitotic structural components was primarily investigated in an immortal, non-neoplastic cell line known as Chinese hamster ovary (CHO) cells. In addition, this chapter covers a less extensive examination of similar attributes upon dexrazoxane exposure in a mortal, primary heart fibroblast cell line, as well as in a previously established dexrazoxane-resistant (DZR) CHO cell line. In Chapter 3 the preceding principal effects of dexrazoxane exposure were explored further on a novel level using a multipotential, human erythroleukemic immortal cell line known as K562. Specifically, the capability of the bisdioxopiperazines, including dexrazoxane to induce hematopoietic cell differentiation

towards erythroid and/or megakaryocyte progenitors, as well as induce apoptosis was investigated. Finally, Chapter 4 covers the selection and isolation of a dexrazoxane-resistant K562 cell line, its characterization, and analysis of cross-resistance towards other antineoplastic and/or topoisomerase II inhibitory agents. In addition, a preliminary examination was conducted on the susceptibility of these dexrazoxane-resistant K562 cells towards topoisomerase II inhibitor-induced differentiation and apoptosis.

1.4 References

1. Toyokuni, S. Iron-induced carcinogenesis: the role of redox regulation. *Free Radic. Biol. Med.*, **20**: 553-566, 1996.

2. Stohs, S.J. and Bagchi, D. Oxidative mechanisms in the toxicity of metal ions. *Free Radic. Biol. Med.*, **18**: 321-336, 1995.

3. Halliwell, B. and Gutteridge, J.M.C. Free Radicals in Biology and Medicine. Oxford: Clarendon, 1989.

4. Gutteridge, J.M.C. Free radicals in disease processes: A compliation of cause and consequence. *Free Radical Research Communications*, **19**: 141-158, 1993.

5. Halliwell, B. and Gutteridge, J.M.C. Oxygen free radicals and iron in relation to biology and medicine: some problems and concepts. *Arch. Biochem. Biophysics*, **246**: 501-514, 1986.

6. Gianni, L., Corden, B.J., and Myers, C.E. The biochemical basis of anthracycline toxicity and anti-tumor activity. *Reviews in Biochemical Toxicology*, **5**: 1-82, 1983.

7. Demant, E.J. and Norskov-Lauritsen, N. Binding of transferrin-iron by adriamycin at acidic pH. *FEBS Lett.*, **196**: 321-324, 1986.

8. Healy, T., Fevang, L., and Gillis, C.M. Compendium of Pharmaceuticals and Specialties. Toronto,ON: Canadian Pharmaceutical Association, 1997.

9. Carter, S.K. Adriamycin - a review. *J. Natl. Cancer Inst.*, **55**: 1265-1274, 1975.

10. Ferrans, V. Overview of cardiac pathology in relation to anthracycline toxicity and anti-tumor activity. *Cancer. Treat. Rep.*, **62**: 955-961, 1978.

11. Gutteridge, J.M.C. Lipid peroxidation and possible hydroxyl radical formation stimulated by the self-reduction of a doxorubicin-iron(III) complex. *Biochem. Pharmacol.*, **33**: 1725-1728, 1984.

12. Malisza, K.L. and Hasinoff, B.B. Production of hydroxyl radical by iron(III)-anthraquinone complezes through self-reduction and through reductive activation by the xanthine oxidase/hypoxanthine system. *Arch. Biochem. Biophysics*, **321**: 51-60, 1995.

13. Myers, C. The role of iron in doxorubicin-induced cardiomyopathy. *Semin. Oncol.*, **25**: 10-14, 1998.

14. Hasinoff, B.B., Hellmann, K., Herman, E.H., and Ferrans, V.J. Chemical, biological and clinical aspects of dexrazoxane and other bisdioxopiperazines. *Curr. Med. Chem.*, **5**: 1-28, 1998.

15. Hasinoff, B.B. Chemistry of dexrazoxane and analogues. *Semin. Oncol.*, **25**: 3-9, 1998.

16. Synold, T.W., Tetef, M.L., and Doroshow, J.H. Antineoplastic activity of continuous exposure to dexrazoxane: potential new role as a novel topoisomerase II inhibitor. *Semin. Oncol.*, **25**: 93-99, 1998.

17. Doroshow, J.H., Locker, G.Y., and Myers, C.E. Enzymatic defenses of the mouse heart against reactive oxygen metabolites. *J. Clin. Invest.*, **65**: 128-135, 1980.

18. Nogrady Medicinal Chemistry. A Biochemical Approach. New York, N.Y.: Oxford University Press, 1988.

19. Duarte-Karim, M., Ruysschaert, J.M., and Hildebrand, J. Affinity of adriamycin to phospholipids a possible explanation for cardiac mitochondrial lesions. *Biochem. Biophys. Res. Comm.*, **71**: 658-663, 1976.

20. Doroshow, J.H., Tallent, C., and Schechter, J.E. Ultrastructural features of adriamycin-induced skeletal and cardiac muscle toxicity. *Am. J. Pathol*, **118**: 288-297, 1985.

21. Bachur, N.R., Gordon, S.L., Gee, M.V., and Kon, H. NADPH cytochrome P-450 reductase activation of quinone anticancer agents to free radicals. *Proc. Natl. Acad. Sci.U.S.A.*, **76**: 954-957, 1979.

22. Hasinoff, B.B. Inhibition and inactivation of NADH-cytochrome c reductase activity of bovine heart submitochondrial particles by the iron(III)-adriamycin. *J. Biochem.*, **265**: 865-870, 1990.

23. Butler, J., Hoey, B.M., and Swallow, A.J. Reactions of the semiquinone free radicals of antitumor agents with oxygen and iron complexes. *FEBS Lett.*, **182**: 95-98, 1985.

24. Andrae, U., Singh, J., and Ziegler-Skylakakis, K. Pyruvate and related alpha-ketoacids protect mammalian cells in culture against hydrogen peroxide-induced cytotoxicity. *Toxicol. Lett.*, **28**: 93-98, 1985.

25. Rice-Evans, C.A. and Diplock, A.T. Current status of antioxidant therapy. *Free Radic. Biol. Med.*, **15**: 77-96, 1989.

26. Speyer, J.L., Green, M.D., Zeleniuch-Jacquotte, A., Wernz, J.C., Rey, M., Sanger, J., Kramer, E., Ferrans, V., Hochster, H., and Meyers, M. ICRF-187 permits longer treatment with doxorubicin in women with breast cancer [published erratum appears in *J. Clin. Oncol* 1992 May;10(5):867]. *J. Clin. Oncol.*, **10**: 117-127, 1992.

27. Wexler, L.H. Ameliorating anthracycline cardiotoxicity in children with cancer: clinical trials with dexrazoxane. *Semin. Oncol.*, **25**: 86-92, 1998.

28. Lopez, M. and Vici, P. European trials with dexrazoxane in amelioration of doxorubicin and epirubicin-induced cardiotoxicity. *Semin. Oncol.*, **25**: 55-60, 1998.

29. Creighton, A.M., Hellmann, K., and Whitecross, S. Antitumour activity in a series of bisdiketopiperazines. *Nature*, **22**: 384-385, 1969.

30. Atherton, A. The effect of (+/-)-1,2-bis(3,5-dioxopiperazin-1-yl) propane (ICRF 159) on liver metastases from a hamster lymphoma. *Eur. J. Cancer*, **11**: 383-388, 1975.

31. Swain, S.M., Whaley, F.S., Gerber, M.C., Ewer, M.S., Bianchine, J.R., and Gams, R.A. Delayed administration of dexrazoxane provides cardioprotection for patients with advanced breast cancer treated with doxorubicin-containing therapy. *J. Clin. Oncol.*, **15**: 1333-1340, 1997.

32. Imondi, A.R. Preclinical models of cardiac protection and testing for effects of dexrazoxane on doxorubicin antitumor effects. *Semin. Oncol.*, **25**: 22-30, 1998.

33. Wexler, L.H., Andrich, M.P., Venzon, D., Berg, S.L., Weaver-McClure, L., Chen, C.C., Dilsizian, V., Avila, N., Jarosinski, P., Balis, F.M., Poplack, D.G., and Horowitz, M.E. Randomized trial of the cardioprotective agent ICRF-187 in pediatric sarcoma patients treated with doxorubicin. *J. Clin. Oncol.*, **14**: 362-372, 1996.

34. Hasinoff, B.B. and Kala, S.V. The removal of metal ions from transferrin, ferritin and ceruloplasmin by the cardioprotective agent ICRF-187 ((+)-1,2-bis(3,5-dioxopiperazinyl-1-yl)propane) and its hydrolysis product ADR-925. *Agents Actions*, **39**: 72-81, 1993.

35. Hasinoff, B.B. Enzymatic ring-opening reactions of the chiral cardioprotective agent (+)(S)-ICRF-187 and its (-)(R)-enantiomer ICRF-186 by dihydropyrimidine amidohydrolase. *Drug Metab. Dispos.*, **21**: 883-888, 1993.

36. Hasinoff, B.B. The enzymatic hydrolysis-activation of the adriamycin cardioprotective agent (+)-1,2-bis(3,5-dioxopiperazinyl-1-yl)propane. *Drug Metab. Dispos.*, **19**: 74-80, 1991.

37. Hasinoff, B.B. The hydrolysis-activation of the doxorubicin cardioprotective agent (+)-1,2-bis(3,5-dioxopiperazinyl-1-yl)propane. *Drug Metab. Dispos.*, **18**: 344-349, 1990.

38. Hasinoff, B.B. Pharmacodynamics of the hydrolysis-activation of the cardioprotective agent (+)-1,2-bis(3,5-dioxopiperazinyl-1-yl)propane. *J. Pharm. Sci.*, **83**: 64-67, 1994.

39. Huang, Z.-X., May, P.M., Quinlan, K.M., Williams, D.R., and Creighton, A.M. Metal binding by pharmaceuticals. Part 2. Interactions of Ca(II), Cu(II), Fe(II), Mg(II), Mn(II) and Zn(II) with the intracellular hydrolysis products of the anti-tumour agent ICRF-159 and its inactive homologue ICRF-192. *Agents Actions*, **12**: 536-542, 1982.

40. Hasinoff, B.B. The interaction of the cardioprotective agent ICRF-187 ((+)-1,2-bis(3,5-dioxopiperazinyl-1-yl)propane), its hydrolysis product ICRF-198, and other chelating agents with the Fe(III) and Cu(II) complexes of adriamycin. *Agents Actions*, **26**: 378-385, 1989.

41. Dawson, K.M. Studies on the stability and cellular distribution of dioxopiperazines in cultured BHK-21S cells. *Biochem. Pharmacol.*, **24**: 2249-2253, 1975.

42. Hasinoff, B.B. NADPH-cytochrome-P450 reductase promotes hydroxyl radical production by the iron complex of ADR-925, the hydrolysis product ICRF-187 (dexrazoxane). *Free Radical Research Communications*, **22**: 319-325, 1995.

43. Buss, J.L. and Hasinoff, B.B. The one-ring open hydrolysis product intermediates of the cardioprotective agent ICRF-187 (dexrazoxane) displace iron from iron-anthracycline complexes. *Agents Actions*, **40**: 86-95, 1993.

44. Burden, D.A. and Osheroff, N. Mechanism of action of eukaryotic topoisomerase II and drugs targeted to the enzyme. *Biochem. Biophys. Acta.*, **1400**: 139-154, 1998.

45. Pommier, Y., Leteurtre, F., Fesen, M.R., Fujimori, A., Bertrand, R., Solary, E., Kohlhagen, G., and Kohn, K.W. Cellular determinants of sensitivity and resistance to DNA topoisomerase inhibitors. *Cancer Investigation*, **12**: 530-542, 1994.

46. Berger, J.M., Gamblin, S.J., Harrison, S.C., and Wang, J.C. Structure and mechanism of DNA topoisomerase II [published erratum appears in Nature 1996 Mar 14;380(6570):179]. *Nature*, **379**: 225-232, 1996.

47. Wang, J.C. DNA topoisomerases. *Ann. Rev. Biochem.*, **54**: 665-697, 1985.

48. Anderson, H.J. and Roberge, M. DNA topoisomerase II: a review of its involvement in chromosome structure, DNA replication, transcription and mitosis. *Cell Biol. Int. Rep.*, **16**: 717-724, 1992.

49. Larsen, A.K., Skladanowski, A., and Bojanowski, K. The roles of DNA topoisomerase II during the cell cycle. *Prog. Cell Cycle Res.*, **2**: 229-239, 1996.

50. Corbett, A.H. and Osheroff, N. When good enzymes go bad: conversion of topoisomerase II to a cellular toxin by antineoplastic drugs. *Chem. Res. Toxicol.*, **6**: 585-597, 1993.

51. Osheroff, N. Biochemical basis for the interaction of type I and type II topoisomerases with DNA. *Pharmacol. Ther.*, **41**: 223-241, 1989.

52. Nitiss, J.L. Roles of DNA topoisomerases in chromosomal replication and segregation. *Adv. Pharmacol.*, **29A**: 103-134, 1994.

53. Heck, M.M., Hittelman, W.N., and Earnshaw, W.C. Differential expression of DNA topoisomerase I and II during the eukaryotic cell cycle. *Proc. Natl. Acad. Sci.U.S.A.*, **85**: 1086-1090, 1988.

54. Osheroff, N. DNA topoisomerases. *Biochem. Biophys. Acta.*, **1400**: 1-2, 1998.

55. Roca, J. and Wang, J.C. The capture of a DNA double helix by an ATP-dependent protein clamp: A key step in DNA transport by type II DNA topoisomerases. *Cell*, **71**: 833-840, 1992.

56. Roca, J. and Wang, J.C. DNA transport by a type II DNA topoisomerase: evidence in favor of a two-gate mechanism. *Cell*, **77**: 609-616, 1994.

57. Tsai-Pflugfelder, M., Liu, L.F., Liu, A.A., Tewey, K.M., Whang-Peng, J., Knutsen, T., Huebner, K., Croce, C.M., and Wang, J.C. Cloning and sequencing of cDNA encoding human DNA topoisomerase II and localization of the gene to chromosome region 17q21-22. *Proc. Natl. Acad.Sci.U.S.A.*, **85**: 7177-7181, 1988.

58. Zechiedrich, E.L. and Osheroff, N. Eukaryotic topoisomerases recognize nucleic acid topology by preferentially interacting with DNA crossovers. *EMBO J.*, **9**: 4555-4562, 1990.

59. Woessner, R.D., Mattern, M.R., Mirabelli, C.K., Johnson, R.K., and Drake, F.H. Proliferation- and cell cycle-dependent differences in expression of the 170 kilodalton and 180 kilodalton forms of topoisomerase II in NIH-3T3 cells. *Cell Growth Differ.*, **2**: 209-214, 1991.

60. Hsiang, Y.H., Wu, H.Y., and Liu, L.F. Proliferation-dependent regulation of DNA topoisomerase II in cultured human cells. *Cancer Res.*, **48**: 3230-3235, 1988.

61. Sengupta, S.K. Topoisomerase II inhibitors, inhibitors of DNA topoisomerases. In: W.O. Foye (ed.), Cancer Chemotherapeutic Agents, pp. 205-260, Washington, D.C.: ACS Professional Reference Book Massachusetts College of Pharamcy and Allied Health Sciences. 1995.

62. Osheroff, N., Corbett, A.H., and Robinson, M.J. Mechanism of action of topoisomerase II-targeted antineoplastic drugs. *Adv. Pharmacol.*, **29B**: 105-126, 1994.

63. Gabbay, E.J., Grier, D., Fingerle, R.E., Reimer, R., Levy, R., Pearce, S.W., and Wilson, W.D. Interaction specificity of the anthracyclines with deoxyribonucleic acid. *Biochemistry*, **15**: 2062-2070, 1976.

64. Tewey, K.M., Rowe, T.C., Yang, L., Halligan, B.D., and Liu, L.F. Adriamycin-induced DNA damage mediated by mammalian DNA topoisomerase II. *Science*, **226**: 466-468, 1984.

65. Chen, G.L., Yang, L., Rowe, T.C., Halligan, B.D., Tewey, K.M., and Liu, L.F. Nonintercalative antitumor drugs interfere with the breakage-reunion reaction of mammalian DNA topoisomerase II. *J. Biol. Chem.*, **259**: 13560-13566, 1984.

66. D'Arpa, P. and Liu, L.F. Topoisomerase-targeting antitumor drugs. *Biochem. Biophys. Acta.*, **989**: 163-177, 1989.

67. Holm, C., Covey, J., Kerrigan, D., and Pommier, Y. Differential requirement of DNA replication for the cytotoxicity of DNA topoisomerase I and II inhibitors in Chinese hamster DC3F cells. *Cancer Res.*, **49**: 6365-6368, 1989.

68. Darby, M.K., Schmitt, B., Jongstra-Bilen, J., and Vosberg, H.P. Inhibition of calf thymus type II DNA topoisomerase by poly(ADP-ribosylation). *EMBO J.*, **4**: 2129-2134, 1985.

69. Solary, E., Bertrand, R., and Pommier, Y. Apoptosis induced by DNA topoisomerase I and II inhibitors in human leukemic HL-60 cells. *Leuk. Lymphoma.*, **15**: 21-32, 1994.

70. Drake, F.H., Hofmann, G.A., Mong, S.M., Bartus, J.O., Hertzberg, R.P., Johnson, R.K., Mattern, M.R., and Mirabelli, C.K. In vitro and intracellular inhibition of topoisomerase II by the antitumor agent merbarone. *Cancer Res.*, **49**: 2578-2583, 1989.

71. Boritzki, T.J., Wolfard, T.S., Besserer, J.A., Jackson, R.C., and Fry, D.W. Inhibition of type II topoisomerase by fostriecin. *Biochem. Pharmacol.*, **37**: 4063-4068, 1988.

72. Bojanowski, K., Lelievre, S., Markovits, J., Couprie, J., Jacquemin-Sablon, A., and Larsen, A.K. Suramin is an inhibitor of DNA topoisomerase II in vitro and in Chinese hamster fibrosarcoma cells. *Proc. Natl. Acad.Sci.U.S.A.*, **89**: 3025-3029, 1992.

73. Jensen, P.B., Jensen, P.S., Demant, E.J., Friche, E., Sorensen, B.S., Sehested, M., Wassermann, K., Vindelov, L., Westergaard, O., and Hansen, H.H. Antagonistic effect of aclarubicin on daunorubicin-induced cytotoxicity in human small cell lung cancer cells: relationship to DNA integrity and topoisomerase II. *Cancer Res.*, **51**: 5093-5099, 1991.

74. Hasinoff, B.B., Kuschak, T.I., Creighton, A.M., Fattman, C.L., Allan, W.P., Thampatty, P., and Yalowich, J.C. Characterization of a Chinese hamster ovary cell line with acquired resistance to the bisdioxopiperazine dexrazoxane (ICRF-187) catalytic inhibitor of topoisomerase II. *Biochem. Pharmacol.*, **53**: 1843-1853, 1997.

75. Hasinoff, B.B., Kuschak, T.I., Yalowich, J.C., and Creighton, A.M. A QSAR study comparing the cytotoxicity and DNA topoisomerase II inhibitory effects of bisdioxopiperazine analogs of ICRF-187 (dexrazoxane). *Biochem. Pharmacol.*, **50**: 953-958, 1995.

76. Tanabe, K., Ikebuchi, K., Ishida, R., and Andoh, T. Inhibition of topoiosmerase II by antitumour agents bis(2,6-dioxopiperazine) derivatives. *Cancer Res.*, **51**: 4903-4908, 1991.

77. Ishida, R., Miki, T., Narita, T., Yui, R., Sato, M., Utsumi, K.R., Tanabe, K., and Andoh, T. Inhibition of intracellular topoisomerase II by antitumor bis(2,6-dioxopiperazine) derivatives: mode of cell growth inhibition distinct from that of cleavable complex-forming type inhibitors. *Cancer Res.*, **51**: 4909-4916, 1991.

78. Roca, J., Ishida, R., Berger, J.M., Andoh, T., and Wang, J.C. Antitumor bisdioxopiperazines inhibit yeast DNA topoisomerase II by trapping the enzyme in the form of a closed protein clamp. *Proc. Natl. Acad. Sci.U.S.A.*, **91**: 1781-1785, 1994.

79. Fattman, C.L., Allan, W.P., Hasinoff, B.B., and Yalowich, J.C. Collateral sensitivity to the bisdioxopiperazine dexrazoxane (ICRF-187) in etoposide (VP-16)-resistant human leukemia K562 cells. *Biochem. Pharmacol.*, **52**: 635-642, 1996.

80. Gorbsky, G.J. Cell cycle progression and chromosome segregation in mammalian cells cultured in the presence of the topoisomerase II inhibitors ICRF-187 [(+)-1,2-bis(3,5-dioxopiperazinyl-1-yl)propane; ADR-529] and ICRF-159 (Razoxane). *Cancer Res.*, **54**: 1042-1048, 1994.

81. Sehested, M., Jensen, P.B., Sorensen, B.S., Holm, B., Friche, E., and Demant, E.J. Antagonistic effect of the cardioprotector (+)-1,2-bis(3,5-dioxopiperazinyl-1-yl)propane (ICRF-187) on DNA breaks and cytotoxicity induced by the topoisomerase II directed drugs daunorubicin and etoposide (VP-16). *Biochem. Pharmacol.*, **46**: 389-393, 1993.

82. Andoh, T. and Ishida, R. Catalytic inhibitors of DNA topoisomerase II. *Biochem. Biophys. Acta.*, **1400**: 155-171, 1998.

83. Salsbury, A.J., Burrage, K., and Hellmann, K. Histological analysis of the antimetastatic effect of (+/-)-1,2-bis(3,5-dioxopiperazin-1-yl)propane. *Cancer Res.*, **34**: 843-849, 1974.

84. Hasinoff, B.B., Yalowich, J.C., Ling, Y., and Buss, J.L. The effect of dexrazoxane (ICRF-187) on doxorubicin- and daunorubicin- mediated growth inhibition of Chinese hamster ovary cells. *Anticancer Drugs*, **7**: 558-567, 1996.

85. Ishida, R., Iwai, M., Hara, A., and Andoh, T. The combination of different types of antitumor topoisomerase II inhibitors ICRF-193 and VP-16, has synergistic and antagonistic effects on cell survival, depending on treatment schedule. *Anticancer Res.*, **16**: 2735-2740, 1996.

Chapter 2 Characterization of the effects of dexrazoxane on morphological, structural, and cell cycle properties of Chinese hamster ovary cells, and related cell lines.

2.1 Introduction

2.1.1 The eukaryotic cell cycle

A typical eukaryotic cell cycle consists of four successive phases (Fig 2.1). During S phase, which entails DNA synthesis the normal diploid (2N) complement of DNA is doubled resulting in the replication of chromosomes. M phase consists of nuclear division (mitosis) and cytoplasmic division (cytokinesis). Mitosis itself is composed of several stages: prophase, prometaphase, metaphase, anaphase, and telophase. In general, chromosomes are first condensed, followed by the break down of the nuclear envelope, separation of sister chromatids, and the formation of two separate nuclei, identical in DNA content. Finally, separating both S and M phases and completing the cell cycle are two intervening gap phases, G2 and G1 [1].

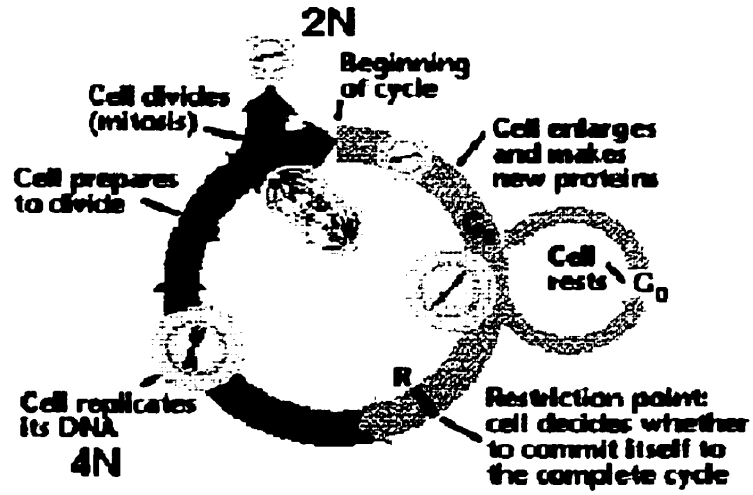

Fig. 2.1. The stages of a typical eukaryotic cell cycle. [2]

The sequence of events during the cell cycle are normally tightly regulated so as to ensure precision in the replication and segregation of cellular material. As discussed later in further detail, negative feedback mechanisms known as checkpoint controls exist throughout the cell cycle to ensure the proper timing and completion of various events subsequent to continued cell cycling [3,4]. With regards to the chemotherapeutic treatment of tumor cells, the fidelity of such checkpoint controls may dicate the degree of their susceptibility towards cell cycle blockage and/or the triggering of cell suicide by apoptosis [4,5].

2.1.2 Polyploidization

In contrast to control tumors, those whose growth has been halted through chemotherapeutic intervention may contain many large multinucleated cells of abnormally enlarged cell volume [6]. As a consequence, such cells are considered to be polyploid in that they contain more than the normal diploid complement of chromosomal DNA, as well as other various intracellular constituents. Polyploidization results from the disruption of certain cellular events relative to others whereby cells undergo an endomitotic or endoreduplication event after each round of DNA replication. As cell cycle checkpoints are either aborgated or delayed these events occur in the absence of cytokinesis [7].

Naturally occurring polyploid cells can be found in angiosperms and insects, as well as in mammals in liver parenchyma, heart muscle, and in the form of differentiating megakaryocytes which fragment into blood platelets. Such cells possess accentuated levels of gene expression and are often involved in functions requiring high metabolic activity [7]. In the context of studying cell cycle regulation and/or differentiation,

polyploid cells can be induced in a cell line dependent manner by some types of topoisomerase II inhibitors which uncouple chromosome dynamics from other cell cycle events [8], as well as by tubulin-depolymerizing agents including colchicine and colcemid [9], and inhibitors of actin polymerization such as cytochalasin B [10].

2.1.3 The project under study

Bisdioxopiperazines including ICRF-187 (dexrazoxane), ICRF-154, and ICRF-193 were originally synthesized as potential antitumor [11] and antimetastatic agents [12]. It was believed that due to their structural similarity to EDTA, a powerful chelating agent that they would be able to chelate trace metals crucial to the activity of many enzyme systems and therefore retard the growth of human or experimental tumors [11]. Early investigations revealed that although ICRF-159 (razoxane) and ICRF-154 were both active against experimental mouse tumors [11], the observed cellular effects including toxicity were mediated through an inhibition of DNA synthesis [13]. Since that time the bisdioxopiperazine derivatives have been shown to disrupt essential cellular functions such as DNA synthesis, chromosome condensation, and segregation through the inhibition of DNA toposiomerase II activity [14,15]. Further studies have demonstrated the existence of a structure-activity relationship between topoisomerase II inhibition, the level of induced cytotoxicity [16], and cell line-specific growth inhibition [13,15,17,18] induced by the bisdioxopiperazines.

In light of the above studies a great deal is known about the growth inhibitory and cell cycle perturbation effects of ICRF-159 on a number of different cell lines [17,19]. Additionally, only a few studies involving a limited variety of cell lines have identified an

obstruction of normal chromosome segregation by ICRF-193 [8,20] and dexrazoxane [3] resulting in polyploidization. Because of poor water solubility and variable bioavailability of ICRF-159, the study and clinical use of the more soluble (+)-(*S*)-enantomier dexrazoxane has become more prominent in recent years [21]. Therefore the present study was designed to provide a comprehensive analysis of the *in vitro* effects of dexrazoxane on the growth, cytotoxicity, morphology and cell cycle progression of normal (primary), and immortal cells of the rodent origin. Specifically, Chinese hamster ovary (CHO) and isolated primary rat heart fibroblast cells were exposed to dexrazoxane and examined for the alteration of a number of properties, as compared to control cells. Furthermore, a dexrazoxane-resistant CHO cell line (DZR) was used as a control for most of these experiments. The results obtained in the present study, in combination with previous published reports have permitted herein some insight into the variable effects of prolonged dexrazoxane exposure on different cell lines, including the mechanistic mitotic consequences with respect to dexrazoxane-induced topoisomerase II inhibition.

2.2 Cell lines and culturing conditions

2.2.1 Materials

Dexrazoxane (Zinecard®, ICRF-187) was a gift of Pharmacia & Upjohn (Columbus, OH, U.S.A.). Trypan blue dye (cat. No. T-6146), HEPES (cell culture grade, cat. No. H-9136) was obtained from Sigma Chemical Co. (St. Louis, MO, U.S.A.). Sodium bicarbonate ($NaHCO_3$, cat. No. BP328-079) and Wheaton double sidearm suspension culture flasks (125 mL, Cat. No. 06-416-2C) were obtained from Fisher Scientific (Fairlawn, NJ, U.S.A.). Dulbecco's phosphate buffered saline (PBS, cat. No. D-5652), Dulbecco's alpha minimum essential medium (α-MEM, cat. No. 12000-022), Dulbecco's modified eagle medium/F-12 (DMEM/F-12, cat. No. 12500-062), penicillin-streptomycin (cat. No. 25200-072), fetal bovine serum (FCS, cat. No. 26140-079), and trypsin, 0.25% (w/v) in Hank's buffered salt solution (HBSS, without Ca^{2+} or Mg^{2+}) with 1 mM Na_4EDTA (cat. No. 25200-072) were obtained from Gibco-BRL, Life Technologies Inc. (Burlington, ON). Na_2EDTA (cat. No. 10093) was obtained from BDH Chemicals Ltd. (Toronto, ON). Sodium hydroxide (5N NaOH, cat. No. H369) was obtained from Mallinckrodt Specialty Chemicals Co. (Paris, KT, U.S.A.). Isoton II Coulter balanced electrolyte solution (cat. No. PN 8546719) was obtained from Beckman Coulter Inc. (Burlington, ON). Carbon dioxide (standard grade) was purchased from Welder's Supply (Winnipeg, MB). Microtitre plates (96-well, sterile, cat. No. 83.1835), 50 mL sterile PP conical centrifuge tubes (29x114 mm, cat. No. 62.547.004), T-25cm^2 (cat. No. 83.1810) and T-75cm^2 (cat. No. 83.1813) PE red plug capped flasks for attached cultures, 35x10 mm (cat. No. 83.1800) and 6-well (cat. No. 83.1839) tissue culture plates, 0.2 μm acetate

syringe filters (cat. No. 83.1826.001) and all other plasticware were obtained from Sarstedt Inc. (St. Leonard, PQ). Glucometer Elite® Blood Glucose Meter and test strips (Bayer Inc., Healthcare Division, Etobicoke, ON).

2.2.2 Cell growth and culturing conditions

Cell lines: Three cell lines were used to various lengths in the experiments outlined in the following sections of this chapter. First, a wild type Chinese hamster ovary (CHO) cell line (type AA8; ATCC CRL-1859) was obtained from the American type Culture Collection (Rockville, MD). Second, a dexrazoxane-resistant (DZR) cell line was previously established in our laboratory by exposure of the CHO cell line to increasing concentrations of dexrazoxane over an extended period of time. Dexrazoxane resistance in DZR cells is 1500-fold greater than parental CHO cells [22], and is presumably attributed to a recently localized Thr48Ile mutation at the dimer interface of DNA topoisomerase II [23]. Finally, a primary neonatal fibroblast cell line was isolated from 2-day-old Sprague-Dawley rat hearts in combination with neonatal ventricular myocytes by GuQi Wang in our laboratory, as previously described [24].

Preparation of media: Cell culture media were prepared by dissolving one pack (10 g) of α-MEM or DMEM/F-12, 4.76 g of HEPES, and 2.2 g of $NaHCO_3$ in 700 mL of ddH_2O. The pH of the solution was adjusted to 7.1 with 5 N NaOH. Next, 10 mL of penicillin-streptomycin and 200 mL of ddH_2O were added aseptically to bring the final volume to 900 mL, followed by sterile filteration through a 0.2 μm Nalgene bottle top filter (Nalgene Company, Rochester, New York). The solution was stored at 4°C for up to one month,

where upon use 100 mL, or 10% (v/v) of fetal bovine serum (FCS) was added under sterile conditions.

Culturing of cells: CHO and DZR cell lines were grown in α-MEM/FCS, as either adherent/attached cultures in T-flasks or tissue culture plates, or as suspension cultures in double sidearm suspended bar, magnetic spinner flasks. In the case of the latter method, stirring speed was adjusted to ~1-2 rotations/sec with the use of an voltage controlling device (Variac) so as to minimize shear forces and adverse effects on cell viability. Heart fibroblast cells were grown in DMEM/F-12/FCS as adherent cultures in T-flasks or tissue culture plates. Cells were grown in an atmosphere of 5% (v/v) CO_2 at 37°C.

Harvesting and seeding of cells: Adherent cells in exponential growth approaching confluence (T-25cm^2 flasks: 10x10^6 cells, T-75cm^2 flasks: 30x10^6 cells, and 35x10 mm or 6-well tissue culture plates: 3x10^6 cells) were harvested as follows: After removal of conditioned medium from the flask, cells were washed once with 10 mL of Dulbecco's phosphate buffered saline (PBS). Next, 1 mL of 0.25% (w/v) trypsin in Hank's buffered salt solution (without Ca^{2+} or Mg^{2+}) with 1 mM EDTA was added (2 mL for T-75cm^2 flasks and 0.3 mL for 35x10 mm plates), and the flask was tottered back and forth gently for up to 5 min until cells had detached from the bottom of the flask. Trypsin was then inactivated by the addition of 9 equivalent volumes of complete cell culture medium followed by the transfer of the entire contents into a sterile conical centrifuge tube and centrifugation at 250 *g* for 10 min. Afterwards, the supernatant was removed and cells were resuspended in 10 mL of cell culture medium. Suspension cells in exponential growth approaching maximum cell density (~1x10^6 cells/mL) were simply diluted to lower starting concentrations (≥ 25,000 cells/mL). A model Z_f Coulter counter (Coulter

Electronics, Hialeah, FL, U.S.A.) was used to assess cell densities (cells/mL) from aseptically removed samples in order to subsequently seed cells at desired levels (see Appendix A.2)

Drug preparation and delivery: Dexrazoxane (M_w = 268.28 g/mol) was dissolved in cell culture medium, filter sterilized through a 0.2 μm acetate syringe filter and added to cell cultures at ~1-10 % (v/v) as per concentration used.

Assessment of viability: Trypan blue dye (0.6% w/v) was prepared by dissolving 0.6 g of dye in ddH_2O containing 150 mM NaCl and 1 mM Na_2EDTA. Cell viability was assessed in a trypan blue dye exclusion analysis by diluting culture samples 1:1 with trypan blue dye. A minimum of 500 cells were counted under a hemacytometer chamber followed by the determination of the percentage non-viable (blue) cells per total number of cells counted.

Assessment of glucose levels: Depletion of media nutrients was followed indirectly by measuring the glucose content level from conditioned culture media. This was accomplished by the use of a blood glucose meter (Glucometer Elite®, Bayer Inc.). For each measurement individual test strips were removed from their package by carefully folding back the foil ends to expose the meter ends of the test strip. Next, the test strip was inserted into the meter registering a beep, as it was held between the foil ends. The base of the test strip was then applied to a small drop of the sample media placed onto the foil wrapper. After 29 sec the final glucose content level was diplayed on the meter in units of mmol/L.

2.3 Cytotoxicity analysis of dexrazoxane on CHO and DZR cells

2.3.1 Introduction

A series of dexrazoxane cytotoxicity experiments were conducted on CHO and DZR cells in order to assess and compare the level of growth inhibition determined by two separate methods of analysis. Cytotoxicity was first evaluated using a colorimetric MTT (3-(4,5-dimethylythiazol-2-yl)-2,5-diphenyltetrazolium bromide) assay. MTT is a soluble tetrazolium salt which is enzymatically reduced into an insoluble dark blue formazan crystal by actively metabolizing cells [25]. In general, a linear relationship exists between the number of viable cells in culture and level of formazan production, evaluated by absorbance after solubilization in DMSO. As a more direct measurement of cytotoxicity, the actual number of intact cells remaining in culture after dexrazoxane treatment was additionally assessed in a cell counting analysis with the use of a model Z_f Coulter counter. Finally, dexrazoxane cytotoxicity of CHO cells was assessed by MTT analysis under different conditions of drug exposure and media replacement so as to determine their effect on cell proliferation and hence median inhibitory concentration values.

2.3.2 Materials

MTT (98%, TLC, cat. No. M-5655) was obtained from Sigma Chemical Co. (St. Louis, MO, U.S.A.). Dulbecco's phosphate buffered saline (PBS, cat. No. D-5652), Dulbecco's alpha minimum essential medium (α-MEM, cat. No. 12000-022), fetal bovine serum (FCS, cat. No. 26140-079), and trypsin, 0.25% (w/v) in HBSS (without Ca^{2+} or Mg^{2+}) with 1 mM Na_4EDTA (cat. No. 25200-072) were obtained from Gibco-BRL, Life

Technologies Inc. (Burlington, ON). DMSO (used for MTT assay, cat. No. 4948) was obtained from Mallinckrodt Specialty Chemicals Co. (Paris, KT, U.S.A.). Microtitre plates (96-well, cat. No. 83.1835) were obtained from Sarstedt Inc. (St. Leonard, PQ).

2.3.3 Methods

2.3.3.1 Cytotoxicity experiments by MTT analysis

2.3.3.1.1 Seeding of cells and delivery of drug to microtitre plates

Exponentially growing CHO and DZR cultures were harvested from T-flasks with trypsin-EDTA and then seeded onto sterile 96-well microtitre plates in 100 μL of α-MEM/FCS per well. CHO cells were seeded at 2000 cells/well, and DZR cells at 5000 cells/well, and allowed to attach for 24 hr before drug solutions were added. After the appropriate quantity of dexrazoxane was weighed and solubilized, as described in Section 2.2.2 drug stock solutions were prepared and added to the microtitre plates using a multichannel pipettor. Appropriate volumes of α-MEM/FCS were added to the wells with cells for a final volume of 200 μL/well. Six replicates were performed at each concentration of dexrazoxane. Into all outer wells that did not contain cells (rows A and H, and column 1) was placed 200 μL of PBS for spectrophotometer blanking and to prevent evaporation of media from inner wells which contained cells and drug.

DZR cells were incubated in the presence of dexrazoxane for 72 hr with no intervention. CHO cells were also incubated for 72 hr, but were exposed to dexrazoxane under 3 separate conditions: (i) no intervention over the 72 hr period, (ii) media only

changed after 48 hr, or (iii) media and drug changed after 24, 48 hr of incubation. The changing of media in the latter two protocols was achieved by gently aspirating off the conditioned media followed by the addition of 200 μL of either fresh media or media with drug in the same manner as before.

2.3.3.1.2 Measurement of cytotoxic effects

After 72 hr of growth in the presence of dexrazoxane, cell survival was measured by the MTT assay [26,27]. MTT is a yellow tetrazolium salt (3-(4,5-dimethylthiazol-2-yl)-2,5-diphenyltetrazolium bromide) which is converted into water-insoluble blue formazan crystals by mitochondrial cytosolic dehydrogenase whereby the amount of formazan produced is directly proportional to the number of viable cells. To the wells of each plate was added 20 μL of 0.25% (w/v) MTT tetrazolium salt prepared in PBS. Plates were then incubated for 4 hr at 37°C in a humidifed 5% (v/v) CO_2 atmosphere followed by the removal of cell culture medium and the addition of 100 μL of DMSO to dissolve the crystals. A Thermomax 96-well plate reader (Molecular Devices, Menlo Park, CA, U.S.A.) was used to measure absorbance at 490 nm in the wells. Absorbance was corrected for non-specific, scattered light by subtracting the absorbance at 650 nm from the absorbance at 490 nm.

2.3.3.1.3 Dose-response curves

Data from all cytotoxicity experiments was inputted into SigmaPlot (Jandel Corp., San Rafael, CA, U.S.A.) and used to determine the 50% median inhibitory concentration (IC_{50}). Prior to graphical representation of dose-response curves outlier absorbances were removed empirically with statistical relevance using the provided transform file entitled *!outlier.xfm* (integral equations not shown). Non-linear, least-squares fitting of the absorbance-drug concentration data was performed in SigmaPlot using the following three- or four-parameter logistic equation,

$$Abs_{490/650} = (a - d) / (1 + (x / c)^b) + d$$

where $Abs_{490/650}$ is the absorbance at 490 nm minus the absorbance at 650 nm, x is the drug concentration, c is the median inhibitory concentration (IC_{50}), b is the Hill-type exponential factor indicative of the rate at which toxicity increases with increasing drug concentration, a is the estimated maximal absorbance and d is the estimated background absorbance at the highest drug concentration. When the background absorbance is close to zero d was set equal to 0, thus giving a three-parameter equation. The values of b and c were initially computed from a two-parameter fit after substitution of the a and d values. Subsequently, more accurate values of b and c were determined upon the iteration of a three- or four-parameter fit equation with the inclusion of the same a and d values and the b and c values computed from the two-parameter fit equation.

2.3.3.2 Cytotoxicity experiments by cell counting analysis

Colorimetric assays such as MTT are one of the most common methods for evaluating the effect of drugs on growth and survival of cells in culture. In general, the MTT assay gives a good concordance between the number of viable cells in culture and the production of formazan, based on the mitochondrial dehydrogenase activity in viable cells [28]. However, on occassion in similar tumor cell lines [28] discrepancies may exist between the actual number of cells and the level of formazan production. To that effect, dexrazoxane-mediated cytotoxicity in CHO and DZR cells was evaluated directly by cell counting, and subsequently compared to results obtained by MTT cytotoxicity analysis.

Cells in exponential growth were harvested and seeded into individual wells of 6-well tissue culture plates and brought to 3.4 mL with α-MEM/FCS. CHO cells were seeded at 2.5×10^4 cells/well, and DZR cells at 6.5×10^4 cells/well followed by a 24 hr incubation period at 5% (v/v) CO_2 and 37°C to allow for cell attachment. Next, 0.1 mL of requisite stock solutions of dexrazoxane were added in replicate (x2 wells) to produce the desired final concentration (total volume 3.5 mL). After 72 hr of growth, cells were harvested with trypsin-EDTA followed by quenching to volumes of 3 mL/well with α-MEM/FCS, as outlined previously (Section 2.2.2). Cell concentrations, and then total number of cells per well in the 3 mL volume were determined from removed sample aliquots on a model Z_f Coulter counter using a threshold setting of 7 (140 μm aperture tube, 1/amp. = 2, 1/ap.current = 2, diameter cutoff ≅ 7.7 μm) for DZR cells and a threshold setting of 7 (100 μm aperture, 1/amp = 2, 1/ap.curr = 8, diameter cutoff ≅ 8.7 μm) for CHO cells, as explained in Appendix A.2. The median dexrazoxane inhibitory concentration

(IC_{50}) was determined in the same fashion as before (Section 2.3.3.1.3) from constructed dose-response curves of the total number of cells/well versus dexrazoxane concentration.

2.3.4 Results

2.3.4.1 Cytotoxicity of dexrazoxane towards CHO and DZR cells

The individual values of the median inhibitory concentration (IC_{50}) of each cytotoxicity Experiment are presented in Table 2.1. Illustrated in Fig. 2.2 and 2.3 are the cytotoxicity profiles for dexrazoxane towards CHO and DZR cells as determined by either MTT or cell counting analysis. The corresponding mean inhibitory concentration values of dexrazoxane on CHO cells was 5.2 ± 0.4 μM and 3.5 ± 0.1 μM, and on DZR cells was 2236.0 ± 172.1 μM and 1648.0 ± 91.9 μM as determined by MTT and cell counting analysis, respectively. The resistance factor for dexrazoxane in DZR cells as compared to CHO cells was determined to be 430-fold by MTT analysis, and 471-fold by cell counting analysis. Daily exposure to dexrazoxane with media replacement gave an IC_{50} value of 5.0 ± 0.6 μM, and media replacement only at 48 hr produced an IC_{50} value of 4.8 ± 0.3 μM, as determined by MTT analysis. Although CHO cells were seeded at the same number of cells/well in each plate absorbance values were noticably higher in the MTT cytotoxicity profile for cells exposed daily to dexrazoxane accompanied by media replacement. This result possibly suggests the maintenance of a healthy culture with media and nutrients replacement.

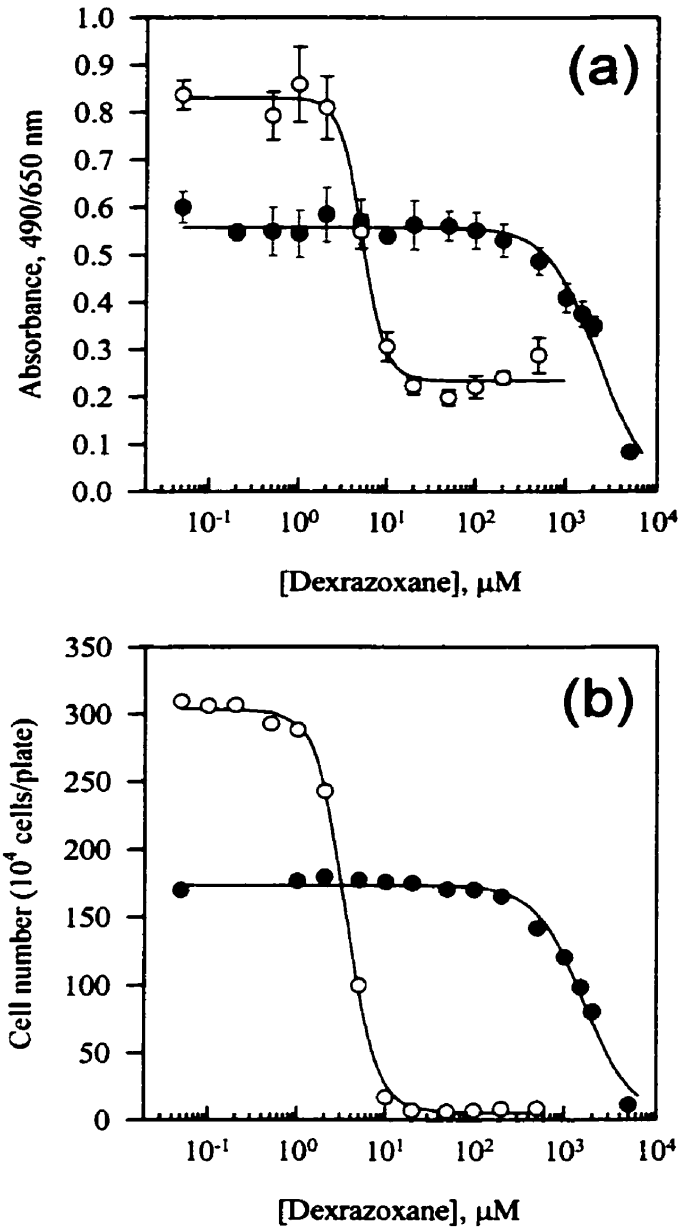

Fig. 2.2. CHO and DZR cell growth inhibition by dexrazoxane without media replacement. CHO (○) and DZR (●) cells were incubated for 72 hr in the presence of dexrazoxane; (a) IC_{50} ± S.E. were 5.2 ± 0.4 μM and 2236.0 ± 172.1 μM for CHO and DZR cell lines, respectively as determined by MTT analysis; (b) IC_{50} ± S.E. were 3.5 ± 0.1 μM and 1648.0 ± 91.9 μM on CHO and DZR cell lines, respectively as determined by cell counting analysis on a model Z_f Coulter counter. The curves represent the results of least squares non-linear regression fits of measured values to three- or four-parameter logistic equations. The error bars represent standard deviations. Concentrations of 0 μM are plotted for convenience with an arbitrary value for the purpose of clarity.

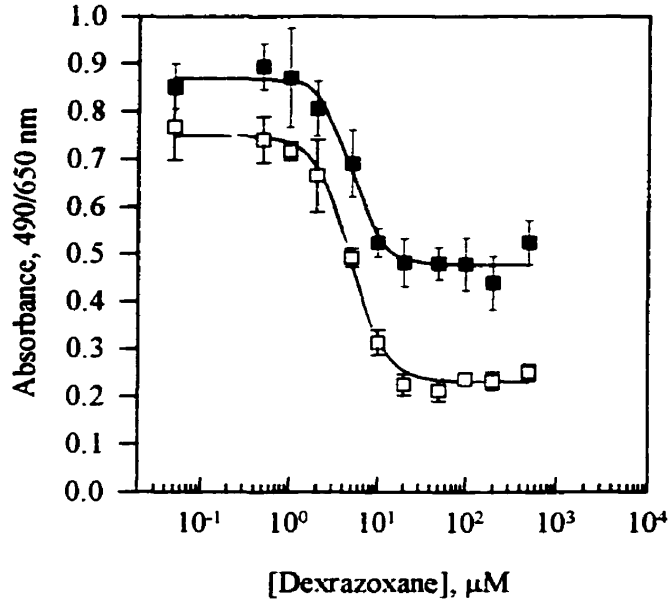

Fig. 2.3. CHO cell growth inhibition by dexrazoxane with media/drug replacement. CHO cells were incubated for 72 hr in the presence of dexrazoxane with media and drug replaced every 24 hr (■), or with only media replaced after 48 hr (□). Growth inhibition was quantitated by MTT analysis, producing $IC_{50} \pm$ S.E. values of 5.0 ± 0.6 μM and 4.8 ± 0.3 μM for the above media/drug replacement protocols, respectively. The curves represent the results of least squares non-linear regression fits of measured values to four-parameter logistic equations. The error bars represent standard deviations. The lowest concentrations are the zero values, plotted for convenience on a logarithmic scale with arbitrary values.

Table 2.1 Cytotoxicity of dexrazoxane towards CHO and DZR cell lines.

Method of analysis	Cell line	IC_{50}[a] (μM)	S.E. (μM)	C.V. (%)	Resistance factor[c]
MTT assay	CHO	5.2	0.4	6.8	
	DZR	2236.0	172.1	7.7	430
	CHO[1]	5.0	0.6	12.3	
	CHO[2]	4.8	0.3	6.9	
Cell counting analysis[b]	CHO	3.5	0.1	3.2	
	DZR	1648.0	91.9	5.6	471

[1] CHO cells exposed to dexrazoxane daily with media replacement.

[2] CHO cells exposed to dexrazoxane once with media replaced at 48 hr.

[a] The individual median inhibitory concentrations of dexrazoxane on CHO and DZR cell lines and their S.E. and % C.V. Cytotoxicity was measured by MTT assay or cell counting analysis on a model Z_f Coulter counter after a 72 hr exposure to dexrazoxane. The IC_{50} is the concentration of dexrazoxane at which cell growth is 50% of the maximum observed inhibition. These values were obtained by fitting absorbance or cell number data to three- or four-parameter logistic equations.

[b] Cell counting analysis using a Coulter counter threshold of 7 (140 μm aperture, 1/amp.= 2, 1/ap.current = 2, diameter cutoff ≅ 7.7 μm) for DZR cells and threshold of 7 (100 μm aperture, 1/amp.= 2, 1/ap.current = 8, diameter cutoff ≅ 8.7 μm) for CHO cells

[c] Resistance factor: the ratio of the median inhibitory concentration of dexrazoxane on CHO and DZR cells after one exposure.

2.4 Effects of dexrazoxane on the proliferation and normal growth of suspension and adherent cell cultures

2.4.1 Introduction

In the following section, under similar conditions of dexrazoxane exposure the characteristics of cell growth, including doubling time and viability were examined in various cell lines. It was important to investigate how both immortal (CHO and DZR) and non-immortal (primary heart fibroblasts) cell lines behaved in the presence of dexrazoxane, as well to as assess the growth patterns of these cells under different conditions of exposure and culturing. Furthermore, the conditions established at the conclusion of this section, with respect to dexrazoxane exposure and nutrience replenishment helped to serve a fundamental basis for the design of all subsequent experiments.

2.4.2 Methods

2.4.2.1 Growth curve characteristics of CHO cells exposed to dexrazoxane under different conditions

In the following experiment CHO cells were exposed separately to 3 different concentrations of dexrazoxane and allowed to grow as adherent cultures for up to 96 hr alongside unexposed control cells. Cells were treated to different concentrations of dexrazoxane under separate exposure and media replacement conditions, and the depletion of nutrients were followed by monitoring glucose levels, as described in Section 2.2.2. The purpose of this initial experiment was first, to establish an ideal concentration of dexrazoxane to sufficiently inhibit cell proliferation and second, determine how often

media should be replaced in order to maintain the basic necessities for the continuation of cell growth, if possible.

Cells in exponential growth were harvested and seeded onto 60 individual 35x10 mm tissue culture plates at $1.3x10^5$ cells/plate, and brought to 3.4 mL with α-MEM/FCS. This was followed by a 24 hr incubation period at 5% (v/v) CO_2 and 37°C to allow for cell attachment. To each set of 18 individual plates was added 0.1 mL of the requisite stock drug solution to produce final dexrazoxane concentrations of either 5, 20, or 100 μM (total volume 3.5 mL). Three separate drugging protocols were performed alongside control cultures to examine the effects of different dexrazoxane treatment periods on cell growth. In the first protocol, cells were treated once with 5, 20, or 100 μM dexrazoxane at 0 hr and were allowed to grow with media replaced aseptically after 48 hr of exposure. In the second protocol, cells were treated daily with 5, 20, or 100 μM dexrazoxane combined with media replacement in the same manner as before. And in the third protocol, cells were treated with 5, 20, or 100 μM dexrazoxane at 0 hr and 48 hr of exposure, with media replacement at these time intervals. After every 24 hr interval of growth 2 replicate plates respective for each dexrazoxane concentration and drugging protocol were analyzed for glucose content followed by harvesting with trypsin-EDTA and quenching to volumes of 3 mL/plate with α-MEM/FCS, as outlined previously (Section 2.2.2). Cell densities, and then total number of cells per plate in the 3 mL volume was determined from removed sample aliquots on a model Z_f Coulter counter using a threshold setting of 7 (140 μm aperture tube, 1/amp. = 2, 1/ap.current = 2, diameter cutoff ≅ 7.7 μm), as explained in Appendix A.2.

2.4.2.2 Comparing the effects of dexrazoxane on the growth curves and proliferation rate in CHO, DZR, and rat heart fibroblast cells

As determined in the previous section, inhibition of CHO cell proliferation was achieved with minimal immediate effect on viability when a dexrazoxane drugging protocol of twice or daily exposure at 100 μM was combined with media replacement (Section 2.4.3.1). The growth curves and proliferation rates of these cell lines exposed under such conditions were examined. In particular, the growth of CHO cells exposed to dexrazoxane was directly compared to DZR cells, a dexrazoxane-resistant cell line, as well as to a mortal isolated primary fibroblast cell line from the heart tissue of neonatal rats. Furthermore, the growth potential of adherent vs. suspension CHO cells cultures exposed to dexrazoxane was additionally contrasted in light of the context of future experiments. Finally where applicable, proliferation rates and percent viability of cultures were examined.

2.4.2.2.1 Growth and exposure of adherent CHO cells to dexrazoxane

CHO cells in exponential growth were harvested and seeded onto 42 individual 35x10 mm tissue culture plates at $1.1x10^5$ cells/plate, and brought to 3.4 mL with α-MEM/FCS. This was followed by a 24 hr incubation period at 5% (v/v) CO_2 and 37°C to allow for cell attachment. To 24 of the 42 individual plates was added 0.1 mL of a requisite stock drug solution to produce a final dexrazoxane concentration of 100 μM, and to the other 18 plates was added 0.1 mL α-MEM/FCS (total volume 3.5 mL). Cells initially treated with 100 μM of dexrazoxane were subsequently exposed on a daily basis in a similar manner as before. Specifically, media was gently aspirated off these plates

followed by the addition of 3.5 mL of relatively fresh media (30:70 conditioned to fresh α-MEM/FCS), containing 100 μM dexrazoxane. At each indicated time interval of growth 2 replicate plates respective of control and exposed cultures were harvested with trypsin-EDTA followed by quenching to volumes of 3 mL/plate with α-MEM/FCS, as outlined previously (Section 2.2.2). Cell densities, and then total number of cells per plate in the 3 mL volume were determined from removed sample aliquots on a model Z_f Coulter counter using a threshold setting of 7 (140 μm aperture tube, 1/amp. = 2, 1/ap.current = 2, diameter cutoff ≅ 7.7 μm), as explained in Appendix A.2.

2.4.2.2.2 Growth and exposure of suspension CHO and DZR cells to dexrazoxane

Exponentially growing adherent CHO and DZR cultures were harvested from T-flasks and seeded to inital concentrations of $0.25x10^5$ cells/mL into double sidearm suspension culture spinner flasks. Upon reaching a state of exponential growth in suspension culture, CHO cells were diluted to starting densities of $0.25x10^5$ cells/mL and $2.25x10^5$ cells/mL in control and dexrazoxane exposed spinner flasks, respectively. Similarly, DZR cells were diluted to a starting density of $0.25x10^5$ cells/mL. This was followed by the addition of 1-10 mL of requisite stock drug solutions to designated flasks in order to produce a final dexrazoxane concentration of 100 μM (total volume 50-300 mL). On a daily basis following removal of the required number of cells for analysis, the remaining dexrazoxane-treated CHO or DZR cells were aseptically combined separately, centrifuged at 250 *g* for 12 min in 50 mL sterile conical tubes, and resuspended in an appropriate volume of ~80% fresh α-MEM/FCS in an attempt to maintain cell densities approximately equivalent to that of before centrifugation. In some cases, where indicated

this was followed by the subsequent re-addition of dexrazoxane administered to the same concentration of 100 μM, and in the same fashion as before. CHO cells were exposed to dexrazoxane either at 0, 24 hr or daily, whereas DZR cells were exposed only at 0, 24 hr.

Depletion of nutrients in cultures were followed indirectly by monitoring the change in glucose levels with the use of a glucometer, as described in Section 2.2.2. Media was consequently replaced in control CHO cultures to approximately equivalent cell densities after 36 and 60 hr of growth when the glucose level had diminished to half of its initial value. In a similar manner, media was replaced in dexrazoxane-treated DZR cultures at 24, 62, and 85 hr of growth.

At indicated time intervals 1-2 mL aliquots were aseptically removed from each culture using a sterile Pasteur pipet. Cell viability was assessed as explained earlier in Section 2.2.2. Cell densities were determined by counting on a model Z_f Coulter counter with a threshold setting of 7 (140 μm aperture tube, 1/amp. = 2, 1/ap.current = 2, diameter cutoff ≅ 7.7 μm), as explained in Appendix A.2. The validity of these densities were assessed in a separate trial by comparing to cell counts determined in a hemacytometer chamber. Final growth curves were corrected for slight changes in cell density with media replacement so as to maintain continuity. In brief, this normalization was achieved by multiplying in series by a differing numerical factor (+/-) in which the cell density changed from its determination after centrifugation and resuspension to the following 24 hr interval, as explained later in Section 3.2.2.2.1.

2.4.2.2.3 Growth and exposure of adherent rat heart fibroblast cells to dexrazoxane

Due to their limited lifespan, neonatal rat heart fibroblast cells were allowed to reach exponential growth 5 days after their initial isolation. At this time cells were harvested with trypsin-EDTA and seeded onto 35x10 mm tissue culture plates at $2.5x10^4$ cells/plate for 24 control plates and at $7.5x10^4$ cells/plate for 24 dexrazoxane treated plates, all brought to 3.4 mL with DMEM/F-12/FCS. This was followed by a 48 hr incubation period at 5% (v/v) CO_2 and 37°C to allow for cell attachment. To 24 of the 48 individual plates was added 0.1 mL of a requisite stock drug solution to produce a final dexrazoxane concentration of 100 μM, and to the other 24 plates was added 0.1 mL DMEM/F-12/FCS (total volume 3.5 mL). Cells initially treated with 100 μM of dexrazoxane were subsequently exposed on a daily basis with media replacement in an identical manner with respect to adherent CHO cells (Section 2.4.2.2.1). In addition, media alone was replaced daily in all control unexposed plates. At each indicated time interval of growth 2 replicate plates respective of control and exposed cultures were harvested with trypsin-EDTA followed by quenching to volumes of 3 mL/plate with DMEM/F-12/FCS, as outlined previously (Section 2.2.2). Cell densities, and then total number of cells per plate in the 3 mL volume were determined from removed sample aliquots on a model Z_f Coulter counter using a threshold setting of 7 (100 μm aperture tube, 1/amp. = 2, 1/ap.current = 8, diameter cutoff ≅ 8.7 μm), as explained in Appendix A.2. Viability was assessed as explained in Section 2.2.2 after a brief centrifugation at 250 *g* for 5 min in order to obtain quantifiable cell densities.

2.4.2.2.4 Determination of growth rates and doubling times of cultured cells

In most control unexposed cultures it is a common occurrence to observe a decline in growth ability beyond a point of confluence. In the case of suspension cells this begins to occur at maximum cell densities above 1 x 10^6 cells/mL. As explained later in further detail (Section 3.2.2.2.2) the following single exponential rise equation was used in SigmaPlot (Jandel Corp., San Rafael, CA, U.S.A.) to empirically calculate the growth rate and doubling time of the above mentioned cell cultures when conditions of exponential growth were evident.

$C_t = C_o e^{\kappa t}$

where, C_t = the cell density at time t (cells/mL)
C_o = the starting initial seeded cell density (cells/mL)
e = the base of the natural logarithm
κ = the growth rate constant (hr^{-1})
t = the time at which C_t is determined

2.4.3 Results

2.4.3.1 CHO cell growth after exposure to different dexrazoxane drugging regimens

Initial experiments investigating the effects of various exposures of dexrazoxane on CHO cell growth are demonstrated in Fig. 2.4. Single, daily, or intermittent exposure of cells to either 20, or 100 μM of dexrazoxane was able to immediately inhibit further cell growth, irrespective of the number of dosages and/or the frequency with which media was replaced (Fig. 2.4b, c). These cells were noticably larger in size after 96 hr of exposure. Exposure of cells to 5 μM of dexrazoxane did not produce an immediate inhibition of cell growth in any of the drugging regimens examined (Fig. 2.4a). After 96 hr of daily

exposure to 5 μM dexrazoxane cell numbers appeared to no longer increase, as compared to the single or intermittment 5 μM drugging regimens.

Deprivation of glucose content levels in all treated cultures were monitored as displayed in Fig. 2.5. At indicated intervals when media was replaced the new glucose level of 6.1 mmol/L was not shown for the purpose of clarity and continuity in these plots. The increase in glucose level from 48-72 hr in cultures having media replaced only at 48 hr is reflective of this trend and should not be taken in context of an actual increase of culture media glucose level. Cultures treated with either 20, or 100 μM dexrazoxane revealed similar decreasing trends in glucose content when comparing the individual drugging protocols (Fig. 2.5b and c). As cells gradually became larger in these cultures daily media replacement was able to sustain the continued depletion of glucose and other nutrients as the energy demands in these non-dividing cells remained. Glucose content levels decreased slightly faster in 5 μM dexrazoxane-treated cultures due to continued exponential cell growth. Overall, these results suggest that 100 μM of dexrazoxane combined with daily media replacement will best inhibit CHO cell division while maintaining a consistent level of essential nutrients. Concentrations of dexrazoxane as such, shown above and previously [29] to be slightly cytotoxic are likely capable of sufficiently inhibiting the catalytic activity of topoisomerase II in the majority of the cell population [16] thus producing an immediate inhibition of cell division.

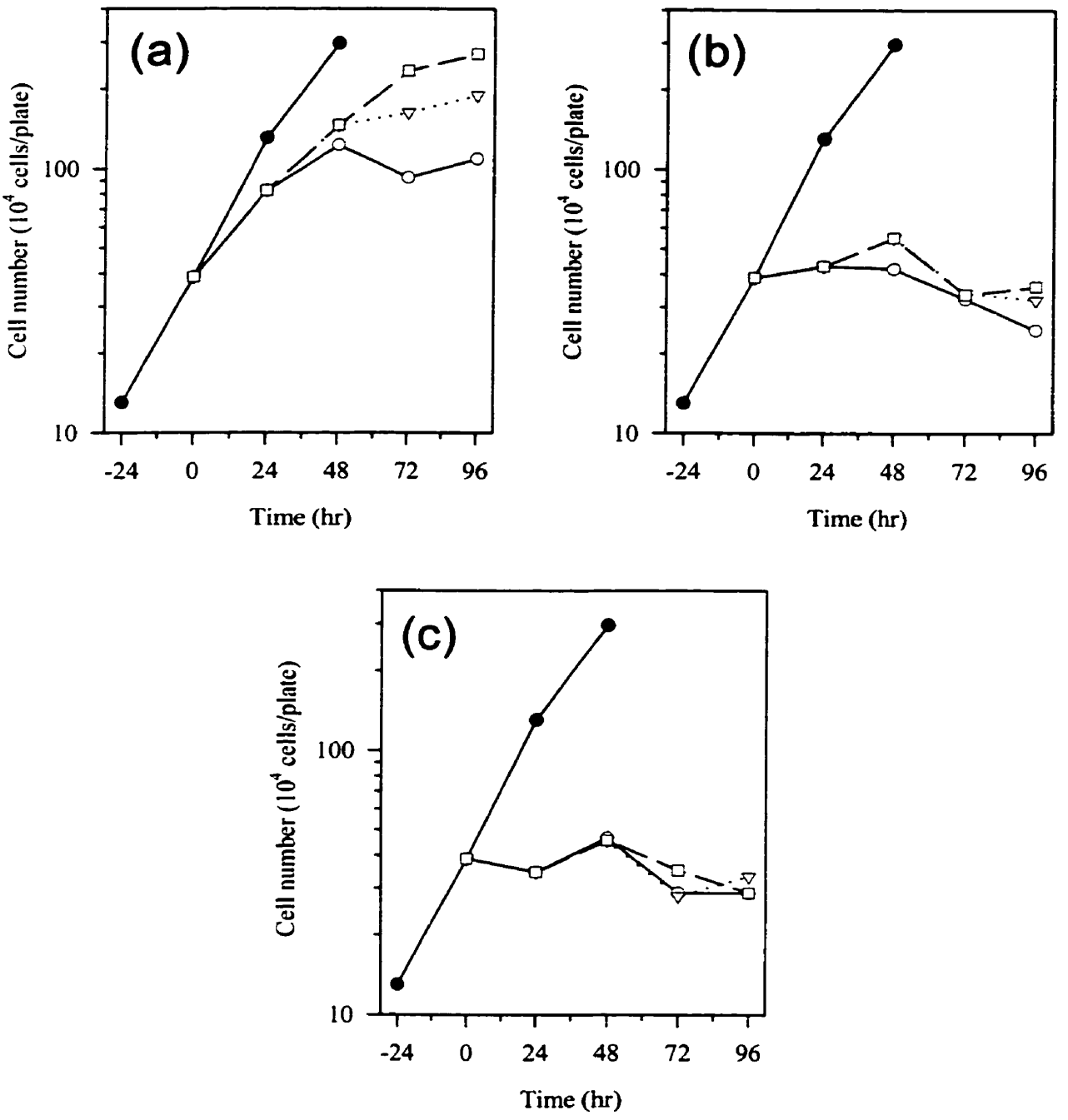

Fig. 2.4. The effects of different dexrazoxane concentrations and drugging protocols on CHO cell growth. CHO cells were seeded onto 35x10 mm plates at initial concentrations of $1.3x10^5$ cells/plate and treated the following day with (a) 5, (b) 20, or (c) 100 μM dexrazoxane. Cells were either treated with dexrazoxane daily with media replacement (○); every other day (at 0, 48 hr) with media replacement at these times (▽); or at only 0 hr with media replacement at 48 hr (□) all alongside non-treated control cells that were allowed to grow without any media replacement (●). At indicated times, the total number of cells were determined from duplicate trypsinized plates with the use of a Coulter counter (threshold of 7, 140 μm aperture, diameter cutoff ≅ 7.7 μm) for each concentration of dexrazoxane.

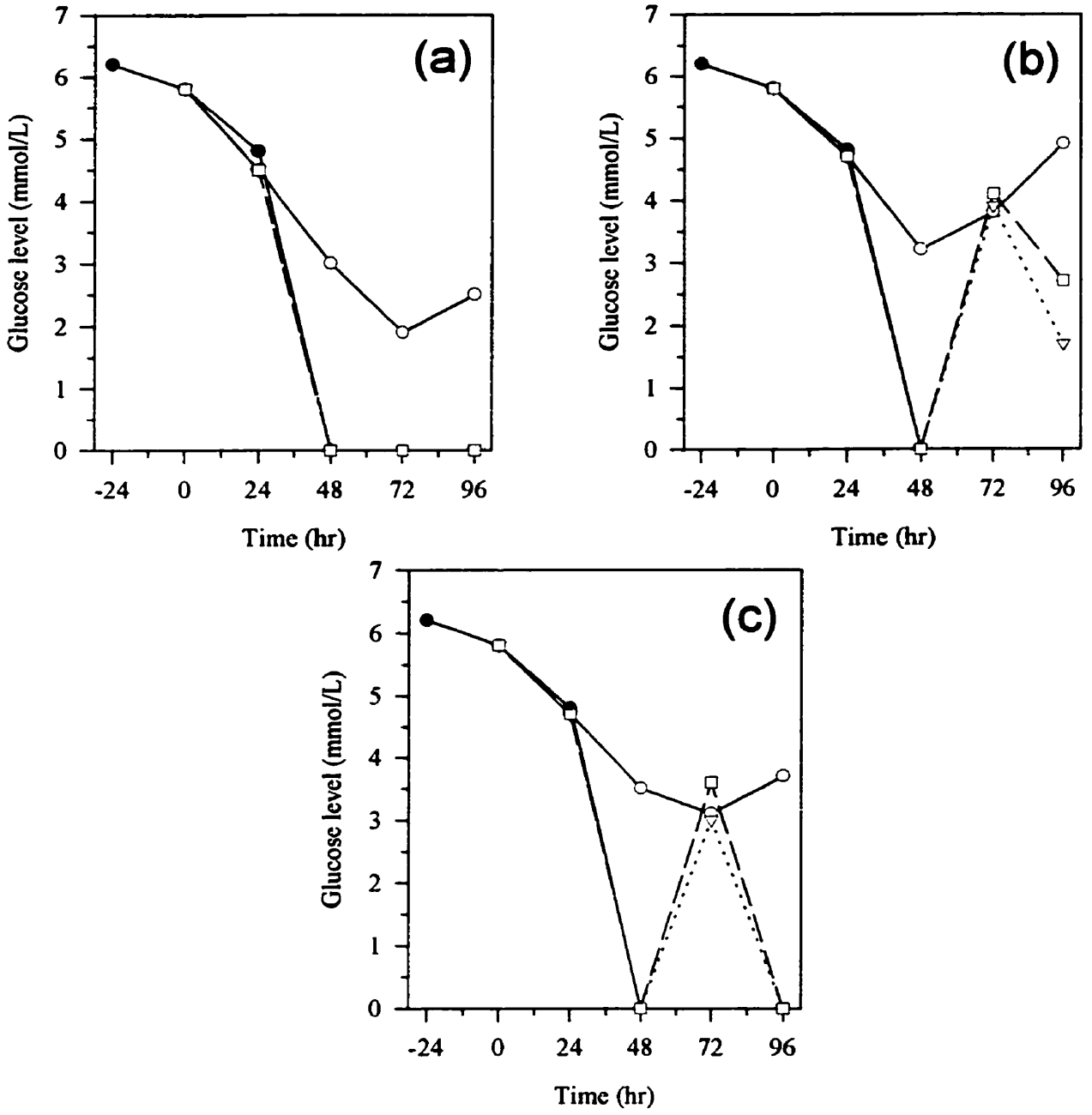

Fig. 2.5. The effects of different dexrazoxane concentrations and drugging protocols on the deprivation of glucose in CHO cell cultures. CHO cells seeded onto 35x10 mm plates at concentrations of $1.3x10^5$ cells/plate were treated the following day with (a) 5, (b) 20, or (c) 100 μM dexrazoxane. Treatment was either daily with media replacement (○); every other day (at 0, 48 hr) with media replacement at these times (▽); or at 0 hr with media replacement at 48 hr (□) all alongside untreated control cells (●). At indicated times glucose content level in the culture media was determined with the use of a glucometer for each concentration of dexrazoxane. Readings below 1.1 mmol/L were unmeasurable and consequently assigned an arbitrary value of 0 mmol/L for plotting purposes. Data represented here is not normalized to media replenished starting glucose levels of 6.1 mmol/L, so as to maintain a continuous linear trend.

2.4.3.2 Growth curves of CHO, DZR, and rat heart fibroblast cells exposed twice or daily to dexrazoxane

An analysis of the growth of CHO, DZR, and neonatal rat heart fibroblast cells in the presence of dexrazoxane essentially forms the basis of all other investigations performed in the remainder of this chapter. In all cases, the conditions of dexrazoxane treatment involved a dual (0, 24 hr) or daily exposure to 100 μM dexrazoxane with daily media replacement. It was presumed that a drug exposure for at least twice the cell cycle time (Table 2.2) would be sufficient to adequately inhibit topoisomerase II within all cells of the population. In addition, an administration of 100 μM dexrazoxane ensured that the unhydrolyzed topoisomerase II-inhibitory form would remain in media for an extended period of time, given its previously demonstrated half-life of 9.3 hr [30]. The daily replacement of media replenished essential nutrients and removed growth inhibitory metabolic products so as to allow for continued survival and/or growth and development.

CHO cells were grown as either adherent or suspension cultures (Fig. 2.6 and 2.7a). The proliferation rate of control cells in suspension was determined to be approximately 16 hr, slightly slower than that estimated for cells grown as adherent cultures, 14 hr (Table 2.2). Although such a marginal discrepancy can be attributed to any number of factors inherent with growth in a suspension spinner flask the fact remains that normal cell growth under either condition was exponential in nature. Cells exposed to dexrazoxane, whether in suspension or as an attached culture behaved in relatively the same manner. In both cases daily exposure to dexrazoxane resulted in a complete immediate inhibition of cell division complemented by a noticable increase in cell size and a gradual decrease of cell numbers. Cell division was inhibited in either drugging regimen in suspension culture of

dual (0, 24 hr) or daily dexrazoxane exposure (Fig. 2.7a), accompanied by comparable gradual decreases in cell number. In addition, cell viability diminished in a similar manner to a level of 82% after 120 hr of growth upon dual or daily exposure (Fig. 2.7b). These results suggest that although CHO cell division is efficiently inhibited upon two exposures (0, 24 hr), a daily exposure protocol does not appear to accelerate a decrease in cell number or viability.

In an effort to attribute the sustained inhibition of CHO cell growth and observable enlargement of cell sizes to the inhibition of topoisomerase II, the growth of DZR cells in the presence of dexrazoxane was examined. Previously it was demonstrated that although DZR cells possess one-half the level of topoisomerase II protein compared to parental CHO cells, their acquired resistance is attributable to an altered target site within the topoisomerase II enzyme, caused by a point mutation [22,23]. As shown in Fig. 2.7a when DZR cells were grown in suspension in a similar manner to CHO cells and exposed twice (0, 24 hr) to dexrazoxane exponential cell growth continued, unaltered. The doubling rate of dexrazoxane exposed DZR cells was found to be 17 hr (Table 2.2), and compared identically to previously reported values of untreated DZR cells [22]. Furthermore, after 72 hr of exposure cells appeared morphologically identical to untreated cells, and viability was still nearly 100% (Fig. 2.7b).

The effects of dexrazoxane on the proliferation of primary heart fibroblast cells is displayed in Fig. 2.8a. These cells, previously isolated from neonatal rats were chosen for investigation due to their mortal limited existence. It has been well established that similar normal, diploid cell lines derived from a variety of tissue types display limited proliferative life spans [31]. Control untreated heart fibroblast cells were shown to attain a level of

exponential growth (Fig. 2.8a), with an approximate doubling time of 67 hr (Table 2.2). Daily exposure of heart fibroblast cells to dexrazoxane resulted in a complete inhibition of cell division which was not complemented by any noticable decrease in total cell number. Although cell viability did decrease in treated cultures with time (Fig. 2.8b), an identical trend was observed in control cultures. This raises the possibility that other factors besides dexrazoxane-induced topoisomerase II inhibition may be acting synergistically to cause a decrease in cell viability to between 80-90% after extended periods of growth. One suggestion is that perhaps these cells were not capable of sustaining a healthy state of growth outside of their natural environment *in vivo*.

Table 2.2. Growth rates and doubling times of cells exposed to dexrazoxane for various periods of time.

Duration of dexrazoxane exposure	κ (hr^{-1})	S.E.	C.V. (%)	t (hr)
Unexposed control adherent CHO cells	4.90E-02	2.55E-03	5.2	14
Unexposed control suspension CHO cells	4.22E-02	1.51E-03	3.6	16
Suspension DZR cells exposed at 0, 24 hr with media replaced at 24, 62, 85 hr	4.01E-02	1.91E-03	4.8	17
Unexposed control adherent neonatal rat heart fibroblast cells	1.03E-02	3.51E-04	3.4	68

NOTE: Determinations were made using cell concentrations which fell below confluence, still in exponential growth.

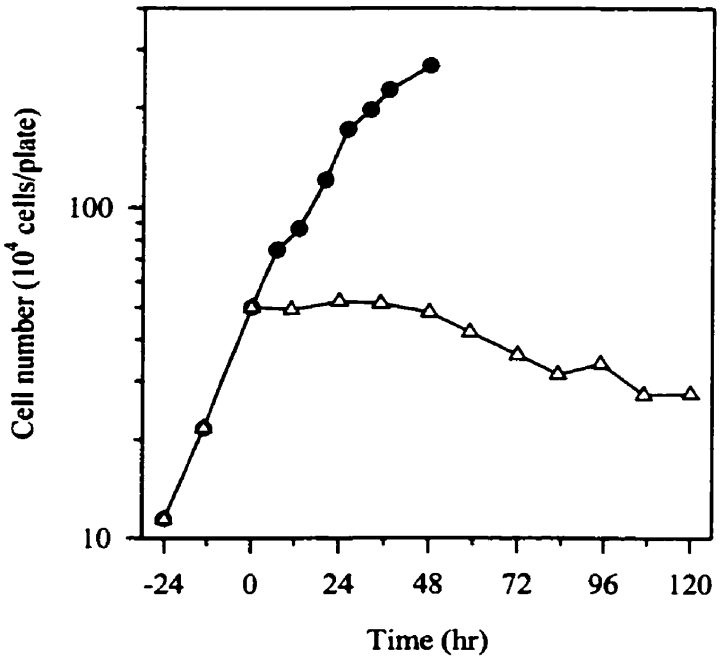

Fig. 2.6. Effects of dexrazoxane on the growth of adherent CHO cells. Following a 24 hr attachment period after seeding onto 35x10 mm plates at $1.1x10^5$ cells/plate cells were either exposed to 100 μM dexrazoxane daily with media replacement (●), or left untreated (Δ). In addition, at indicated time intervals plates were harvested in duplicate and cell densities were determined with the use of a Coulter counter (threshold of 7, 140 μm aperture, diameter cutoff ≅ 7.7 μm). Viability of cells was not assessed in this experiment.

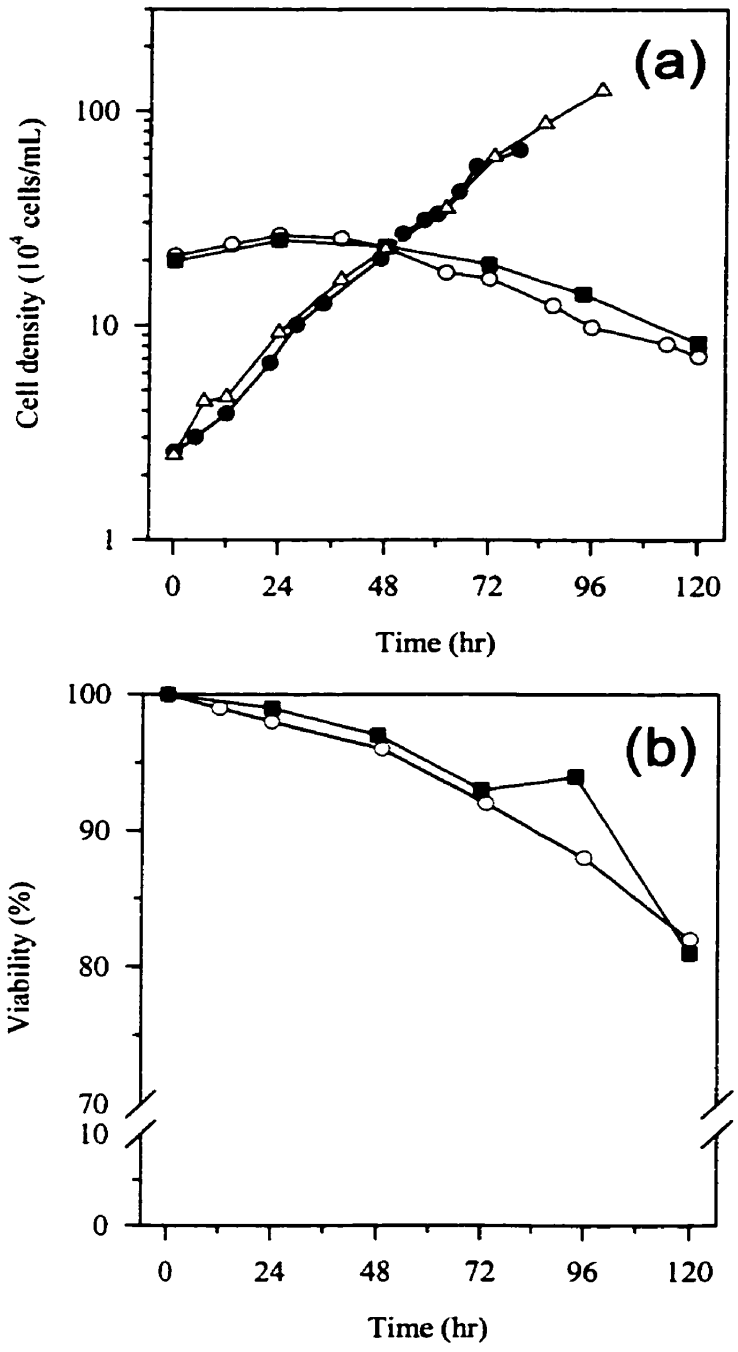

Fig. 2.7. Effects of dexrazoxane on the growth of suspension CHO and DZR cells. CHO cells were seeded at 2.25×10^5 cells/mL and treated with 100 μM dexrazoxane daily with media replacement (○), or at 0, 24 hr with media replacement daily (■). Control CHO cells were seeded at 0.25×10^5 cells/mL with media replacement at 36, 60 hr (●). DZR cells were seeded at 0.25×10^5 cells/mL and treated with 100 μM dexrazoxane at 0, 24 hr with media replacement at 24, 62, 85 hr when glucose levels had decreased by half (Δ). At indicated times (a) cell densities were determined on a Coulter counter (threshold of 7, 140 μm aperture, diameter cutoff ≅ 7.7 μm) followed by normalization; and (b) viability was assessed using a trypan blue dye exclusion analysis.

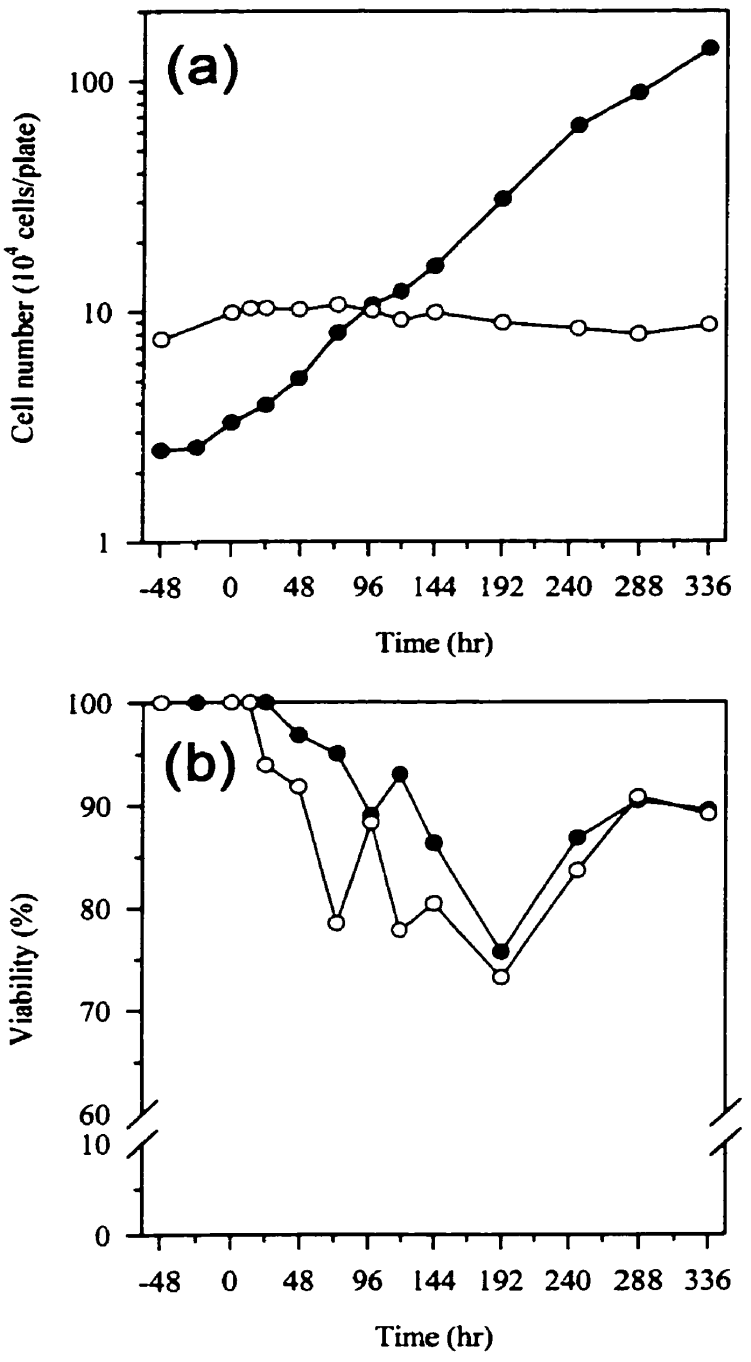

Fig. 2.8. Effects of dexrazoxane on the growth of attached neonatal rat heart fibroblast cells. Heart fibroblast cells were seeded onto 35x10 mm plates at $2.5x10^4$ cells/plate for control cells (●) and at $7.5x10^4$ cells/plate for dexrazoxane exposed cells (○). Cells were exposed to 100 μM dexrazoxane 49 hr after seeding and at every 24 hr interval thereafter with media replacement. In addition, media alone was replaced daily in all control unexposed plates. At indicated time intervals, plates were harvested in duplicate and (a) cell densities and then total cell number were determined with the use of a Coulter counter (threshold of 7, 100 μm aperture, diameter cutoff ≅ 8.7 μm); and (b) viability was assessed using a trypan blue dye exclusion analysis.

2.5 Morphology and morphometry analysis of dexrazoxane-treated cells

2.5.1 Introduction

The number of cells and their sizes are the fundamental basic elements which help to define the growth of an organism, its organs, and/or a cell population. The determination of cell number and size assists in the analysis of pathological changes which may be occurring within the original cell population. Changes in mean cellular volume and diameter of a population may be a consequential result of depressed or enhanced growth characteristics after drug or reagent administration. Essentially, cell sizing data can play a vital role in many single or multiparameter systems in which different cellular features including cell volume, DNA content, or even immunological surface features can be determined simultaneously [32].

In the following section, the profile-size distributions of various cell types including CHO, DZR, and heart fibroblast cells were followed by one of two methods after exposure to dexrazoxane. In the first method cells were sized electrically in a flowing system through a Coulter counter. As explained in further detail in Appendix A, cells suspended in an electrolyte solution were counted at a rate of a few thousand cells per second through a range of set threshold volume-class divisions until the entire profile had been accounted for. The second method used to generate profile-size distributions was based on principles of stereology. The two-dimensional profile area of cells were determined from photographic images in an attempt to empirically calculate their respective individual, and mean profile volume and diameter values. And finally, the

morphology of dexrazoxane-treated cells was initially examined from these photographic images as a prelude to further investigation.

2.5.2 Materials

Isoton II Coulter balanced electrolyte solution (cat. No. PN 8546719) was obtained from Beckman Coulter Inc. (Burlington, ON).

2.5.3 Methods

2.5.3.1 Drug treatment

CHO and DZR cells were grown as suspension cultures in double sidearm suspension spinner flasks seeded initially at 2.25×10^5 cells/mL and 0.25×10^5 cells/mL respectively. Both cell types were seeded from control suspension cultures, and treated with 100 μM dexrazoxane at 0, 24 hr as described explicitly in Section 2.4.2.2.2. Media was replaced daily in dexrazoxane-treated CHO cell cultures, and at 24, 62, and 85 hr in dexrazoxane-treated DZR cell cultures. Cells were aseptically removed, centrifuged at 250 *g* for 12 min, and resuspended in an appropriate volume of ~80% fresh α-MEM/FCS in an attempt to maintain cell densities approximately equivalent to that of before centrifugation. Cell densities were determined by counting on a model Z_f Coulter counter with a 140 μm aperture, threshold setting of 7 (1/amp = 2, 1/ap.current = 2, diameter cutoff ≅ 7.7 μm).

Neonatal rat heart fibroblast cells in exponential growth were harvested with trypsin-EDTA and seeded onto 35x10 mm tissue culture plates, as described in Section 2.4.2.2.3. Control plates were seeded at $2.5x10^4$ cells/plate followed by daily replacement of media with ~80% fresh DMEM/F-12/FCS. All other plates were seeded at $7.5x10^4$ cells/plate and exposed daily to 100 μM dexrazoxane with media replacement. At each indicated period of growth 2 replicate plates, respective of control and exposed cultures were harvested with trypsin-EDTA followed by quenching to volumes of 3 mL/plate with DMEM/F-12/FCS. Cell densities were determined by counting on a model Z_f Coulter counter with a 100 μm aperture, threshold setting of 7 (1/amp = 2, 1/ap.current = 8, diameter cutoff ≅ 8.7 μm).

2.5.3.2 Cell sizing and quantitation by use of a Coulter counter

The first method utlized to follow changes in cell size distributions after dexrazoxane exposure was by collecting and analyzing cell number data from a model Z_f Coulter counter using a 140 μm aperture tube, as explained in detail in Appendix A.4. In brief, approximately $1x10^7$ cells were removed at each specified time interval of dexrazoxane exposure and diluted 3:50 mL as needed in a 50 mL glass beaker with Isoton II balanced electrolyte solution. Each dilution mixture was counted through a span of threshold volume-class divisions from 0-100, increasing by 4 divisions with each counting determination. Counting was performed in replicate (x2) through a series of different amperage and aperture current settings, chosen so as to cover the entire cell size distribution profile. Subsequently, the number of cells falling within set threshold ranges was determined, followed by the normalization of cell counts to a single amperage and

aperture current setting so as to account for the various volume intervals used (see Appendix A.4.2.3). Finally, these cell counts were expressed as a function of cell volume and/or diameter in the form of frequency distribution histograms. Estimations of mean cell volume (MCV) and mean cell diameter (MCD) were made only for those distributions which appeared Gaussian-like (see Appendix A.4.2.4).

For reasons of clarity, cell counts of distribution peaks were subsequently normalized to the undrugged control. In the case of 12 and 24 hr derazoxane-treated CHO cells, and dexrazoxane-treated DZR cells the peak height of these profile distributions were normmalized to the equivalent peak height of the control distribution. Profiles of 48-120 hr dexrazoxane-treated CHO cells were normalized such that cell counts became half that of the corresponding peak volume interval in the control profile.

2.5.3.3 Cell sizing and morphology analysis from photographic images

The second method used to obtain profile-size distributions of dexrazoxane-treated cell populations was accomplished by estimating the two-dimensional profile area of cells from photographic images. The following method of sizing analysis was based in part on techniques used to quantitate megakaryocyte size and number using the principles of stereology, a branch of morphometry [33]. The stereological basis of this method allowed for the estimation of three-dimensional structural parameters from measurements made on two-dimensional images using computer software. It was believed that unlike the Coulter counter sizing method, complete Gaussian-like size distributions could be obtained by this method of analysis, thus allowing for the estimation of such fundamental parameters as mean cell volume (MCV) and mean cell diameter (MCD).

After indicated periods of dexrazoxane exposure 1 mL aliquots were aseptically removed directly from suspension cultures, or upon trypsinization in the case of adherent cultures. Samples were then diluted 1:1 with 0.6% (w/v) trypan blue dye and concomitant with the assessment of cell viability and morphology photographic images were taken under a 10X or 40X objective lens using a Nikon camera with Kodak 400 colour film. Once developed these pictures were then photocopied and individual cells were coloured in with a fine black magic marker. The necessity for filling in cell images was due to the operational constraints of the computer software program SigmaScan (Jandel Corp., San Rafael, CA, U.S.A.) used to determine their two-dimensional profile area. Structural parameters could not be adequately determined over the entire surface area of individual two-dimensional cells if the brightness/contrast inside the cells were at all similar to their surroundings.

All blackened, photocopied cell images were then scanned using a Hewlett Packard ScanJet 5p and saved as bitmap images. Using SigmaScan, a 2-point calibration of a known 50 μm distance was performed from a scanned image of a hemacytometer chamber grid, photographed under the same magnification as cells. Next, each bitmap image respective for a particular duration of dexrazoxane exposure was opened in turn within SigmaScan. The profile area of between 250-500 cells in units of μm^2 was then determined empirically upon their manual selection and placed automatically into a worksheet column. Assuming a spherical model for all analyzed cells, cell profile diameter (d) and consequently cell profile volume (V) were then calculated from the measurements of profile area (A) using the following equations:

$A = \pi r^2$ where r = radius
$\therefore r = \sqrt{A/\pi}$
and since $d = 2r$
$\therefore d = 2\sqrt{A/\pi}$

$V = 4/3\ \pi r^3$ and once diameter (d) is known, then
$\therefore V = 4/3\ \pi\ (d/2)^3$

As shown in Table 2.3 for control CHO cells, all calculated measurements for each individual cell were sorted into numerical order. Next, using a volume-class size of 100 μm^3, the number of cells possessing volume determinations within each volume class was counted, i.e. 0-100, 100-200, 200-300 μm^3, etc. The value of the midpoint of a given class was used as the volume value for that class. Distributions were subsequently plotted as histograms of the number of cells per volume-class size of 100 μm^3 after normalization to 500 total cells counted. Overall, the number of size classes ranged from 100-70000 μm^3. Mean cell volume (MCV) and diameter (MCD) were calculated simply by averaging together all of the collected profile data before sorting into volume-class divisions (see Table 2.3).

Table 2.3. Morphometric sizing of control CHO cells from 2-D photographic images.

Area of 2-D Cells	Sorted Area (μm^2)	Sorted Diameter (μm)	Sorted Volume (μm^3)	Volume Class (μm^3)	Plotted Volume Class Midpoint (μm^3)	Equivalent Plotted Diameter Midpoint (μm)	#cells Within Each Volume Class	Normalized to 500 total #cells
166.4	96.1	11.1	708.6	700	750	11.3	2	4
193.2	102.9	11.4	785.4	800	850	11.8	2	4
141.2	106.6	11.7	827.8	900	950	12.2	1	2
168.0	110.8	11.9	877.3	1000	1050	12.6	8	15
187.9	120.2	12.4	991.9	1100	1150	13.0	16	30
173.2	121.3	12.4	1004.9	1200	1250	13.4	16	30
200.0	121.8	12.5	1011.4	1300	1350	13.7	16	30
168.0	122.8	12.5	1024.5	1400	1450	14.0	20	38
130.7	124.9	12.6	1050.9	1500	1550	14.4	19	36
143.8	126.0	12.7	1064.2	1600	1650	14.7	25	47
172.7	126.5	12.7	1070.9	1700	1750	15.0	20	38
156.4	127.0	12.7	1077.5	1800	1850	15.2	27	51
144.4	127.6	12.7	1084.2	1900	1950	15.5	20	38
181.1	129.1	12.8	1104.4	2000	2050	15.8	20	38
200.5	129.7	12.9	1111.1	2100	2150	16.0	14	26
171.1	130.2	12.9	1117.9	2200	2250	16.3	16	30
194.8	130.7	12.9	1124.6	2300	2350	16.5	6	11
165.4	131.2	12.9	1131.4	2400	2450	16.7	6	11
150.1	131.2	12.9	1131.4	2500	2550	17.0	2	4
170.1	132.8	13.0	1151.8	2600	2650	17.2	2	4
202.6	132.8	13.0	1151.8	2700	2750	17.4	2	4
181.1	133.3	13.0	1158.7	2800	2850	17.6	1	2
208.9	133.3	13.0	1158.7	2900	2950	17.8	0	0
166.4	133.3	13.0	1158.7	3000	3050	18.0	1	2
190.0	133.9	13.1	1165.5	3100	3150	18.2	1	2
182.7	134.9	13.1	1179.3	3200	3250	18.4	1	2
'	'	'	'	3300	3350	18.6	0	0
'	'	'	'	3400	3450	18.8	0	0
'	'	'	'	3500	3550	18.9	0	0
'	'	'	'	3600	3650	19.1	0	0
110.8	227.8	17.0	2587.9	3700	3750	19.3	0	0
106.6	230.5	17.1	2632.7	3800	3850	19.4	0	0
161.7	232.6	17.2	2668.8	3900	3950	19.6	0	0
227.8	237.3	17.4	2750.5	4000	4050	19.8	0	0
169.6	239.4	17.5	2787.1	4100	4150	19.9	0	0
193.2	241.5	17.5	2823.9	4200	4250	20.1	0	0
168.0	252.0	17.9	3010.0	4300	4350	20.3	0	0
169.0	259.9	18.2	3152.2	4400	4450	20.4	0	0
137.5	264.1	18.3	3228.9	4500	4550	20.6	0	0
162.7	338.6	20.8	4688.6	4600	4650	20.7	1	2
	Mean:	**14.8 μm**	**1752.6 μm^3**			**Total #cells:**	**265**	**500**
	S.E.	**0.1**	**28.7**					

2.5.4 Results

After 120 hr of dexrazoxane exposure CHO cells were clearly larger in size and exhibited various shapes and morphologies (Fig. 2.9b) which differed from control cells (Fig. 2.9a). Such features were also prevalent in adherent dexrazoxane-treated CHO cells (see later, Fig. 2.24). The complexity and granular organization within these cells suggested that cell swelling might not exclusively account for their enlargement, and thus prompted further investigation. A 1500-fold dexrazoxane-resistant CHO derived cell line known as DZR [22] served as a negative control for these such effects. No observable changes in DZR size or morphology were seen after 96 hr of dexrazoxane exposure (Fig. 2.9c and 2.9d). Neonatal rat heart fibroblast cells were initially variable in shape and size within the control population (Fig. 2.9e). This was perhaps due to the heterogenity of the population, a direct result of their isolation from 2-day old neonatal rats. After 300 hr of dexrazoxane exposure some heart fibroblasts cells were found to appear slightly larger in size while others remained unchanged (Fig. 2.9f). This observation though was not specific to dexrazoxane-treated cells. Some control cells grown for the same duration of time were also slightly larger in size (data not shown) suggesting that these cells may simply be progressively adapting to *in vitro* culture conditions. Pignolo *et al.* [31] have attributed such a development of irregular morphologies and cell enlargement of fibroblast cells derived from normal rat tissue to be the result of an *in vitro* senescence or a functional decline.

In order to fully characterize any increase in size, particularly with respect to CHO cells, quantitation of cell sizes was carried out by one of two methods. Frequency size distribution histograms were generated either from collected electronic sizing data using a

Coulter counter or from morphometric analysis of two-dimensional photographic images. Analysis of CHO cells exposed to dexrazoxane at 0, 24 hr revealed by both procedures a progressive increase in maximum peak volumes as the distributions broadened (Fig. 2.10). After 48 hr of exposure, distribution profiles by Coulter counter analysis were no longer Gaussian-like and began to exhibit a decay-like pattern at low diameter values (Fig. 2.10a). As a result, mean cell volume and diameter quantitations could not be accurately resolved from such distributions. This is a common drawback of Coulter counter sizing analysis. As noted here and by others [34], Window Counts can become erroneous and exponentially increase logarithmically as cell size decreases, particularly within the range of 0-900 μm^3.

The largest recorded CHO cell size using a Coulter counter was 45000 μm^3 (a 44 μm diameter) after 120 hr of dexrazoxane exposure. This corresponded to a 31-fold increase in volume compared to the MCV of control CHO cells. In contrast, sizing analysis from photographic revealed the appearance of cells that were 73600 μm^3 in volume (or 52 μm in diameter) images after an identical length of dexrazoxane exposure. This corresponded to a 42-fold increase in volume compared to the MCV of control CHO cells. Sizing analysis of CHO cells by this second method produced profile distributions which greatly broadened over 120 hr (Fig. 2.10b), concomitant with a 9-fold increase in MCV (Table 2.4). Unlike during Coulter counter analysis, these profile distributions were Gaussian-like in nature and consequently accurate values of MCV and MCD were determined (Table 2.4). When plotted, a highly significant linear relationship ($p < 0.001$) was identified between the duration of dexrazoxane exposure and the increase in mean CHO cell volume (Fig. 2.13a).

In agreement with an unaltered cell morphologies, the size distribution profiles of dexrazoxane-treated DZR cells remained normal-like and unchanged from that of control distributions (Fig. 2.11). The mean cell volume of control DZR cells was found to be 1520 μm^3 by imaging sizing analysis and 1392 μm^3 by Coulter counter analysis (Table 2.4). By comparison, the corresponding mean cell diameter values were 14.1 μm and 13.9 μm, respectively. Although MCV values fluctuated slightly, no significant relationship was identified between MCV and the duration of dexrazoxane exposure (Fig. 2.13b)

The size distribution profile of heart fibroblast cells remained relatively unchanged between 48 hr and 300 hr of dexrazoxane exposure (Fig. 2.12). As compared to control heart fibroblast cells the size distribution profile of dexrazoxane-treated cells appeared to shift only slightly to higher values with some initial unpronounced broadening. The largest recorded heart fibroblast cell size after 300 hr of dexrazoxane exposure was 22400 μm^3 (a 35 μm diameter), which corresponded to a 20-fold increase in volume compared to the MCV of control cells. Although a few larger cells were identified, overall the MCV increased by only 1.8-fold after 300 hr of exposure (Table 2.4). In addition, when MCV was plotted versus duration of dexrazoxane exposure the apparent increasing trend was deemed non-significant by statistical linear regression analysis (Fig. 2.13c).

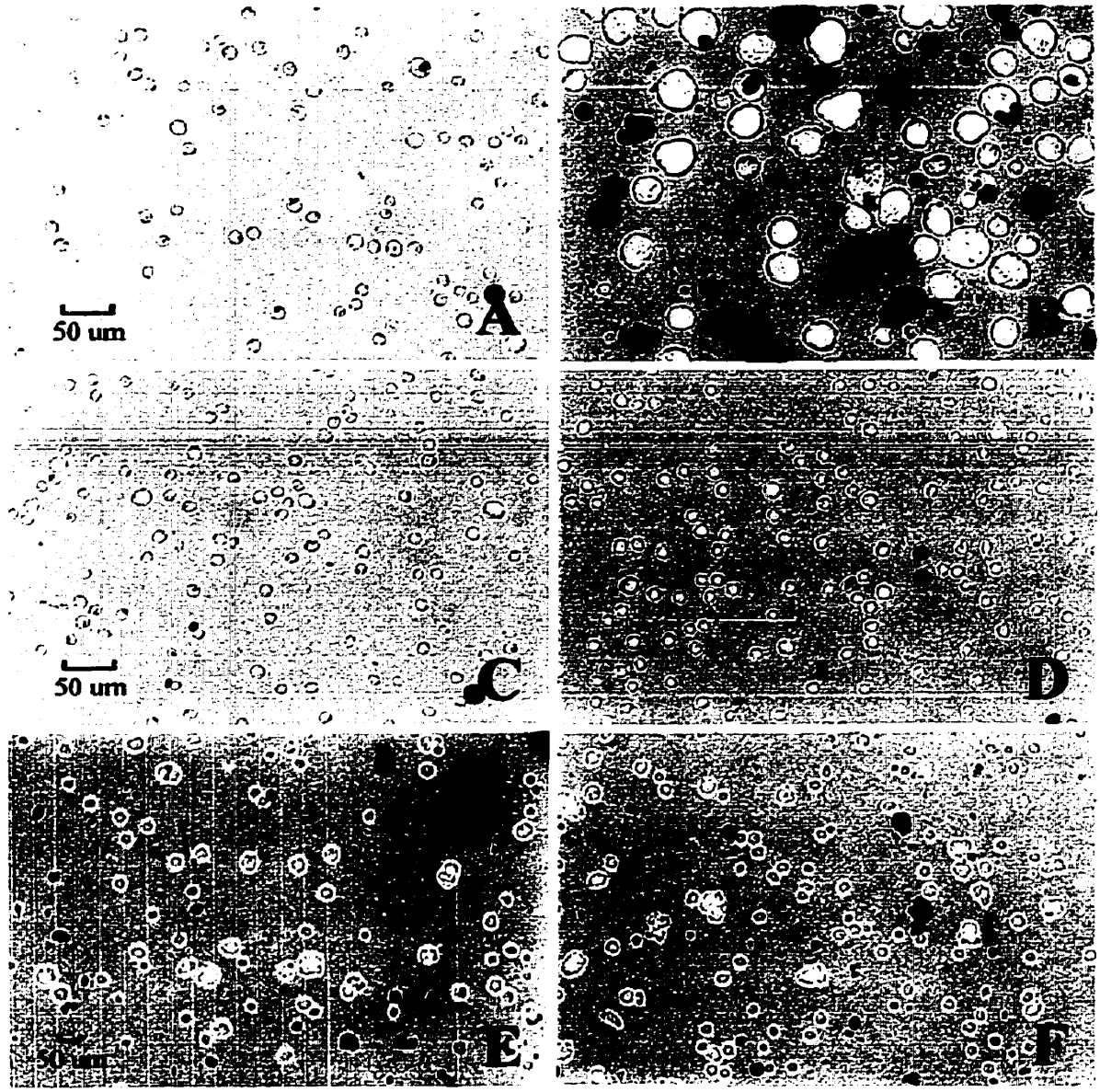

Fig. 2.9. Bright-field photomicrographs of dexrazoxane-treated cells in suspension stained with trypan blue dye. Cells were photographed after staining with 0.6% (w/v) trypan blue under a 40X (CHO and DZR), or a 10X objective lens (heart fibroblasts). CHO and DZR cells were grown as suspension cultures, treated with 100 μM dexrazoxane at 0, 24 hr with daily media replacement. Heart fibroblast cells were grown as attached cultures treated with 100 μM dexrazoxane daily with media replacement. (A) Control CHO cells. (B) CHO cells after 120 hr of dexrazoxane exposure were significantly larger in size, exhibiting differing morphologies. (C) Control DZR cells. (D) DZR cells exposed to dexrazoxane for 96 hr exhibited no observable changes in cell size or shape. (E) Control heart fibroblast cells were initially variable in size and shape. (F) After 300 hr of dexrazoxane exposure these features became only slightly more accentuated. Bar scale (50 μm) in left panels is the same for each pair of photographs.

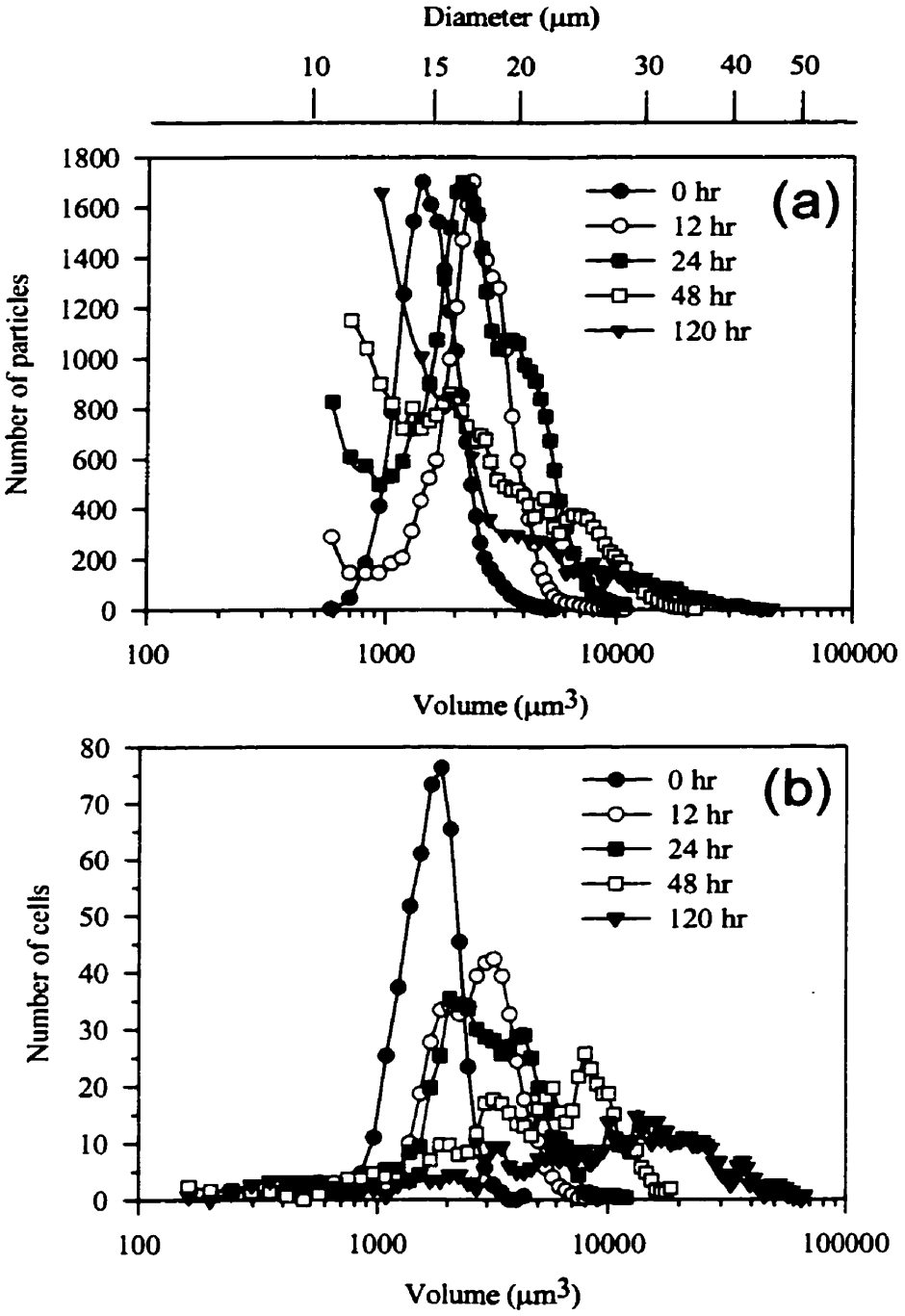

Fig. 2.10. Size distribution histograms of dexrazoxane-treated CHO cells. CHO cells were grown as a suspension culture at 2.25×10^5 cells/mL and exposed to 100 μM dexrazoxane at 0, 24 hr with daily media replacement. (a) Electronic Coulter counter sizing using a 140 μm aperture tube. For clarity peak cell counts were normalized to the undrugged control. (b) Morphometry analysis of 2-D cell images. Counted cells were distributed into classes of volume (100 μm^3 in size) followed by normalization to 500 cells total. Distributions are expressed relative to volume measurements on a logarithmic scale (*bottom x-axis*) with approximate corresponding diameter values on a non-linear scale (*top x-axis*). The data obtained at 72, and 96 hr were not plotted for clarity.

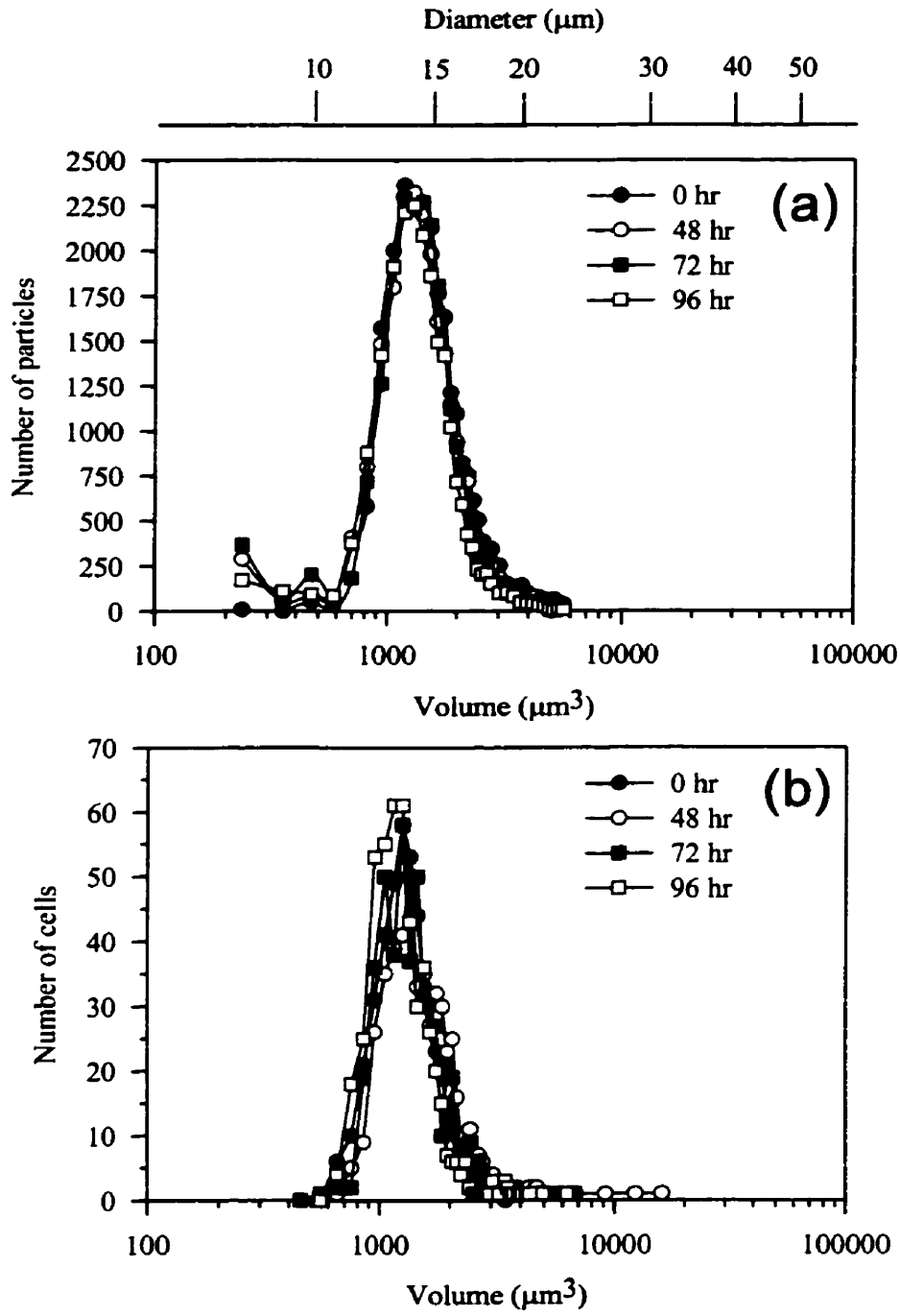

Fig. 2.11. Size distribution histograms of dexrazoxane-treated DZR cells. DZR cells were grown as a suspension culture seeded at 0.25×10^5 cells/mL and exposed to 100 μM dexrazoxane at 0, 24 hr with daily media replacement. (a) Electronic Coulter counter sizing using a 140 μm aperture tube. For clarity peak cell counts were normalized to the undrugged control. (b) Morphometry analysis of 2-D cell images. Counted cells were distributed into classes of volume (100 μm^3 in size) followed by normalization to 500 cells total. Distributions are expressed relative to volume measurements on a logarithmic scale (*bottom x-axis*) with approximate corresponding diameter values on a non-linear scale (*top x-axis*). The data obtained at 12, and 24 hr were not plotted for clarity.

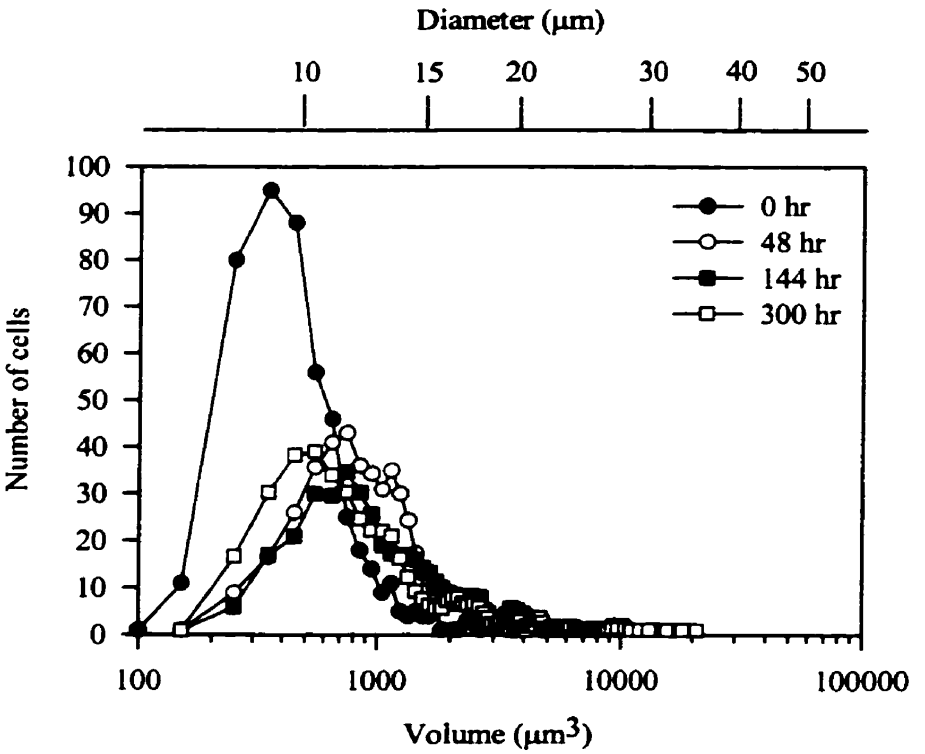

Fig. 2.12. Size distribution histogram of dexrazoxane-treated heart fibroblast cells. Isolated neonatal rat heart fibroblast cells were grown in DMEM/F-12/FCS on 35x10 mm tissue culture plates, seeded at $7.5x10^4$ cells/plate. Cells were exposed to 100 μM dexrazoxane daily, with media replacement. Frequency size distributions were generated by morphometry analysis of 2-D cell images upon harvesting. Counted cells were distributed into classes of volume (100 μm^3 in size) followed by normalization to 500 cells total. Distributions are expressed relative to volume measurements on a logarithmic scale (*bottom x-axis*) with approximate corresponding diameter values on a non-linear scale (*top x-axis*). The data obtained at 24, 72, 96, 120, 196, 250 hr were not plotted for clarity.

Table 2.4. Mean cell volume (MCV) and diameter (MCD) of dexrazoxane-treated cells, as estimated by separate quantitation procedures.

		2-D morphometry analysis using Sigma Scan					Coulter counter analysis	
Cell Line	Length of exposure (hr)	MCV (μm^3)	S.E.	MCD (μm)	S.E.	Factor of MCV increase	MCV (μm^3)	MCD (μm)
CHO	0	1752.6	28.7	14.8	0.1	1.0	1465.2	14.1
	12	2809.7	54.9	17.1	0.1	1.6	-	-
	24	3364.2	77.5	18.1	0.1	1.9	-	-
	48	6317.4	212.5	21.9	0.3	3.6	-	-
	72	9193.9	383.8	23.9	0.4	5.2	-	-
	96	12323.1	479.0	26.3	0.4	7.0	-	-
	120	15845.3	762.3	28.7	0.5	9.0	-	-
DZR	0	1520.0	20.9	14.1	0.1	1.0	1392.2	13.9
	12	1705.6	41.8	14.6	0.1	1.1	-	-
	24	1356.9	24.3	13.5	0.1	0.9	-	-
	48	1729.1	30.0	14.6	0.1	1.1	1330.2	13.6
	72	1583.8	32.8	14.2	0.1	1.0	1328.4	13.6
	96	1403.4	26.2	13.7	0.1	0.9	1287.5	13.5
Heart Fibroblasts	0	1130.2	68.9	11.9	0.2	1.0	-	-
	24	1234.7	32.4	12.9	0.1	1.1	-	-
	48	1194.1	35.5	12.7	0.1	1.1	-	-
	72	1817.5	62.0	14.4	0.2	1.6	-	-
	96	2648.7	108.0	16.4	0.2	2.3	-	-
	120	1966.1	79.3	14.6	0.2	1.7	-	-
	144	2134.7	141.3	14.5	0.2	1.9	-	-
	196	2050.0	99.8	14.0	0.2	1.8	-	-
	250	1877.3	107.7	13.5	0.2	1.7	-	-
	300	2061.2	135.7	14.0	0.2	1.8	-	-

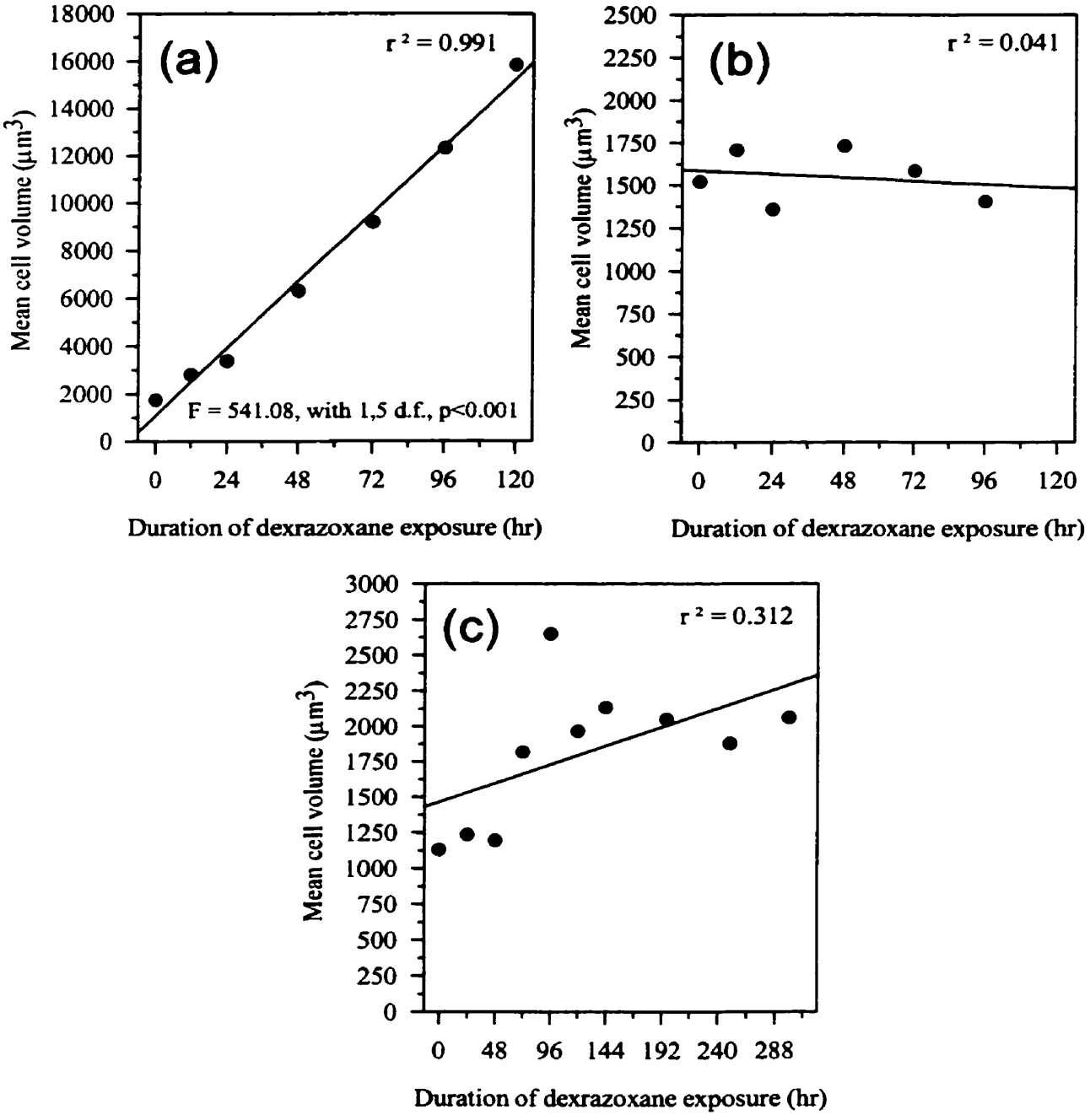

Fig. 2.13. Linear regression analysis of mean cell volume and the duration o dexrazoxane exposure in various cell types. Mean cell volumes determined from morphometry 2-D image analysis of dexrazoxane-treated (a) CHO, (b) DZR, and (c) heart fibroblast cells were plotted vs. the duration of dexrazoxane exposure. As demonstrated by statistical linear regression analysis a highly significant relationship ($p<0.001$) was identified in CHO cells only.

2.6 Effect of dexrazoxane on mean protein and DNA content

2.6.1 Introduction

One of the first observations made of CHO cells exposed to dexrazoxane for extended periods of time was an obvious increase in cell size (Section 2.5.3). Initially, before more extensive studies were conducted it was important to determine quantitatively whether cell enlargement was accompanied by an increase of various cellular constituents. To that effect the mean content level of protein and DNA in dexrazoxane-treated CHO cells was measured over an extended period of time. As explained in the following section, both protein and DNA were measured from the same samples using a modified Bradford assay [35] and a fluorometric assay [36], respectively. In addition, the mean protein and DNA content of dexrazoxane-treated DZR cells was conducted as a control. Finally, the existence of a correlation between protein/DNA content in dexrazoxane-treated CHO cells and the change in mean cell volume was examined.

2.6.2 Materials

Lauryl sulfate (SDS, cat. No. L-4390), bovine serum albumin (BSA, cat. No. A-3350), bisBenzimide (Hoechst 33258, M_w = 533.9 g/mol, cat. No. B-2883), and Coomassie brilliant blue G-250 (cat. No. B-0770) were obtained from Sigma Chemical Co. (St. Louis, MO, U.S.A.). Calf thymus DNA (cat. No. 2618) was obtained from Calbiochem Corp. (La Jolla, CA, U.S.A.). Dulbecco's Phosphate buffered saline (PBS, cat. No. D-5652) was obtained from Gibco-BRL, Life Technologies Inc. (Burlington, ON). Sodium chloride (NaCl, cat. No. AC-8304) was obtained from Anachemia Ltd. (Toronto, ON). Sodium

citrate (cat. No. C-614), o-phosphoric acid 85% (cat. No. A242P-500), fluorometric disposable cuvettes (cat. No. 14-386-20) were obtained from Fisher Scientific (Fairlawn, NJ, U.S.A.). Ethyl alcohol anhydrous (ethanol, 100%, cat. No. UN 1170) was obtained from Commercial Alcohols Inc. (Toronto, ON).

2.6.3 Methods

2.6.3.1 Preparation of reagents

1% (w/v) SDS: Prepared by dissolving 0.1 g of lauryl sulfate (SDS) in 10 ml ddH_2O.

0.15 mM bisBenzimide (Hoechst 33258) dye: Prepared by completely dissolving Hoechst 33258 (M_w = 533.9 g/mol) in ddH_2O, stored at 4°C in a foil wrapped amber bottle.

SSC solution: This solution contained 0.015 M sodium citrate (M_w = 294.10 g/mol), 0.154 M NaCl (M_w = 58.44 g/mol), adjusted to pH 7.0 and stored at room temperature.

Standard calf thymus DNA stock solution (1 μg/μL): This solution was prepared by dissolving calf thymus DNA into SSC solution using high intensity sonication.

Standard calf thymus DNA working solution: This solution contained 0.05 μg/μL of calf thymus DNA made by diluting calf thymus DNA stock solution (1 μg/μL) 1:20 in SSC solution.

1 M NaCl stock solution: Prepared by dissolving sodium chloride in ddH_2O.

Standard BSA protein stock solution (200 μg/mL): Prepared by dissolving bovine serum albumin (BSA) in 0.15 M NaCl.

Coomassie brilliant blue solution (0.01% w/v): A 500 mL solution was prepared by completely dissolving 0.05 mg Coomassie brilliant blue G-250 in 25 mL of 95% ethanol. This was followed by the addition of 50 mL of o-phosphoric acid 85%, 425 mL ddH_2O, and filtering through Whatman No. 1 filter paper, stored at 4°C in an amber bottle.

2.6.3.2 Drug treatment

CHO and DZR cells were grown as suspension cultures in double sidearm suspension spinner flasks. Protein and DNA content levels were quantified from the same cell cultures in which growth curves were analyzed concurrently (Section 2.4.2.2.2). Both cell types were seeded from control suspension cultures, and treated with 100 μM dexrazoxane at 0, 24 hr with daily replacement of media, as explained explicitly in Section 2.4.2.2.2. Media was replaced in the control CHO cultures at 36, 60 hr and in the dexrazoxane treated DZR culture at 24, 62, and 85 hr of growth. Media replacement involved resuspension in ~80% fresh media which allowed for maintenance of relatively unaltered cell densities. Cell densities were determined by counting on a model Z_f Coulter counter with a threshold setting of 7 (140 μm aperture, 1/amp = 2, 1/ap.current = 2, diameter cutoff ≅ 7.7 μm).

2.6.3.3 Preparation of cell samples

After each 24 hr period of growth $1x10^6$ cells were aseptically removed in replicate (x4), placed into 15 mL conical sterile centrifuge tubes, brought to 10 mL with PBS, and centrifuged 18 min at 150 *g*. Next, the supernatants were carefully removed to

approximately the 50 μL mark using a beveled Pasteur pipet. The cell pellet was then dispersed, but not resuspended by the addition of 10 mL PBS, followed by another centrifugation at 150 *g* for 18 min. Afterwards, the cell pellet was reuspended gently in 1 mL PBS approximately 10 times to ensure monodispersion of cells. Using an electronic repeat pipettor a volume of 600 μL was removed, placed into a microcentrifuge tube, centrifuged at 150 *g* for 10 min, and followed with the careful removal of 550 μl of the supernatant. Cell pellets were left in the remaining 50 μL of PBS and stored at –4°C until assayed. The actual number of cells in this 600 μL volume, and consequently in the cell pellet was calculated empirically from a separately removed sample of 300 μL using a model Z_f Coulter counter (see Appendix A.2.3).

2.6.3.4 Lyzing of cell pellets

Prepared cell samples in 50 μL PBS were thawed briefly in a 37°C incubator. To each sample was added 20 μL of 1% (w/v) SDS, followed by a gentle resuspension ~5-10 times so as to disperse the cell pellet without creating many soap bubbles. Samples were then placed back in the 37°C incubator for 45 min with periodic inversion. Afterwards sample volumes were brought to 500 μL with PBS.

2.6.3.5 Fluorometric determination of DNA content

2.6.3.5.1 Measuring DNA content from prepared samples

For each determination of DNA content 75 μL of cell lysate was placed into a polystyrene fluorometric cuvette followed by the addition of SSC solution to a total volume of 2990 μL. To avoid assay interference the final SDS concentration in 3000 μL was kept below 0.01% (w/v).

$$\text{i.e.}\quad 1\%\ \text{SDS} \times \frac{20\ \mu\text{L}}{500\ \mu\text{L total lysate vol.}} \times \frac{75\ \mu\text{L lysate assayed}}{3000\ \mu\text{L total assay vol.}} = 0.001\%\ \text{SDS}$$

Cell lysate volumes around 75 μL were used to obtain reasonable fluorescence measurements in all samples analyzed. As explained in Section 2.6.3.5.2, when a range of lysate volumes were analyzed adjustments in samples and/or standard curves were made for the maintenance of an equivalent final SDS concentration. Sample cuvettes were mixed in turn several times using a plastic plunger. This was followed by the determination of a blank fluorescence on a Shimadzu RF5000U spectrophoto-fluorometer (Shimadzu Scientific Instruments Inc., Columbia, MD, U.S.A.) tuned to excitation and emission wavelengths of 360 nm and 450 nm, respectively. Next, 10 μL of 0.15 mM Hoechst 33258 dye was added to each sample bringing the total volume to 3000 μL. This was followed by mixing in the same manner as before, and then determining the 'sample fluorescence' after 10 min in an enclosed space protected from light. The corrected 'sample fluorescence' was calculated by the subtraction of the blank fluorescence from the 'sample fluorescence'.

2.6.3.5.2 Constructing a DNA standard curve

DNA standards were prepared from a calf thymus DNA working solution of 0.05 μg/μL calf thymus DNA in SSC solution. SDS concentration was adjusted to an equivalent concentration as in the measured cell lysate samples as outlined in Table 2.5 by the addition of a small volume of dilute SDS.

i.e. $\frac{13\ \mu L}{3000\ \mu L}$ x 0.231% SDS = 0.001% (w/v) SDS

Each DNA standard was prepared to a volume of 2990 μL followed by a blank fluorescence determination, and then an 'actual fluorescence' determination upon the addition of 10 μL of 0.15 mM Hoechst 33258 in the same manner as before. Corrected 'actual fluorescence' was calculated by subtraction of these two values as shown in Table 2.5, and then plotted vs. the amount of standard DNA in units of micrograms (Fig. 2.14). First order linear regression analysis of graphically displayed data was accomplished using SigmaPlot (Jandel Corp., San Rafael, CA, U.S.A.) so as to determine the values of the slope (m), and the y-axis intercept point (b).

Table 2.5. Preparation and measurement of calf thymus DNA standards.

Amnt of 0.05 μg/μL calf thymus DNA (μL)	Amnt of 0.231% SDS (μL)	Amnt of SSC solution (μL)	Blanks Readings #1	#2	Fluor. after 10 min #1	#2	Corr. Fluor. #1	#2	Mean Fluor.	S.E.	C.V.%	*Final SDS conc.* (%)	*Absolute amnt of DNA* (μg)
0	13	2977	2.9	3.4	11.9	12.7	9.0	9.3	9.2	0.15	2.32	0.001	0.00
2	13	2975	5.2	5.4	16.5	16.2	11.3	10.8	11.1	0.25	3.20	0.001	0.10
5	13	2972	6.1	6.5	22.4	21.8	16.3	15.3	15.8	0.50	4.48	0.001	0.25
10	13	2967	9.2	8.4	31.9	32.1	22.7	23.7	23.2	0.50	3.05	0.001	0.50
20	13	2957	10.5	10.3	47.7	49.1	37.2	38.8	38.0	0.80	2.98	0.001	1.00
25	13	2952	10.2	10.9	56.5	57.7	46.3	46.8	46.6	0.25	0.76	0.001	1.25
30	13	2947	10.6	8.5	65.9	64.1	55.3	55.6	55.5	0.15	0.38	0.001	1.50
35	13	2942	8.3	7.6	73.1	72.9	64.8	65.3	65.1	0.25	0.54	0.001	1.75
40	13	2937	9.3	8.8	80.9	81.2	71.6	72.4	72.0	0.40	0.79	0.001	2.00
45	13	2932	7.6	7.7	89.4	87.7	81.8	80.0	80.9	0.90	1.57	0.001	2.25

Fig. 2.14. DNA standard curve of calf thymus DNA concentration vs. relative fluorescence after reaction with Hoescht 33258.

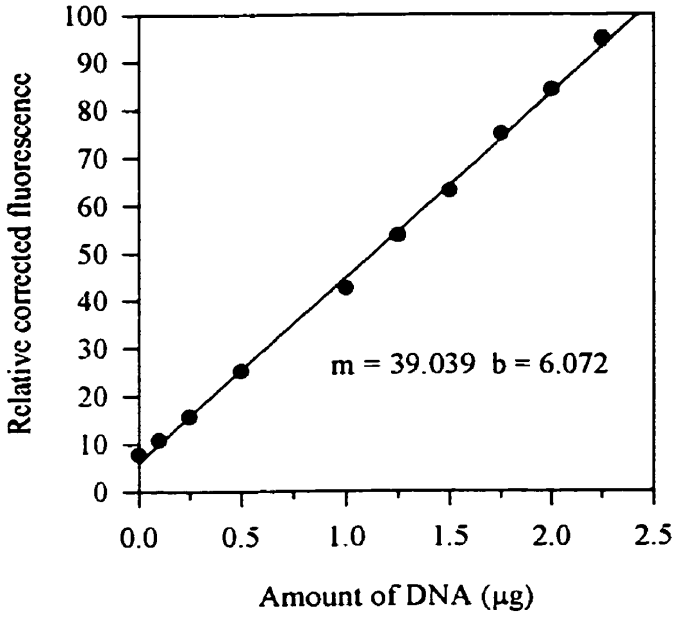

2.6.3.5.3 Calculating mean DNA content in samples using the standard curve

Using the data obtained from 75 µL of cell lysate sample replicate #1 of 0 hr control CHO cells as an example, the amount of DNA per million cells was calculated, and outlined inTable 2.6 as follows:

Since, $y = mx + b$ where x is the amount of DNA in the 75 µL cell lysate, y is the corrected fluorescence value of this replicate, and from Fig. 2.14: m = 39.039 and b = 6.072

$$\therefore \quad x = \frac{y-b}{m} = \frac{62.4-6.072}{39.039} = 1.44 \text{ µg of DNA}$$

Then, the amount of DNA in the total cell lysate volume was determined by:

$$1.44 \text{ µg} \times \frac{\text{total cell lysate vol}}{\text{vol. of cell lysate assayed}} = 1.44 \text{ µg} \times \frac{500 \text{ µL}}{75 \text{ µL}}$$

Finally, the amount of DNA per million cells was determined by dividing this value by the number of cells in the sample prior to lyzing, and then multiplying by a factor of $1x10^6$. The number of cells lyzed was approximately equivalent to the number of cells in the 600 µL volume prior to centrifugation and the removal of supernatant, which left a 50 µL cell pellet that was subsequently lyzed and brought to 500 µL with PBS (Section 2.6.3.3).

Overall then,

$$\text{Amount of DNA in replicate \#1} = \frac{y-b}{m} \times \frac{\text{total cell lysate vol.}}{\text{vol. of cell lysate assayed}} \times \frac{1x10^6}{\text{\#cells lyzed}}$$

$$= \frac{62.4-6.072}{39.039} \times \frac{500 \text{ µL}}{75 \text{ µL}} \times \frac{1x10^6}{8.07x10^5 \text{ cells}}$$

$$= 11.9 \text{ µg DNA}/10^6 \text{ cells}$$

Total DNA content was determined as follows, using control 0 hr CHO cells as an example by multiplying the mean DNA content per million cells by the cell density value at that time interval (Table 2.6).

i.e. Total DNA content after 0 hr exposure = mean DNA content of all 4 replicates x cell density at 0 hr

$$= 12.5\ \mu g/10^6 \text{ cells} \times 2.58 \times 10^4 \text{ cells/mL}$$

$$= \frac{12.5\ \mu g}{1 \times 10^6 \text{ cells}} \times \frac{2.58 \times 10^4 \text{ cells}}{1 \text{ mL}}$$

$$= 0.3\ \mu g/mL$$

Table 2.6. Determination of mean and total DNA content.

Rep. No.	Blank Fluor.	Fluor.	Corr. Fluor.	DNA from Std. Curve	Amnt of lysate used (µL)	#cells/ 600 µL	DNA content (µg/10^6 cells)	Mean DNA content (µg/10^6 cells)	S.E.	Total # cells/ml in flask	Total DNA content (µg/ml)	S.E.
1	9.0	71.4	62.4	1.44	75	8.07E+05	11.9	**12.5**	**0.4**	2.58E+04	**0.3**	**0.0**
2	5.8	67.2	61.4	1.42	75	7.89E+05	12.0					
3	4.6	64.1	59.5	1.37	75	6.77E+05	13.5					
4	3.9	65.7	61.8	1.43	75	7.51E+05	12.7					

2.6.3.6 Quantitation of protein content using a modified Bradford assay

2.6.3.6.1 Preparation of samples for protein content assessment

Cell lysate samples were prepared for protein analysis as outlined in the following section so as to obtain measurable protein concentrations between 2-8 µg/mL, the linear range of the BSA protein standard curve. To that extent various quantities of each cell lysate sample were on occassion assayed at once using the same standard curve in order to obtain protein concentration values within this valid range. Consequently, all analyzed

obtain protein concentration values within this valid range. Consequently, all analyzed samples and BSA standards were adjusted to equivalent final SDS and NaCl concentrations of 0.001% (w/v) and 0.105 M, respectively. To avoid assay interference final concentrations of SDS and NaCl were kept below these levels. Protein assay samples containing 5-25 μL of cell lysates were prepared in microcentrifuge tubes to 200 μL as outlined in Table 2.7 by the addition of various amounts of 0.1% SDS and 0.15, 0.375, and 1 M NaCl. This was followed by the addition of 800 μL of 0.01% (w/v) Coomassie brilliant blue dye to a volume of 1000 μL.

SDS was adjusted to a final concentration of 0.001% (w/v in 1000 μL total volume) as follows, using 1000 μL prepared samples containing 15 μL of cell lysate as an example:

i.e. Prior to adjustment the final SDS concentration was:

$$1\%\ \text{SDS} \times \frac{20\ \mu\text{L}}{500\ \mu\text{L total lysate vol.}} \times \frac{15\ \mu\text{L lysate assayed}}{1000\ \mu\text{L total assay vol.}} = 0.0006\%\ \text{SDS}$$

This was followed by the addition of 0.1% SDS such that,

$$0.1\%\ \text{SDS} \times \frac{4\ \mu\text{L}}{1000\ \mu\text{L total assay vol.}} = 0.0004\%\ \text{SDS}$$

overall the final SDS concentration was: 0.001% SDS

NaCl concentration was adjusted to a final concentration of 0.105 M in prepared samples of a total volume 1000 μL containing 15 μL of cell lysate so as to maintain equivalence with BSA standards (Section 2.6.3.6.2).

i.e.

$$0\ \text{M NaCl} \times \frac{15\ \mu\text{L lysate assayed}}{1000\ \mu\text{L total assay vol.}} = 0\ \text{M NaCl}$$

$$0.15\ \text{M NaCl} \times \frac{85\ \mu\text{L}}{1000\ \mu\text{L total assay vol.}} = 0.01275\ \text{M NaCl}$$

$$1\text{ M NaCl} \times \frac{90\ \mu L}{1000\ \mu L\text{ total assay vol.}} = 0.09\text{ M NaCl}$$

overall the final NaCl concentration was: 0.105 M NaCl

Table 2.7. Outline of sample preparation used prior to protein content quantitation.

Volume of cell lysate (μL)	Amnt of 0.15 M NaCl (μL)	Amnt of 0.375 M NaCl (μL)	Amnt of 0.1% SDS (μL)	Amnt of 1 M NaCl (μL)	Amnt of Coomassie Dye (μL)	*Final SDS conc.* (%)	*Final NaCl conc.* (M)
5	95	2	8	90	800	0.001	0.105
10	90	4	6	90	800	0.001	0.105
15	85	6	4	90	800	0.001	0.105
20	80	8	2	90	800	0.001	0.105
25	75	10	0	90	800	0.001	0.105

2.6.3.6.2 Preparation of BSA protein standards

BSA protein standards ranging from 0-16 μg/mL were prepared to a volume of 1000 μL with the addition of 800 μL of Coomassie dye, as shown in Table 2.8. Final concentrations of SDS and NaCl equivalent to the prepared cell lysate samples were maintained in the same manner as before.

SDS was adjusted by the addition of 0.1% (w/v) SDS.

i.e. $$0.1\%\text{ SDS} \times \frac{10\ \mu L}{1000\ \mu L\text{ total assay vol.}} = 0.001\%\text{ SDS}$$

overall the final SDS concentration was: 0.001% SDS

As well, using standard #2 as an example (Table 2.8) NaCl concentration was adjusted to 0.105 M. This included the 0.15 M NaCl in which BSA was dissolved in to make the standard BSA protein stock solution (200 μg/mL).

i.e.

$$0.15\text{ M NaCl} \times \frac{5\ \mu\text{L BSA}}{1000\ \mu\text{L total assay vol.}} = 0.00075\text{ M NaCl}$$

$$0.15\text{ M NaCl} \times \frac{95\ \mu\text{L}}{1000\ \mu\text{L total assay vol.}} = 0.01425\text{ M NaCl}$$

$$1\text{ M NaCl} \times \frac{90\ \mu\text{L}}{1000\ \mu\text{L total assay vol.}} = 0.09\text{ M NaCl}$$

overall the final NaCl concentration was: 0.105 M NaCl

Finally, a blank sample was prepared containing 0.001% SDS, 0.105 M NaCl and 800 μL of ddH_2O in instead of Coomassie dye. The mean abosrbance value of the blank measurements was subsequently subtracted from the absorbance values of all quantified samples.

Table 2.8. Preparation of BSA protein standards prior to quantitative assessment.

Std. #	Amnt of 0.15 M NaCl (μL)	Amnt of 200 μg/mL BSA in 0.15 M NaCl (μL)	Amnt of 0.1% SDS (μL)	Amnt of 1 M NaCl (μL)	Amnt of Coomassie Dye (μL)	*Final SDS conc.* (%)	*Final NaCl conc.* (M)	*Final BSA conc.* (μg/mL)	*Absolute amnt of BSA* (μg)
1	100	0	10	90	800	0.001	0.105	0	0
2	95	5	10	90	800	0.001	0.105	1	1
3	90	10	10	90	800	0.001	0.105	2	2
4	85	15	10	90	800	0.001	0.105	3	3
5	80	20	10	90	800	0.001	0.105	4	4
6	75	25	10	90	800	0.001	0.105	5	5
7	60	40	10	90	800	0.001	0.105	8	8
8	40	60	10	90	800	0.001	0.105	12	12
9	20	80	10	90	800	0.001	0.105	16	16
Blank	100	0	10	90	**800 μL ddH_2O**	0.001	0.105	0	

2.6.3.6.3 Spectrophotometric determination of protein content on a microplate reader

Prepared cell lysate samples were briefly vortexed followed by loading in replicate (3-4x) into specified wells of a 96-well microtitre plate. Using an electronic repeat pipettor 200 µL/well was loaded from prepared 1000 µL samples. Absorbances at 589 nm were then immediately measured and recorded using a Thermomax 96-well plate reader (Molecular Devices, Menlo Park, CA, U.S.A.), and a standard curve, fit to a quadratic equation was automatically constructed (Fig. 2.15).

Fig. 2.15. BSA protein concentration vs. absorbance at 589 nm after reaction with Coomassie brilliant blue dye.

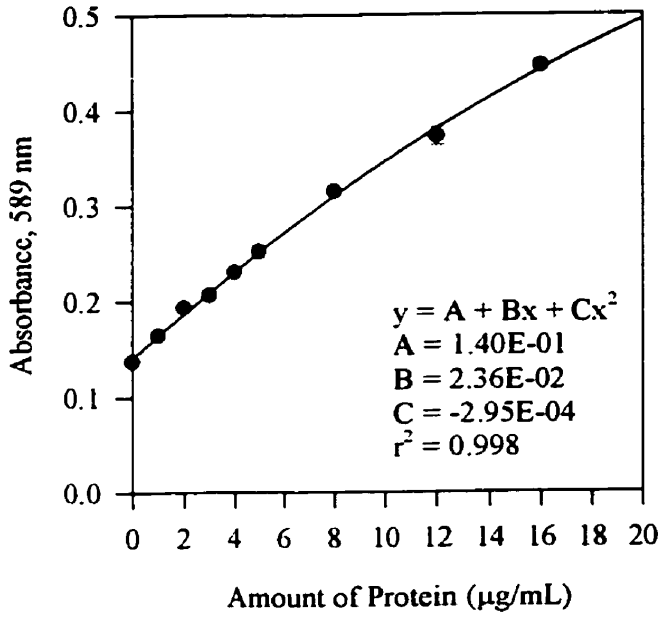

2.6.3.6.4 Calculating corrected absolute protein content from microplate reader data

The amount of protein in the original cell lysate sample was determined as follows, based on the raw data output from the Thermomax 96-well plate reader (Table 2.9). The final protein concentration was determined using the data collected from one set of

replicate determinations from a single assayed cell lysate volume. Only those samples which yielded a mean protein concentration value within the linear range of 2-8 μg/mL on the BSA standard curve (Fig. 2.15) were used. With the data obtained from replicate #1 of 0 hr control unexposed CHO cells as an example, the amount of protein per million cells was calculated as follows.

First, the mean protein concentration of 4 separate 200 μL/well determinations from cell lysate sample #1 was determined to be 4.095 μg/mL from the BSA protein standard curve (Table 2.9). Although this value of 4.095 μg is not representative of the amount of protein in the measured 200 μL aliquot it is representative of the amount of protein in the original 1 mL prepared volume prior to dispensing. For simplicity protein concentration on the x-axis of the BSA protein standard curve was expressed in units of μg/mL rather than μg in the 200 μL aliquot. The units of the *x*-axis (Fig. 2.15) can be made representative in terms of the measured 200 μL aliquot by dividing by 5.

i.e. The amount of protein in 200 μL aliquot $= 4.095\ \mu g/mL \times 200\ \mu L$

$$= \frac{4.095\ \mu g}{1000\ \mu L} \times 200\ \mu L$$

$$= 0.819\ \mu g$$

However, this calculation would be followed by a multiplication by 5 in determining the abolute amount of protein that contained within the original 1 mL sample volume prior to dispensing.

i.e. Amount of protein in the 1 mL prepared sample $= 0.819\ \mu g \times \frac{1000\ \mu L}{200\ \mu L}$

$$= 4.095\ \mu g$$

Therefore, to avoid these extra calculation for every sample the units on the *x*-axis of the BSA protein standard were expressed in terms of μg/mL or μg. Next, the corresponding amount of protein in the total cell lysate volume was determined as follows.

$$\text{i.e. Amount of protein in original cell lysate} = \text{Amount of protein in prepared 1 mL sample from standard curve} \times \frac{\text{total cell lysate vol}}{\text{vol. of cell lysate assayed}}$$

$$= 4.095\ \mu g \times \frac{500\ \mu L}{15\ \mu L}$$

$$= 136.50\ \mu g$$

The amount of protein per million cells was determined by dividing this value by the number of cells in the sample prior to lyzing, and multiplying by a factor of $1x10^6$. The number of cells lyzed was approximately equivalent to the number of cells in the 600 μL volume prior to centrifugation and the removal of supernatant, which left a 50 μL cell pellet that was subsequently lyzed and brought to 500 μL with PBS (Section 2.6.3.3).

Overall then,

$$\text{Amount of protein in replicate \#1} = \text{Amount of protein in prepared 1 mL sample from standard curve} \times \frac{\text{total cell lysate vol.}}{\text{vol. of cell lysate assayed}} \times \frac{1x10^6}{\text{\#cells lyzed}}$$

$$= 4.095\ \mu g \times \frac{500\ \mu L}{15\ \mu L} \times \frac{1x10^6}{8.07x10^5\ \text{cells}}$$

$$= 169.2\ \mu g\ \text{protein}/10^6\ \text{cells}$$

Total protein content in the culture at each assayed time interval was determined by multiplying the mean protein content per million cells by the cell density at that time interval (Table 2.9).

i.e. Total protein content after 0 hr exposure = mean protein content from all 4 replicates x cell density at 0 hr

$= 176.4\ \mu g/10^6$ cells x 2.58×10^4 cells/mL

$= \frac{176.4\ \mu g}{1 \times 10^6 \text{ cells}} \times \frac{2.58 \times 10^4 \text{ cells}}{1 \text{ mL}}$

$= 4.5\ \mu g/mL$

Table 2.9. Determination of mean and total protein content.

Rep. No.	Protein from Std. Curve (mg)	Amnt of lysate used (ml)	#cells/ 600 ml	Protein content ($mg/10^6$ cells)	Mean Protein content ($mg/10^6$ cells)	S.E.	Total # cells/ml in flask	Total Protein content (mg/ml)	S.E.
1	4.095	15	8.07E+05	169.2	**176.4**	**7.4**	2.58E+04	**4.5**	**0.2**
2	4.040	15	7.89E+05	170.7					
3	4.029	15	6.77E+05	198.5					
4	3.764	15	7.51E+05	167.1					

2.6.4 Results

As shown in the following results, concomitant with an inhibition of CHO cell prolferation and an increase in mean cell volume, the mean content levels of both protein (Fig. 2.16a) and DNA (Fig. 2.16b) increased upon exposure to dexrazoxane. Over a 120 hr period the mean protein and DNA content of dexrazoxane-treated cells increased in a linear fashion by 5.4-fold and 3.8-fold, respectively as compared to control 0 hr levels. The mean protein and DNA content per million cells at each time interval (N = 4) of exposure was significantly different ($p < 0.001$) from the mean content level of control unexposed cell samples (N = 16) when analyzed individually using an unpaired Student's *t*-test. DZR cells exposed to dexrazoxane under the same conditions did not significantly increase in mean protein or DNA content levels over 96 hr of growth as compared to the

mean content level of control 0 hr DZR samples (N = 4), using the same method of statistical analysis (Fig. 2.16).

A closer examination of the mean protein and DNA content levels of dexrazoxane-treated cells was obtained by plotting this data as a ratio of mean protein/DNA content vs. duration of exposure (Fig. 2.16c). The slight increasing trend of this ratio in dexrazoxane-treated CHO cells as compared to control and DZR cells indicated that protein production was either increasing relative to DNA production, or DNA production was slowing down as protein production continued on at the same rate. This suggestion was further confirmed by an analysis of the total protein (Fig. 2.17a) and total DNA (Fig. 2.17b) content per milliliter of culture. Both protein and DNA production in dexrazoxane-treated cells appeared to increase steadily over the first 72 hr, with only DNA production plateauing off after this time period.

Mean protein and DNA content levels from dexrazoxane-treated CHO cells were additionally compared separately to previously determined mean cell volumes at each respective time interval (Fig. 2.18). Using statistical linear regression analysis a highly significant dependency relationship was demonstrated in both cases ($p < 0.001$). This result clearly associates the larger cell volumes of dexrazoxane-treated CHO cells with accentuated protein and DNA levels in a time and/or cell cycle dependent manner, although the lack of intersection at the point of origin (0,0) does raise a key point of interest. This trend may be attributable simply due to a lack of a sufficient number of data points to accurately demonstrate the actual relationship. Although this seems reasonable, it may be impossible to completely demonstrate due to quantifiable limitations of protein and DNA analysis, as well as the absence of any mean cell volume values below 2000 μm^3.

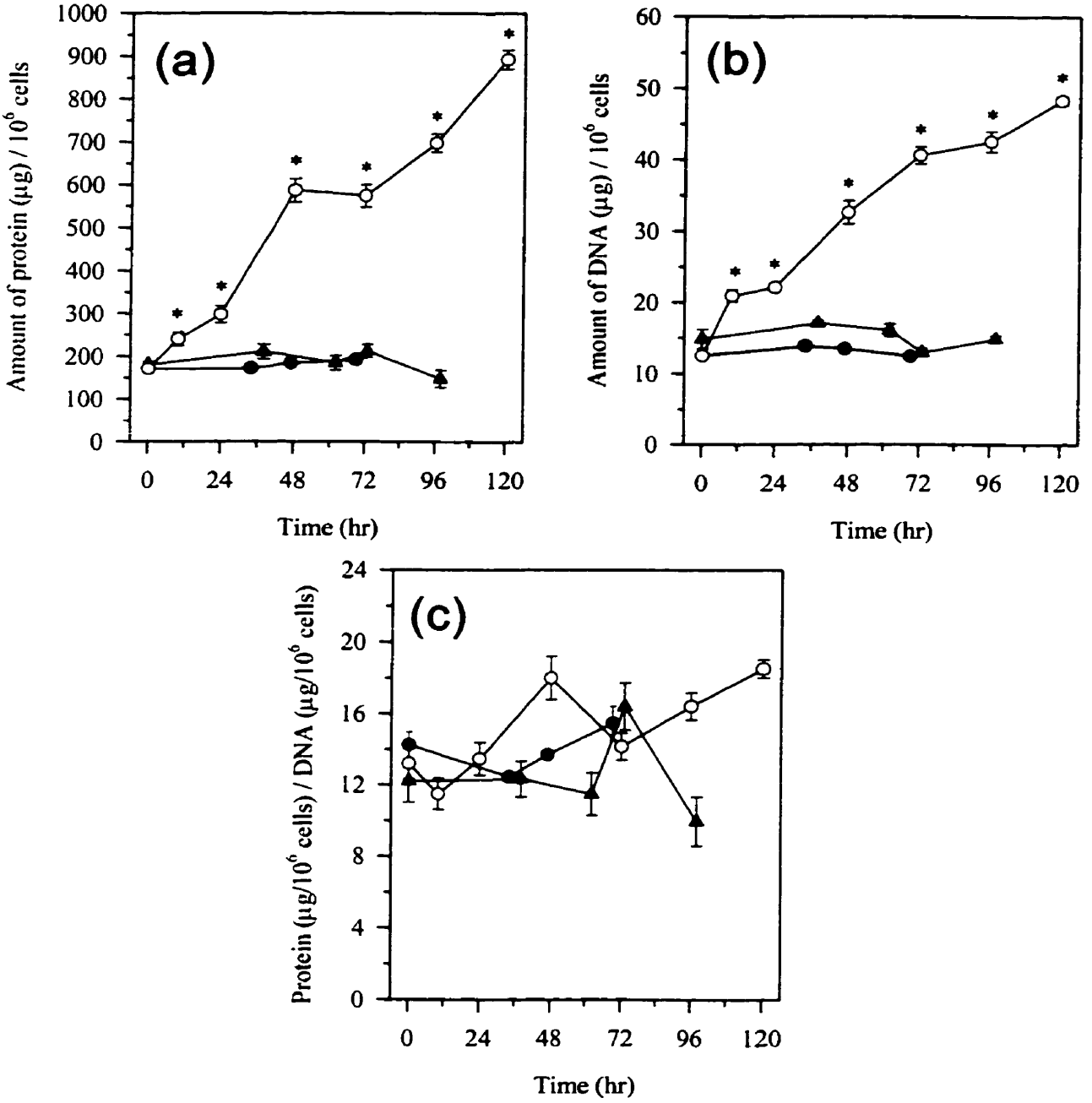

Fig. 2.16. Mean protein and DNA content levels in suspension CHO and DZR cells exposed to dexrazoxane. CHO cells seeded at 2.25×10^5 cells/mL were exposed to 100 μM dexrazoxane at 0, 24 hr with daily media replacement (○). DZR cells were treated at 0, 24 hr with media replacement at 24, 62, and 85 hr (▲). Control CHO cells (●) and DZR cells were seeded at 0.25×10^5 cells/mL. Cell densities were determined on a Coulter counter (140 μm aperture, diameter cutoff ≅ 7.7 μm). Protein (a) and DNA (b) content levels per million cells were determined by a modified Bradford assay and a Hoechst dye fluorometric analysis, respectively. Protein/DNA ratio values were determined for each analyzed time interval (c). Data points represent the mean of 4 replicate samples ± S.E. Asterisks (*) indicate a statistically significant difference ($p < 0.001$, unpaired Student's *t*-test) from the mean of control unexposed CHO cell values.

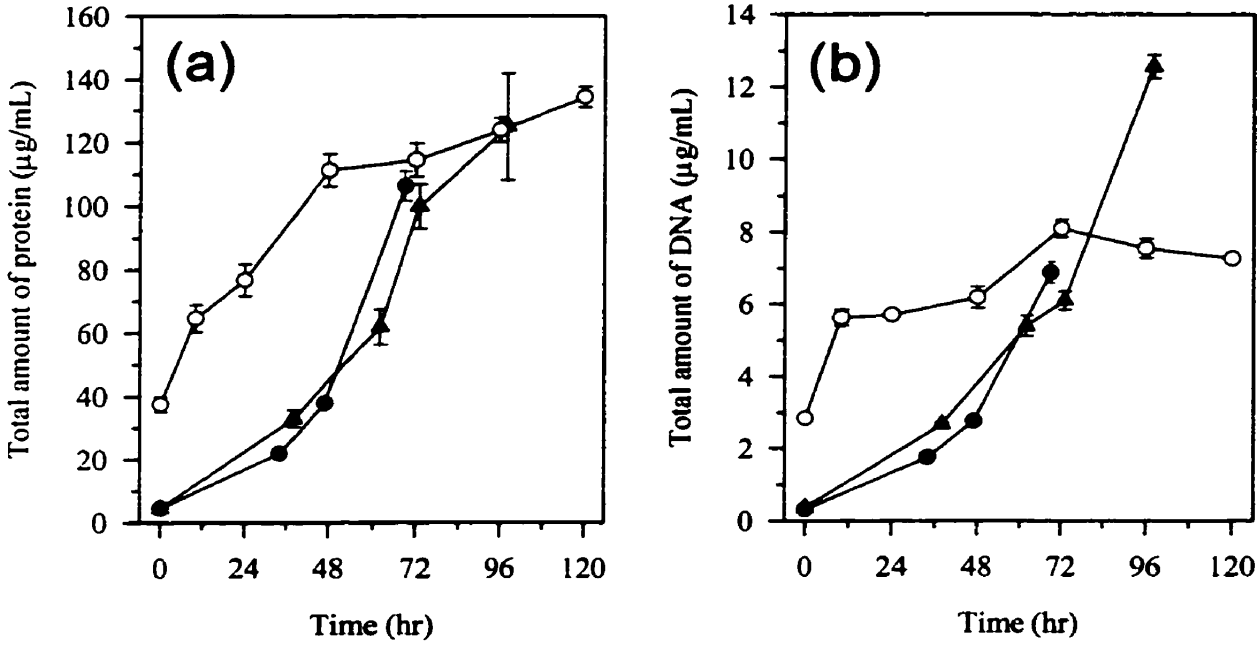

Fig. 2.17. Total cell protein and cell DNA content levels in dexrazoxane-exposed CHO and DZR suspension cell cultures. The overall amount of protein and DNA per milliliter of cell culture was determined by multiplying individual mean protein and DN content levels by the cell density at their respective time intervals, taken directly from Fig. 2.7. Control CHO cells (●) were grown alongside cells exposed to 100 µM dexrazoxane at 0, 24 hr with media replaced daily (○). DZR cells were treated in the same fashion with media replacement at 24, 62, and 85 hr (▲). Cell densities were determined with the use of a Coulter counter (140 µm aperture, diameter cutoff ≅ 7.7 µm) as displayed in Fig. 2.7. Mean protein and DNA content levels were determined as shown in Fig. 2.16. Data points represents the mean of 4 replicate samples ± S.E.

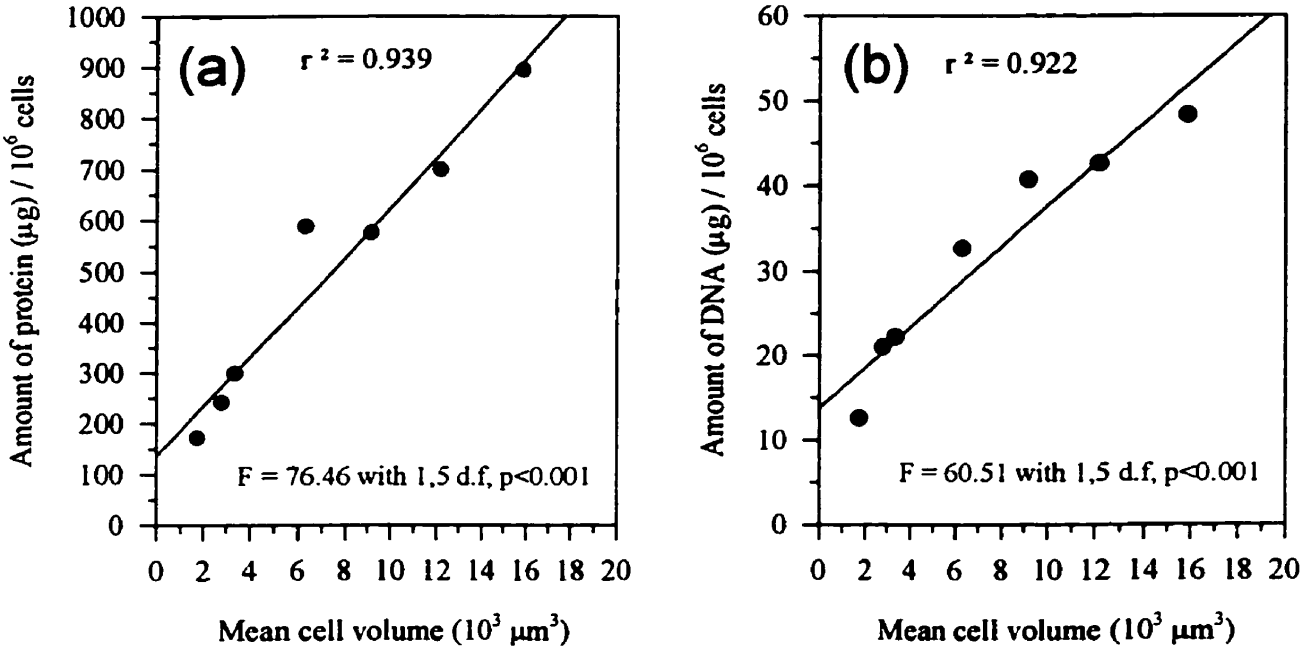

Fig. 2.18. Dependency relationship between mean protein or DNA content and mean CHO cell volume upon exposure to dexrazoxane. Mean protein (a) and DNA (b) content from dexrazoxane-treated CHO cells were plotted vs. previous stereometrically determined (Section 2.5.4) mean cell volumes at each respective analyzed time interval. Dependency relationships were identifed in either case, and shown to be highly significant ($p<0.001$) by statistical linear regression analysis.

2.7 Cell cycle analysis of dexrazoxane-treated cells by flow cytometry

2.7.1 Introduction

In the following section flow cytometry was used to characterize the effect that dexrazoxane has on the cell cycling of CHO, DZR, and heart fibroblast cell lines. The cell cycle perturbation effects of dexrazoxane were examined not only after an extended period of exposure but also on a logarithmic scale of DNA fluorescence, which together illustrate some of the shortcomings of similar studies [18,19,37]. Specifically, the DNA ploidy content of individual cells was quantitated after the stoichiometric binding of a fluorophore (propidium iodide) to double stranded DNA, and the delivery of these cells in a flow system past an excitation beam. In addition, other parameters including forward (FALS) and right (90°LS) angle light scattering were measured. The intensity of light scattered in the forward direction generally correlates with cell size, and the light intensity scattered at right angles to the excitation laser beam correlates with granularity and the ability of intracellular structures to reflect light [38]. Finally, the above parameters were correlated using sophisticated data processing software so as to identify the existence of cell subpopulations which may be otherwise indistinguishable by other methods of analysis.

2.7.2 Materials

RNase A (stored at –20°C, cat. No. R-5503) and propidium iodide (cat. No. P-4170), were obtained from Sigma Chemical Co. (St. Louis, MO, U.S.A.). Triton X-100 (cat. No. X198-5) was obtained from J.T. Baker Chemical Co. (Phillipsburg, NJ, U.S.A.). Dulbecco's Phosphate buffered saline (PBS, cat. No. D-5652) was obtained from Gibco-

BRL, Life Technologies Inc. (Burlington, ON). Ethyl alcohol anhydrous (ethanol, 100%, cat. No. UN 1170) was obtained from Commercial Alcohols Inc. (Toronto, ON).

2.7.3 Methods

2.7.3.1 Drug treatment

CHO cells were grown as suspension cultures in double sidearm suspension spinner flasks, seeded initially at $2.0x10^5$ cells/mL and treated with 100 μM dexrazoxane at 0, 24 hr, or daily. DZR cells were grown as adherent cultures in T-75 flasks, seeded at $0.20x10^5$ cells/flask and treated with 100 μM dexrazoxane daily. Media was replaced daily in all CHO and DZR dexrazoxane-treated cell cultures. In suspension cultures this was achieved by the aspetic removal of cells followed by centrifugation at 250 *g* for 12 min, and resuspension in an appropriate volume of ~80% fresh α-MEM/FCS in an attempt to maintain cell densities approximately equivalent to that of before centrifugation. At indicated times of dexrazoxane exposure cells were either removed directly from culture or harvested with trypsin-EDTA followed by sample preparation for flow cytometry analysis. Cell densities were determined by counting on a model Z_f Coulter counter with a 100 μm aperture, threshold setting of 7 (1/amp = 2, 1/ap.current = 8, diameter cutoff ≅ 8.7 μm).

Neonatal rat heart fibroblast cells in exponential growth were harvested with trypsin-EDTA, and subsequently seeded onto separate T-75 flasks at $1.8x10^6$ cells/flask. Media was replaced every other day in control flasks with ~80% fresh DMEM/F-12/FCS. All other flasks were exposed daily to 100 μM dexrazoxane with media replacement. After 326 hr of dexrazoxane-exposure all cultures were harvested with trypsin-EDTA

followed by quenching with DMEM/F-12/FCS. Cell densities were also determined by counting on a model Z_f Coulter counter with a 100 μm aperture, threshold setting of 7.

2.7.3.2 Preparation of staining solution, and samples for analysis

Propidium iodide (PI) stock solution (1 mg/mL): A stock solution of PI was made by dissolving 1 mg of PI in 1 mL ddH_2O, stored in a microcentrifuge tube at 4°C wrapped in foil for several months.

DNase-free RNase A: A solution of RNase A was first prepared by dissolving 1 mg of RNase A into 1 mL ddH_2O, prepared in a glass test tube. Contaminating DNase enzymes in the solution were inactivated by boiling the test tube for 5 min.

Propidium iodide (PI)/Triton X-100 staining solution with RNase A: A 10 mL staining solution containing 0.02 mg/mL PI was prepared by adding to a volume of 0.1% (v/v) Triton X-100 in PBS, the DNase-free RNase A (1 mg/mL), and 200 μL of the PI stock solution (1 mg/mL).

Sample preparation by fixation and staining: After different periods of dexrazoxane exposure $5x10^6$ cells were removed from CHO and DZR cultures, and $8x10^6$ cells from heart fibroblast cultures. Cells were then centrifuged at 200 *g* for 6 min, and gently resuspended as monodispersed single cell suspensions in 0.5 mL PBS using a Pasteur pipet or a 22½ G syringe. This was followed by the addition, dropwise of the prepared cell suspensions into 4.5 mL of 70% (v/v) cold ethanol whilst being vortexed, followed by fixation overnight at -20°C. Samples were then centrifuged and washed once with 5 mL PBS as before, and resuspended in 1 mL of the propidium iodide (PI)/Triton X-100

staining solution containing RNase A. Finally, samples were incubated for 15 min at 37°C, and stored on ice wrapped in foil until analyzed.

2.7.3.3 Determination of the percentage of cell aggregates

The percentage of cell aggregates in all prepared samples was determined microscopically so as to assess their contribution towards cell cycling analysis. Monodipersed cell suspensions ensure a high degree of accuracy in attributing ploidy levels to actual individual cells. Clumps of cells can distort the analysis of DNA histograms and lead to a false-positive ploidy level. In particular, two aggregated cells in G0/G1 of the cycle will equate to one cell in G2/M in terms of DNA content. After staining with propidium iodide, 20 μL of each sample was removed and diluted with PBS to ~100 μL in a careful manner so as not to cause any disruption. Next, a minimum of 300-500 total cells were counted under a 10X objective lens in a hemacytometer chamber. Each observed cell doublet, triplet, quadruplet, or quintuplet was attributed with a single count. The percentage of each types of cell aggregate was then determined by dividing by the overall total number of aggregates counted.

2.7.3.4 Flow cytometry, and analysis of collected fluorescence raw data

Cell cycle analysis was carried out on an EPICS V multiparameter flow cytometer (Coulter Electronics, Hialeah, FL, U.S.A.) in the Department of Immunology (University of Manitoba, Winnipeg, MB) with the assistance of Dr. Edward Rector. PI-stained cells were passed through a 75 μm chamber orifice, and excited with an argon ion laser tuned to 488 nm. This was followed by the collection of red fluorescence emissions at 610 nm

using 3.5 decade logarithmic amplifiers over a span of 256 channels of increasing fluorescence intensity, directly proportional to increasing DNA ploidy level. A total of 10,000 cells were analyzed per trial and the number of cells falling within each channel was counted. Regions of interest or gates were defined to select certain populations of cells for the display of a number of select parameters. Specifically, forward and orthogonal (90° or side) light scatter were recorded together with red (PI) DNA fluorescence followed by the correlation of each on bivariate histograms. The relative position of the 2N diploid peak from control samples was used for instrument alignment of the DNA fluorescence histograms from dexrazoxane-treated samples.

A hard copy of the collected raw data from a total of 10,000 cells per sample was outputted displaying the number of cells that fell within each channel from 0-255 of increasing fluorescence These values were entered into a SigmaPlot spreadsheet (Jandel Corp., San Rafael, CA, U.S.A.), and consequently 3-D plots were generated displaying DNA fluorescence histograms of each analyzed sample. The designation of the respective axes were as follows: *x*-axis, level of DNA fluorescence; *y*-axis, duration of dexrazoxane exposure; *z*-axis, number of cells contained within each channel of DNA fluorescence. The collected data was expressed on a logarithmic scale (*x*-axis) of increasing DNA content vs. the number of cells. The following SigmaPlot transform function was utilized to generate a range of 256 equally spaced numbers, which when taken the log of, extented from 1-1000, as displayed on the DNA content frequency histograms:

```
Col(1) = data(0,3,0.0117647)
Col(1) = 10**Col(1)
```

The relative fraction of cells residing within each discrete DNA ploidy level was determined empirically from the collected raw data. The delineation between where successive phases 2N, 4N, 8N, etc. began or ended could not be determined absolutely due to the extent of overlap of non-definable S phases. Therefore, approximations of the number of cells residing within each DNA ploidy peak was determined by dividing the number of counted cells between the midpoints of two successive valley regions on either side of a particular peak by 10,000 or the total number of cells counted overall.

2.7.4 Results

Upon staining with propidium iodide the distribution of ploidy content in various cell lines were examined by flow cytometry in order to analyze any cell cycle perturbations caused by exposure to dexrazoxane. The DNA content of CHO cells grown in suspension were examined at various intervals of growth after exposure to 100 μM dexrazoxane at 0, 24 hr or daily (Fig. 2.19 and 2.20, respectively). Under both treatment conditions an increasing trend towards a high level of polyploidization appeared with increasing durations of dexrazoxane exposure. Adherent CHO cells grown and exposed to dexrazoxane under the same conditions as suspension cells resulted in similar levels of polyploidization after extended periods of time (data not shown). The identification of cells with higher multiples of a normal diploid content of DNA after dexrazoxane exposure is suggestive of cells undergoing multiple rounds of DNA synthesis in the absence of cell division. Depicted in the DNA histogram profile of control CHO cells are the typical normal successive phases of a eukaryotic cell cycle. A greater number of cells exhibit a sharp 2N, diploid peak during the long G0/G1 phase, followed by an intermediate DNA

synthesis phase (S phase), and finally a G2/M phase prior to division represented by a 4N, tetraploid peak.

After 96 hr of daily dexrazoxane exposure CHO cells with a DNA content as high as 32N were detectable, indicative of four successive rounds of DNA synthesis (Fig. 2.19 and 2.20). Exposure to dexrazoxane at 0, 24 hr with daily media replacement lead to the appearance of cells with a DNA content of 32N, as well as 64N (Fig. 2.19). Although cell aggregation can commonly lead to false positive ploidy levels, microscopic examination of propidium iodide-stained cells revealed that very few cells were clumped together at these long time periods (Table 2.10). The percentages of doublets in each prepared sample was on average less than 7%, with triplets accounting for less than 1% of the analyzed population. By 92 hr, a slightly higher proportion of 32N and 64N cells were present after a 0, 24 hr treatment with dexrazoxane than were present after a comparative time of daily exposure (Table 2.11). Despite a similar trend towards higher ploidy content from either drugging protocol, the replacement of media alone after two dexrazoxane exposures may have established more adequate conditions for further cycling than the protocol involving daily exposure. The presence of nearly twice as many 2N, diploid cells after 92 hr (Table 2.11) lends support to this theory of a healthier cell population, although earlier viability studies demonstrated no pronounceable difference between the separate treatment protocols (Section 2.4.3.2).

The range of ploidy content in dexrazoxane-treated CHO cells appeared to be relatively evenly distributed with increasing times of exposure, complemented by the presence of multiple or continuous S-phase(s). More specifically, after 48 hr of continuous exposure the percentage of 4N, 8N, and 16N cells remained relatively constant without a

clear progression of the entire population towards a single high ploidy level (Table 2.11). These results can perhaps be explained by a cell cycle blockage induced at differential ploidy levels as seen by the eventual depletion of 2N cells from the population. Additionally, the possibility remains that some high ploidy cells may have been able to undergo division in spite of a high degree of topoisomerase II inhibition.

Light scatter signals resulting from the flow cytometric analysis of dexrazoxane exposed CHO cells were compared and correlated with other simulataneously analyzed parameters. The upper (I, II, III) and lower panels (IV, V, VI) of Fig. 2.21 correspond to control and 92 hr dexrazoxane-treated CHO cells, respectively. Bivariate dot plots of light scattering (Fig. 2.21I and IV) are representative of 10,000 analyzed cells plotted according to the intensity of forward angle (FALS) and right angle (90°LS) light scattering. After a 0, 24 hr dexrazoxane treatment regimen and growth for a total of 92 hr a greater number of cells with increased FALS and 90°LS properties appeared, representative of significantly larger and more granular cells respectively. The encircled region of cells on these and other light scattering histograms was the subject of a gating selection based on physical cell characteristics that were carried forward for further analysis of fluorescence properties.

The subsequent histograms of Fig. 2.21 display the analyzed relative fluoresence detected from control and 92 hr dexrazoxane-exposed CHO cells. Normally when a cell passes through a laser beam the scattering of fluorescent light is detected and an electronic signal or pulse is generated. Two measurements are made on these propidium iodide stained cells: (i) the integrated relative fluorescence (IRFL) emitted from these cells, which is proprotional to their DNA content, and (ii) the width of the pulse signal in time (PRFL) [39]. Since PRFL is proportional to the size of the measured particle a direct correlation

was made between increased DNA ploidy level and increased cell size. When displayed on separate axes of bivariate histograms these parameters revealed distinct sub-populations of various DNA content levels after 92 hr of dexrazoxane exposure. In particular, five separate sub-population regions were identified on the histogram of 92 hr dexrazoxane-treated cells (Fig. 2.21V). When viewed from the perspective of the *x*-axis (IRFL) looking forward these sub-populations correspond to the ploidy levels 2N, 4N, 8N, 16N, 32N identified in Fig. 2.21VI as C, D, E, F, J. These final DNA content vs. cell count bivariate histograms (Fig. 2.21II and VI) are a re-representation of control and 92 hr individual histograms previously shown in Fig. 2.19.

Ultimately, aside from the correlation postulated between increasing PRFL or cell size and increasing DNA ploidy a strategy known as back-gating [40] was employed to determine the physical characteristics of the various sub-populations of cells. By placing a gate around these regions with distinct fluorescence characteristics (Fig. 2.21II and V) the light scattering characteristics of these cells were highlighted in distinct regions of the histogram I and IV. Specifically, higher ploidy cells possessed increased FALS and 90°LS properties representative of being significantly larger and more granular. Furthermore, the lack of the appearance of cells with sub-diploid DNA content and the absence of a significantly reduced FALS properties indicated that apoptotic bodies were not present and suggests that dexrazoxane did not induce apoptosis in CHO cells [38,41].

In addition to the flow cytometry analysis of dexrazoxane treated CHO cells, two other cell lines, namely DZR and heart fibroblasts were examined with respect to the effects of dexrazoxane on cell cycle perturbations. After 96 hr of continuous dexrazoxane exposure the profile of DNA ploidy in DZR cells remained relatively unchanged from that

of control cells (Fig. 2.22). This result was as expected, due to the inherent resistance towards dexrazoxane [22], and their previously demonstrated unchanging distribution in cell size upon exposure to dexrazoxane (Section 2.5.4). The insignificant increase in the fraction of 16N and 32N DZR cells after 96 hr dexrazoxane exposure (Table 2.11) can be attributed to some cell aggregation (Table 2.10), and perhaps a partial unproven reversion in dexrazoxane resistance of some cells.

When heart fibroblast cells were exposed to dexrazoxane continuously for 326 hr DNA content did not increase to such high ploidy levels as seen with respect to CHO cells (Fig. 2.23). Instead, as cells continued to cycle a significant proportion of the population presumably became blocked in the G2/M phase. This result was indicated by an increased fraction of 4N cells after 326 hr, paralleled by a decreased fraction of 2N cells, compared to control levels (Table 2.11). In addition after 326 hr of dexrazoxane exposure 8N and 16N ploidy cells were present, and the S phase which had previously existed between 2N and 4N ploidy peaks was no longer present. This result suggests that while some cells were able to cycle onto higher ploidy levels in the absence of cell division others became quiescent and stopped cycling altogether, and remained in a G0/G1 phase. Overall, the effects of dexrazoxane on CHO and heart fibroblast cell cycling appeared similar with respect to an obvious increasing trend towards a high level of polyploidization. Furthermore, the differing propensities between these two cell lines towards a possible G2/M blockage may be attributed to their respective doubling rates, inherent life spans, and/or topoisomerase II levels.

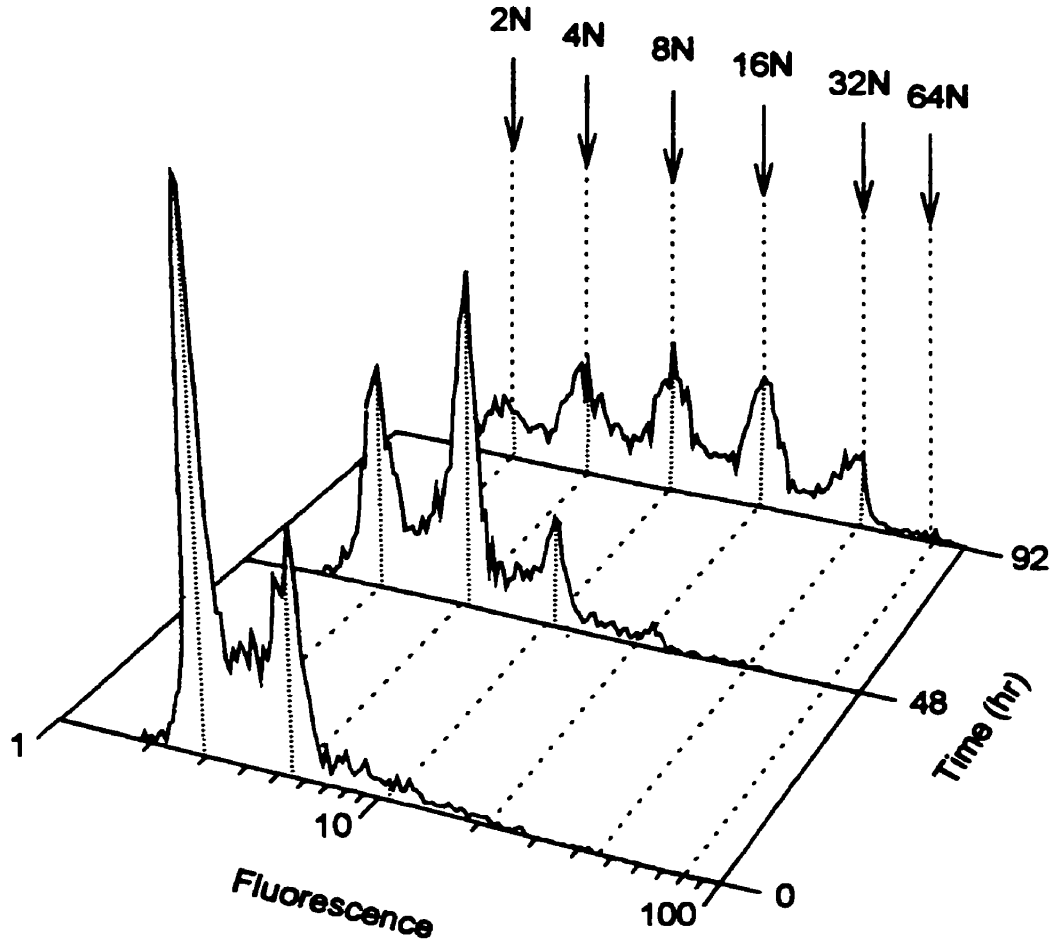

Fig. 2.19. Cell cycle analysis of CHO cells exposed to derazoxane at 0, and 24 hr with daily media replacement. Cells were taken directly from suspension cultures at the indicated times, stained with propidium iodide and analyzed by flow cytometry as described in Section 2.7.3.4. Shown here is integrated red fluorescence on a logarithmic scale, reflective of increasing DNA content vs. the number of cells. The leftmost peak in the control (0 hr) culture represents G0/G1 (2N) cells. Cells with twice the fluorescence of G0/G1 cells represent the G2/M cells with tetraploid (4N) levels of DNA. At subsequent times, higher multiples of the G0/G1 peak can be seen, representative of higher ploidy levels (8N, 16N, 32N respectively). A total of 5000 cells were analyzed per time interval.

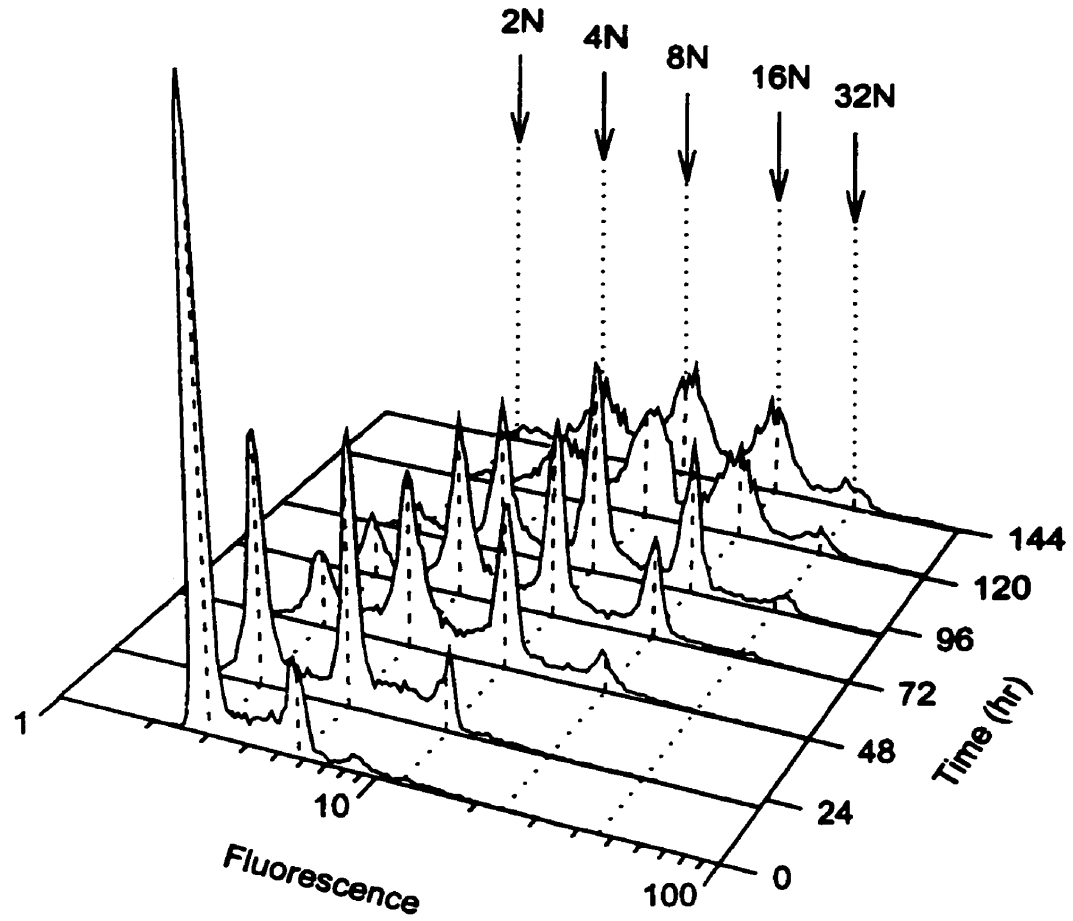

Fig. 2.20. Cell cycle analysis of CHO cells exposed daily to derazoxane with media replacement. Cells were taken directly from suspension cultures at the indicated times, stained with propidium iodide and analyzed by flow cytometry as described in Section 2.7.3.4. Shown here is integrated red fluorescence on a logarithmic scale, reflective of increasing DNA content vs. the number of cells. The leftmost peak in the control (0 hr) culture represents G0/G1 (2N) cells. Cells with twice the fluorescence of G0/G1 cells represent the G2/M cells with tetraploid (4N) levels of DNA. At subsequent times, higher multiples of the G0/G1 peak can be seen, representative of higher ploidy levels (8N, 16N, 32N respectively). A total of 10,000 cells were analyzed per time interval.

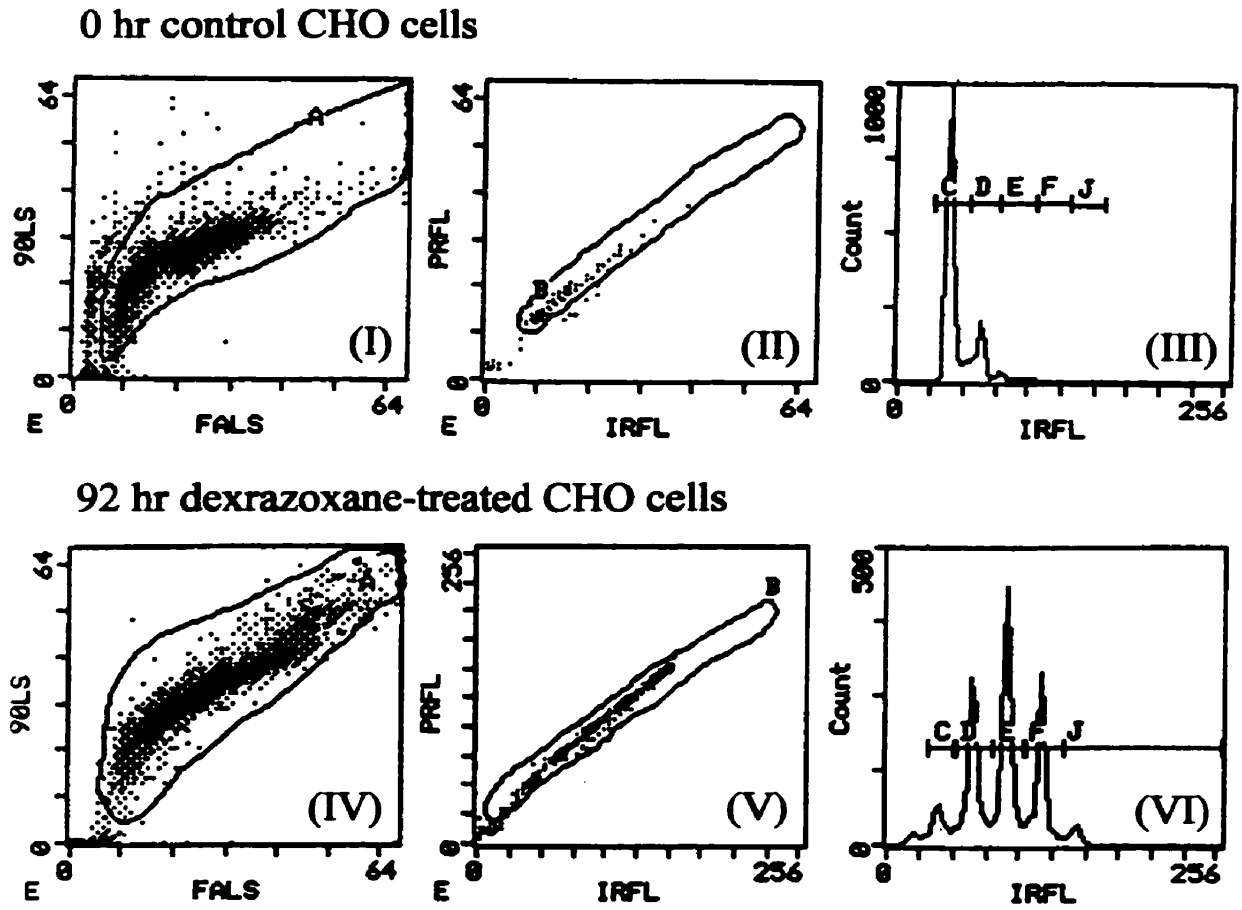

Fig. 2.21. Correlation of physical light scattering properties with DNA ploidy level in dexrazoxane-treated CHO cells. Upper (I, II, III) and lower panels (IV, V, VI) correspond to control and 92 hr dexrazoxane-treated CHO cells, respectively. Cells were exposed to dexrazoxane at 0, 24 hr with daily media replacement. Light scattering analysis (I and IV) revealed an increasing trend towards a greater intensity of forward angle (FALS) and side angle (90°LS) light scattering in dexrazoxane-treated cells, reflective of increasing cell size and granularity. An analysis of gated cells in terms of pulse-width (PRFL) vs. integrated relative fluorescence (IRFL) in histograms II and V revealed the existence distinct sub-populations of cells. As displayed in histograms III and VI, a clearer analysis of IRFL or DNA content vs. cell count shows the range of ploidy levels in these cell samples. Back-gating analysis of fluorescence sub-populations demonstrated a clear correlation between increased ploidy levels and increased FALS and 90°LS properties.

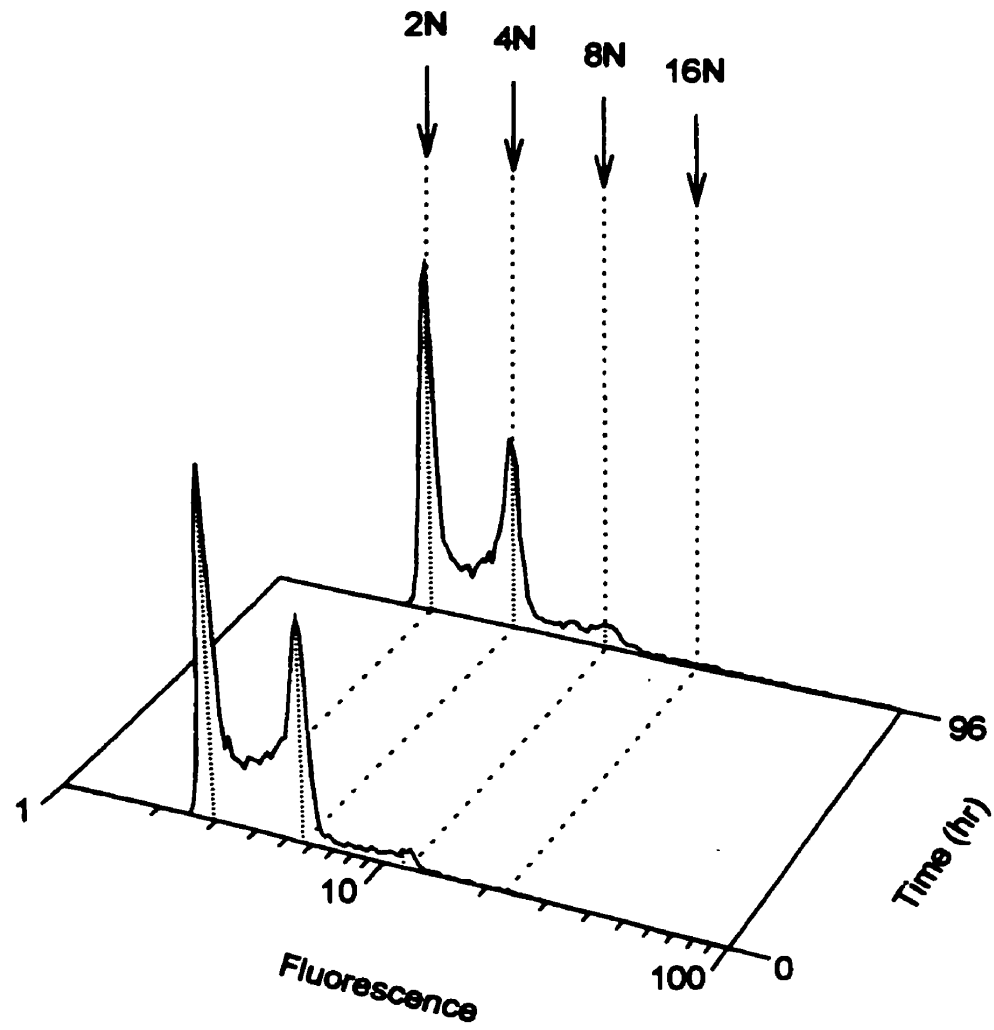

Fig. 2.22. Cell cycle analysis of DZR cells exposed daily to derazoxane with media replacement. Cells were harvested from T-flasks at indicated times, stained with propidium iodide and analyzed by flow cytometry as described in Section 2.7.3.4. Shown here is integrated red fluorescence on a logarithmic scale, reflective of increasing DNA content vs. number of cells. The leftmost peak in the control (0 hr) culture represents G0/G1 (2N) cells. Cells with twice the fluorescence of G0/G1 cells represent the G2/M cells with tetraploid (4N) levels of DNA. At subsequent times, higher multiples of the G0/G1 peak were not seen indicative of the inherent resistance of DZR cells to dexrazoxane. A total of 10,000 cells were analyzed per time interval.

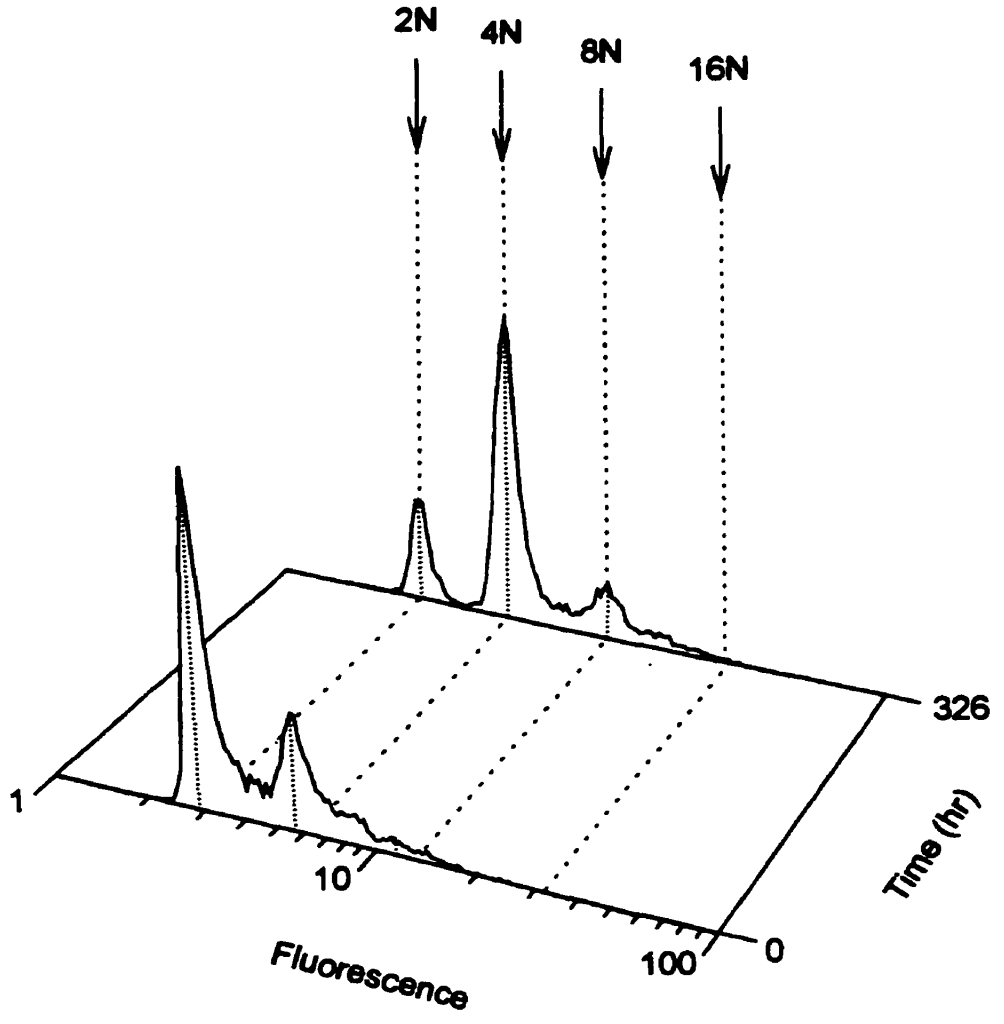

Fig. 2.23. Cell cycle analysis of heart fibroblast cells exposed daily to derazoxane. Cells were harvested from T-flasks at indicated times, stained with propidium iodide and analyzed by flow cytometry as described in Section 2.7.3.4. Shown here is integrated red fluorescence on a logarithmic scale, reflective of increasing DNA content vs. number of cells. The leftmost peak in the control (0 hr) culture represents G0/G1 (2N) cells. Cells with twice the fluorescence of G0/G1 cells represent the G2/M cells with tetraploid (4N) levels of DNA. After 326 hr of dexrazoxane exposure, cells with 4-fold the DNA content of G0/G1 cells can be seen, represented by 8N. A total of 10,000 cells were analyzed per time interval.

Table 2.10. Percentage of cell aggregates contributing to flow cytometry analysis.

Cell Line	Duration of dexrazoxane exposure	Time (hr)	Single cells (%)	Doublets (%)	Triplets (%)	Quadruplets (%)	Quintuplets (%)
CHO	Exposed daily	0	93.9	6.1	0.0	0.0	0.0
		21	89.1	8.4	2.4	0.2	0.0
		48	91.5	7.1	1.2	0.2	0.0
		72	92.1	7.1	0.8	0.0	0.0
		93	93.1	5.9	0.8	0.2	0.0
		121	93.7	5.5	0.8	0.0	0.0
		144	91.0	8.2	0.8	0.0	0.0
	Exposed at 0, 24 hr	0	82.8	11.8	3.7	1.0	0.7
		48	80.8	14.7	2.5	1.0	1.0
		92	87.5	9.6	2.6	0.3	0.0
DZR	Exposed daily	0	91.1	8.4	0.5	0.0	0.0
		96	87.5	10.5	2.0	0.0	0.0
Heart Fibroblasts	Exposed daily	0	89.4	5.8	2.7	1.8	0.4
		326	87.6	10.7	1.3	0.4	0.0

Table 2.11. Cell cycle distribution of cells exposed to derazoxane.

Cell Line	Duration of dexrazoxane exposure	Time (hr)[a]	Cell cycle distribution (%)[b] 2N	4N	8N	16N	32N	64N
CHO	Exposed daily	0	78.0	18.3	3.2	0.4	0.1	0.0
		21	42.3	41.7	15.0	0.9	0.1	0.0
		48	21.3	39.5	30.2	8.5	0.5	0.0
		72	14.5	34.6	33.4	16.1	1.3	0.0
		93	8.5	27.1	37.2	23.6	3.6	0.0
		121	2.8	21.4	41.7	29.1	4.9	0.0
		144	3.1	21.2	37.5	31.4	6.6	0.0
	Exposed at 0, 24 hr	0	58.5	33.4	5.9	1.8	0.4	0.0
		48	34.8	44.0	16.9	3.6	0.6	0.0
		92	14.2	23.6	26.3	23.9	11.3	0.8
DZR	Exposed daily	0	50.8	43.2	5.2	0.7	0.1	0.0
		96	50.8	39.7	8.0	1.3	0.4	0.0
Heart Fibroblasts	Exposed daily	0	53.1	36.7	9.8	0.5	0.0	0.0
		326	16.7	59.2	20.4	3.7	0.0	0.0

[a]Duration of exposure of cells to the dexrazoxane

[b]The cell cycle distribution was calculated by computer analysis ftom red (DNA) fluorescence histograms displayed in Fig. 2.19, 2.22, and 2.23
The number of cells residing within each successive ploidy phase was approximated by first, assuming non-definable S phases and second, dividing the number of counted cells between successive valley region midpoints by the total overall number of cells analyzed.

2.8 Epi-illumination fluorescence microscopy analysis of dexrazoxane-treated CHO cells

2.8.1 Introduction

Fluorescent molecules absorb light at one wavelength and emit light at another, longer wavelength. Through the use of specific fluorescent probes and stains various cellular structures, biological macromolecules, and organelles can be labelled and subsequently viewed microscopically. This is the concept of fluorescence microscopy. Sometimes the fluorescent molecule itself is a direct stain for specific structures. In other situations the fluorescent dye is bound to another non-fluorescent probe such as an antibody which recognizes specific structures. In the following section, the effects of dexrazoxane on essential mitotic structural components including DNA/nucleus, F-actin, microtubulin, and centrosomes was analyzed upon immunofluorescent and fluorescent labelling. Furthermore, the effect of dexrazoxane on the spatial localization and morphologies of such organelles as mitochondria, endoplasmic reticulum, and golgi apparatus was also examined by fluorescence microscopy. Finally, the structure of nuclear chromatin in dexrazoxane-treated CHO cells was examined for the purpose of correlating with the morphological development of their cellular state. More specifically, by the use of fluorescent dyes the posibility of dexrazoxane-induced apoptosis in CHO cells was investigated according to the degree of chromatin condensation or staining.

2.8.2 Materials

Cover glass slips (22x22 mm, no. 1½, cat. No. 12-541B) and glass slides (75x25 mm, cat. No. 12-550A) were obtained from Fisher Scientific (Fairlawn, NJ, U.S.A.). Culture plates (100x20 mm, cat. No. 25020) were obtained from Corning Glass Works (Corning, N.Y., U.S.A.). Hoechst 33258 (cat. No. B-2883), ethidium bromide (95%, cat. No. E-8751), acridine orange (cat. No. A-6014), bovine serum albumin (BSA, cat. No. A-3350), paraformaldehyde (cat. No. P-6148), anti-mouse IgG1 FITC conjugated secondary antibody (Cy3, cat. No. 2181) were obtained from Sigma Chemical Co. (St. Louis, MO, U.S.A.). Triton X-100 (cat. No. X198-5) was obtained from J.T. Baker Chemical Co. (Phillipsburg, NJ, U.S.A.). Rhodamine-labelled phalloidin (cat. No. R-415), DiOC6(3) (cat. No. D-273), BODIPY FLC_5-Ceramide (cat. No. D-352), JC-1 (cat. No. T-3168), ER-Tracker Blue White DPX (cat. No. E-12353), Mito-Tracker Green FM (cat. No. M-7514) were obtained from Molecular Probes, Inc. (Eugene, OR, U.S.A.). Anti-acetylated α-tubulin primary antibody (C3B9) was donated by K. Gull, (University of Manchester, UK). Mouse monoclonal antibody (TU-30) was donated by P. Draber, (Czechoslovakia). Acetone was obtained from Anachemia Ltd. (Toronto, ON). Methanol was obtained from Commerical Alcohols Inc. (Toronto, ON).

2.8.3 Methods

2.8.3.1 Drug treatment

CHO cells were grown as adherent cultures in T-75 flasks seeded at $2x10^6$ cells/flask or on sterile 22x22 mm (no. 1½) cover glass slips in 100x20 mm culture plates, seeded at $1.0x10^5$ cells/plate. After a 24 hr attachment period cells were treated twice at 0, 24 hr with 100 μM dexrazoxane, followed by daily media replacement. Control cells were seeded 24 hr prior to analysis. In Section 2.8.3.3, with respect to apoptosis quantitation both control and 96 hr dexrazoxane-treated CHO cells were harvested from T-75 flasks with trypsin-EDTA followed by resuspension in fresh media to an appropriate cell density.

2.8.3.2 Examining structural organization and organelle localization in dexrazoxane-treated CHO cells using fluorescence microscopy

After 96 or 144 hr of dexrazoxane exposure, both control and drug treated cells were prepared and stained for various cellular constituents according to the following procedures. As indicated where required, cells were either pre- or post-fixed using freshly prepared 3.7% (w/v) paraformaldehyde in PBS. In some instances unfixed live cells were stained prior to viewing. For the purpose of simplicity, protocols used for the preparation of live cells have not been included where the results of fixed cells were shown to be very similar if not identical. Cells were viewed on an Zeiss Photo II inverted microscope through 20X and/or 40X objective lens. Fluorescence was detected using DIC and/or epifluorescence optics with the appropriate filter sets, and images were captured with a Sony 3 chip colour cooled charge-coupled device (CCD) camera using the Northern

Exposure Imaging system. All images were processed by subtraction of camera dark noise and archived for later retrieval using custom designed software.

For the purpose of later discussion, previous unpublished fluorescence microscopy results attained from the staining of DNA, F-actin, microtubules, and centrosomes are included herein. CHO cells cultured and treated with dexrazoxane for these experiments were performed by Dr. Gaik-Lean Chee, previously in our laboratory. Fluorescent staining and viewing of microtubules and centrosomes from dexrazoxane-treated CHO cells was performed by Dr. Edward Byard (Department of Biology, University of Winnipeg). All other fluorescent staining and viewing was performed by Dr. Erwin Huebner (Department of Zoology, University of Manitoba).

DNA/nucleus staining: Cover slips were gently removed from media, fixed for 1 hr at RT after the addition of a few drops of 4% (w/v) paraformaldehyde in PBS, and then washed (3x) with 1-2 mL of PBS. Next, cells were stained for 30 min at RT after the addition of a 5:1000 μL dilution of stock Hoechst 33258 (1 mg/mL in 0.9% NaCl) with PBS, followed by washing with PBS (3x) as before. Cells were observed in fluorescence with the filter set for Hoechst.

F-actin staining: Cover slips were gently removed from media, fixed for 1 hr at RT after the addition of a few drops of 4% (w/v) paraformaldehyde in a microfilament stabilizing buffer (PEME, pH 6.9). Cells were then permeabilized and washed (3x) by incubation in 0.2% (v/v) Triton X-100 in PBS for 10 min each at RT. Next, cells were stained for 1 hr at RT after the addition of a 5:1000 μL dilution of rhodamine-labelled phalloidin (1 mg/mL in methanol) with PBS, followed by washing with PBS (2x) as before. Cells were observed in fluorescence with the filter set for rhodamine.

Microtubule staining: Cover slips were gently removed from media, fixed for 1 hr at RT after the addition of a few drops of 4% (w/v) paraformaldehyde in a microfilament stabilizing buffer (PEME, pH 6.9). Cells were then permeabilized and washed (3x) by incubation in 0.2% (v/v) Triton X-100 in PBS for 10 min each at RT, followed by blocking for 30 min with 0.5% (w/v) BSA in PBS-Triton X-100. Next, an anti-acetylated α-tubulin primary antibody (C3B9, from K. Gull, University of Manchester, UK) was added to each cover slip diluted 1:5 with PBS and incubated for 1 hr at 37°C. Cells were then washed (5x) for 10 min with PBS-Triton X-100, and incubated 1 hr at 37°C in the presence of a secondary FITC conjugated antibody (Cy3, Sigma). After a final washing step with PBS-Triton X-100 cells were observed in fluorescence with the filter set for fluorescein.

Centrosome (gamma tubulin) and DNA/nucleus double staining: Cover slips were gently removed from media, and washed (3x) with PBS. Cells were permeabilized, first by incubation in 100% methanol at –20°C for 20 min, followed by washing (3x) for 5 min with 33% (v/v) methanol in PBS. This was followed by further permeabilization (2x) with 0.2% (v/v) Triton X-100 in PBS for 10 min each at RT, followed by blocking for 30 min with 0.5% (w/v) BSA in PBS-Triton X-100. Cells were then post-fixed for 15 min at 37°C by the addition of a few drops of 4% (w/v) paraformaldehyde in PBS to the cover slip, followed by washing with PBS (2x) as before. Next, a mouse monoclonal IgG1 primary antibody (TU-30, P. Draber, Czechoslovakia) specific for γ-tubulin was added and incubated 1 hr at 37°C. Cells were then washed (2x) for 10 min with PBS, and incubated 1 hr at RT in the presence of a secondary FITC conjugated antibody (Cy3, Sigma). Cover slips were then washed with PBS and stained for 10 min with 10 μg/mL Hoechst 33342 in

PBS. After a final washing step with PBS cells were observed in fluorescence with filter sets for fluorescein and Hoechst.

Endoplasmic reticulum membrane staining: Cover slips were gently removed from media, fixed for 5 min at 37°C after the addition of a few drops of 3.7% (w/v) paraformaldehyde, and then washed twice with PBS. Cells were then permeabilized by incubation in 0.1% (v/v) Triton X-100 for 10 min at RT. Next, cells were stained for 30 min at 37°C after the addition of a 1:1000 μL dilution of stock ER-Tracker Blue White DPX (1 mM in DMSO) with PBS, followed by washing with PBS (2x) as before and placing in the dark. Cells were observed in fluorescence with the filter set for Hoechst.

Endoplasmic reticulum and/or mitochondria membrane staining: Cover slips were gently removed from media, and washed twice with PBS. Next, cells were stained for 10 min at RT after the addition of a 1:1000 μL dilution of stock DiOC6(3) (0.5 mg/mL in 100% ethanol) with PBS, followed by washing with PBS (2x) as before and placing in the dark. Cells were observed in fluorescence with the filter set for fluorescein.

Mitochondria membrane staining: Cover slips were gently removed from media, and washed twice with PBS. Next, cells were stained for 15 min at 37°C after the addition of 100 μL of stock Mito-Tracker green FM (1 mM in DMSO), followed by washing with PBS (2x) as before. Cells were then post-fixed fixed for 15 min at 37°C after the addition of a few drops of 3.7% (w/v) paraformaldehyde in PBS, followed by washing with PBS (2x) as before and placing in the dark. Cells were observed in fluorescence with the filter set for fluorescein.

Active vs. inactive mitochondria membrane staining: Cover slips were gently removed from media, and washed twice with PBS. Next, cells were stained for 10 min at RT after the addition of a 10:1000 μL dilution of stock JC-1 (1 mg/mL in DMSO) with PBS, followed by washing with PBS (2x) as before. Cells were observed in fluorescence with a long pass filter set for fluorescein. Active and inactive mitochondria were distinguished by a red or green fluorescence, respectively.

Golgi apparatus staining: Cover slips were gently removed from media, and washed twice with PBS. Next, cells were stained for 10 min at 37°C after the addition of a 1:200 μL dilution of stock BODIPY Ceramide (2.5 mM in ethanol) with BSA-MEM (0.34 mg/mL fatty acid-free BSA in MEM), followed by washing with PBS (2x) as before and placing in the dark. Cells were observed in fluorescence with the filter set for fluorescein.

2.8.3.3 Quantitation of apoptosis in dexrazoxane-treated CHO cells using fluorescent dyes

The chromatin organization in 96 hr dexrazoxane-treated CHO cells was examined by fluorescence microscopy for the purpose of quantitating the degree of apoptotic induction [42]. An explicit description of the protocol utilized for apoptosis quantitation, including sample preparation and evaluation criteria is explained later in Section 3.5.2.3 with respect to K562 cells. In brief, CHO cells were double stained by the addition of 4 μL of ethidium bromide/acridine orange (100 μg/mL in PBS) to 100 μL of cells in α-MEM/FCS, previously harvested with trypsin-EDTA. Cells were then mounted onto 75x25 mm glass cover slides and viewed by epifluorescence microscopy under a 40X objective lenses, employing an XF-19 filter set (Omega Optical, Brattleboro, VT). A

minimum of 1000 cells of normal size and larger were counted per sample. Apoptotic and necrotic positive control samples were generated by the treatment of CHO cells with 10 μM camptothecin daily for 48 hr and 70% (v/v) ethanol, respectively.

Acridine orange is a membrane permeable dye taken up by cells which may or may not possess an intact membrane. Upon binding DNA acridine orange fluoresces green in viable cells (and red-orange upon binding RNA or single stranded DNA). Conversely, ethidium bromide is a charged dye taken up by necrotic cells which possess damaged outer membranes and overwhelms acridine orange fluorescence. Upon binding DNA ethidium bromide fluoresces orange in non-viable and necrotic cells.

Based on the various morphological appearances, chromatin structures, and membrane integrity observed the percentage of each cell type was determined in relation to the total number of cells counted. Viable and non-viable apoptotic cells were identified on the basis of their fragmented nuclei and condensed chromatin beads around the periphery of the nucleus. The number of cells of each of the following four cellular states were counted: (i) VNA, viable cells with green non-apoptotic chromatin/nuclei and diffuse fluorescence intensity; (ii) VA, viable cells with green apoptotic chromatin/nuclei; (iii) NEC, necrotic or non-viable cells with orange normal chromatin/nuclei and diffuse fluorescence intensity; (iv) NVA, non-viable cells with orange apoptotic chromatin/nuclei. Photographs of cells were taken with a Nikon camera mounted on a photomicroscope with epifluorescence attachment. Kodak Ektachrome (Elitechrom) 400 daylight color slide film was used with the following setting under 40x objective lens: shutter control on, step setting of +1, set time of 4 sec, actual exposure time ~10 sec.

2.8.4 Results

2.8.4.1 Structural appearance and localization of fluorescently labelled cellular constituents

The effects of dexrazoxane on the structural organization and localization of various cellular constituents in CHO cells was assessed by epi-fluorescence microscopy after preparation and staining as described in Section 2.8.3.2. As shown in Fig. 2.24a under differential interference contrast (DIC), adherent CHO cells exposed to dexrazoxane for 144 hr were significantly larger in size with extensively developed pseudopodia as compared to control cells (inset). This result complements earlier observed morphologies of suspension cells (Section 2.5.4), and confirms as expected that culture conditions do not contribute to the observed effects of dexrazoxane on CHO cells. Preceeding the following results it was determined that CHO cells did not emit any natural fluorescence.

When compared to the control (Fig. 2.24, inset images) a number of significant changes in various structural components occurred in CHO cells after 144 hr of dexrazoxane exposure. DNA fluorescent staining of dexrazoxane-treated CHO cells with Hoechst 33258 showed large, highly fragmented, multi-lobed nuclei exhibiting varying morphologies (Fig. 2.24b). The variable number of individual nuclear lobes detected in these such cells is consistent with flow cytometry data of an increasing variation in DNA ploidy level with dexrazoxane exposure. However, it remains uncertain whether the exact number of nuclear lobes constitutes a good estimate of the actual ploidy level of these cells. In some cases, these DNA-stained nuclear lobes were separated by pockets of space within the cell, thus suggesting a conceivable attempt of the dexrazoxane-treated CHO cells to separate daughter chromatids (data not shown).

When stained with rhodamine-labelled phalloidin 144 hr dexrazoxane-treated CHO cells were shown to possess an elaborate and extensive array of F-actin microfilaments (Fig. 2.24c). This dense network of cross-linking confirms the important role of F-actin in providing mechanical strength to the cytoskeletal structure of a cell, particularly in such enlarged cellular structures as seen here. Similarly, immunofluorescence staining using an anti-acetylated α-tubulin antibody revealed the presence of large, well developed networks of microtubule fibers (Fig. 2.24d). Occasionally it was noticed that a few large dexrazoxane-exposed cells appeared to be in the process of cell division. The role of microtubule fibers in the regulation of cell shape and the plane of division was exemplified by the appearance of a cell division midbody between two such dividing cells (data not shown). Anti γ-tubulin fluorescent staining of centrosomes showed that control cells possessed 1-2 centrosomes (Fig. 2.24e, inset), each presumably containing a pair of centrioles consistent with normal mitotic cell cycling. In comparision, after 144 hr of dexrazoxane exposure, CHO cells possessed multiple spindle poles, or centrosome pairs (Fig. 2.24e). This result combined with the observed presence of multiple nuclear lobes clearly indicates that cell cycling continues to occur in dexrazoxane-treated CHO cells in the absence of cytokinesis.

Fluorescent staining with ER-Tracker Blue-White DPX and Mito-Tracker Green FM specifically identified extensive networks of endoplasmic reticulum (Fig. 2.25a), and mitochondria (Fig. 2.25b) respectively in 96 hr dexrazoxane exposed CHO cells. As compared to control cells (inset) and previous reports of similar fluorescent staining analyses [43,44] these patterns of organelle localization and morphology appeared to be normal. Mitochondria appeared as long discontinuous filaments and as tiny circular or

granular objects clustered mainly about the nuclear region. This was clearly identifiable in dexrazoxane-treated CHO cells, perhaps suggesting increased ATP requirements. On the other hand endoplasmic reticulum were not as distinct in shape or size as mitochondria and their relative localization was found to be generally about the entire cell, with a somewhat heavier staining around the nuclear region. Endoplasmic reticulum were also fluorescently stained with DiOC6(3) (Fig. 2.25d). This dye primarily stains the membrane of endoplasmic reticulum, but when used at high concentrations or for longer durations of exposure mitochondrial membranes are also stained, indiscriminately. In light of this fact, endoplasmic reticulum appeared as a dense network of organelles streaming outward from the nucleus much like Mito-Tracker Green FM staining of mitochondria.

In order to possibly assess the fraction of active mitochondria existing in CHO cells after 96 hr of dexrazoxane treatment cells were stained with JC-1 (Fig. 2.25c). By the use of this fluorescent dye active and inactive mitochondria can be discerned by either a red or green fluorescence, respectively. Due in part to an inadequate solubilization of the dye the image revealed in Fig. 2.25c is not the most ideal. Although both active (red) and inactive (green) mitochondria appeared as tiny dots it is uncertain whether dexrazoxane-treated cells possessed a relatively higher proportion of one as oppposed to the other. Finally, dexrazoxane-treated CHO cells were fluorescently stained for Golgi apparatus with BODIPY ceramide (Fig. 2.25e). These organelles appeared normal without any distinctive shape, size, or discernment of separate components much like the speckled appearance of endoplasmic reticulum as previously noted. Also, in a similar fashion to other organelles golgi apparatus were generally distributed about the entire area of the cell with a greater proportion centered around the nuclear region.

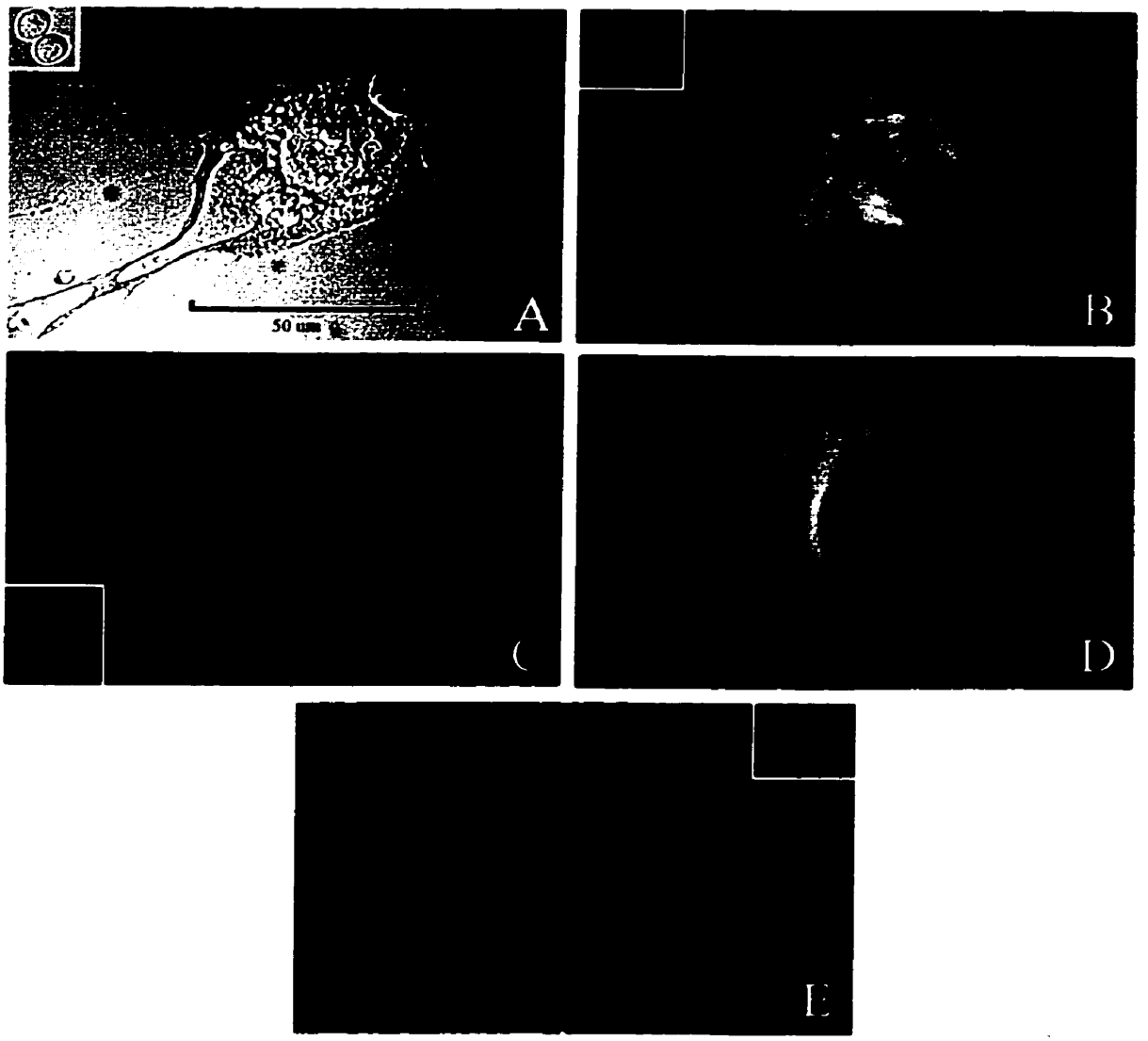

Fig. 2.24. Bright field and fluorescent photomicrographs depicting the structural organization of attached CHO cells treated with dexrazoxane twice for 144 hr. Under DIC optics **(A)**, there was an evident enlargement in cell size, change in morphology, and the development of pseudopodia as compared to control cells ***(inset A-E)***. DNA staining with Hoechst 33258 **(B)**, revealed significantly enlarged nuclear regions that contained a variable number of multiple lobes. An extensive F-actin microfilament array **(C)** was seen in these cells, as revealed by rhodamine-labelled phalloidin staining. As well, an extensive microtubule array **(D)** was revealed by immunofluorescence upon secondary FITC staining to a specific anti-acetylated α-tubulin primary antibody. As compared to control cells, dexrazoxane-treated cells possessed multiple centrosomes **(E)**, upon immunofluorescence staining with anti-gamma tubulin. This observation indicates that cell cycling and centrosome doubling is continuing to occur in the absence of cytokinesis. All images are as seen under a 40X objective lens. Control images for **(D)** were unfortunately not taken.

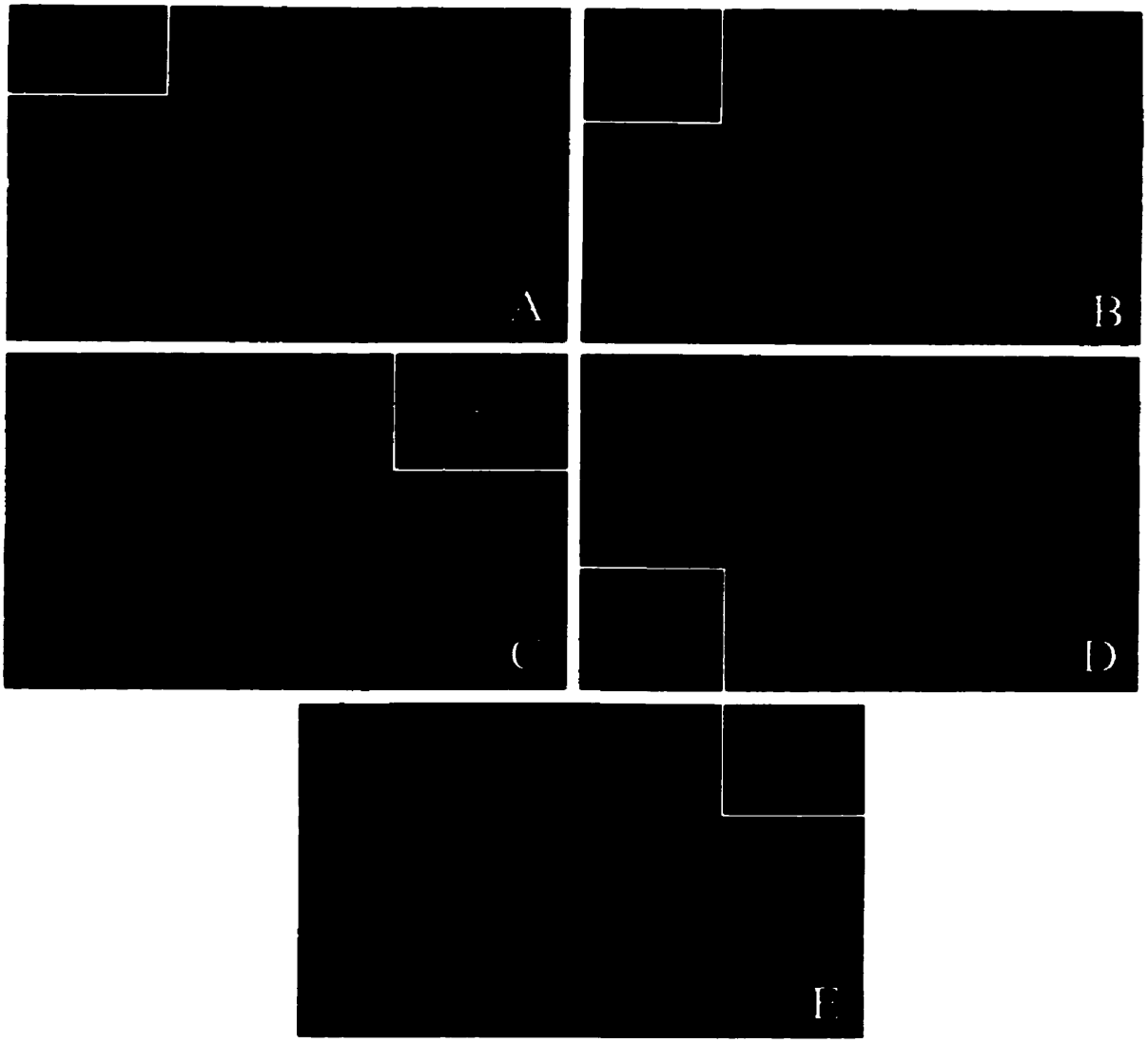

Fig. 2.25. Fluorescent photomicrographs depicting the localization of various organelles in attached CHO cells treated with dexrazoxane twice for 96 hr. Fluorescent staining with ER-Tracker Blue White DPX and MitoTracker Green FM clearly identified an extensive network of endoplasmic reticulum **(A)**, and mitochondria **(B)**, respectively which streamed outward as elongated discontinuous filaments. The intense concentration of mitochondria about the nuclear region **(B)** is suggestive of area requiring a high demand for ATP. Fluorescent staining with JC-1 **(C)** revealed that these mitochondria were both active (red) and inactive (green). The extensive network of both of endoplasmic reticulum and mitochondria was further confirmed after non-discriminate fluorescent staining with DiOC6(3) **(D)**. Fluorescent staining for Golgi apparatus with BODIPY Ceramide **(E)** revealed an inconclusive extensive network similar to the other examined organelles. All images are as seen under a 40X objective lens.

2.8.4.2 Morphological characterization of chromatin patterns

As shown in Fig. 2.26d, fluorescent photomicrographs taken of 96 hr dexrazoxane-treated CHO cells revealed chromatin patterns and staining consistent with nonapoptotic cells, either viable (green) or nonviable/necrotic (orange). These cells which were enlarged in size as compared to control cells (Fig. 2.26c) exhibited relatively normal variations in fluorescent intensity, although they possessed multiple nuclear lobes. This non-uniform staining of chromatin is reflective of a normal distribution of heterochromatin (condensed and nontranscribed) and euchromatin (less condensed and transcribed) [42], and perhaps suggests normal mitotic cycling in the absense of cytokinesis. In order to validate the ethidium bromide/acridine orange staining technique positive controls for apoptotic and necrotic cell death (Fig. 2.26a and 2.26b) were generated by exposure to 10 μM camptothecin and 70% (v/v) ethanol, respectively. The chromatin pattern in apoptotic nuclei appeared uniformly stained taking the form of crescents around the periphery of the nucleus, or as groups of featureless, bright spherical beads (*arrow #1*). Necrotic control cells on the other hand possessed normal variations in chromatin staining, and were generally the same size as untreated CHO cells. Quantitation of the percentage of morphogical cell types present upon dexrazoxane exposure revealed very little change as compared to control cells (Table 2.12). After 96 hr of dexrazoxane treatment the cell population consisted of 88% viable non-apoptotic (VNA), and 12% necrotic (NEC), and essentially no apoptotic cells, viable or non-viable. Overall, these results suggest that although dexrazoxane induces a small decrease in CHO cell viability with time (Section 2.4.3.2) it is not necessarily attributable to the induction of apoptosis.

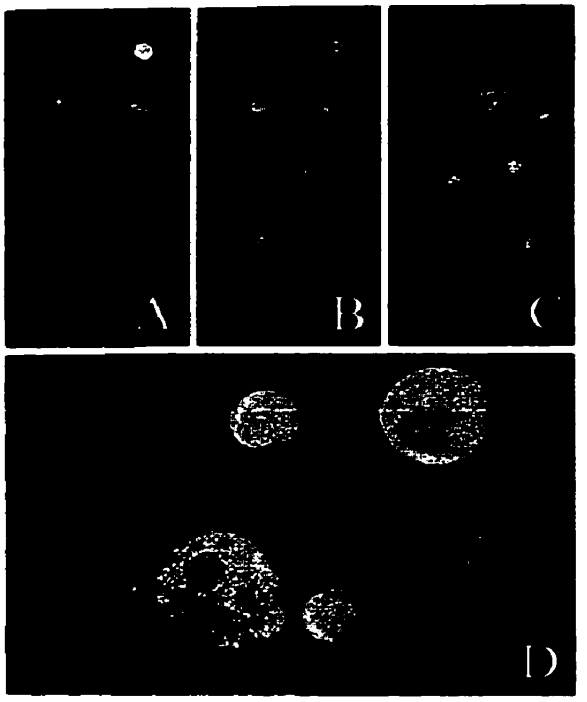

Fig. 2.26. A comparison of chromatin organization in 96 hr dexrazoxane-treated CHO cells with apoptotic and nectrotic controls. Apoptotic **(A)** and necrotic **(B)** controls were prepared by exposure to 10 μM camptothecin for 48 hr and overnight exposure to 70% (v/v) ethanol, respectively. Exponentially growing CHO cells **(C)** were exposed to 100 μM of dexrazoxane at 0, 24 hr with daily media replacement and subsequently examined and characterized **(D)** as described in Section 3.5.2.3. Apoptotic cells were identified by fragmented nuclei, and bright, uniformly fluorescent spherical beads of condensed chromatin spread around the periphery of the nucleus ***(arrow #1)***. Non-apoptotic cells undergoing mitosis in the absence of cytokinesis were identified by the presence of multiple nuclear lobes, and varying degrees of fluorescent staining chromatin and nuclear compaction ***(arrow #2)***. All images are as seen under a 40X objective lens.

Table 2.12. Characterization of various morphological cellular states in CHO cells by chromatin pattern analysis after dexrazoxane exposure.

Duration of dexrazoxane exposure[a] (hr)	Number of cells counted[b] VNA (%)	NEC (%)	VA (%)	NVA (%)	Total (%)
0	1066 (91%)	105 (9%)	0 (0%)	0 (0%)	1171 (100%)
96	1465 (88%)	204 (12%)	0 (0%)	1 (0%)	1670 (100%)

[a] Attached CHO cells were exposed to dexrazoxane at 0, 24 hr with daily media replacement, then harvested and double stained with ethidium bromide/acridine orange.

[b] The percentage of viable non-apoptotic (VNA), necrotic (NEC), viable apoptotic (VA), and non-viable apoptotic (NVA) were determined as described in Section 3.5.2.3 after mounting onto glass slides and viewing by epi-fluorescence microscopy.

2.9 Ultrastructural examination of cell morphology in dexrazoxane-treated CHO cells using transmission electron microscopy

2.9.1 Introduction

The limiting separation at which two objects can still be seen as distinct under a light microscope is just under 0.2 μm. By comparison the resolution achieved under an electron microscope is about 100 times greater [45]. Although the prinicpal features of both types of microscopes are very similar, one focuses light while the other focuses electrons. Contrast in an electron microscope is directly proportional to the atomic number of the atoms in a specimen. As electrons impinge upon the sample some are scattered according to the local density of the specimen whereas others pass through and are focused to form an image, thus achieving a very high degree of ultrastructural resolution [45]. It was primarly due to this reason alone that dexrazoxane-treated CHO cells were structurally analyzed further using transmission electron microscopy as described in the following section.

2.9.2 Materials

Potassium phosphate monobasic (KH_2PO_4, cat. No. P-286) was obtained from Fisher Scientific (Fairlawn, NJ, U.S.A.). Potassium hydroxide (1M KOH, cat. No. 5282) was obtained from Mallinckrodt Specialty Chemicals Co. (Paris, KT, U.S.A.). Glutaraldehyde (50%, cat. No. G-7651) was obtained from Sigma Chemical Co. (St. Louis, MO, U.S.A.).

2.9.3 Methods

Phosphate buffer: A solution of 0.1 M phosphate buffer was prepared by dissolving 0.54436 g of KH_2PO_4 in ddH_2O, titrated to 40 mL and a pH of 7.4 with 1 M KOH.

Glutaraldehyde fixative: A 40 ml solution of 2.5% (w/v) glutaraldehyde was prepared by adding 2 mL of 50% (w/v) glutaraldehyde to 38 mL of 0.1 M phosphate buffer, pH 7.4 followed by filtration through a 0.2 μm acetate filter, and storage at 4°C in an amber bottle.

CHO cells were grown as suspension cultures in double sidearm suspension spinner flasks, seeded initially at $2.0x10^5$ cells/mL and exposed to 100 μM dexrazoxane daily with media replacement as previously described (Section 2.7.3.1). Approximately $5x10^6$ cells were collected in replicate from control and 96 hr dexrazoxane-treated cultures, washed once with PBS by centrifugation at 250 *g* for 7 min, and resuspended in 0.5 mL of 2.5% (w/v) glutaraldehyde fixative solution in PBS with a Pasteur pipet. Samples were then sent to Dr. Victor Ferrans at NIH, Bethesda, MD, U.S.A. on top of partially frozen ice packs. Upon arrival, samples were post-fixed with 1% (v/v) osmic acid in 0.1 M phosphate buffer, pH 7.3, dehydrated with graded ethanol and propylene oxide, and embedded in PolyBed #812 Epoxy resin. After trimming, ultrathin sections were made using a microtome. Sections were then stained with uranyl acetate and lead citrate, and viewed on a JEOL 1200EX electron microscope.

2.9.4 Results

Transmission electron microscopy was used in part to structurally analyze the nuclear architecture of dexrazoxane-treated cells under a higher resolution as well as a means to examine for characteristic features of apoptosis. As expected, electron photomicrographs of control CHO cells under 800X magnification were shown to contain 1-2 nuclear lobes, consistent with the normal progression of the cell cycle (Fig. 2.27a). CHO cells treated with dexrazoxane for 96 hr displayed varying degrees of hypersegmentation into multiple nuclear lobes, suggesting continued cycling in the absence of cell division (Fig. 2.27b). This result complements earlier observations made using fluorescence microscopy (Section 2.8.4.1) and is consistent with the varying ploidy levels previously identified in these cells (Section 2.7.4). Due to the nature of this photomicrograph being acquired from a single thin section, it is very likely that some of these lobes may be one in the same, going into and out of the page. The lack of separation amongst these structures further suggests that they may in fact be nuclear lobes as opposed to individual nuclei.

Upon further examination of ultrastructural morphology it was seen that after 96 hr of dexrazoxane exposure CHO cell structure, in terms of size and shape diversified from that of the control. For the most part control cells appeared circular in nature with some blebbing or degeneration of the outer membrane, perhaps associated with the fixation treatment. In addition, some cells did not possess a definable nuclear structure suggesting that these were interphase cells with diffuse forms of chromatin. Dexrazoxane-treated cells were obviously larger in size with slightly more extensive morphologies. Although a few cells contained cytoplasmic hydrophobic vacuoles the increased cell size was clearly

not attributable to osmotic changes. In addition, some dexrazoxane-treated cells exhibited features of outer membrane blebbling and on occasion degeneration of the entire cellular structure into fragments.

When cells were viewed under an even higher magnification (3000X) nuclear and cytoplasmic structures such as chromatin and organelles could be resolved (data not shown). Mitochondria and endoplasmic reticulum appeared normal in shape and size, and could be found generally distributed about the nuclear region. In addition, nuclear lobes contained several nucleoli exhibiting various normal degrees of chromatin granularity or condensation. Overall, dexrazoxane-treated cells did not exhibit any of the characteristic ultrastructural features of apoptosis. Such features would have included margination of condensed chromatin to the periphery of the nucleus, accompanied by convolution of the nuclear membrane. Furthermore, late-stage apoptotic cells would have possessed very large uniformly dense areas of condensed chromatin, and possibly no identifiable cytoplasmic structures [46]. The cell death of some dexrazoxane-treated cells appeared to be instead consistent with necrosis, as characterized by uncontrolled cell swelling and the disruption of membrane integrity followed by cell lysis.

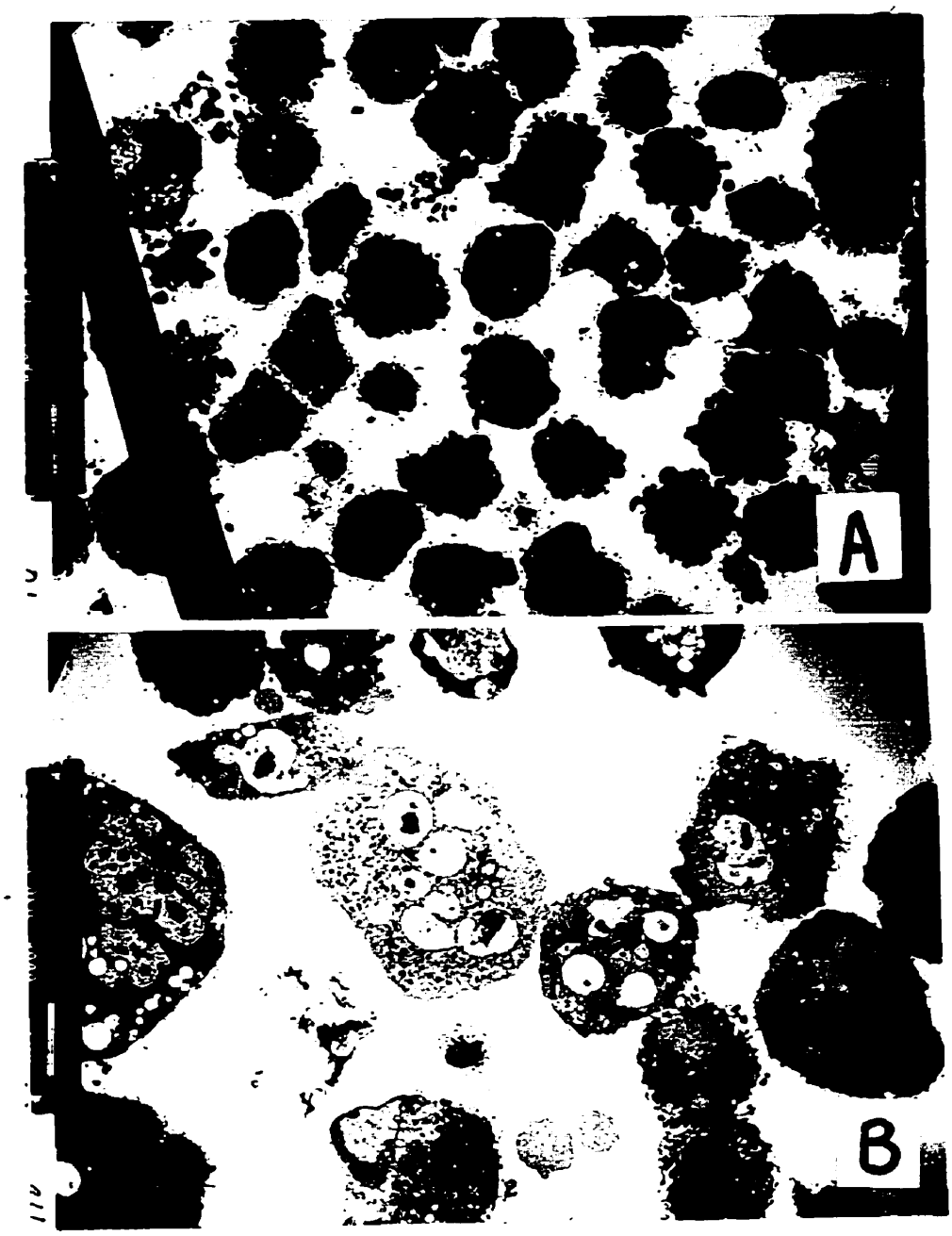

Fig. 2.27. Transmission electron photomicrographs of suspension CHO cells exposed to dexrazoxane daily for 96 hr. CHO cells were fixed with glutaraldehyde, embedded in epoxy, sectioned, stained with heavy metals, and analyzed for ultrastructural organization using transmission electron microscopy (800X). Control cells **(A)**, were generally circular in nature, possessing a single nuclear structure. After 96 hr of dexrazoxane exposure **(B)**, cells were noticably different in shape and size, and possessed multilobed nuclei. With respect to the single section nature of this micrograph some individual nuclear lobes may actually be adjoined through a separate sectioning. Measurement bar at the side is representative of 10 μm.

2.10 Three-dimensional examination of nuclear organization in dexrazoxane-treated CHO cells using confocal fluorescence microscopy

2.10.1 Introduction

Biological material is essentially organized into four dimensions: three spatial ones and one temporal one. With respect to resolution and cellular organization, confocal scanning microscopy clearly permits this information to be more accessible than conventional methods of microscopic analysis. With the best attributes of both light and electron microscopy, confocal scanning microscopy allows for the direct visualization of the three-dimensional structure of biological objects without the need for fixation or dehydration. With the use of a computer, stereoscopic images are collected in series using optical sectioning to create a three-dimensional array of the biological material. The main advantage over normal light microscopy is its ability to generate a high quality of transverse resolution by effectively suppressing the contributions of out-of-focus areas in the specimen [47]. In the following section, dexrazoxane-treated CHO cells were stained for DNA and viewed using confocal scanning fluorescence microscopy in an effort to achieve improved resolution of the structure and orientation of the multiple nuclear lobes previously identified (Section 2.8).

2.10.2 Materials

Cover glass slips (22x22 mm, no. 1, cat. No.12-542B) were obtained from Fisher Scientific (Fairlawn, NJ, U.S.A.). Culture plates (100x20 mm, cat. No. 25020) were obtained from Corning Glass Works (Corning, N.Y., U.S.A.). Propidium iodide (cat. No. P-4170) and formaldehyde (37% formalin, cat. No. F-1635) were obtained from Sigma Chemical Co. (St. Louis, MO, U.S.A.). Dulbecco's phosphate buffered saline (PBS, cat. No. D-5652) was obtained from Gibco-BRL, Life Technologies Inc. (Burlington, ON).

2.10.3 Methods

CHO cells were grown as adherent cultures on sterile 22x22 mm (no. 1) cover glass slips in 100x20 mm culture plates, seeded at $1.0x10^5$ cells/plate. After a 24 hr attachment period cells were treated twice at 0, 24 hr with 100 μM dexrazoxane, followed by daily media replacement. Control cells were seeded 24 hr prior to analysis. After 96 hr of dexrazoxane exposure both drugged and control cover slips were placed into individual 50 mL conical centrifuge tubes containing 10% (v/v) formaldehyde prepared fresh in PBS. These cover slips, containing cells were then sent to Dr. Victor Ferrans at NIH, Bethesda, MD, U.S.A. where they were treated with Rnase A and stained for DNA with propidium iodide. Samples were then examined by optical sectioning using confocal scanning fluorescence microscopy with excitation at 568 nm on a Leica TCS (Deerfield, IL, U.S.A.) microscope equipped with an argon-krypton laser.

2.10.4 Results

In an effort to better visualize the multiple nuclear lobes generated in dexrazoxane-treated CHO cells with greater stereoscopic effectiveness confocal scanning fluorescence microscopy was used. The serial photomicrograph images displayed in Fig. 2.28 with respect to both control (*upper panel*) and 96 hr dexrazoxane-treated (*bottom panel*) cells clearly allowed for a three-dimensional visualization of the number of nuclear lobes present and their configuration about the cell, as a whole. As expected, control cells contained 1-2 nuclear lobes consistent with normal mitotic cell cycling. After 96 hr of dexrazoxane exposure, CHO cells possessed multiple nuclear lobes oriented in a donut-shape pattern about the central region of the cell. Previous two-dimensional epi-fluorescence double staining for DNA and centromeres had suggested that multiple centrosomes pairs were coordinated in this central region of the cell (data not shown). These results acquired from three-dimensional scanning clearly implies that the development and arrangement of multiple nuclear lobes in dexrazoxane-treated cells occurs in a concerted manner.

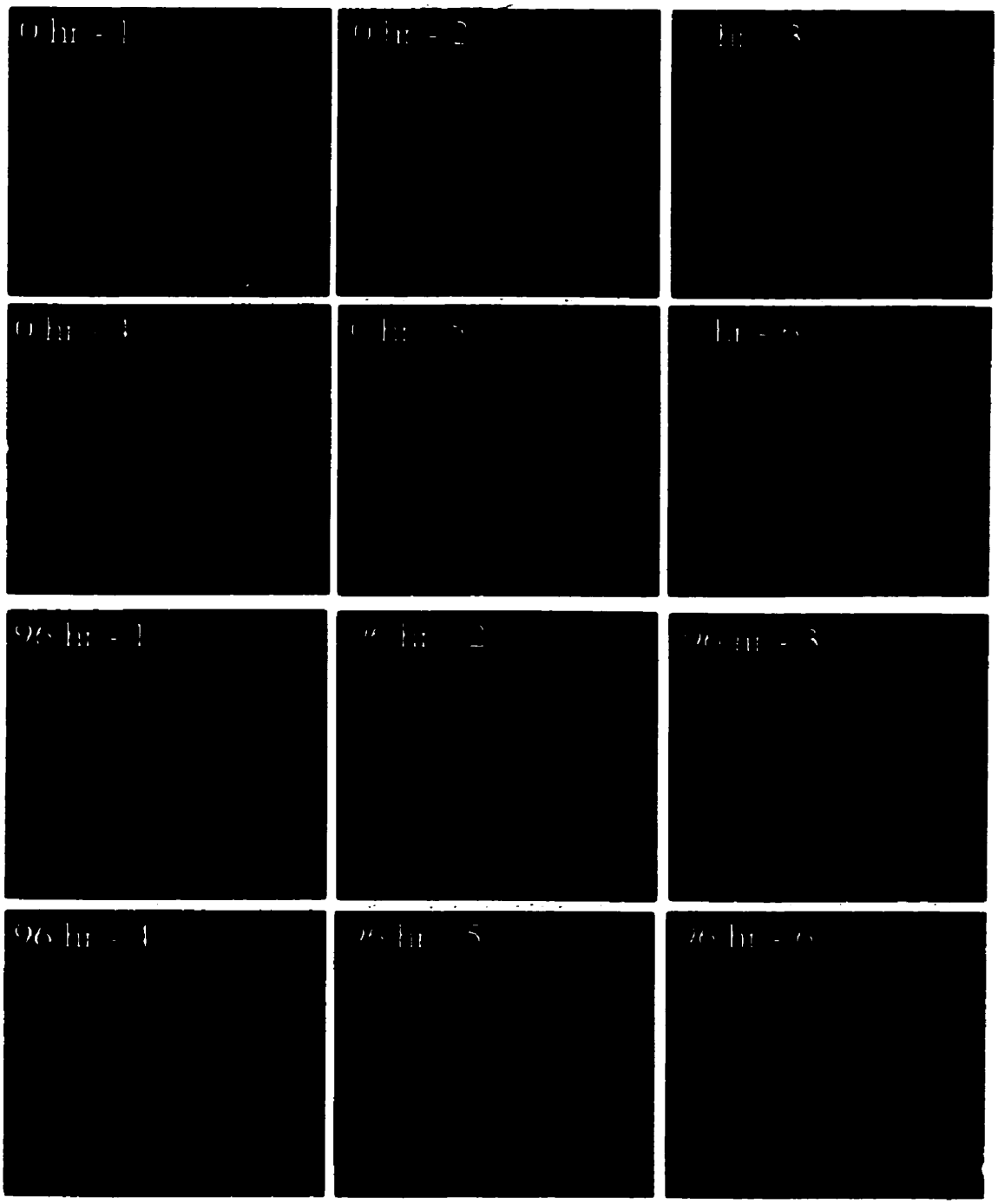

Fig. 2.28. Confocal photomicrographs of adherent fluorescent-stained (DNA) CHO cells treated with dexrazoxane twice for 96 hr. Cells were fixed with formalin, stained for DNA with propidium iodide, and imaged in serial sections (1000X) using confocal microscopy. Control, unexposed cells contained as expected, 1-2 nuclear lobes (*top panel*). After 96 hr of dexrazoxane exposure, cells possessed multiple nuclear lobes (*bottom panel*), arranged in a donut-shape orientation about the central region of the cell.

2.11 Discussion

2.11.1 MTT vs. cell counting cytotoxicity analysis

The cytotoxicity of dexrazoxane towards CHO and DZR cells as determined by MTT and cell counting analysis is discussed in the following section. The cytotoxicity survival curves for CHO and DZR cells generated by either method of analysis resulted in nearly identical monophasic curves (Fig. 2.2), and consequently IC_{50} values which differed by ~30% (Table 2.1). Although these slight discrepancies existed, the dexrazoxane resistance factor of DZR cells to CHO cells by either method were nearly the same; 430-fold resistant by MTT analysis and 471-fold resistant by cell counting analysis. This result suggests that either method of cytotoxicity analysis is equally reliable in accurately assessing the level of drug-resistance as compared to parental cells.

The main principle of the MTT assay states that the level of formazan produced by the bioreduction of MTT is directly proportional to the number of viable cells present [25]. However, a direct comparison of the cytotoxicity profiles generated by MTT and cell counting analysis for CHO cells revealed a slight discordance with this principle (Fig. 2.2). Although each curve appeared to be monophasic in nature the MTT cytotoxicity profile plateaued at about 30%, never dropping to near zero. Previous determinations have shown that for concentrations of dexrazoxane above 1000 μM the cytotoxicity profile does in fact drop to near zero, creating a biphasic curve [22]. It is suspected that the cytotoxicity at these high dexrazoxane concentrations for both CHO and DZR cell lines might be due to the depletion of free calcium or magnesium from the growth medium by ADR-925 [22]. Although few CHO cells remained in culture after 72 hr of exposure to high dexrazoxane

concentrations (10-1000 μM) these cells are presumed to have possessed an increased capacity for reducing MTT to formazan, as revealed by the higher absorbance values seen in this region. Upon microscopic examination these cells were observed to be significantly larger than normal. It is likely that an increased mitochondrial reductase potential in these cells permitted the same level of formazan production as would be a higher number of normal sized cells. As a result, the MTT cytotoxicity profile plateaued at higher dexrazoxane concentrations creating the illusion that cell kill was not as significant as the cell counting analysis had proven it to be. The growth-inhibiting activity of agents similar to dexrazoxane which may induce such effects should therefore be evaluated by MTT with caution due to the possible underestimation of its actual cytotoxic effects.

When CHO cell growth inhibition by dexrazoxane was evaluated under conditions of periodic media/drug replacement (Fig. 2.3) the resulting IC_{50} values did not differ much from single exposure non-intervening trials (Table 2.1). This result suggests that an increased number of exposures does not necessarily increase the rate of cytotoxic cell death, provided that others factors such as nutrience deprivation are eliminated as possible contributors. Additionally, this complements subsequent data which showed irrespective of the number of exposures cell viability gradually depreciated at the same rate (Fig. 2.7). The cytotoxicity profiles from all three dexrazoxane exposure protocols indicated in Fig. 2.2a and Fig. 2.3 were generally the same. When daily exposure was accompanied by media replacement absorbance values were noticably higher than the other drugging regimens even though all plates were seeded with the same number of cells and the profile trends were generally the same. This result presumably occurred due to the maintenance

of optimal growth conditions with daily replacement of media which possibly allowed for a greater number of large cells to remain viable.

2.11.2 Continuation of balanced growth in the absence of cell division

The cytotoxic effects of the bisdioxopiperazines have previously been examined both *in vivo* and *in vitro* in a variety of different cell types [13,15,17,48]. One of the most prominent observations in these and other studies is that the drug concentration and the length of exposure required to produce a inhibition of cell division and/or the desired cytotoxic effect varies with cell type. A single exposure to ICRF-159 has been shown to completely halt the division of such cell lines as CHO [18], B16 melanoma [49], and BHK-21S [17]. In other cases, upon replacement with drug-free media cell division is only transiently inhibited by ICRF-159 and such cell lines as EMT6 [19], lymphoma P_3J [48], and HeLa [6] proceed to divide once again.

These and other studies together suggest that in order to successfully inhibit the division of a given population, two important factors must be considered: (i) drug concentration; is it sufficient enough to adequately provide maximum topoisomerase II inhibition, and/or (ii) the exposure protocol used; will it ensure that cell proliferation is not transiently inhibited. Normally under physiological conditions dexrazoxane undergoes a slow ring-opening hydrolysis [30,50] with a half-life of 9.3 hr such that after a 12 hr period from initial exposure ~40% of the unhydrolyzed topoisomerase II-inhibitory form [16] remains in the growth medium. With the knowledge that dexrazoxane effects cells cycling through the G2 phase [37,48] and that a typical cell population cycles in a non-synchronous manner it was important in the present study to choose a dexrazoxane

concentration and exposure protocol that would ensure that eventually all cells in the population would be effected.

A concentration of 100 μM dexrazoxane was chosen combined with a dual (0, 24 hr) or daily drugging protocol to ensure maximum inhibition of growth in all cell lines tested. Initial experiments with respect to CHO cells demonstrated that this concentration, which was 20 times greater than the median inhibitory concentration of 5.2 ± 0.4 μM (Fig. 2.2) would sustain growth inhibition irrespective of the number of exposures (Fig. 2.4). Therefore, given a CHO doubling time of ~12-16 hr (Table 2.2) a dexrazoxane treatment protocol of at least two exposures (0, 24 hr or daily) was presumed to establish a condition of continual topoisomerase II inhibition whereby those cells not already in G2 phase would eventually be affected. In fact, other studies have similarly found that complete growth inhibition could be established either with daily media and drug changing as in the case of RPMI 8402 cells exposed to 50 μM ICRF-154 or 10 μM ICRF-193 [15], or drug exposure for twice the cell cycle time as in the case of P_3J cells exposed to 37 μM dexrazoxane [48].

As one of several explanations discussed herein, the propensity of a given cell population to seemingly overcome topoisomerase II inhibition and to continue to divide may be in part related to their inherent rate of proliferation. Rapidly growing cell populations are commonly more sensitive to brief exposures to ICRF-159 or dexrazoxane than slower growing populations [48]. As a consequence, cytotoxicity is commonly more pronounced in faster dividing populations [6,48]. Although our results do not entirely agree with this theory, perhaps due to the concentration and type of topoisomerase II inhibitor used it is likely that other factors inherent to each particular cell line such as the

level of topoisomerase II expression or activity [51] influence the degreee of cytotoxicity incurred irrespective of being fast or slow growing.

In the present study, CHO cells grown as adherent or suspension cultures and exposed to dexrazoxane twice (at 0, 24 hr) or daily were completely inhibited from further cell division (Fig. 2.6 and 2.7). In a similar fashion, a normal slow growing population of primary heart fibroblast cells were also completely inhibited from further division (Fig. 2.8). Although cell division was clearly inhibited in both cell lines, the growth inhibitory effect of dexrazoxane was not distinctly apparent. Instead cells became progressively less viable only after extended periods of exposure, suggesting that although topoisomerase II was being inhibited, key downstream events necessary for the initiation of cytodestruction were not readily occurring as quickly as citied in other cell lines [48]. Perhaps as well, the replenishment of nutrients with daily media changing may have contributed in part to the maintenance of a healthier population.

Concomitant with the inhibition of cell division by dexrazoxane, CHO cells observably increased in size and shape taking on a variety of morphologies (Fig. 2.9). After 120 hr of exposure a wide distribution of CHO cell sizes were identified (Fig. 2.10) with the largest observed cells exhibiting diameters of 52 μm (Fig. 2.10b), and a mean population-wide cell volume which had increased 9-fold from the control (Table 2.4). In contrast, the marginal increase in heart fibroblast cell volume after 300 hr of dexrazoxane exposure was deemed insignificant, although cell division was similarly completely inhibited (Fig. 2.12 and 2.13). Alterations in morphology and cell size is not an uncommon effect of the bisdioxopiperazines. Although similar features of cell enlargement have been citied in BHK-21S [52,53], B16 melanoma cells [49], hamster

fibrosarcoma T17 cells [6], and RPMI 8402 human leukemic cells [15] exposed to ICRF-159 a key question to be considered is whether this form of cell growth occurs in an unbalanced fashion.

Exposure of proliferating cells to chemotherapeutic agents that interfere with DNA synthesis and arrest cells in the division cycle can result in a state of unbalanced cell growth in which cell volume can become abnormally enlarged [54-56]. In some instances this abnormal increase in cell size may simply signal an immediate response of tumor cells to therapy, wherby the consequential endpoint is cell death [56]. Unbalanced growth is characterized by the disportionate synthesis of proteins, RNA and other macromolecules [55] leading to the accumulation of cell mass [54] and eventual hydrolytic cell death [55]. Upon analysis after 120 hr of dexrazoxane exposure the mean protein and DNA content in CHO cells increased 5.4-fold and 3.8-fold respectively in a relatively linear fashion (Fig. 2.16a, b). Furthermore, as CHO cell size increased without further cell division the ratio of protein/DNA content fluctuated slightly and compared highly with control levels taken at the same time intervals (Fig. 2.16c). These results clearly suggest the continuation of a balanced form of growth, and lend some explanation to the maintenance of cell viability in absence of cell division. Similar conclusions made in earlier studies of murine leukemia L1210 [18] and mouse-embryo fibroblast cells [13] exposed to ICRF-159 further serve to complement our findings.

2.11.3 Polyploidization through the inhibition of cytokinesis

Cell cycle studies have indicated that the cytotoxicity of the bisdioxopiperazines is cell cycle phase dependent. Specifically, ICRF-159 [18,48,57], dexrazoxane [37,48], and ICRF-193 [15] have been proposed to effect cells cycling through G2 phase. As a result it is not uncommon to identify cells presumably arrested in a G2/M state, or cycling on towards higher ploidy levels as cell size increases concomitantly [6,52]. An accumulation of cells with a tetraploid (8N) content of DNA have been identified in BHK-21S [17], murine leukemia L1210, and Friend leukemia cells [18] treated with razoxane (ICRF-159), and in P_3J [48], murine sarcoma S180 [58], and human ovarian carcinoma A2780 cells [37] treated with dexrazoxane. In each of these cases due to a constrained and limited linear scale analysis of DNA fluorescence, and/or a shorter duration of exposure, the highest observed ploidy levels fell short of those levels detected herein.

CHO cells exposed to dexrazoxane were found to increase in cell size, continue to cycle, and undergo further DNA synthesis without cell division attaining ploidy levels ranging from 2N to 64N (Fig. 2.19 and 2.20). By using back-gating analysis a direct correlation was made between increasing DNA ploidy level and increasing cell size (Fig. 2.21). The identification of ploidy levels as high as 64N after an extended period of dexrazoxane exposure indicates that in CHO cells the catalytic inhibition of topoisomerase II does not per se result in a complete cell cycle arrest. While these results do not indicate a clear selective depletion of G0/G1 cells for a single high ploidy level there does appear to be a progressive inhibition towards further cycling. Some cells presumably became held up from further synthesizing DNA while others were permitted to cycle on towards even higher ploidy levels (Table 2.11). Another, perhaps complementary explanation would

suggest that some dexrazoxane-induced polyploid CHO cells were able to segregate their entangled chromsomes enough to permit division. This possibility is not totally without reason given that a razoxane-induced mutant polyploid (6-12N) EMT6 mouse tumor cell line has been previously established, able to stably divide [19]. Contrary to the trend identified in dexrazoxane-treated CHO cells, primary heart fibroblasts cells exposed to dexrazoxane were found to accumulate in G2/M phase, suggesting a cell cycle phase-specific blockage. This determination was arrived at due to the clear depletion of S phase cells after 326 hr of exposure, complemented by the accumulation of 4N cells in G2/M, and a small fraction of cells with tetraploid (8N) DNA content (Fig. 2.23).

A key factor which may serve to define the differing propensities of cell lines towards polyploidization is the fidelity of the topoiosmerase II-dependent G2 cycle checkpoint control mechanism. Different drugs have been citied to induce, in susceptible mammalian cell populations an accumulation of cells at a number of distinct stages in the G2 phase of the cell cycle [59]. In part, the G2 checkpoint system is sensitive to the decatenation activity of topoisomerase II [60] or the catenation state of DNA [20,51,60]. Additionally, a G2 arrest can be induced by any number of cellular responses to DNA damage, such as the phosphorylation state of topisomerase II [51] and/or $p34^{cdc2}$ cyclin-dependent kinase [4,61] which when inactivated delays entry into mitosis until the cellular repair of DNA lesions has been completed [61].

Based on the above statements, the degree of resistance towards a G2/M cell cycle arrest may also contribute towards the competency of further cycling in the midst of topoisomerase II inhibition. While it may seem that a number of cell lines may not possess a G2 phase checkpoint system, as evidenced by continued DNA synthesis in the absence of

cell division it remains possible that this checkpoint may in part be most sensitive to the direct induction of DNA damage, rather than the functionality of topoisomerase II [3]. Agents such as teniposide [3], etoposide [61], and doxorubicin [58] which stabilize the cleavable topoisomerase II-DNA complex may be more apt to induce a complete G2 cell cycle blockage [3] due to the rapid formation of DNA strand breaks and inhibition of $p34^{cdc2}$ kinase activity rather than through the inhibition of topoisomerase II per se [61,62]. The bisdioxopiperazines, which inhibit the catalytic activity of topoisomerase II without the formation of the cleavable complex [15,16] have been citied to induce temporary [18,48], or progressive/cumulative G2/M phase arrests at successive ploidy levels [37,48] as well as delayed $p34^{cdc2}$ kinase inactivation [8] in a dose and cell line dependent manner. As first suggested with respect to ICRF-159 treated BHK-21S cells [17], and more recently with ICRF-154 and ICRF-193 treated RPMI 8402 cells [15] the induction of polyploid cells may be more reflective of abnormal mitosis rather than any form of G2 arrest, transient, progressive or otherwise. This form of cell cycle progression entails a slow progression through G2 to G1 via an abnormal mitosis with immaturely condensed chromosomes [3,15] and the inhibition of chromatid segregation through anaphase [3,20,63]. Therefore, the propensity for further cell cycling and DNA synthesis may in part be dependent on the ability of a cell line to transverse an abnormal mitosis established by dexrazoxane-induced topoisomerase II inhibition.

Another critical factor that determines the outcome of drug treatment once drug-target interaction has been achieved is the stability of cells while repair is underway and the fidelity of the p53-dependent G1 checkpoint control mechanism [4]. In the case of DNA damage the tumor suppressor gene p53 acts as a checkpoint at the end of the G1

phase to inhibit cell cycle progression and allow the cells to either activate pathways involved in repair for survival, and/or engage enzymatic machinery that result in apoptosis [46,64]. Other cell systems which lack or possess mutant forms of p53 exhibit a deficiency in the G1-checkpoint control. In the case of undetected DNA damage these cells have an increased tendency to undergo S phase DNA synthesis before becoming arrested in G2 [4]. With respect to CHO cells, it remains a possibility that an absent p53-dependent G1 checkpoint may have assisted continued cell cycling upon dexrazoxane exposure.

Despite the fact that dexrazoxane inhibits topoisomerase II without stablizing the cleavable topoisomerase II-DNA complex [15], it is interesting to ponder whether through bona fide endonuclease cleavage that DNA was at all damaged in CHO cells. If so, then the possibly remains, as in the case of cleavable complex forming topoisomerase II inhibitors that detectable DNA damage by G1 or G2 checkpoint mechanisms may trigger the initiation of apoptotic pathways [4,46,64]. Although the ability of the bisdioxopiperazines to induce apoptosis has not been well characterized, it has been identified in non-proliferative murine thymocytes exposed to ICRF-154 [65], and in dexrazoxane-treated human leukemic CEM [66], and K562 cells (Section 3.5). After an extended period of dexrazoxane exposure, CHO cells did not exhibit some of the previously characterized features of apoptosis [41,42,46]. Bivariate flow cytometry analysis did not reveal diminished stainability for DNA, or decreased forward and right angle light scattering properties (Fig. 2.21), which would have been consistent with the sub-diploid DNA content of apoptotic bodies; morphological and staining analysis of chromatin patterns by fluorescence microscopy did not reveal apoptotic features (Fig. 2.26); and electron microscopy furthermore confirmed the absence of apoptotic features,

such as large uniformly condensed areas of chromatin (Fig. 2.27). Although some uncontrolled, necrotic cell death was detected using fluorescence microscopy (Fig. 2.26 and 2.27), this does not necessarily preclude that higher dexrazoxane concentrations would lead only to necrotic cell death [46]. These results suggest that dexrazoxane-induced cytotoxicity in CHO cells may not necessarily be due to the induction of apoptosis, but rather other means of cytodestruction linked directly or indirectly to the non-cleavable complex form of topoisomerase II inhibition. With respect to this presumption Kung *et al.* [67] was able to demonstrate in CHO cells that the cytotoxicity of cell cycle phase specific agents, aphidicolin and vincristine was not attributable to their direct biochemical action. Instead, as may be the case upon dexrazoxane exposure cell death was evoked by the dissociation of normally coupled or integrated cell cycle events such as replicative/mitotic events or cytokinetic/nuclear reformation events.

Although dexrazoxane-treated CHO cells did not exhibit features characteristic of apoptosis a detailed examination of morphology using fluorescence microscopy revealed several changes which complemented earlier studies [3,6,15]. Exposure of CHO cells to dexrazoxane resulted in the appearance of cells with multilobed nuclei (Fig. 2.24b) which complements the variable ploidy content at these time intervals. Confocal fluorescent microscopy later confirmed the concentric orientation of these structures about the cell (Fig. 2.28). Gamma tubulin fluorescent staining of centrosomes revealed a greater number of centrosomes in dexrazoxane-treated CHO cells (Fig. 2.24e), thus clearly indicating that cells were continuing to cycle and becoming polyploid in the absence of cytokinesis. Cytoskeletal components (F-actin, and microtubules) extensively encompassed these enlarged cells and generally appeared structurally normal (Fig. 2.24c, d). Furthermore,

upon dexrazoxane exposure organelles such as mitochondria, endoplasmic reticulum, and golgi apparatus were apparently greater in number (Fig. 2.25) but generally appeared normal, as similarly seen in ICRF-159 treated hamster fibrosarcoma T17 cells [6].

The terms multilobed nuclei [15] and multinucleation [6,15] have been used interchangeably to define the morphological appearance of fluorescently-labelled DNA in cells treated with the bisdioxopiperazines. However, while one definition implies one nuclei with several lobes and the other implies multiple individual nuclei it remains clear that they appear to be linked by nuclear threads or bridges of chromatin [6,15,18]. It is possible that this contact maintained between the daughter nuclei does not allow for their separation and thus leads to the inhibition of cytokinesis [18]. Ishida *et al.* [8] has previously demonstrated that ICRF-193 does not block the reassembly of the nuclear envelope in HeLa cells during telophase. As nuclear envelopes formed around the periphery of fused, unsegregated chromosomes that were incompletely decondensed this prompted the formation of multilobed nuclei [8].

As previously mentioned, in yeast topoisomerase mutants the activity of topoisomerase II can be complemented by that of topoisomerase I in controlling torsional strain accumulated during DNA replication and transcription. However, topoisomerase II plays an essential role during mitosis acting to anchor and organize chromatin, as well as decatenating DNA necessary for chromosome condensation and segregation [51,68,69]. Upon the inactivation of topoisomerase II by bisdioxopiperazine analogs, polyploid cells can develop as other mitotic events, uncoupled from chromosome dynamics proceed normally [8]. Such cellular processes, which are triggered by the activation of $p34^{cdc2}$ kinase include the disassembly and reassembly of nuclear membrane envelopes and

spindle apparatus formation [3,8,15,70]. Additionally, aberrantly occurring cytokinesis has been citied in HeLa and PtK_2 cells treated with ICRF-193 [20].

Previous studies have shown through detailed cytological analysis that in the presence of ICRF-193 [8,15,20,63], ICRF-159, and dexrazoxane [3] cells continue to transverse the cell cycle synthesizing DNA and becoming polyploid in the absence of a G2 arrest and cytokinesis. Cells progress slowly from G2 to G1 via an abnormal mitosis phase generally characterized by the inhibition of late stage chromosome condensation, segregation, as well as delayed decondensation [8,15]. Earlier reports seemed to suggest that topoisomerase II inhibition caused a mitotic delay only during anaphase through the prevention of chromatid segregation [20]. While this remains valid, due to an inability to completely segregate entangled masses of elongated chromosomes during anaphase, it is believed as well that a mitotic checkpoint exists within metaphase to delay the transition to anaphase [3,63,70]. Although inhibitors of microtubule formation have been shown to delay metaphase progression through the improper attachment of kinetochore spindles to chromosomes [63], alternative explanations have suggested that this checkpoint detects the alignment of centromeres at the metaphasic plate [3]. However, the observed elimination of high concentrations of topoisomerase II at the centromeres in dexrazoxane-treated Ptk1 epithelial cells [3] did not necessary inhibit centromere alignment during metaphase. Overall, these findings tend to suggest that topoisomerase II activity is not essential for metaphase centromere alignment, the initiation of centromere separation during anaphase, or continued cell cycling although it is required for the proper organization and the complete separation of centromeric chromatid arms at the onset of anaphase [3,20].

Normally, mitosis and cytokinesis are coordinated both temporally and spatially, such that upon the completion of mitosis a cleavage furrow bisects the cell at the equatorial plane between the spindle poles, corresponding to the prior location of the metaphasic plate. Contrary to the conventional model in which the location of the centrosomes dictates the plane of cleavage, Wheatley *et al.* [71] have demonstrated that in dexrazoxane-treated normal rat kidney (NRK) epithelial cells cleavage activity is determined by the organization of the chromosomes and midzone microtubules. Specifically, microtubules emanating laterally from the region of tangled chromosomes act as a vehicle for chromosome-mediated signalling to the cell cortex to initiate cytokinesis at these sites. Although cytokinesis was completed ~40% of the time, the position of the cleavage furrow deviated from the equator, thus producing distorted furrows and irregular shaped daughter cells [71]. This result was similarly seen in dexrazoxane and ICRF-159 treated Ptk1 cells in which cytokinesis proceeded upon unequal, random partitioning of chromatin into daughter cells [3].

With respect to dexrazoxane-treated CHO cells, cytokinesis appeared to be completely inhibited, as judged by the unchanging cell numbers (Fig. 2.7), and the appearance of polyploid (Fig. 2.19), multinucleated cells (Fig. 2.24b). However, as detected by fluorescence microscopy upon anti-acetylated α-tubulin staining a few enlarged cells were present in the process of cytokinesis possessing distorted cleavage furrows (data not shown). While this may have been true of only a few cells, it would seem that the majority of the population continued to cycle in the absence of any division as determined by the multiple number of spindle poles (centrosomes) identified within each cell (Fig. 2.24e). The shortened distance between the centrosomes may have clearly

affected cytokinesis due to the inhibition of spindle elongation. In addition, as noted by Wheatley *et al.* [71] and proposed herein, the absence of any concerted contraction of F-actin along the equatorial plane may have prevented the proper progression of the cleavage furrow in dexrazoxane-treated cells.

In conclusion, the results of this study show that the topoisomerase II catalytic inhibitor dexrazoxane, which is unable to directly induce DNA strand breaks is capable of permitting continued cell cycling without cell division, thus implying a complementary role of topoisomerase I during non-essential processes. The propensity for further cell cycling onto higher ploidy levels is clearly cell line specific. Inherent factors such as proliferation rate, expression level or activity of topoisomerase II, ability to segregate chromosomes, the fidelity of checkpoint controls, as well as susceptibility to apoptosis may all dictate the extent of polyploidization or cytotoxicity incurred. The use of a dexrazoxane-resistant CHO cell line (DZR) [22], possessing a Thr48Ile mutation at the dimer interface of topoisomerase II [23] served as a negative control for most characterized features present in dexrazoxane-treated parental CHO cells. The absence of any alteration in growth (Fig. 2.7), morphology (Fig. 2.9c, d), protein and DNA content (Fig. 2.16), or cell cycling (Fig. 2.22) upon exposure of DZR cells to dexrazoxane further confirmed, as previously believed that the catalytic inhibition of topoisomerase II was the key source of the above mentioned cell cycle perturbations in other cell lines. Although normal primary heart fibroblasts were completely inhibited by dexrazoxane *in vitro* it remains unclear how these or other mortal, non-neoplastic cell types will behave *in vivo* upon extensive, continuous exposure to dexrazoxane and whether their recovery can be permitted through intermittent dosing. Further studies may determine if the cumulative cytostatic effect of

dexrazoxane serves any rational for the design of anti-tumor chemotherapeutic regimens or whether it at all creates complications in its current clinical usage.

2.12 References

1. Alberts, B., Bray, D., Lewis, J., Raff, M., Roberts, K., and Watson, J.D. Cell growth and division. In: Molecular Biology of the Cell., pp. 727-790, New York, N.Y.: Garland Publishing, Inc. 1989.

2. Weinberg, R.A. How cancer arises. *Sci. Am.*, **275**: 62-70, 1996.

3. Gorbsky, G.J. Cell cycle progression and chromosome segregation in mammalian cells cultured in the presence of the topoisomerase II inhibitors ICRF-187 [(+)-1,2-bis(3,5-dioxopiperazinyl-1-yl)propane; ADR-529] and ICRF-159 (Razoxane). *Cancer Res.*, **54** : 1042-1048, 1994.

4. O'Connor, P.M. and Kohn, K.W. A fundamental role for cell cycle regulation in the chemosensitivity of cancer cells? *Semin. Cancer Biol.*, **3**: 409-416, 1992.

5. Dubrez, L., Goldwasser, F., Genne, P., Pommier, Y., and Solary, E. The role of cell cycle regulation and apoptosis triggering in determining the sensitivity of leukemic cells to topoisomerase I and II inhibitors. *Leukemia*, **9**: 1013-1024, 1995.

6. Hallowes, R.C., West, D.G., and Hellmann, K. Cumulative cytostatic effect of ICRF 159. *Nature*, **247**: 487-490, 1974.

7. Erusalimsky, J.D. and Martin, J.F. The regulation of megakaryocyte polyploidization and its implications for coronary artery occlusion. *Eur. J. Clin. Invest.*, **23**: 1-9, 1993.

8. Ishida, R., Sato, M., Narita, T., Utsumi, K.R., Nishimoto, T., Morita, T., Nagata, H., and Andoh, T. Inhibition of DNA topoisomerase II by ICRF-193 induces polyploidization by uncoupling chromosome dynamics from other cell cycle events. *J. Cell Biol.*, **126**: 1341-1351, 1994.

9. Baatout, S., Chatelain, B., Staquet, P., Symann, M., and Chatelain, C. Augmentation of the number of nucleolar organizer regions in human megakaryocyte cell lines after induction of polyploidization by a microtubule inhibitor. *Eur. J. Clin. Invest.*, **28** : 138-144, 1998.

10. Baatout, S., Chatelain, B., Staquet, P., Symann, M., and Chatelain, C. Induction and enhancement of normal human megakaryocyte polyploidization are concomitant with perturbation in the actin metabolism. *Eur. J. Clin. Invest.*, **28**: 845-855, 1998.

11. Creighton, A.M., Hellmann, K., and Whitecross, S. Antitumour activity in a series of bisdiketopiperazines. *Nature*, **22**: 384-385, 1969.

12. Atherton, A. The effect of (+/-)-1,2-bis(3,5-dioxopiperazin-1-yl) propane (ICRF 159) on liver metastases from a hamster lymphoma. *Eur. J. Cancer*, **11**: 383-388, 1975.

13. Creighton, A.M. and Birnie, G.D. Biochemical studies on growth-inhibitory bisdioxopiperazines. I. Effect on DNA, RNA and protein synthesis in mouse-embryo fibroblasts. *Int. J. Cancer*, **5**: 47-54, 1970.

14. Tanabe, K., Ikebuchi, K., Ishida, R., and Andoh, T. Inhibition of topoiosmerase II by antitumour agents bis(2,6-dioxopiperazine) derivatives. *Cancer Res.*, **51**: 4903-4908, 1991.

15. Ishida, R., Miki, T., Narita, T., Yui, R., Sato, M., Utsumi, K.R., Tanabe, K., and Andoh, T. Inhibition of intracellular topoisomerase II by antitumor bis(2,6-dioxopiperazine) derivatives: mode of cell growth inhibition distinct from that of cleavable complex-forming type inhibitors. *Cancer Res.*, **51**: 4909-4916, 1991.

16. Hasinoff, B.B., Kuschak, T.I., Yalowich, J.C., and Creighton, A.M. A QSAR study comparing the cytotoxicity and DNA topoisomerase II inhibitory effects of bisdioxopiperazine analogs of ICRF-187 (dexrazoxane). *Biochem. Pharm.*, **50**: 953-958, 1995.

17. Edgar, D.H. and Creighton, A.M. ICRF 159-induced cell-cycle perturbation in vitro: its relationship to inhibition of colony-forming ability. *Br. J. Cancer*, **44**: 236-240, 1981.

18. Traganos, F., Darzynkiewicz, Z., and Melamed, M.R. Effects of the L isomer (+)-1,2-bis(3,5-dioxopiperazine-1-yl)propane on cell survival and cell cycle progression of cultured mammalian cells. *Cancer Res.*, **41**: 4566-4576, 1981.

19. Taylor, I.W. and Bleehen, N.M. Razoxane-induced polyploidy. *Br. J. Cancer*, **38**: 143-147, 1978.

20. Clarke, D.J., Johnson, R.T., and Downes, C.S. Topoisomerase II inhibition prevents anaphase chromatid segregation in mammalian cells independently of the generation of DNA strand breaks. *J. Cell Sci.*, **105**: 563-569, 1993.

21. Speyer, J.L., Green, M.D., Zeleniuch-Jacquotte, A., Wernz, J.C., Rey, M., Sanger, J., Kramer, E., Ferrans, V., Hochster, H., and Meyers, M. ICRF-187 permits longer treatment with doxorubicin in women with breast cancer [published erratum appears in J Clin Oncol 1992 May;10(5):867]. *J. Clin. Oncol.*, **10**: 117-127, 1992.

22. Hasinoff, B.B., Kuschak, T.I., Creighton, A.M., Fattman, C.L., Allan, W.P., Thampatty, P., and Yalowich, J.C. Characterization of a Chinese hamster ovary cell line with acquired resistance to the bisdioxopiperazine dexrazoxane (ICRF-187) catalytic inhibitor of topoisomerase II. *Biochem. Pharm.*, **53**: 1843-1853, 1997.

23. Yalowich, J.C., Thampatty, P., Allan, W.P., Chee, G.-L., and Hasinoff, B.B. Acquired resistance to ICRF-187 (dexrazoxane) in a CHO cell line is associated with a point mutation in DNA topoisomerase II-alpha (topo II) and decreased drug-induced DNA-enzyme complexes. *Proc Am Assoc Cancer Res*, **39**: 375, 1998.

24. Kirshenbaum, L.A. and de Moissac, M.D. The bcl-2 gene product prevents programmed cell death of ventricular myocytes. *Circulation*, **96**: 1580-1585, 1997.

25. Engelhard, H.H., Krupka, J.L., and Bauer, K.D. Simultaneous quantification of c-myc oncoprotein, total cellular protein, and DNA content using multiparameter flow cytometry. *Cytometry*, **12**: 68-76, 1991.

26. Vistica, D.T., Skehan, P., Scudiero, D., Monks, A., Pittman, A., and Boyd, M.R. Tetrazolium-based assays for cellular viability: a critical examinatoin of selected parameters affecting formazan production. *Cancer Res.*, **51**: 2515-2520, 1991.

27. Sobottka, S.B. and Berger, M.R. Assessment of antineoplastic agents byMTT assay: partial underestimation of antiproliferative properties. *Cancer Chemother. Pharmacol.*, **30**: 385-393, 1992.

28. Pagliacci, M.C., Spinozzi, F., Migliorati, G., Fumi, G., Smacchia, M., Grignani, F., Riccardi, C., and Nicoletti, I. Genistein inhibits tumour cell growth *in vitro* but enhances mitochondrial reduction of tetrazolium salts: A further pitfall in the use of the MTT assay for evaluating cell growth and survival. *Eur. J. Cancer*, **29A**: 1573-1577, 1993.

29. Hasinoff, B.B., Creighton, A.M., Kozlowska, H., Thampatty, P., Allan, W.P., and Yalowich, J.C. Mitindomide is a catalytic inhibitor of DNA topoisomerase II that acts at the bisdioxopiperazine binding site. *Mol. Pharmacol.*, **52**: 839-845, 1997.

30. Hasinoff, B.B. Pharmacodynamics of the hydrolysis-activation of the cardioprotective agent (+)-1,2-bis(3,5-dioxopiperazinyl-1-yl)propane. *J. Pharm. Sci.*, **83**: 64-67, 1994.

31. Pignolo, R.J., Masoro, E.J., Nichols, W.W., Bradt, C.I., and Cristofalo, V.J. Skin fibroblasts from aged fischer 344 rats undergo similar changes in replicative life span but not immortalization with caloric restriction of donors. *Exp. Cell Res.*, **201**: 16-22, 1992.

32. Volker, K. Sizing of cells by the electrical resistance pulse technique. In: Catsimpoolas and Nicholas (eds.), Cell Analysis, pp. 195-199, New York: Plenum Press. 1985.

33. Cullen, W.C. and McDonald, T.P. Comparison of stereologic techniques for the quantification of megakaryocyte size and number. *Exp. Hematol.*, **14**: 782-788, 1986.

34. Lines, R.W. The electrical sensing zone method (The Coulter principle). In: J.Z. Knapp, T.A. Barber and A. Lieberman (eds.), Liquid-and-surface-borne particle measurement handbook, pp. 113-140, New York, N.Y.: Marcel Dekker, Inc. 1996.

35. Bradford, M.M. A rapid and sensitive method for the quantitation of microgram quantities of protein utlizing the principle of protein-dye binding. *Anal. Biochem.*, **72**: 248-254, 1976.

36. Cesarone, C.F., Bolognesi, C., and Santi, L. Improved microfluorometric DNA determination in biological material using 33258 Hoechst. *Anal. Biochem.*, **100**: 188-197, 1979.

37. Scambia, G., Della, B.R., Benedetti, P.P., De, V.R., Contu, G., Ercoli, A., Bonanno, G., Pierelli, L., and Mancuso, S. Bisdioxopiperazine, (+)-1,2-bis(3,5-dioxopiperazinyl-1-yl)propane (ICRF 187), enhances the antiproliferative effect of cisplatin on human ovarian cancer cells. *Gynecol. Oncol.*, **57**: 16-22, 1995.

38. Gorman, A.M., Samali, A., McGowan, A.J., and Cotter, T.G. Use of flow cytometry techniques in studying mechanisms of apoptosis in leukemic cells. *Cytometry*, **29**: 97-105, 1997.

39. Ormerod, M.G. Flow Cytometry. Oxford, UK: BIOS Scientific Publishers Ltd., 1994.

40. Givan, A.L. Flow Cytometry First Principles. New York,N.Y.: Wiley-Liss, Inc., 1992.

41. Darzynkiewicz, Z., Bruno, S., Del, B.G., Gorczyca, W., Hotz, M.A., Lassota, P., and Traganos, F. Features of apoptotic cells measured by flow cytometry. *Cytometry*, **13**: 795-808, 1992.

42. Mercille, S. and Massie, B. Induction of apoptosis in nutrient-deprived cultures of hybridoma and myeloma cells. *Biotechnology and Bioengineering*, **44**: 1140-1154, 1994.

43. Chen, L.B. Fluorescent labeling of mitochondria. In: D. Lansing Taylor and Y. Wang (eds.), Fluorescence Microscopy of Living Cells in Culture Part A., pp. 103-123, San Diego, CA: Academic Press, Inc. 1989.

44. Terasaki, M. Fluorescent labeling of endplasmic reticulum. In: D. Lansing Taylor and Y. Wang (eds.), Fluorescence Microscopy of Living Cells in Culture Part A., pp. 125-135, San Diego, CA: Academic Press, Inc. 1989.

45. Alberts, B., Bray, D., Lewis, J., Raff, M., Roberts, K., and Watson, J.D. How cells are studied. In: AnonymousMolecular Biology of the Cell., pp. 135-198, New York, N.Y.: Garland Publishing, Inc. 1989.

46. Solary, E., Bertrand, R., and Pommier, Y. Apoptosis induced by DNA topoisomerase I and II inhibitors in human leukemic HL-60 cells. *Leuk. Lymphoma.*, **15**: 21-32, 1994.

47. Brakenhoff, G.J., Van Spronsen, E.A., Van Der Voort, H.T.M., and Nanninga, N. Three-dimensional confocal fluorescence microscopy. In: D. Lansing Taylor and Y. Wang (eds.), Fluorescence Microscopy of Living Cells in Culture Part B., pp. 379-398, San Diego, CA: Academic Press, Inc. 1989.

48. Wheeler, R.H., Clauw, D.J., Natale, R.B., and Ruddon, R.W. The cytokinetic and cytotoxic effects of ICRF-159 and ICRF-187 in vitro and ICRF-187 in human bone marrow in vivo. *Invest. New Drugs*, **1**: 283-295, 1983.

49. Lazo, J.S., Ingber, D.E., and Sartorelli, A.C. Enhancement of experimental lung metastases by cultured B16 melanoma cells treated with (+/-)-1,2-bis(3,5-dioxopiperazin-1-y)propane (ICRF- 159). *Cancer Res.*, **38**: 2263-2270, 1978.

50. Hasinoff, B.B., Kuschak, T.I., Fattman, C.L., and Yalowich, J.C. The one-ring open hydrolysis intermediates of the cardioprotective agent dexrazoxane (ICRF-187) do not inhibit the growth of Chinese hamster ovary cells or the catalytic activity of DNA topoisomerase II. *Anticancer Drugs*, **9**: 465-471, 1998.

51. Larsen, A.K., Skladanowski, A., and Bojanowski, K. The roles of DNA topoisomerase II during the cell cycle. *Prog Cell Cycle Res.*, **2**: 229-239, 1996.

52. Stephens, T.C. and Creighton, A.M. Mechanism of action studies with ICRF 159: Effects on the growth and morphology of BHK-21S cells. *Br. J. Cancer*, **29**: 99-100, 1974.

53. Stephens, T. C. An investigation of the effects of the antitumour agent ICRF 159 on the growth of BHK-21S cells in culture. 1974. University of London, London. (Thesis/Dissertation)

54. Ross, D.W. The nature of unbalanced cell growth caused by cytotoxic agents. *Virchows Arch [Cell Pathol]*, **37**: 225-235, 1981.

55. Malec, J., Przybysewski, W.M., Grabarczyk, M., Sitarska, E., and Czartoryska, B. Mechanism of unbalanced growth-induced cell damage. I. A probable role for hydrolytic enymes synthesis. *Chem. Biol. Interactions*, **57**: 315-324, 1986.

56. Ross, D.W. Cell volume growth after cell cycle block with chemotherapeutic agents. *Cell Tissue Kinet.*, **9**: 379-387, 1976.

57. Hellmann, K. and Field, E.O. Effect of ICRF 159 on the mammalian cell cycle: Significance for its use in cancer chemotherapy. *J. Natl. Cancer Inst.*, **44**: 539-543, 1970.

58. Wadler, S., Green, M.D., Basch, R., and Muggia, F.M. Lethal and sublethal effects of the combination of doxorubicin and the bisdioxopiperazine, (+)-1,2,-bis (3-5-dioxopiperazinyl-1-yl) propane (ICRF 187), on murine sarcoma S180 in vitro. *Biochem. Pharm.*, **36**: 1495-1501, 1987.

59. Tobey, R.A. Different drugs arrest cells at a number of distinct stages in G2. *Nature*, **254**: 245-247, 1975.

60. Downes, C.S., Clarke, D.J., Mullinger, A.M., Gimenez-Abian, J.F., Creighton, A.M., and Johnson, R.T. A topoisomerase II-dependent G2 cycle checkpoint in mammalian cells/ [published erratum appears in Nature 1994 Dec 15;372(6507):710]. *Nature*, **372**: 467-470, 1994.

61. Lock, R.B. and Ross, W.E. Inhibition of p34cdc2 kinase activity by etoposide or irradiation as a mechanism of G2 arrest in Chinese hamster ovary cells. *Cancer Res.*, **50**: 3761-3766, 1990.

62. Lock, R.B. Inhibition of p34cdc2 kinase activation, p34cdc2 tyrosine dephosphorylation, and mitotic progression in Chinese hamster ovary cells exposed to etoposide. *Cancer Res.*, **52**: 1817-1822, 1992.

63. Iwai, M., Hara, A., Andoh, T., and Ishida, R. ICRF-193, a catalytic inhibitor of DNA topoisomerase II, delays the cell cycle progression from metaphase, but not from anaphase to the G1 phase in mammalian cells. *FEBS Lett.*, **406**: 267-270, 1997.

64. Kaufmann, S.H. Cell death by topoisomerase-targeted drugs: more questions than answers. *Biochem. Biophys. Acta.*, **1400**: 195-211, 1998.

65. Kizaki, H. and Onishi, Y. Topoisomerase II inhibitor-induced apoptosis in thymocytes and lymphoma cells. *Adv. Enzyme Regul.*, **37:403-23**: 403-423, 1997.

66. Khelifa, T. and Beck, W.T. Induction of apoptosis by dexrazoxane (ICRF-187) through caspases in the absence of c-jun expression and c-jun NH2-terminal kinase 1 (JNK1) activation in VM-26-resistant CEM cells. *Biochem. Pharm.*, **58**: 1247-1257, 1999.

67. Kung, A.L., Zetterberg, A., Sherwood, S.W., and Schimke, R.T. Cytotoxic effects of cell cycle phase specific agents: result of cell cycle perturbation. *Cancer Res.*, **50**: 7307-7317, 1990.

68. Anderson, H.J. and Roberge, M. DNA topoisomerase II: a review of its involvement in chromosome structure, DNA replication, transcription and mitosis. *Cell Biol. Int. Rep.*, **16**: 717-724, 1992.

69. Nitiss, J.L. Investigating the biological functions of DNA topoisomerases in eukaryotic cells. *Biochem. Biophys. Acta.*, **1400**: 63-81, 1998.

70. Nurse, P. Universal control mechanism regulating onset of M-phase. *Nature*, **344**: 503-508, 1990.

71. Wheatley, S.P., O'Connell, C.B., and Wang, Y. Inhibition of chromosomal separation provides insights into cleavage furrow stimulation in cultured epithelial cells. *Mol. Biol. Cell*, **9**: 2173-2184, 1998.

Chapter 3 Induction of differentiation and apoptosis in K562 human erythroleukemic cells by dexrazoxane and other topoisomerase II inhibitors

3.1 Introduction

3.1.1 Blood cell formation by pluripotent stem cells

The development and survival of an individual, from the fetal stage onward depends on the continual regeneration of different types of blood cells by a process known as hematopoiesis. These cells are responsible for a variety of functions (Table 3.1), whereby they necessitate cellular interactions for the cognitive and activation phases of specific immune responses within the vascular system or at other distant sites [1]. The generation of all blood cells occurs remarkably from a common self-renewing stem cell in the bone marrow. This hematopoietic stem cell is therefore pluripotent, giving rise to many different types of terminally differentiated blood cells, i.e. erythroid, megakaryocytic, granulocytic, monocytic, and lymphocytic (Fig. 3.1). In this scheme of hematopoiesis, the pluripotent stem cells may divide infrequently to generate more stem cells or committed progenitor cells when then divide rapidly for a limited number of amplification divisions. Depending on the nature of the immune response, these committed progenitor cells irreversibly mature towards specific terminally differentiated cell types, which usually divide no further and die after several days or weeks. Proteins that regulate cell death, multiplication, and differentiation of the different hematopoietic cell lineages are called cytokines. Many of these cytokines are also known as colony-stimulating factors (CSFs) or interleukins (ILs). Essentially, a multigene family or

network of interacting cytokines exist, some with overlapping functions that provides flexibility with respect to the part of the network activated, as well as allowing for the amplification of responsive precursor cells to a particular stimulus [2]. Abnormalities in this normal development program for blood cell formation can occasionally result in hematological diseases such as leukemia [2]. Such abnormalities may entail genetic changes that uncouple the normal balance in hematopoietic cell multiplication and differentiation. The result is too many growing cells concurrent with differentiating cells blocked at some step in the maturation process which prevent them from reaching the normal end-point which ultimately is cell death [3]. In view of such occurrences, new approaches towards the clinical therapeutic use of cytokines and other compounds have currently offered a means of suppressing such malignancies and bypassing genetic defects in certain leukemic cell types by the induction of differentiation [3].

Table 3.1. Typical blood cells and their functions. (Adapted from [1])

Type of Cell	**Main Functions**
Red Blood Cells (erythrocytes)	transport O_2 and CO_2
White blood cells (leucocytes)	
Granulocytes	
Neutrophils	phagocytose and destroy invading bacteria
Eosinophils	destroy larger parasites and modulate allergic inflammatory responses
Basophils	release histamine in immune reactions
Monocytes	become tissue macrophages, which phagocytose and digest invading microorganisms, foreign bodies, and senescent cells
Lymphocytes	
B cells	make antibodies
T cells	kill virus-infected cells and regulate activities of other leucocytes
Platelets (cell fragments, arising from megakaryocytes in bone marrow)	initiate blood clotting

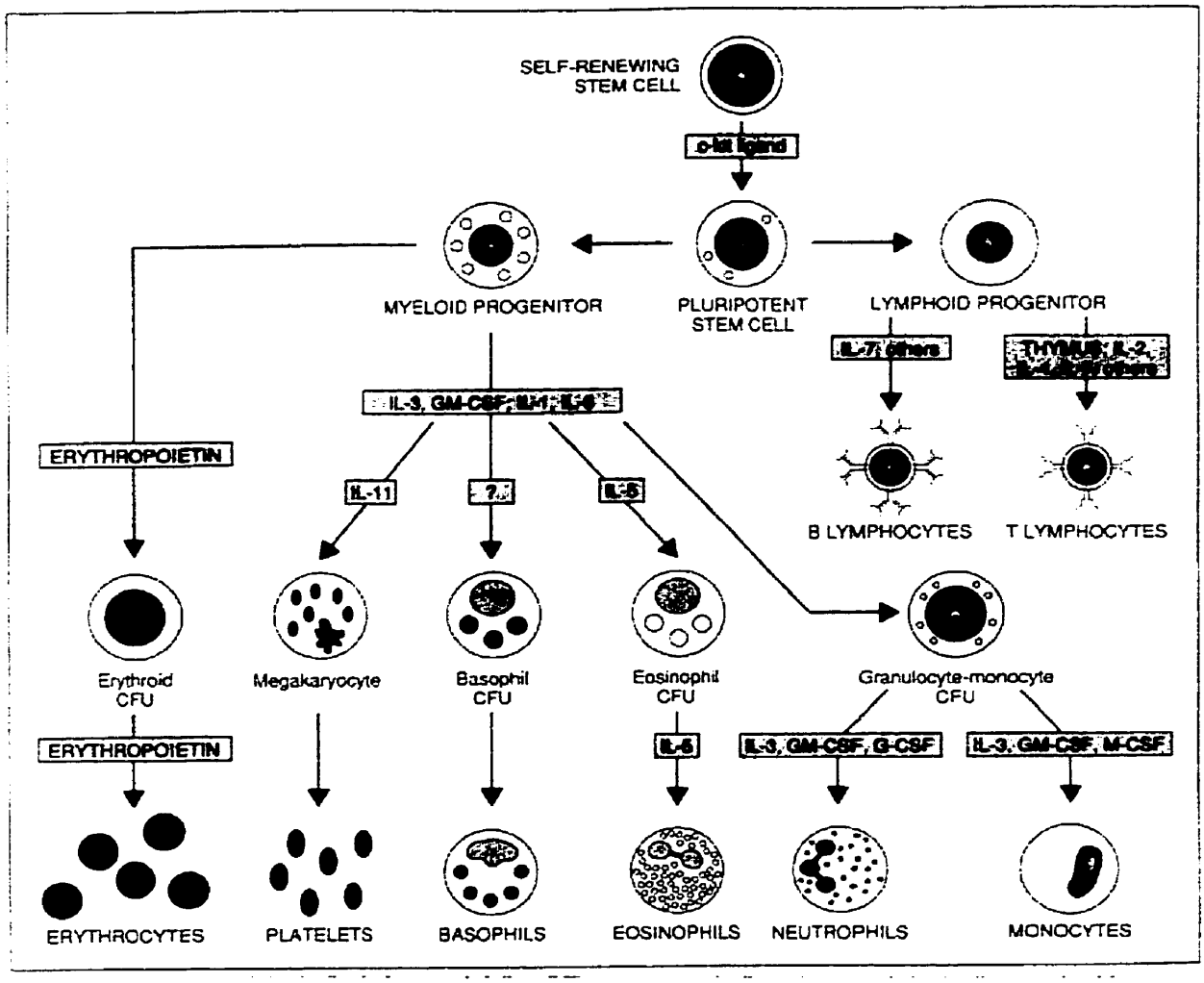

Fig. 3.1. Maturation of blood cells: the hematopoietic "tree". The maturation of different lineages of blood cells is regulated by various cytokines. CFU, colony forming unit; IL, interleukin; GM-CSF, granulocyte-macrophage colony-stimulating factor. (Adapted from [1]).

3.1.2 K562 human leukemic cells: A model system for studying the induction of differentiation and apoptosis

A number of different hematopoietic human and rodent cell lines have been established for the purpose of studying the mechanisms regulating differentiation and maturation with respect to leukemia [4]. The development of permanent leukemic cell lines able to undergo a series of differentiation events in the presence of a variety of inducing agents has not only increased our understanding of hematopoiesis and leukemia but also assisted in providing new approaches towards therapeutic treatment of such hematological diseases. One such immortal cell line known as K562, has been cited to serve a number of applications and usefulness in relation to such studies [5].

The K562 cell line was established by Lozzio and Lozzio [6] from the pleural effusion of a 53-year-old female with chronic myelogenous leukemia (CML) in terminal blast crisis, a disease characterized by the progressive accumulation of myeloid cells in the peripheral blood and bone marrow [7]. Initially, K562 cells were considered highly undifferentiated myeloid cells of the granulocytic series [5] with a leukemic origin confirmed by their retention of a characteristic CML cytogenetic marker, the Philadelphia (Ph^1 +) chromosome [8]. Although Lozzio and Lozzio maintain that K562 represents a primitive cell of the myeloid lineage, other studies have firmly established the presence and biosynthesis of glycophorin A, hemoglobin, and spectrin, all well known markers of an erythroid lineage [9,10]. In addition, several laboratories have shown that K562 cells can be induced to express erythroid, granulocytic, monocytic, and megakaryocytic antigens to varying degrees and possibly concurrently, depending upon the inducer [11-13]. Studies such as these have led to the conclusion that despite its malignant origin, the K562 cell line retains some capacity for the expression of alternative programs of differentiation, a

characteristic of a multipotent hematopoietic stem cell [12,14]. Normal hematopoietic differentiation would involve a stem cell losing its multipotentiality in the process of commitment towards the expression of genes of a particular lineage. The K562 cell line on the other hand does not follow an orderly differentiation program in that they may simultaneously express markers of more than one lineage, unlike what is observed in normal bone marrow cells [11,12]. This concept of lineage infidelity may be a normal feature of early progenitor cells, whereby they may express a variety of markers specific for each of the lineages within the stem cell repertoire. As differentiation is induced, lineage-specific features are amplified while repressing the immunophenotype expression of other lineages [11].

The existence of a leukemic cell line with the capacity for the expression of multilineage markers is not without a rationale theory. One hypothesis suggests that since chronic myeloid leukemia is a clonal disease of a pluripotent stem cell that some degree of mulitpotentiality together with gene dysregulation, led to the expression of multilineage markers in what became the K562 cell line [14]. Another possibility is that the phenotype of K562 cells could also be observed during normal ontogenesis [14]. Clearly though, the establishment of a continuous leukemic cell line, like K562, with multilineage differentiation capacities has made it possible to further study mechanisms of normal and abnormal hematopoiesis, while at the same time in a clinical sense attempt to generate new means of inducing remission in leukemic patients expressing similar features of lineage infidelity. One aspect of the following study, which will be explained further was to investigate the existence of a relationship between the induction of erythroid and megakaryocytic lineages in K562 cells.

As alluded to earlier, in hematopoietic tissues the survival of progenitor cells and the turnover of terminally differentiated cells is controlled by an implemented controlled program of cell death. This process, commonly known as apoptosis is a genetically regulated process that can be induced by a variety of extrinsic or intrinsic signals. Such stimuli include signaling via surface receptors, radiation therapy, deprivation of hormonal and other growth factors, and treatment with DNA-damaging agents or inhibitors of macromolecular synthesis which accordingly activate an internally encoded suicide program via a cascade of cellular events [15]. Apoptotic cell death is characterized by plasma membrane blebbing, cell volume loss, nuclear condensation, and endonucleolytic degradation of DNA at nucleosomal intervals [16].

The efficacy of current antineoplastic therapy is determined by a sequential cascade of events including drug delivery, drug-target interaction, induction of cellular damage, and the response of the cell to that damage (death or repair). Clinically, most leukemias exhibit parallel sensitivity or cross-resistance to most cytotoxic anticancer agents, despite their differing mechanisms of action. Although the cause of treatment failure in most leukemias remains unclear, emerging evidence has demonstrated that the apparent resistance to apoptotic induction by anticancer drugs is probably a function of multiple signals that influence apoptosis [17]. In addition to its differentiation capacities, the K562 cell line derived from a patient with CML exhibits such anti-apoptotic attributes, making it an ideal *in vitro* model system for the testing of new therapeutic treatment strategies.

The existence of the Philadelphia (Ph^1) chromosome ($22q^-$) in K562 cells and most CML patients is perhaps the most prominent attribute of these cells which contributes to their enhanced survival potential during antileukemic chemotherapy treatment.

Specifically, the Philadelphia chromosome results from a reciprocal translocation between chromosome 9 and 22. The breakpoint on chromosome 22 where the *c-abl* gene of chromosome 9 is inserted is known as the breakpoint cluster region (*bcr*). This translocation produces the *bcr-abl* fusion gene and the constitutive expression of the *BCR-ABL* tyrosine kinase which transduces signals to suppress apoptosis [7,18]. Consequently, the K562 cell line can be used to test its susceptibility to apoptosis by various agents and therapeutic drugs for the purpose of the development of an ideal effective treatment strategy for CML and other leukemias. Moreover, it may be desirable to aim the design of future treatment therapies at the activity of anti-apoptotic genes such as *bcr-abl*, rather than further attempting to inhibit the activity of genes which promote apoptosis.

3.1.3 Erythropoiesis

Erythropoiesis as it normally occurs over the entire lifespan of an individual results in the formation of erythrocytes, commonly known as red blood cells (RBCs). These cells, which are transported via the bloodstream function in the exchange of O_2 for CO_2 at sites of tissue respiration. Progenitor stem cells are committed to erythrocyte-specific differentiation in response to the hormone glycoprotein erythropoietin, and to a lesser extent IL-3. Over the course of this process the developing red blood cell (erythroblast) extrudes its nucleus to become an immature erythrocyte (reticulocyte) shortly before leaving the bone marrow and entering into circulation. Maturation of erythrocytes then continues to a terminal point with the further loss of mitochondria, ribosomes, endoplasmic reticulum, and proliferative capacity. In their final mature state red blood cells produce and express specific surface membrane proteins such as glycophorin A, a membrane

sialoglycoprotein, and to a much greater extent an oligomeric protein known as hemoglobin (Hb). In adults hemoglobin is composed of 4 globin polypeptide chains ($\alpha_2\beta_2$) in a tetrahedral ferrous photoporphyrin arrangement around 4 heme prosthetic groups [19].

3.1.4 Induction of K562 erythroid-like differentiation

The study of the regulation of human erythropoiesis and hemoglobin synthesis at different stages of development has been hampered by the lack of easily accessible self-sustaining populations of primitive erythropoietic stem cells [8]. The need for such a cell line has been further exemplified by the fact that harvested erythroid precursor cells can only be maintained in culture for short periods of time before they are committed to terminal differentiation. The K562 cell line has since provided valuable potential for studying the dynamics of erythropoiesis and hemoglobin switching, representative in humans. Andersson *et al.* [10] was the first to demonstrate that K562 cells synthesize glycophorin A, as well as hemoglobin after induction with sodium butyrate [20]. Subsequently, others have shown that uninduced K562 cells possess fetal ($\alpha_2\gamma_2$) and embryonic ($\xi_2\varepsilon_2$ or $\xi_2\gamma_2$) globin chains, and globin mRNAs [21] which accumulate in these forms upon exposure to hemin or sodium butyrate [19,21-25].

During ontogeny hemoglobin synthesis normally proceeds from an embryonic pattern through a period of fetal hemoglobin production until adult hemoglobin ($\alpha_2\beta_2$) synthesis is established. Although analysis of many K562 subclones have shown a great heterogeneity in hemoglobin synthesis patterns, no evidence of a complete switch to adult hemoglobin has been seen. It remains unclear exactly why K562 cells should synthesize embryonic hemoglobin when the cells were obtained from an adult patient. The current

postulation was that normal cells determinant for embryonic erythropoiesis laid dormant and were more susceptible for leukemogenesis over normal adult stem cells, and that it was from these extremely immature stem cells that the K562 cell line was likely derived [23].

Although key erythroid features are expressed in K562 cells upon induction, differentiation neither seems to be complete or normal. Differentiated K562 cells lack the typical morphology, ABO and Rh antigens normally present in mature proerythroblasts [8,21]. Wide distributional differences in globin gene and glycophorin A expression in uninduced K562 cells is reflective of unequal expression within the population, and it is possible that only a proportion of cells may actually be participating in the erythropoietic process [8,26]. Although K562 cells undergo a seemingly partial erythroid differentiation this does not preclude their importance to the further study of erythropoiesis and hemoglobin switching.

3.1.5 Megakaryocytopoiesis

Megakaryocytes are unique bone marrow cells by virtue of their large size, ranging in diameter from 10 - 60 μm, and by their rarity, comprising only 0.02 - 0.05% of all marrow cells [27]. These cells are further characterized by highly defined invaginated membranes (demarcation membranes), in addition to possessing a large, multilobular nucleus containing several multiples of the normal 2N complement of DNA ranging from 8-64N, and membrane proteins necessary for the production of platelets [28,29]. Primarily found in the bone marrow and in the lungs, megakaryocytes result in the formation of platelets by the extension of attenuated cytoplasmic processes (pseudopodiae) through holes in the endothelial sinus wall lining, which pinch off at various lengths and are swept

away in the blood as putative platelets [30,31]. The number of platelets produced from a typical megakaryocyte can be on the order of 10,000 whereby megakaryocytes of higher ploidy result in the formation of a greater number of large platelets that are hyper-reactive with respect to hemostatic efficacy [28,30].

Platelets have important physiological functions in hemostasis, blood coagulation, and the maintenance of vascular integrity. In addition, platelets participate physiologically in the healing repair of tissue injury, by the release of factors which favor the formation of connective tissue. Located in regions called α-granules these factors include platelet derived growth factor (PDGF), and transforming growth factor β1 (TGFβ1) [32]. Due to the heterogenity of platelet size, density, and reactivity they also are involved pathologically in atherosclerotic elements of ischaemic heart disease [33]. Although originating from polyploid megakaryocytes, platelets are essentially devoid of DNA, and possess a negligible capacity for protein synthesis [33].

Megakaryocytopoiesis is the cellular developmental process prior to the release of platelets into circulation. Upon commitment, small mononuclear megakaryocyte precursor cells are amplified by multiple rounds of mitosis followed by a gradual loss of the capacity for proliferation as these cells then begin a process of endomitosis and endoreduplication in the absence of cell division. Pleiotropic cytokines such as thrombopoietin, IL-3, M-CSF, IL-6, and M-CSF control the growth, survival and maturation of these cells which will eventually produce platelets [29]. In their final state, mature megakaryocyte cells are significantly larger in size, possess increased DNA ploidy and cytoplasmic granulation [34,35], and express platelet specific proteins such as platelet peroxidase (PPO), and glycoproteins Ib (CD42b), and IIb/IIIa (CD41) [33,36]. The heterodimer gpIIb/IIIa

belongs to the receptor family of integrins and participates it the specific binding of fibrinogen, fibronectin, and vitronectin thus facilitating platelet aggregation [33,36].

3.1.6 Induction of K562 megakaryocyte-like differentiation

Mechanisms regulating megakaryocyte development have not been fully elucidated in part because of the technical difficulty in isolating samples, as well as due to the rarity of these cells in the marrow. In an effort to circumvent these problems, various human leukemic cell lines such as HEL and LAMA-84 [37] have been established as ideal models for studying the induction of megakaryocyte characteristics. Comparably, the K562 cell line has also been observed to possess and accumulate megakaryocyte properties, aside from its obvious inducible erythroid-like characteristics. Vainchenker *et al.* [38] was the first to demonstrate on an ultrastructural level that ~1-2% of K562 cells possessed peroxidase activity in the nuclear envelope and rough endoplasmic reticulum, consistent with platelets and megakaryocytes and that the number of positive cells increased to 30% upon exposure to sodium butyrate. Gewirtz *et al.* [39] later reported that ~35% of K562 cells constitutively express platelet glycoprotein, and Tetteroo *et al.* [40] further showed that the expression of platelet gpIIIa is strongly enhanced on the surface of K562 cells upon treatment with phorbol esters such as: 12-O-tetradecanoylphorbol-13-acetate (TPA) [40], phorbol-12,13-dibutyrate (PDBu) [41], and phorbol-12-myristate-13-acetate (PMA) [42]. These agents reportedly activate protein kinase C and consequently regulate the phosphorylation status of many proteins and enzymes, including topoisomerase II [43]. It is interesting to note as well that concomitant with the appearance of megakaryocytic markers, the expression of the erythroid lineage specific glycophorin A has been reported

to be down-regulated [32]. However, in the reverse scenario with the induction of erythroid differentiation by hemin, no modification of constitutive megakaryocyte markers has been seen [14]. Observations such as these, of the co-expression of erythroid and megakaryocytic markers further suggest the complex potentially of the K562 cell line, and its inability to diverge solely towards a single lineage upon induction.

3.1.7 DNA topoisomerase II in cell differentiation and apoptosis

The development and homeostatic maintenance of many hematopoietic cells is regulated by a number of fundamental processes that include stem cell renewal, differentiation, and cell death [15,41]. Partial differentiation of various human and rodent leukemic cell lines have been found to be induced by a number of known topoisomerase II inhibitors [3,44-49]. These include doxorubicin, amsacrine, aclarubicin, etoposide, teniposide, novobiocin, mitoxantrone, suramin, and ICRF-193 [3]. In addition, the action of other known differentiation-inducing drugs such as phorbol esters, have been shown to be associated with an eventual decrease in topoisomerase II activity with an increase phosphorylation [46,50,51], and in the case of retinoic acid, an increase in protein-associated DNA strand breaks [52]. Consequently, induced differentiation of many leukemic cell lines may be coupled with cell cycle arrest and/or terminally result in programmed cell death [3,15]. Following topoisomerase II inhibition the commitment of a cell line to apoptosis depends on such critical elements as the intensity of treatment, the induction of cleavable complexes or otherwise incurred DNA damage, the stage of differentiation, and/or the cell type. All of these factors influence how rapidly leukemic

cells are committed to either of these processes, or whether cell cycle arrest simply occurs (Fig. 3.3) [53].

Fig. 3.2. Pathways of cell commitment upon topoisomerase inhibition. (Adapted from [149]).

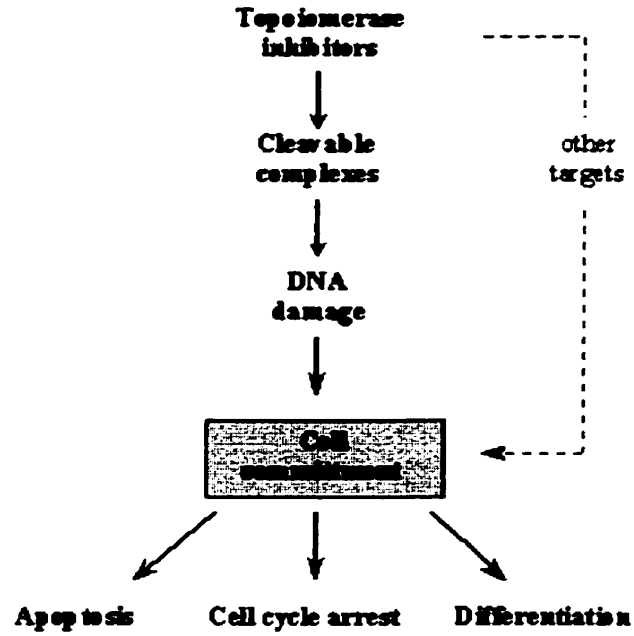

The catalytic activity of topoisomerase II can be inhibited by many of the above mentioned poisons at any stage in the cell cycle. In fact, the clinical action of most of these agents appears to target proliferating cells, which possess higher activity and levels of topoisomerase II [3,54]. As a consequence of their action, the proliferative potential of many cells may be reduced, due to a complete or transient inhibition of passage through the cell cycle. It has been suggested that perturbations of normally integrated cell cycle events may present the stimulus for the cell to engage a program of cell death [55,56]. The action of some topoisomerase II inhibitory agents may induce enzyme-mediated DNA breaks, illegitimate DNA recombinations, and gene alterations in G2/M halted cells

[53,57]. Other inhibitors could equally trigger cell death, by either inhibiting the catalytic activity of topoisomerase II needed for the separation of intertwined chromosomal DNA molecules during mitosis and/or by interfering with the structural functions of topoisomerase II in chromatin organization [3]. Overall, despite the particular mode of topoisomerase II inhibition conferred by various inducers the result is a state of differentiation which appears rarely to proceed with normality or to completeness. Alterations in the expression of various lineage-specific markers suggest that only a partial differentiation is achieved, which accordingly seems to be irreversible [3].

3.1.8 Associated changes in topoisomerase II activity and levels with differentiation/apoptosis induction

Induction of differentiation in many leukemic cell lines has been associated with a decrease in topoisomerase II activity and protein levels [3,51,58]. In contrast, relatively no change is seen in the levels of topoisomerase I in differentiated cells as compared to untreated cells. In the case of differentiation, it is not known whether changes in topoisomerase II levels, induced by inhibitors or other agents essentially triggers differentiation or is simply a result of differentiation process [3,49]. What is known is that the induction of differentiation by topoisomerase II inhibitors depends on such factors as the type of inhibitor, the dosage, the cell line being tested, as well as the lineage-specific evaluation criteria. Furthermore, support for at least a causal role of topoisomerase II in the induction of differentiation has been supported by the use of topoisomerase II inhibitors to block differentiation induced by other types of agents [3].

Induction of apoptosis in leukemic cell lines has been associated with changes in topoisomerase II levels in a strikingly similar fashion to differentiated cells [58,59]. Signs

of apoptosis can appear suddenly by the induction of lethal cleavage complexes, or more gradually by other means such as DNA damage induced by topoisomerase II inhibition, cell cycle arrest, or terminal differentiation [3,56]. In HL-60 cells induced to differentiate with retinoic acid it was found that only the topoisomerase IIα isoenzyme decreased in cellular content, whereby degradation of topoisomerase IIβ was not seen until much later when the early stages of apoptosis were evident [58]. When the same cells were subjected to etoposide-induced apoptotic conditions, the level of topoisomerase IIα remained constant while topoisomerase IIβ was completely degraded. These results, obtained by Sugimoto *et al.* [58] were amongst the first to demonstrate that topoisomerase IIα and IIβ played a fundamental role in cell proliferation and cell survival respectively, and that both were coincidentally lost upon the induction of differentiation and apoptosis.

3.1.9 Changes in gene expression and chromatin structure during differentiation and apoptosis

Since various inducers differ in their mechanisms of action, there remains a great deal of complexity and uncertainty enshrouding the nature of cell sensory and signaling events that determine which pathway a cell is committed towards upon exposure. Whether or not the initial metabolic changes involve such signal transduction pathways as exemplified by the Ca^{2+}-dependency of protein kinase C signaling [53,60], important and significant changes do occur during the processes of gene expression and post-transcriptional regulation [3]. In fact, there is a widespread agreement that induction of differentiation and/or apoptosis requires both the down regulation of several cell cycle related genes and the expression of certain other genes [3,7,55]. An altered regulation of c-

myc, c-*myb*, c-*fos*, and c-*jun* gene expression, which effect the proliferative status of a cell can consequently lead to the prevention of differentiation and the induction of apoptosis [3,61]. The expression of other gene products including c-*fes*, c-*fms*, and MER5 are essential for the differentiation of some leukemic cell lines [3]. Cells may also express any number of other genes including *p53*, *bcl-abl*, *bcl-*X_S, *bcl-*X_L, and *bcl-2* capable of inducing or suppressing programmed cell death, by a variety of methods [7,16,62,63].

The induction of differentiation and/or apoptosis leads to associated features of chromatin reorganization, caused by the opening and closing of large regions of DNA and is thus likely to have an effect on the transcription of some of the above mentioned genes. Such changes are likely to be affected by topoisomerases acting directly as structural elements on the nuclear matrix, or indirectly in altering the degree of DNA supercoiling [64]. The transcription of regions crucial for gene expression may be effected further by altered topoisomerase activities resulting in appearance of DNA strand breaks and/or altered interaction with other proteins involved in the regulation of gene expression [3].

3.1.10 Objectives in studying the effects of dexrazoxane on K562 cells

In the present study, the effect that dexrazoxane, a known topoisomerase II inhibitor has on the immortal human leukemic cell line known as K562 was investigated by a variety of methods. In light of the effects of dexrazoxane on CHO cells as described in Chapter 2, and the above mentioned introductory information, the objectives of this study were multifaceted. Firstly, we wished to show that by virtue of its action, dexrazoxane would have a similar effect on a human-derived cell line as did on CHO cells, in which polyploidization was observed in the absence of cytokinesis. Many clinically

used topoisomerase II inhibitors have been demonstrated as being capable of inducing differentiation and/or apoptosis in a broad spectrum of leukemia cells, a likely important part of their clinical activities [3]. To that effect, it was the further aim of the following study to examine in a variety of situations the ability of dexrazoxane, and to a lesser extent other bisdioxopiperazines and agents to induce erythroid-like differentiation and/or apoptosis in K562 cells. Finally, due to the evident morphological similarities of some dexrazoxane-treated K562 cells to megakaryocytes, the expression of erythroid and megakaryocyte antigens were examined in an immunofluorescence flow cytometry analysis.

3.2 Cytotoxic effects of topoisomerase II inhibitors on normal K562 cell growth

3.2.1 Introduction

In the following section, human leukemic K562 cells were exposed to dexrazoxane under various conditions in order to examine the effect on cell growth, doubling time and viability. First, K562 cells were grown as suspension cultures and exposed to a 100 μM of dexrazoxane under a variety of exposure conditions. Since the half-life of dexrazoxane in media is 9.3 hr at pH 7.4 [65] it was presumed that a concentration of 100 μM would be sufficient enough to inhibit topoisomerase II in the entire cell population if given for at least twice the cell cycle time (~18 hr). To that effect various drugging protocols were tested to examine the extent to which K562 cell proliferation could be inhibited by dexrazoxane. In addition, a series of cytotoxicity experiments were conducted on K562 cells in order to assess the level of growth inhibition caused by dexrazoxane, ADR-925, ICRF-193, ICRF-154, etoposide, and doxorubicin (Fig. 3.3). Cytotoxicity towards the above mentioned agents was first evaluated using a colorimetric MTS (3-(4,5-dimethyl-thiazol-2-yl)-5-(3-carboxymethoxyphenyl)-2-(4-sulfophenyl)-2H-tetrazolium) assay after it was previously optimized. As a more direct measurement of cytotoxicity, the number of cells remaining in culture after dexrazoxane treatment was additionally assessed in a cell counting analysis with the use of a model Z_f Coulter counter.

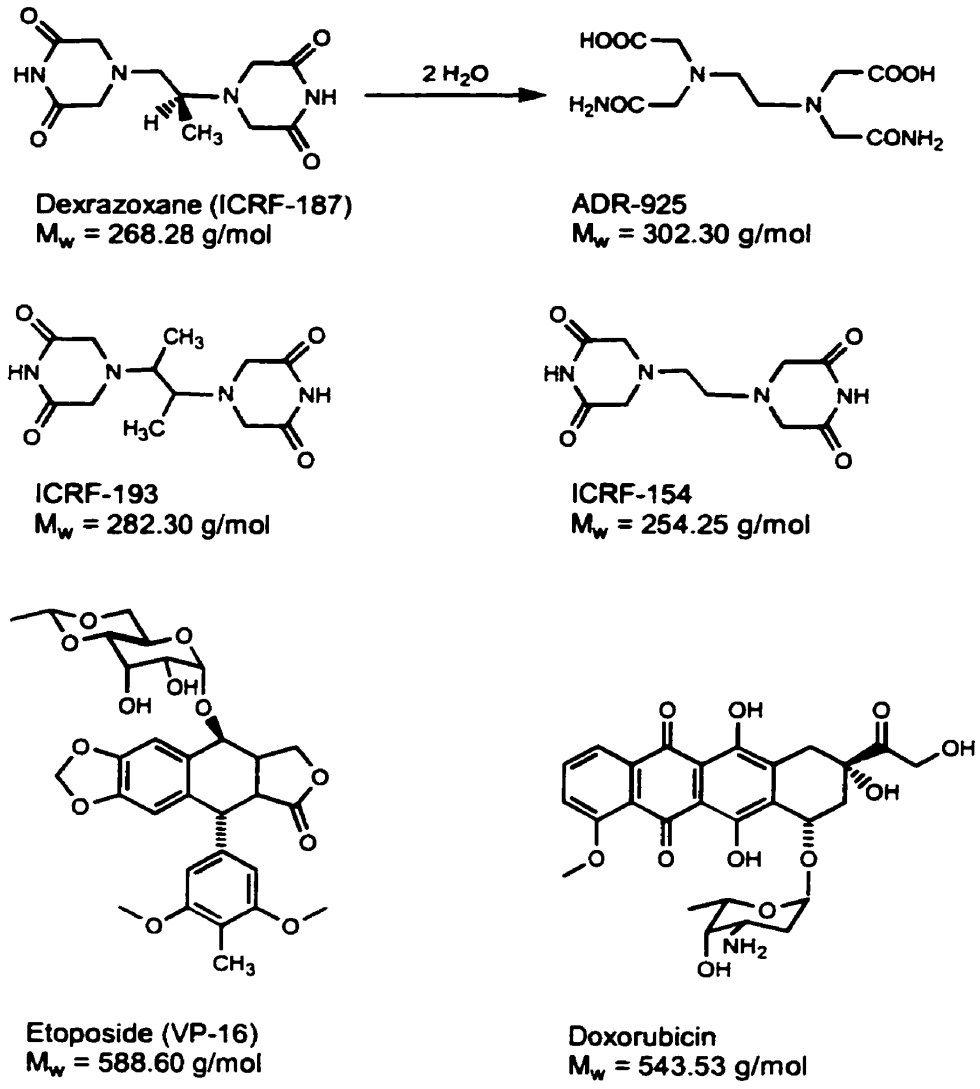

Fig. 3.3. Chemical structures of all drugs tested.

3.2.2 Materials and Methods

3.2.2.1 Materials

3.2.2.1.1 Drugs, chemicals, and reagents

Dexrazoxane (Zinecard®, ICRF-187), ADR-925, and doxorubicin were gifts of Pharmacia & Upjohn (Columbus, OH, U.S.A.). Etoposide, was obtained from Sigma Chemical Co. (cat. No. E-1383), ICRF-193 and ICRF-154 were synthesized previously in our laboratory. DMSO used to dissolve drugs, 99.5% cat. No. D-5879), trypan blue dye (cat. No. T-6146), HEPES (cell culture grade, cat. No. H-9136), were obtained from Sigma Chemical Co. (St. Louis, MO, U.S.A.). Sodium bicarbonate ($NaHCO_3$, cat. No. BP328-079) was obtained from Fisher Scientific (Fairlawn, NJ, U.S.A.). Dulbecco's phosphate buffered saline (PBS, cat. No. D-5652), Dulbecco's modified eagle medium (DMEM, cat. No. 12800-017), penicillin-streptomycin (cat. No. 25200-072), and fetal bovine serum (FCS, cat. No. 26140-079) were obtained from Gibco-BRL, Life Technologies Inc. (Burlington, ON). Na_2EDTA (cat. No. 10093) was obtained from BDH Chemicals Ltd. (Toronto, ON). Sodium chloride (NaCl, cat. No. AC-8304) was obtained from Anachemia Ltd. (Toronto, ON). Sodium hydroxide (5N NaOH, cat. No. H369) was obtained from Mallinckrodt Specialty Chemicals Co. (Paris, KT, U.S.A.). MTS, CellTiter 96® AQ_{ueous} One Solution Reagent (cat. No. G3580) was obtained from Promega Corp. (Madison, WI, U.S.A.) and stored at –20°C protected from light. Isoton II Coulter balanced electrolyte solution (cat. No. PN 8546719) was obtained from Beckman Coulter Inc. (Burlington, ON). Carbon dioxide (standard grade) was purchased from Welder's Supply (Winnipeg,

MB). Microtitre plates (96-well, sterile, cat. No. 83.1835), 50 mL sterile PP conical centrifuge tubes (29x114 mm, cat. No. 62.547.004), T-25cm^2 (cat. No. 83.1810.502) and T-75cm^2 (cat. No. 83.1813.502) PE green 0.2 μm vented plug capped flasks for suspension cultures, and all other plasticware were obtained from Sarstedt Inc. (St. Leonard, PQ).

3.2.2.1.2 Preparation of drugs and reagents

Dexrazoxane (M_w = 268.28 g/mol) and ADR-925 (M_w = 302.3 g/mol) were dissolved in cell culture medium (DMEM/FCS) and filter sterilized through a 0.2 μm acetate filter. Etoposide (M_w = 588.6 g/mol), ICRF-193 (M_w = 282.3 g/mol), ICRF-154 (M_w = 254.25 g/mol), and doxorubicin (M_w = 543.53 g/mol) were dissolved in 99.5% DMSO by brief sonication and heating in a 37°C water bath and subsequently added to cell cultures such that DMSO concentrations would not exceed 0.5% (v/v). Trypan blue dye (0.6% w/v) was prepared by dissolving 0.6 g of dye in a ddH_2O containing 150 mM NaCl and 1 mM Na_2EDTA.

3.2.2.1.3 Culturing of K562 cells

Human erythroleukemic K562 cells were donated by Dr. Jack C. Yalowich (University of Pittsburgh School of Medicine, Pittsburgh, PA, U.S.A.) with whom our laboratory has established a collaboration. In order to cross-correlate future results with Dr. Yalowich's laboratory K562 cells were similarly grown as suspension cultures in T-flasks in DMEM containing 20 mM HEPES, 100 units/mL penicillin G, 100 μg/mL streptomycin, 10% (v/v) fetal bovine serum in an atmosphere of 5% (v/v) CO_2 and 95%

(v/v) air at 37°C (pH 7.1). Cell densities (cells/mL) in cultures were assessed from aseptically removed aliquots by the use of a model Z_f Coulter counter (Coulter Electronics, Hialeah, FL, U.S.A.), as explained in Appendix A.2. Cell viability was assessed in a trypan blue dye exclusion analysis by the dilution of culture samples 1:1 with trypan blue dye. A minimum of 500 cells were counted in a hemacytometer chamber followed by the determination of the percentage of non-viable (blue) cells per total number of cells counted.

3.2.2.2 Growth curve characteristics of K562 cells exposed to dexrazoxane under different conditions

Exponentially growing cultures were diluted to starting cell densities of $2x10^5$ cells/mL in T-75 flasks followed by the addition of 1-2 mL of dexrazoxane such that the final drug concentration produced would be 100 μM (total volume of 15-40 mL). Four separate drugging protocols were performed alongside control cultures to examine the effects of different dexrazoxane treatment periods on cell growth. In the first culture, cells were treated daily with dexrazoxane without media replacement such that the daily drug concentration in the culture would be approximately 100 μM. The second culture was treated in an identical manner as the first except that culture media was replaced daily. The third culture was exposed with 100 μM dexrazoxane at 0, and 48 hr of growth with media replaced after 24, and 48 hr of growth. The fourth and final treated culture was exposed once to 100 μM dexrazoxane at 0 hr without any media replacement at subsequent time intervals.

After every 24 hr interval of growth a 1-2 mL aliquot was removed from each culture using a sterile Pasteur pipet. Cell viability was assessed as explained earlier in Section 3.2.2.1.3. In addition, cell densities were determined by counting on a model Z_f Coulter counter with a 100 μm aperture tube, threshold setting of 7 (1/amp. = 2, 1/ap.current = 8, diameter cutoff ≅ 8.7 μm), as explained in Appendix A.2. For those cultures in which media was replaced at specified intervals cells were aseptically removed, centrifuged at 250 *g* for 12 minutes, and resuspended in an appropriate volume of ~80% fresh DMEM/FCS in an attempt to maintain cell densities approximately equivalent to that of before centrifugation. This was followed by a subsequent exposure to 100 μM of dexrazoxane, administered in the same fashion as before.

3.2.2.2.1 Normalization of cell counts from cultures in which media is replaced

The pattern of cell growth from a suspension culture can easily be followed by measuring the changing cell densities with time through the removal of sample aliquots. However, in the case of researcher intervention such as with the changing of media a normalization of cell counts is required. This is to correct for the slight fluctuation in culture volumes and cell densities in order to obtain a smooth growth curve. In brief, normalization was achieved by multiplying in order of cell densities, by a numerical factor (±) in which the cell density changed from its determination after centrifugation and resuspension, to the following 24 hr interval. In Table 3.2 are shown the quantified cell densities before and after centrifugation from the second K562 cell culture exposed daily to 100 μM dexrazoxane with media replacement. The final normalized cell density for each 24 hr time interval was determined as follows,

Example:

$$\text{Normalized 48 hr Cell density} = \frac{\text{Cell density at 48 hr}}{\text{Cell density at 25 hr}} \times \frac{DT}{AT} \times \text{Cell density at 24 hr}$$

where, ***DT*** = desired time interval between cell density data points on growth curve, (i.e. 24 hr)

AT = actual time interval from the time after centrifugation and resuspension to the following day (i.e. from 25 to 48 hr of growth = 23 hr)

$$\therefore \text{Normalized 48 hr Cell density} = \frac{2.38E+05 \text{ cells/mL}}{2.27E+05 \text{ cells/mL}} \times \frac{24 \text{ hr}}{23 \text{ hr}} \times 2.13E+05 \text{ cells/mL}$$

$$= 2.33E+05 \text{ cells/mL}$$

then,

$$\text{Normalized 72 hr Cell density} = \frac{\text{Cell density at 72 hr}}{\text{Cell density at 49 hr}} \times \frac{DT}{AT} \times \text{Normalized 48 hr Cell density}$$

$$\therefore \text{Normalized 72 hr Cell density} = \frac{2.25E+05 \text{ cells/mL}}{1.77E+05 \text{ cells/mL}} \times \frac{24 \text{ hr}}{23 \text{ hr}} \times 2.33E+05 \text{ cells/mL}$$

$$= 3.09E+05 \text{ cells/mL}$$

and so forth up to 120 hr of growth.

Table 3.2. Initial and final normalized cell densities from a K562 culture exposed daily to dexrazoxane with media replacement.

Time (hr)	Cell density (cells/mL)	Time (hr)	Cell density (cells/mL)
0	2.00E+05	0	2.00E+05
24	2.13E+05	24	2.13E+05
25	2.27E+05	48	2.33E+05
48	2.38E+05	72	3.09E+05
49	1.77E+05	96	3.38E+05
72	2.25E+05	120	3.89E+05
73	1.40E+05		
96	1.47E+05		
97	1.39E+05		
120	1.53E+05		

3.2.2.2.2 Determination of growth rates and doubling times of cultured cells

In most control unexposed cultures it is a common occurrence to observe a decline in growth potential beyond a point of confluence, which in the case of suspension cells begins to occur at cell densities above 1 x 10^6 cells/mL. In the determination of the growth rate of these such cell cultures only those time periods in which exponential growth was observed were used in the following calculations. The doubling time of cultured cells was computed using the following single exponential rise equation,

$C_t = C_o e^{\kappa t}$

where, C_t = the cell density at time t (cells/mL)
C_o = the starting initial seeded cell density (cells/mL)
e = the base of the natural logarithm
κ = the growth rate constant (hr^{-1})
t = the time (hr) at which C_t is determined

Example:

First, a crude rough determination of κ is made using values of C_o , C_t , and t chosen from the collected data. From the fourth K562 culture treated once with 100 μM dexrazoxane at 0 hr without any media replacement at subsequent time intervals the following values were chosen,

C_o = 2.26E+05 cells/mL at the start of the experiment
C_t = 8.03E+05 cells/mL at the end of the experiment
t = the time at which C_t is determined, in this case 119 hr

$$C_t = C_o e^{\kappa t}$$

$$\frac{C_t}{C_o} = e^{\kappa t}$$

$$\frac{8.03E+05}{2.26E+05} = e^{\kappa (119)}$$

$$3.5609 = e^{\kappa (119)}$$

$$1.2700 = \kappa * (119) \qquad \text{(taking the natural logarithm)}$$

$$\kappa = \frac{1.2700}{119}$$

$$\kappa = 0.01067 \text{ hr}^{-1}$$

Next, a more accurate determination of κ is made using this rough estimate as well as the entire span of collected cell density data in a nonlinear regression analysis using SigmaPlot. Under <Statistics> choose <Nonlinear Regression>, then open up the single exponential rise fit file (exprise1.fit). This analysis program performs a series of iterations using the collected cell density data to determine the best value for κ. This equation used is of the same form as $C_t = C_o e^{\kappa t}$, expressed as f = a*exp(b*x) where f = C_t, a = C_o, b = κ, x = t. In the following example under [Parameters] and [Variables], the values of a, b, x, and y are assigned where b is the rough estimate of κ, determined above.

Single exponential rise fit file (exprise1.fit):

```
;f = a exp(bx), starts at f (0) = a and
;rises with a time constant = 1/b
;Modify these values for your data
a = 225500              ;amplitude, initial starting cell density
b = 0.01067             ;rate constant
[Variables]
x = col(1)              ;change to appropriate column
y = col(2)              ;change to appropriate column
[Equations]
f = a*exp (b*x)
fit f to y
[Constraints]
b > 0                   ;prevents exponential decay
```

Afterwards the outputted value of b (or rather κ) is inserted back into the original single exponential rise equation in order to determine the value of t when the cell density has doubled, or increased by a factor of 2.

$C_t = C_o e^{\kappa t}$

$\frac{C_t}{C_o} = e^{\kappa t}$

$2 = e^{\kappa t}$ when $C_t = 2C_o$, or rather cell density has doubled

$0.693 = \kappa t$ (taking the natural logarithm)

$t = \frac{0.693}{\kappa}$

$t = \frac{0.693}{9.63\text{E-}03}$ substituting in the outputted value of κ

$t = 71.94$ hr

3.2.2.3 Optimization of the MTS, CellTiter 96® AQ_{ueous} One Solution cell proliferation assay

3.2.2.3.1 Background information

The MTS, or CellTiter 96® AQ_{ueous} One Solution cell proliferation assay is a colorimetric method licensed exclusively to Promega Corp. (Madison, WI, U.S.A.) which is used for determining the number of viable cells in proliferation or cytotoxicity assays. This one-solution reagent contains, with enhanced chemical stability a yellow tetrazolium dye called MTS or [3-(4,5-dimethylthiazol-2-yl)-5-(3-carboxymethoxyphenyl)-2-(4-sulfo-phenyl)-2H-tetrazolium], and an electron coupling reagent known as PES or (phenazine ethosulfate). When added to cells in tissue culture medium MTS is indirectly bioreduced into a blue colored soluble formazan product (Fig. 3.4) by mitochondrial cytosolic reductases such as NADPH or NADH [66]. The MTS assay is ideal for growth inhibition or cytotoxicity analysis of suspension cells such as K562 since there are no washing, cell harvesting, or solubilization steps involved. Basically, a small amount of the MTS reagent is added directly into culture wells on a 96-well plate, and then incubated for 1-4 hr. Then, the amount of the formazan product produced is measured by the amount of 490 nm absorbance, which is directly proportional to the number of living cells in culture.

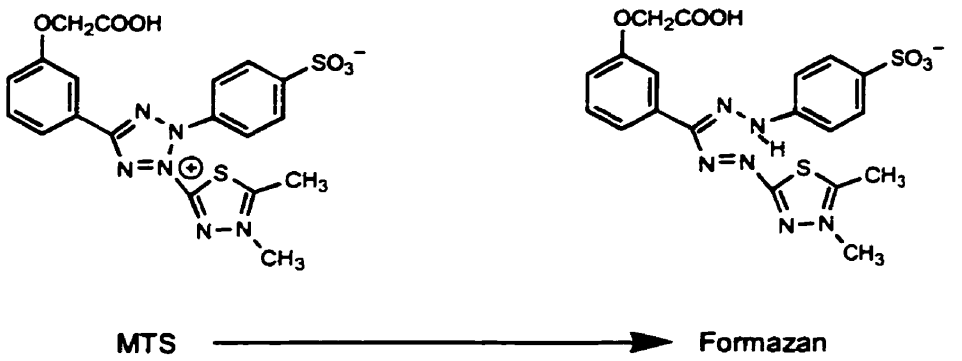

Fig. 3.4. Structure of MTS tetrazolium and its formazan product.

3.2.2.3.2 Maintaining assay sensitivity while optimizing MTS reagent usage

Although the concentrations of tetrazolium and electron transfer reagents had been previously optimized by Promega Corp. (Madison, WI, U.S.A.) as indicated in their technical bulletin, it was of particular interest to determine if assay sensitivity would be compromised by the use of a reagent:medium ratio lower than the suggested ratio of 20μL:100μL. To this effect, various numbers of K562 cells were added in replicate (x6) to the wells of two 96-well microtitre plates in DMEM/FCS to volumes of 100 μL/well. The MTS reagent was thawed for 15 min in a 37°C water bath. Into each well of the first 96-well assay plate was added 10 μL of MTS reagent followed by 10 μL of DMEM/FCS using multichannel pipettors. Into each well of the second 96-well assay plate was added 20 μL of the MTS reagent. Plates were then incubated for 1-3 hr at 37°C in a humidified, 5% (v/v) CO_2 atmosphere. After each 1 hr time interval the plates were removed from incubation and the absorbances at 490 nm for each well were recorded using a Thermomax 96-well plate reader (Molecular Devices, Menlo Park, CA, U.S.A.). Absorbance was

a Thermomax 96-well plate reader (Molecular Devices, Menlo Park, CA, U.S.A.). Absorbance was corrected for non-specific, scattered light by subtracting the absorbance at 650 nm from the absorbance at 490 nm. Subsequently, average absorbances from replicate determinations were plotted versus the number of cells/well in order to examine the limitations of the linear relationship with respect to each plate analyzed.

3.2.2.4 Cytotoxicity experiments by MTS analysis

3.2.2.4.1 Seeding of microtitre plates with cells

Exponentially growing cultures were diluted to starting cell densities of 36,000 cells/mL in the case of dexrazoxane and ADR-925 cytotoxicity analyzes, and to 20,100 cells/mL for all other drugs analyzed which required solubilization in DMSO. It was previously determined through optimization of the MTS assay (Section 3.2.3.2) that a concentration of 32,000 cells/well in control columns at the stage of analysis was ideally within the range of sensitivity for accurately resolving a growth inhibition curve. Therefore, based on an 18 hr doubling time (Table 3.4) cells were seeded at 1800 cells/well such that cell densities would reach 32,000 cells/well in control columns after 72 hr of growth. Cells were delivered into microtitre wells in replicate (x6) between columns 2-12 and rows B-G using a multichannel pipettor. For cytotoxicity analysis of drugs requiring solubilization in DMEM/FCS, 50 μL of cells at 36,000 cells/mL were added to each well, and for drugs requiring solubilization in DMSO, 89.5 μL of cells at 21,000 cells/mL were added in the same manner.

3.2.2.4.2 Delivery of drug to microtitre plates

After the appropriate quantity of drug was weighed and solubilized as described in Section 3.2.2.1.2 drug stock solutions were prepared and added to microtitre plates immediately after seeding. A typical drug map illustrated in Table 3.3 demonstrates an example of how each drug stock solution was prepared and added in replicate (x6) to the wells of each plate such that the drug was used sparingly and the total final volume per well was 90 μL. Drugs solubilized in DMEM/FCS (dexrazoxane, ADR-925) were added at 40 μL/well using a multichannel pipettor, and drugs solubilized in DMSO (ICRF-154, ICRF-193, etoposide, doxorubicin) were added at 0.5 μL/well individually using an Eppendorf 2 μL micropipettor with sterile microtips. When DMSO was used as a solvent its final concentration in cell culture medium was 0.5% (v/v), and controls were included in experiments to ensure that DMSO did not effect cell growth. Into all outer wells that did not contain cells (rows A and H, and column 1) was placed 100 μL of PBS for spectrophotometer blanking and/or the prevention of evaporation from inner wells containing cells and drug. To further maintain a consistent volume of 90 μL/well in all inner wells each plate was wrapped individually with Saran wrap (Dow Brands Canada Inc., Paris, ON) before placing in the incubator at 37°C with 5% (v/v) CO_2.

Table 3.3. A typical drug map for DMSO soluble drugs.

Example: ICRF-193 (M_w = 282.3 g/mol)

Drug Stock #	Prepared from Stock #	Vol_{stock} (µl)	$Vol_{solvent}$ (µl)	$[drug]_{stock}$ (µM)	Vol_{well} (µl)	$[drug]_{well}$ (µM)
A	1.385 mg	-	545.1	9000	0.5	50
B	A	40	60	3600	0.5	20
C	A	20	80	1800	0.5	10
D	A	10	90	900	0.5	5
E	D	40	60	360	0.5	2
F	D	20	80	180	0.5	1
G	D	10	90	90	0.5	0.5
H	G	40	60	36	0.5	0.2
I	G	20	80	18	0.5	0.1
J	G	10	90	9	0.5	0.05
K	J	40	60	3.6	0.5	0.02
L	J	20	80	1.8	0.5	0.01
M	J	10	90	0.9	0.5	0.005
N	M	40	60	0.36	0.5	0.002
O	M	20	80	0.18	0.5	0.001

Plate #1:

	Column Number											
	1	2	3	4	5	6	7	8	9	10	11	12
Vol_{cells} (µl)	-	89.5	89.5	89.5	89.5	89.5	89.5	89.5	89.5	89.5	89.5	89.5
Vol_{drug} (µl)	-	0.5	0.5	0.5	0.5	0.5	0.5	0.5	0.5	0.5	0.5	0.5
$[drug]_{plate}$ (µM)	-	0	0.001	0.002	0.005	0.01	0.02	0.05	0.1	0.2	0.5	1
Drug Stock #	PBS	DMSO	O	N	M	L	K	J	I	H	G	F

Plate #2:

	Column Number											
	1	2	3	4	5	6	7	8	9	10	11	12
Vol_{cells} (µl)	-	89.5	89.5	89.5	89.5	89.5	89.5	89.5	89.5	89.5		
Vol_{drug} (µl)	-	0.5	0.5	0.5	0.5	0.5	0.5	0.5	0.5	0.5		
$[drug]_{plate}$ (µM)	-	0	0.2	0.5	1	2	5	10	20	50		
Drug Stock #	PBS	DMSO	H	G	F	E	D	C	B	A		

3.2.2.4.3 Measurement of cytotoxic effects

After 72 hr of growth in the presence of drug a suitable amount of the MTS one solution reagent (Promega Corp., Madison, WI, U.S.A.) was removed aseptically and placed into a sterile boat after thawing for 15 min in a 37°C water bath. Into the appropriate wells of each microtitre plate was added 10 µL of MTS reagent such that the final volume per well was 100 µL. Plates were then incubated for 3 hr at 37°C in a humidified, 5% CO_2 atmosphere after which time a Thermomax 96-well plate reader (Molecular Devices, Menlo Park, CA, U.S.A.) was used to measure absorbance at 490 nm in the wells. Absorbance was corrected for non-specific, scattered light by subtracting the absorbance at 650 nm from the absorbance at 490 nm.

3.2.2.4.4 Dose-response curves

Data from all cytotoxicity experiments was inputted into SigmaPlot (Jandel Corp., San Rafael, CA, U.S.A.) and used to determine the 50% inhibitory concentration (IC_{50}) for the drugs tested on K562 cells. Prior to graphical representation of dose-response curves outlier absorbances were removed empirically with statistical relevance using the provided transform file entitled *!outlier.xfm*. Non-linear, least-squares fitting of the absorbance-drug concentration data was performed in SigmaPlot using the following three- or four-parameter logistic equation,

$$Abs_{490/650} = (a - d) / (1 + (x / c)^b) + d$$

where $Abs_{490/650}$ is the absorbance at 490 nm minus the absorbance at 650 nm, x is the drug concentration, c is the median inhibitory concentration (IC_{50}), b is the Hill-type exponential factor indicative of the rate at which toxicity increases with increasing drug concentration, a is the estimated maximal absorbance and d is the estimated background absorbance at the highest drug concentration. When the background absorbance is close to zero d was set equal to 0, thus giving a three-parameter equation. The values of b and c were initially computed from a two-parameter fit after substitution of the a and d values. Subsequently, more accurate values of b and c were determined upon the iteration of a three- or four-parameter fit equation with the inclusion of the same a and d values and the b and c values computed from the two-parameter fit equation.

3.2.2.5 Cytotoxicity experiments by cell counting analysis

Colorimetric assays such as MTT and MTS are two of the most common methods for evaluating the effect of drugs on growth and survival of cells in culture. In general, these assays produce a reliable agreement between the number of viable cells in culture and the production of formazan, based on the mitochondrial dehydrogenase activity in viable cells [67]. However, as noticed previously with respect to CHO cells (Section 2.11.1), and by other authors with similar tumor cell lines [67], on occasion discrepancies may exist between the actual number of cells and the quantity of formazan produced. To that effect, it was decided to investigate directly the level of dexrazoxane-mediated cytotoxicity on K562 cells by cell counting, and to compare these results to those obtained by MTS analysis.

Counting analysis of cell proliferation in the presence of various concentrations of dexrazoxane was assessed twice using two slightly different protocols. In the first method, exponentially growing cells were seeded consistently at 0.6×10^5 cells/mL to a volume of 3.4 mL in 6-well tissue culture plates. This was followed by the addition of 0.1 mL of the requisite stock solution of dexrazoxane to produce the desired final concentration as single determinations. After 72 hr of growth at 37°C with 5% (v/v) CO_2 cell densities were determined on a model Z_f Coulter counter using a 100 μm aperture, threshold setting of 20 (1/amp = 2, 1/ap.curr = 8, diameter cutoff ≅ 11.9 μm) for an accurate determination of the actual number of whole cells. The median dexrazoxane inhibitory concentration (IC_{50}) was determined in the same fashion as before (Section 3.2.2.4.4) from constructed dose-response curves of cell density versus dexrazoxane concentration.

In the second method employed for IC_{50} determination cells were seeded at various starting densities before exposure to dexrazoxane. The rationale for this method of analysis is explained later in further detail (Section 3.4.3.2), as it applies directly to the objectives of a subsequent experiment. In brief, for dexrazoxane concentrations of 0-5 μM cells were seeded at $0.6x10^5$ cells/mL, for 10 and 30 μM at $0.75x10^5$ and $1.75x10^5$ cells/mL respectively, and for concentrations of 100-5000 μM were seeded at $3.0x10^5$ cells/mL. All cells were seeded accordingly as single determinations to 14 mL in T-25 flasks, followed by the addition of 1 mL of the requisite stock solution of dexrazoxane to produce the desired final concentration. Cells were then grown, as before for the duration of 72 hr, without any intervention or replacement of media. After this period of time cell densities were determined by counting on a model Z_f Coulter counter with the same settings as before. Dose-response curves were constructed by plotting the factor of increase in cell density or C/C_o (i.e. final cell densities (C) relative to initial seeded densities (C_o)) versus the range of dexrazoxane concentrations tested, and IC_{50} values were subsequently determined as previously explained.

3.2.3 Results

3.2.3.1 Growth curves after dexrazoxane exposure

Initial experiments investigating the effects of various exposures of dexrazoxane on K562 cell growth are demonstrated in Fig. 3.5a. Growth curves displayed here seemed to suggest that single or dual exposures to dexrazoxane were able to partially inhibit cell growth. Daily exposure to dexrazoxane with or without media replacement resulted in a significantly greater inhibition of growth. These observations were complemented by the calculated doubling times and growth rates of the respective cultures studied (Table 3.4). Untreated K562 cells exhibited a doubling time of approximately 19 hr. As cells were exposed to dexrazoxane for longer periods of time the rate of growth declined accordingly. Cell cultures exposed to dexrazoxane up to 5 times with or without media replacement exhibited doubling times that were approximately 2 times longer than cells exposed once or twice to dexrazoxane, and up to 7.5 times longer than control cells. Monitored changes in cell viability correlated well with the doubling rates of their respective cultures. Cells exposed to dexrazoxane for longer periods of time were not only slower to divide but also exhibited a greater decline in percent viability as compared to cells exposed to dexrazoxane for shorter periods of time (Fig. 3.5b). Furthermore, viability did not decline as rapidly in cultures treated under conditions of daily media replacement. Overall, these results indicate that daily exposure to dexrazoxane is able to inhibit the division of K562 cells. Furthermore, when accompanied with daily media replacement any decline in cell viability can be attributed to the effects of dexrazoxane rather than a deprivation nutrients.

Table 3.4. Growth rates of K562 cells exposed to dexrazoxane under different conditions as determined by cell counting on a Coulter counter.

Duration of dexrazoxane exposure	κ (hr^{-1})	S.E.	C.V. (%)	t (hr)
Unexposed control cells	3.69E-02	1.60E-03	4.3	19
Daily (0-120 hr) with media replacement	6.04E-03	5.34E-04	8.8	115
Daily (0-120 hr) without media replacement	4.42E-03	1.41E-03	32.0	141
Exposed at 0,48 hr with media replaced at 24, 48 hr	7.88E-03	9.10E-04	11.6	88
Exposed once at 0 hr without any media replacement	9.63E-03	1.80E-03	18.7	72

NOTE: Determinations were made using only cell densities which fell below 1.0E+06 cells/mL

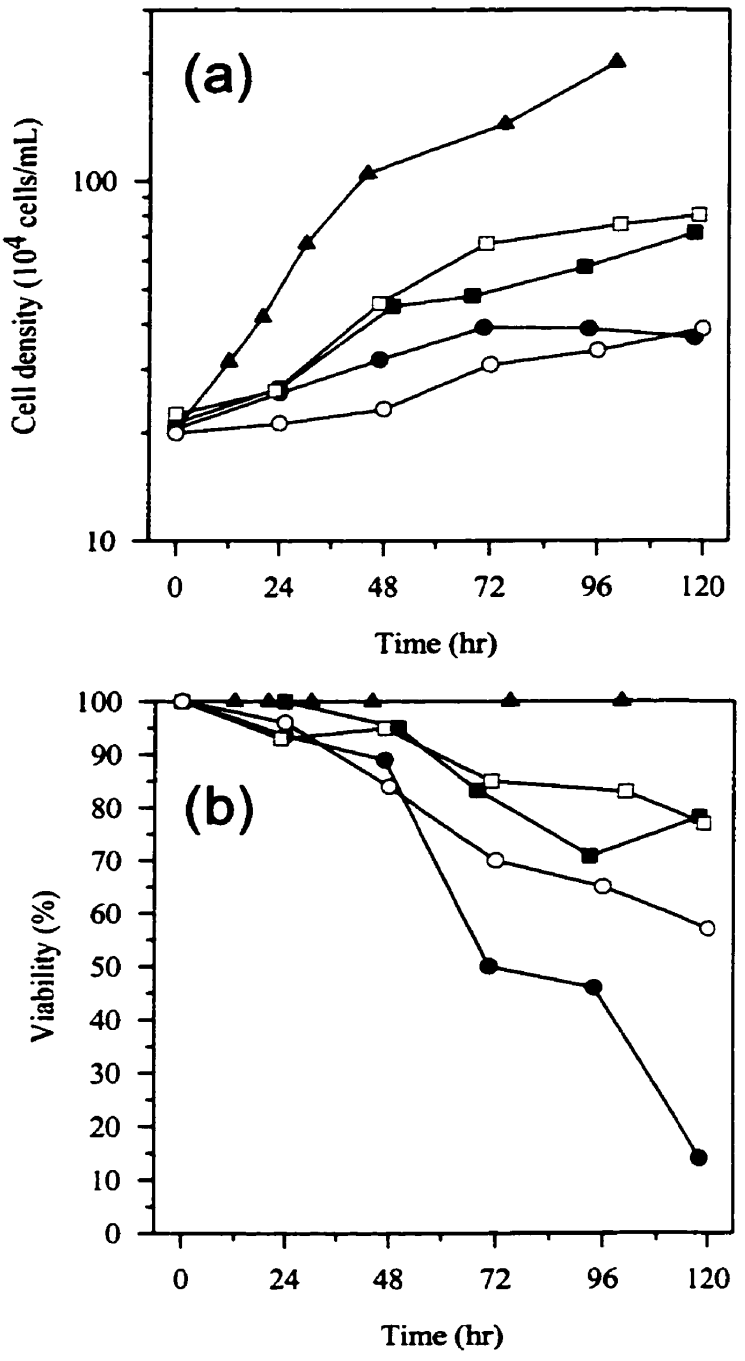

Fig. 3.5. Initial trial results examining the effects of different dexrazoxane drugging protocols on cell proliferation, and viability. Cells were seeded at initial densities of $2x10^5$ cells/mL and treated daily with 100 μM dexrazoxane without media replacement (●); daily with media replacement (○); at 0, 48 hr with media replacement at 24, 48 hr (■); at only 0 hr with no media replacement (□); and non-treated control cells were seeded as well without any media replacement (▲). At indicated times, samples were removed and (a) cell densities were determined with the use of a Coulter counter (threshold of 7, 100 μm aperture, diameter cutoff ≅ 8.7 μm); and (b) viability was determined using a trypan blue dye exclusion analysis.

3.2.3.2 Optimization of MTS reagent usage conditions

Use of a reagent:medium ratio of 20 μL:100 μL in plate B, as suggested by Promega Corp. produced a linear response at each assayed time interval between cell number and absorbance at 490-650 nm from 10,000 – 100,000 cells/well even at high absorbance readings (Fig. 3.6b). The use of a reagent:medium ratio of 10 μL:100 μL in plate A produced a similar linear response between cell number and absorbance at 490-650 nm but only from 10,000 – 50,000 cells/well and at assayed time intervals of 2 and 3 hr of incubation (Fig. 3.6a). Absorbances were approximately on average 1.5 times greater in plate B than in plate A from the interval of 10,000 – 100,000 cells/well. Based on these results MTS assay sensitivity is not compromised by the use of a reagent:medium ratio of 10 μL:100 μL so long as there is between 10,000 – 50,000 cells/well. Therefore, subsequent MTS cytotoxicity protocols were designed such that control wells would contain at the stage of analysis approximately 30,000 cells/well and then incubated with 10 μL/well of MTS reagent for at least 2 hr.

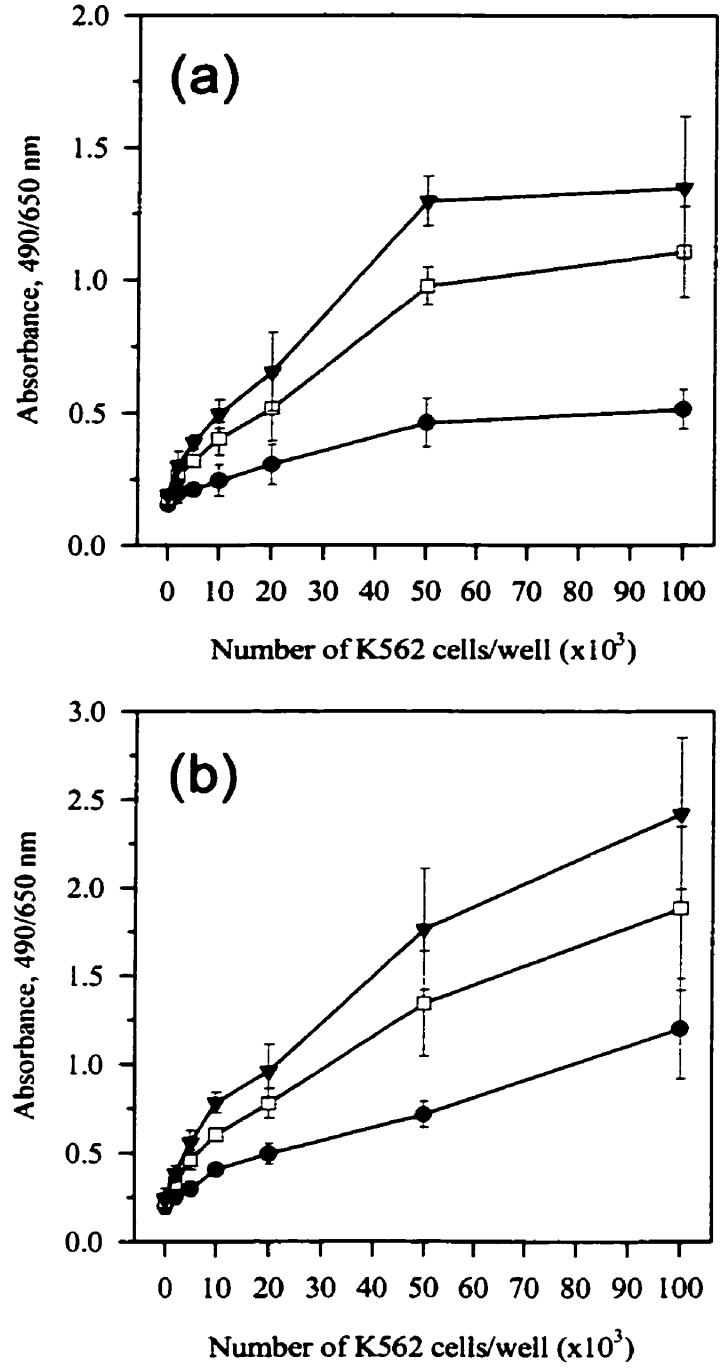

Fig. 3.6. Effect of cell number on absorbance at 490 nm measured using MTS assay. Various numbers of K562 cells were added to the wells of two 96-well plates in DMEM/FCS. Medium was equilibrated to a volume of 100 μL/well with the addition of MTS reagent in the quantities of 10 μL/well to the first plate (a), and 20 μL/well to the second plate (b). After 1 (●), 2 (□), and 3 hr (▼) at 37°C in a 5% (v/v) CO_2 atmosphere, the absorbance at 490-650 nm was recorded using a plate reader. Each point represents the mean ± SD of 6 replicates.

3.2.3.3 Examination of cytotoxicity towards some bisdioxopiperazine analogs and topoisomerase II poisons

The individual values of the median inhibitory concentration (IC_{50}) for each drug cytotoxicity Experiment are presented in Table 3.5. Illustrated in Fig. 3.7 are the cytotoxicity profiles for each of these compounds, as determined by MTS analysis. Concentrations of ICRF-193 and ICRF-154 higher than 50 μM and 150 μM, respectively were limited by the solubility of these drugs. No DMSO-mediated cytotoxicity was observed in control wells containing 0.5% (v/v) DMSO (data not shown). In addition, growth inhibition analysis by cell counting was conducted in two slightly different ways, but only for dexrazoxane-treated cells (Fig. 3.8). With the exception of ADR-925-treated cells, at drug concentrations above the calculated IC_{50} values cells generally appeared larger in size with many particulates, as viewed under a microscope with a 10X objective lens.

Table 3.5. Cytotoxicity of various topoisomerase II inhibitory agents towards K562 cells as determined by MTS and/or cell counting analysis.

Drug	IC_{50}[a] (μM)	S.E. (μM)	C.V. (%)
dexrazoxane	20.3	1.9	9.5
dexrazoxane*	17.0	1.1	6.4
dexrazoxane**	13.8	1.3	9.5
ADR-925[b]	1229.0	20.2	16.4
ICRF-193	0.54	0.05	9.68
ICRF-154	33.52	3.93	11.71
etoposide	0.71	0.12	17.01
doxorubicin	0.073	0.013	17.98

[a] Cytotoxicity was measured by MTS analysis with a 72 hr exposure to the cytotoxic agent. The IC_{50} is the concentration of the agent at which cell growth is 50% of the maximum observed inhibition. Individual median inhibitory concentrations ± S.E. were obtained by fitting absorbance data to a four-parameter logistic equation (Fig. 3.7).

[b] ADR-925, the hydrolyzed form of dexrazoxane was the only known non-topoisomerase II inhibitory agent investigated.

* Dexrazoxane-mediated cytotoxicity as determined by cell counting analysis using a Coulter counter. Cells were seeded at identical concentrations in 6-well plates, grown for 72 hr, and the IC_{50} value calculated in the same manner as before (Fig. 3.8a).

** Dexrazoxane-mediated cytotoxicity as determined by cell counting analysis using a Coulter counter. Cells were seeded at various concentrations in T-75 flasks, grown for 72 hr, and IC_{50} values were calculated as before, but from a plot of the factor of cell density increase after 72 hr versus dexrazoxane concentration (Fig. 3.8b).

Fig. 3.7. MTS assay of cell growth inhibition by bisdioxopiperazines and other topoisomerase II inhibitory agents. K562 cells were incubated for 72 hr with (a) dexrazoxane, (b) ADR-925, (c) ICRF-193, (d) ICRF-154, (e) etoposide, and (f) doxorubicin on 96-well microtitre plates. Absorbances at 490-650 nm were determined after 3 hr of incubation with MTS reagent, except for dexrazoxane plates which were analyzed after 2 hr of incubation. The curves represent the results of least squares non-linear regression fits of measured values to a four-parameter logistic equation. The error bars represent standard deviations. The lowest concentrations are the zero values, plotted for convenience on a logarithmic scale with arbitrary values.

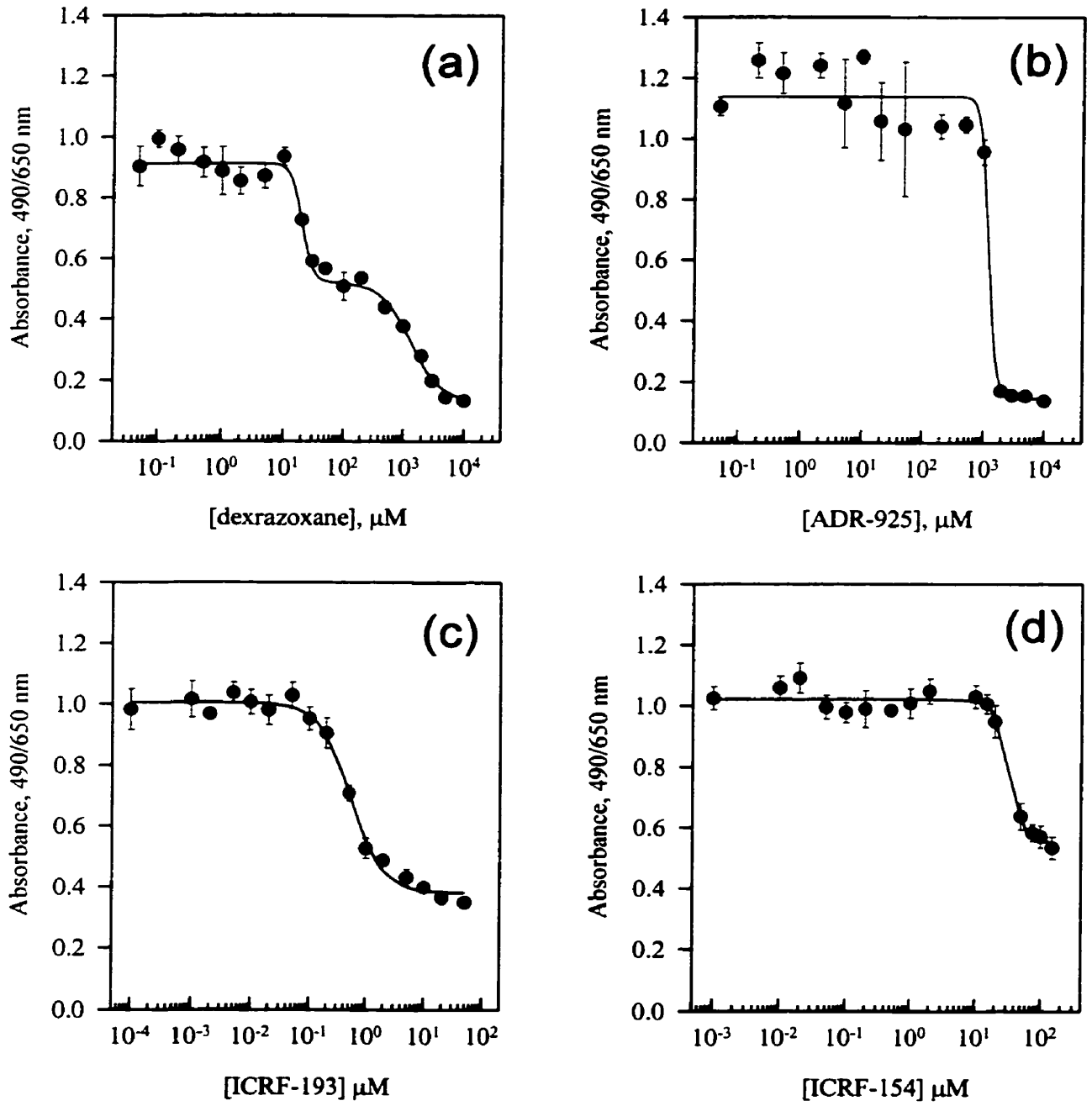

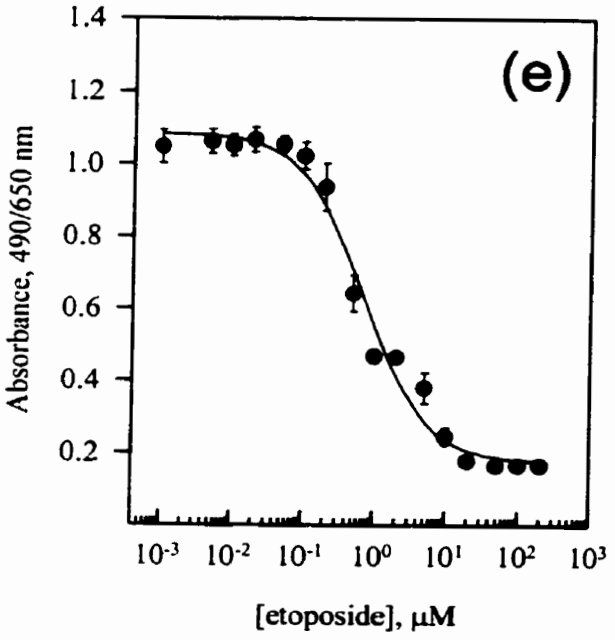
(e)
Absorbance, 490/650 nm
1.4
1.2
1.0
0.8
0.6
0.4
0.2
10^{-3} 10^{-2} 10^{-1} 10^{0} 10^{1} 10^{2} 10^{3}
[etoposide], μM

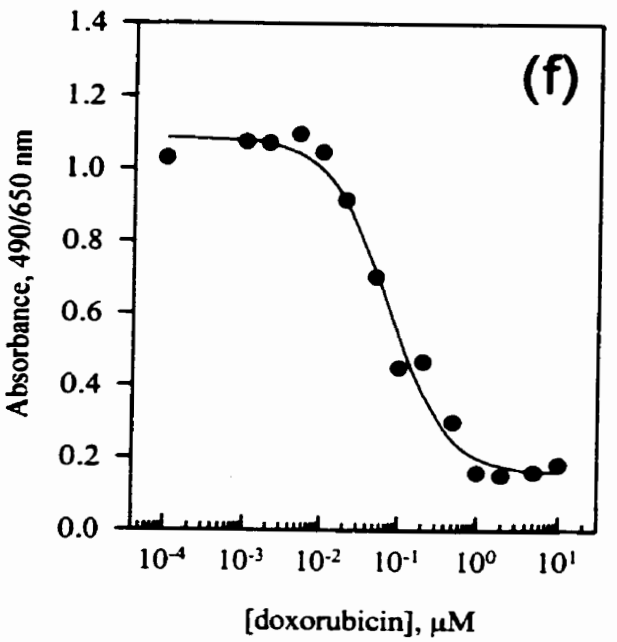
(f)
Absorbance, 490/650 nm
1.4
1.2
1.0
0.8
0.6
0.4
0.2
0.0
10^{-4} 10^{-3} 10^{-2} 10^{-1} 10^{0} 10^{1}
[doxorubicin], μM

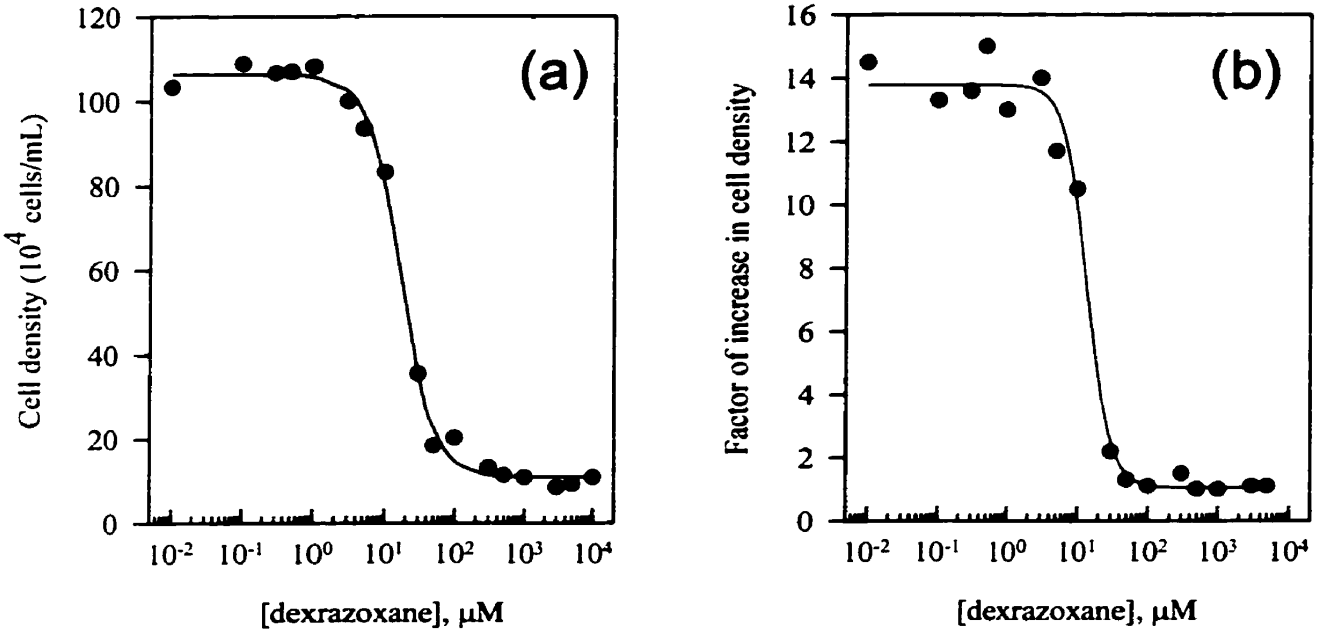

Fig. 3.8. Cell counting analysis of dexrazoxane-mediated cytotoxicity. K562 cells were seeded at (a) identical densities in 6-well plates, or (b) various densities in T-75 flasks. After 72 hr of growth in the presence of dexrazoxane cell densities were assessed on a model Z_f Coulter counter (threshold 20, 100 μm aperture, diameter cutoff ≅ 11.9 μm). The curves represent the results of least squares non-linear regression fits of measured values to a four-parameter logistic equation. The lowest concentrations are the zero values, plotted for convenience on a logarithmic scale with arbitrary values.

3.3 Effect of dexrazoxane on cell size, cycling, and mean protein and DNA content

3.3.1 Introduction

Aside from investigating the effects that a particular agent, such as dexrazoxane has on cell growth and viability there exist a wide range of other general characteristic features which can be examined. As mentioned previously, agents such as dexrazoxane and other bisdioxopiperazines target the topoisomerase IIα enzyme, and are able to affect the mitotic progression of a given cell line by interrupting the process at the G2/M phase boundary [68]. The experiments described in the following section attempt to explore some of the qualitative and molecular effects caused by dexrazoxane-induced topoisomerase II inhibition. First, the profile-size distributions of K562 cells were followed electrically in a flowing system through a Coulter counter, after exposure to dexrazoxane. Second, mean protein and DNA levels in dexrazoxane-treated cells were quantified in an attempt associate a change in cell size with an alteration of cellular constituents. And finally, flow cytometry was used to characterize the effect that dexrazoxane has on the cell cycling of K562 cells by quantifying the ploidy content of individual cells.

3.3.2 Materials and Methods

3.3.2.1 Materials

Dexrazoxane (Zinecard®, dexrazoxane; M_w = 268.28 g/mol) was a gift of Pharmacia & Upjohn (Columbus, OH, U.S.A.) and was prepared as previously described (Section 3.2.2.1.2) in cell culture medium (DMEM/FCS) followed by filter sterilization through a 0.2 μm acetate filter. RNase A (stored at –20°C, cat. No. R-5503), propidium iodide (cat. No. P-4170), Lauryl sulfate (SDS, cat. No. L-4390), bovine serum albumin (BSA, cat. No. A-3350), bisBenzimide (Hoechst 33258, M_w = 533.9 g/mol, cat. No. B-2883), and Coomassie brilliant blue G-250 (cat. No. B-0770) were obtained from Sigma Chemical Co. (St. Louis, MO, U.S.A.). Triton X-100 (cat. No. X198-5) was obtained from J.T. Baker Chemical Co. (Phillipsburg, NJ, U.S.A.). Calf thymus DNA (cat. No. 2618) was obtained from Calbiochem Corp. (La Jolla, CA, U.S.A.). Dulbecco's Phosphate buffered saline (PBS, cat. No. D-5652), DMEM (cat. No. 12800-017), and fetal bovine serum (FCS, cat. No. 26140-079) were obtained from Gibco-BRL, Life Technologies Inc. (Burlington, ON). Isoton II Coulter balanced electrolyte solution (cat. No. PN 8546719) was obtained from Beckman Coulter Inc. (Burlington, ON). Sodium chloride (NaCl, cat. No. AC-8304) was obtained from Anachemia Ltd. (Toronto, ON). Sodium hydroxide (5N NaOH, cat. No. H369) was obtained from Mallinckrodt Specialty Chemicals Co. (Paris, KT, U.S.A.). Sodium citrate (cat. No. C-614) was obtained from Fisher Scientific (Fairlawn, NJ, U.S.A.). Ethyl alcohol anhydrous (ethanol, 100%, cat. No. UN 1170) was obtained from Commercial Alcohols Inc. (Toronto, ON).

3.3.2.2 Drug treatment

For each of the following separately conducted experiments cells were grown and treated with dexrazoxane in an identical manner. Exponentially growing cultures were diluted to starting cell densities of $7x10^5$ cells/mL in T-75 flasks followed by the addition of 1-5 mL of dexrazoxane to produce a final concentration of 100 μM (total volume of 20-80 mL). Untreated control cells were seeded at $0.7x10^5$ cells/mL and were allowed to grow without intervention. On a daily basis, upon removal of the required number of cells for analysis, the remaining dexrazoxane-treated cells were aseptically combined, centrifuged at 250 *g* for 12 min in 50 mL sterile conical tubes, and resuspended in an appropriate volume of ~80% fresh DMEM/FCS in an attempt to maintain cell densities approximately equivalent to that of before centrifugation. This was followed by the subsequent re-addition of dexrazoxane, administered to the same concentration of 100 μM and in the same fashion as before. Cell densities were monitored daily by counting on a model Z_f Coulter counter with a 100 μm aperture tube, threshold setting of 7 (1/amp. = 2, 1/ap.curr. = 8, diameter cutoff ≅ 8.7 μm). Final growth curves for these cultures (data not shown) were normalized for changes in cell densities and volumes as before (Section 3.2.2.2.1), and were identical in nature to growth curves reported later in Section 3.4.3.1.

3.3.2.3 Cell sizing and quantitation by use of a Coulter counter

K562 cell size distributions after dexrazoxane exposure were monitored by collecting and analyzing cell number data from a model Z_f Coulter counter using a 100 μm aperture tube, as explained in detail in Appendix A.4. In brief, approximately $1x10^7$ cells were removed at each specified time interval of dexrazoxane exposure and diluted 3:50 mL as needed in a 50 mL glass beaker with Isoton II balanced electrolyte solution. Each dilution mixture was counted through a span of threshold volume-class divisions from 0-100, increasing by 4 divisions with each counting determination. Counting was performed in replicate (x2) through a series of different amperage and aperture current settings, chosen so as to cover the entire cell size distribution profile. Subsequently, the number of cells falling within set threshold ranges was determined, followed by the normalization of cell counts to a single amperage and aperture current setting so as to account for the various volume intervals used (see Appendix A.4.2.3). Finally, these cell counts were expressed as a function of cell volume and/or diameter in the form of frequency distribution histograms. Estimations of mean cell volume (MCV) and mean cell diameter (MCD) were made only for those distributions which appeared Gaussian-like (see Appendix A.4.2.4).

For reasons of clarity, cell counts of distribution peaks were subsequently normalized to the undrugged control. In the case of 12 and 24 hr dexrazoxane-treated K562 cells the peak height of these profile distributions were normalized to the equivalent peak height of the control distribution. Profiles of 48-96 hr dexrazoxane-treated K562 cells were normalized such that cell counts became half that of the corresponding peak volume interval in the control profile.

3.3.2.4 Quantitation of mean protein and DNA levels

The effect that dexrazoxane had on mean protein and DNA levels in K562 cells was examined in an identical manner as previously described with respect to dexrazoxane-treated CHO cells (Section 2.6.3). In brief, after growth in the presence of dexrazoxane for various periods of time, 4 replicates of $1x10^6$ cells were removed, washed twice with 10 mL PBS by centrifugation at 150 *g* for 18 min. The washed pellets were then gently resuspended in 1 mL PBS to ensure monodispersion. From this suspension a 300 µL volume of cells was removed in order to determine the cell density on model Z_f Coulter counter with a 100 µm aperture tube, threshold setting of 7 (1/amp. = 2, 1/ap.curr. = 8, diameter cutoff ≅ 8.7 µm). The remaining 600 µL of cells were then pelleted to a 50 µL volume and lyzed with 1% (w/v) SDS at 37°C for 45 min. Protein was then quantified in non-sterile 96-well microtitre plates at 589 nm after Coomassie brilliant blue staining in a modified Bradford assay, using bovine serum albumin (BSA) for standards (see Section 2.6.3.6). DNA content from the same samples was quantified in a fluorometric analysis after staining with Hoechst 33258, using calf thymus DNA for standards (see Section 2.6.3.5).

3.3.2.5 Cell cycle analysis using flow cytometry

The effect that dexrazoxane had on the ploidy content of individual K562 cells was examined in an identical manner, as previously described with respect to dexrazoxane-treated CHO, DZR, and heart fibroblast cells (Section 2.7.3) by cell cycle analysis using flow cytometry. In brief, at each specified time interval of dexrazoxane exposure ~$8x10^6$ cells were removed and fixed as monodispersed cell suspensions in 4.5 mL of 70% (v/v) cold ethanol overnight at -20°C. Samples were subsequently washed with PBS, resuspended in 1 mL of a 0.1% (v/v) Triton X-100 in PBS containing 0.02 mg/mL propidium iodide and 0.1 mg/mL DNase-free RNase A, followed by incubation for 15 min at 37°C. The percentage of cell aggregates in all prepared samples was determined microscopically in a hemacytometer chamber, as previously described (Section 2.7.3.3).

DNA content and light scattering analysis was carried out on an EPICS V multiparameter flow cytometer (Coulter electronics, Hialeah, FL, U.S.A.) in the Department of Immunology (University of Manitoba, Winnipeg, MB) with the assistance of Dr. Edward Rector. Propidium iodide-stained cells were passed through a 75 μm chamber orifice, and excited with an argon ion laser tuned to 488 nm. This was followed by the collection of red fluorescence emissions at 610 nm using 3.5 decade logarithmic amplifiers over a span of 256 channels of increasing fluorescence intensity, directly proportional to DNA ploidy level. Specialized analytical software on site was used to process the collected light intensity data, and permitted for the direct output of bivariate light scattering histograms. DNA content frequency histograms were generated in SigmaPlot (Jandel Corp., San Rafael, CA, U.S.A) as described in Section 2.7.3.4 from collected raw data of the number of cells that fell within increasing channels of

fluorescence. The relative fraction of cells residing within each discrete DNA ploidy level was determined empirically from the collected raw data. The delineation between where successive phases 2N, 4N, 8N, etc. began or ended could not be determined absolutely due to the extent of overlap of non-definable S phases. Therefore, approximations of the number of cells residing within each DNA ploidy peak was determined by dividing the number of counted cells between the midpoints of two successive valley regions on either side of a particular peak by 10,000 or the total number of cells counted overall.

3.3.3 Results

3.3.3.1 Cell size distributions of dexrazoxane-treated K562 cells

Frequency size distribution histograms of dexrazoxane-treated K562 cells, generated from collected electronic sizing data progressively increased in maximum peak volume over the first 24 hr of exposure (Fig. 3.9). Untreated control cells exhibited a tight narrow normal-like distribution of cell sizes, with an approximate mean cell volume of 2270 μm^3 (a 16.3 μm diameter). After 48 hr of exposure, distribution profiles were no longer Gaussian-like and began to exhibit a decay-like pattern at low diameter values. This presumably was due to the fact that as some dexrazoxane-treated K562 cells increased in cell size others gradually fragmented into an exceedingly high proportion of cell particles. The largest recorded K562 cell size was 32100 μm^3 (a 40 μm diameter) after 96 hr of dexrazoxane exposure. This corresponded to a 14-fold increase in volume compared to the mean cell volume of control cells. After 240 hr of continuous exposure to dexrazoxane, some cells were identified, microscopically to exhibit diameters of ~100 μm, a 230-fold increase in volume (see later, Fig. 3.14). Morphometric sizing analysis of dexrazoxane-treated K562 cells from two-dimensional photographic images was not conducted due to the difficulty of including the many fine particles within the analysis process. As a result, determinations of mean cell volume and diameter, at each time interval of dexrazoxane exposure could not be accurately resolved.

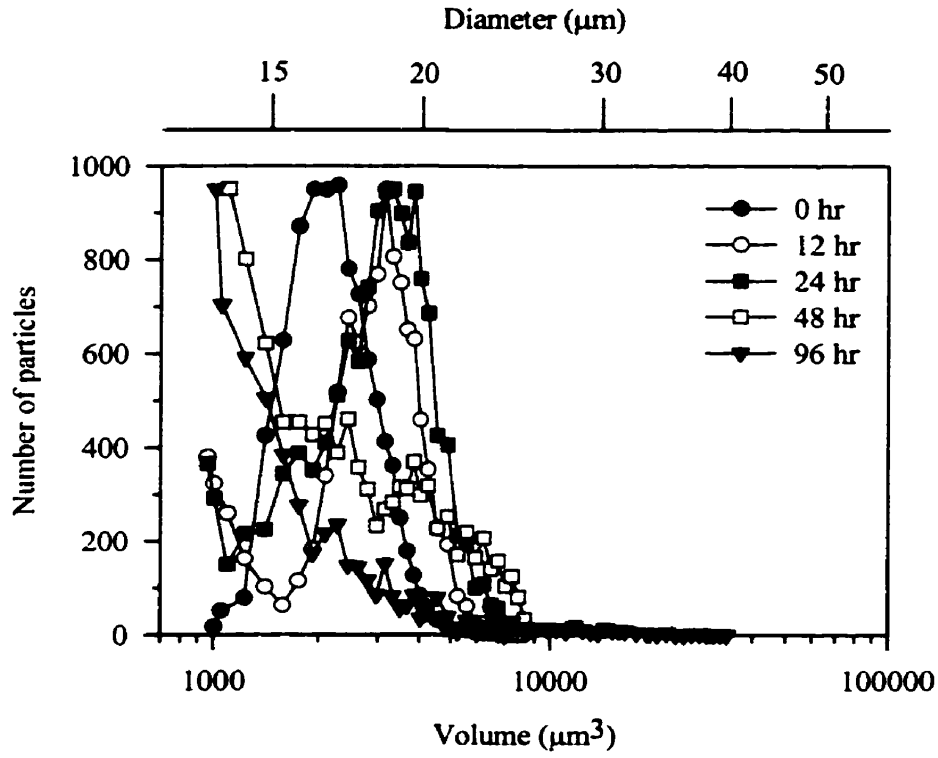

Fig. 3.9. Size distribution histograms of dexrazoxane-treated K562 cells. K562 cells were grown as a suspension culture seeded at $7x10^5$ cells/mL and exposed to 100 μM dexrazoxane daily with media replacement. At indicated time intervals frequency size distributions were generated by electronic Coulter counter sizing. For clarity, peak cell counts were normalized to the undrugged control. Distributions are expressed relative to volume measurements on a logarithmic scale (*bottom x-axis*) with approximate corresponding diameter values on a non-linear scale (*top x-axis*). The data obtained at 72 hr was not plotted for clarity.

3.3.3.2 Mean protein and DNA content levels in dexrazoxane-treated cells

Over the first days of growth in the presence of dexrazoxane, as cell size began to increase, so too did the mean cell content levels of protein and DNA (Fig. 3.10a and 3.10b). The analyzed time period of 48 hr corresponded to approximately two complete rounds of cell cycling, assuming a normal doubling rate of ~18 hr (see Table 3.4). Accordingly, with this duration of time mean protein and DNA content per million cells increased from control levels by 1.6-fold and 2.3-fold, respectively with the inhibition of further cell division by dexrazoxane. When analyzed individually using an unpaired Student's *t*-test, the mean protein and DNA content per million cells at each time interval ($N = 4$) of exposure was significantly different ($p < 0.001$) from the mean content level of control unexposed cell samples ($N = 16$). After a subsequent 120 hr of dexrazoxane exposure totaling 168 hr, mean protein and DNA levels ceased to increase further and began to decrease. This result was presumed to be a consequence of progressive cell fragmentation and the use of a relatively low Coulter counter diameter cutoff ($\cong 8.7$ μm) which overestimated the number of actual whole intact cells. A closer examination of mean protein and DNA content levels of dexrazoxane-treated cells was obtained by plotting as a ratio of mean protein/DNA content vs. duration of exposure (Fig. 3.10c). Protein/DNA ratio values not only remained consistent over 168 hr of dexrazoxane exposure but were also very similar to control levels, thus indicating a continued balanced form of growth.

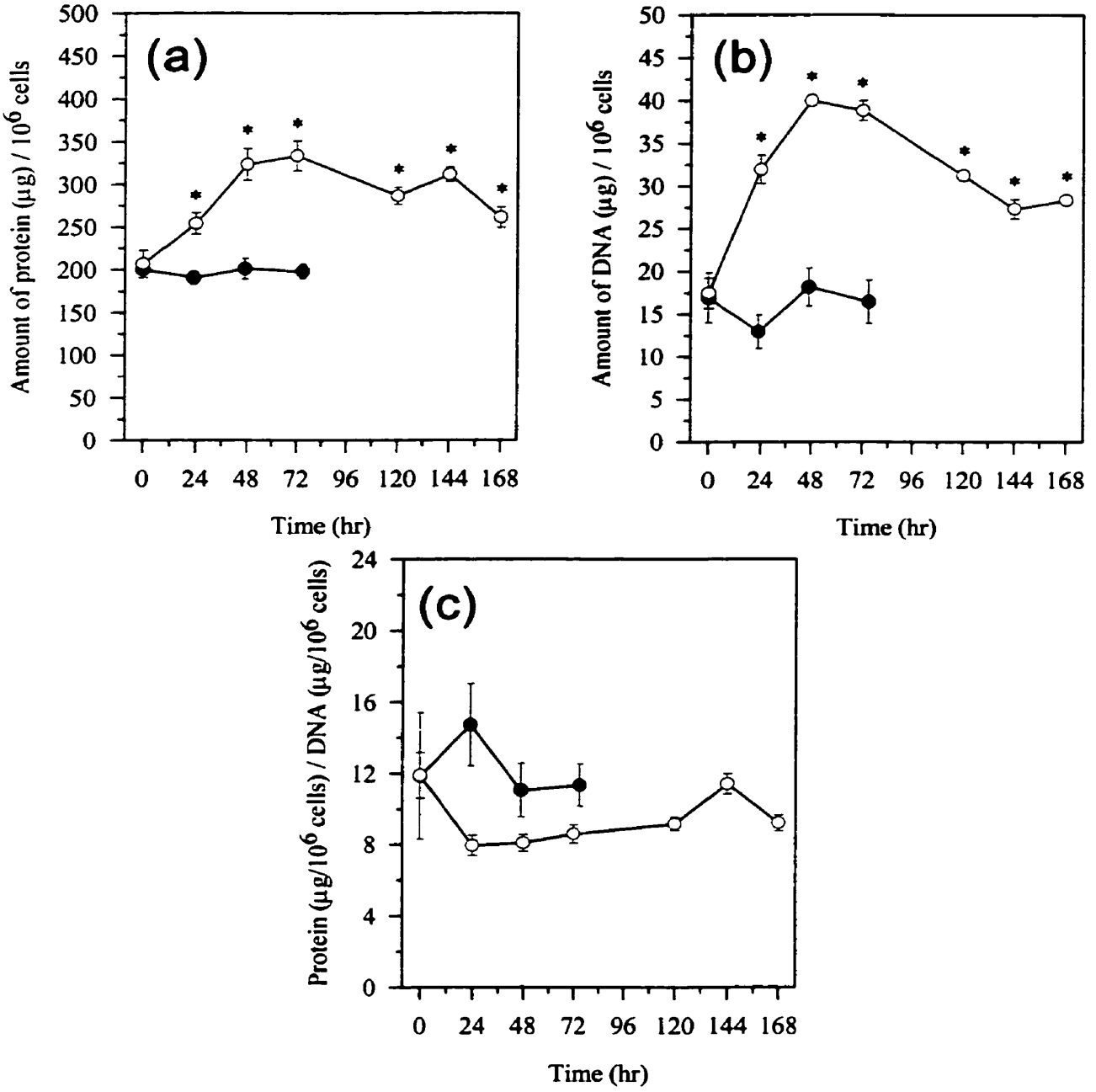

Fig. 3.10. Mean protein and DNA content levels in K562 cells exposed to dexrazoxane. K562 cells seeded at $7x10^5$ cells/mL were exposed to 100 μM dexrazoxane daily with media replacement (○). Control cells (●) seeded at $0.7x10^5$ cells/mL were allowed to reach maximum cell density without intervention. Cell densities were determined on a Coulter counter (100 μm aperture, diameter cutoff ≅ 8.7 μm). Protein (a) and DNA (b) content levels per million cells were determined by a modified Bradford assay and a Hoechst dye fluorometric analysis, respectively. Protein/DNA ratios were determined for each time analyzed time interval (c). Data points represent the mean of 4 replicate samples ± S.E. Asterisks (*) indicate a statistically significant difference ($p<0.001$, unpaired Student's *t*-test) from the mean of control unexposed K562 cell values.

3.3.3.3 Cell cycle analysis of dexrazoxane-treated K562 cells

In order to gain further insight into the effects of dexrazoxane on cell cycling, which had lead to enlargement of some cells (Fig. 3.9) the distribution of DNA ploidy content in dexrazoxane-treated K562 cells was examined by flow cytometry. Consistent with the normal successive phases of a typical eukaryotic cell cycle, the DNA histogram profile of untreated control K562 cells exhibited a sharp G0/G1 (2N, diploid) peak, an S phase, and a G2/M (4N, tetraploid) peak (Fig. 3.11). The presence of a few untreated cells with octaploid (8N) DNA content was not surprising given the variable number of chromosomes within this cell line [61] and relatively high percentage of doublet and triplet cell aggregates in this sample (Table 3.6). With increasing periods of dexraxoxane exposure there appeared an increasing trend towards a high level of polyploidization (Fig. 3.11). After 216 hr of daily dexrazoxane exposure, K562 cells with a DNA content as high as 32N were detected, indicative of four successive rounds of DNA synthesis. Microscopic examination of propidium iodide-stained cells revealed that very few cells were clumped together at these long time periods (Table 3.6). The relative percentage of cells possessing 8, 16, and 32N ploidy content gradually increased after 48 hr of dexrazoxane exposure (Table 3.7), consistent with the previously observed increase in cell sizes (Fig. 3.9). Although there did not appear to be a clear progression towards a single high ploidy level (Table 3.7), perhaps due to cell cycle blockage at different stages, the appearance of higher multiples of normal diploid content indicated multiple rounds of DNA synthesis in the absence of cell division. This was further confirmed by the appearance of a somewhat unbroken S-phase(s), which may also be the result of cells cycling with intermediate irregular ploidy quantities. Finally, the continuous decay-like

pattern between successive ploidy peaks can be attributed to the progressive fragmentation of dexrazoxane-treated K562 cells into particles of intermediate DNA content.

Table 3.6. Percentage of cell aggregates contributing to flow cytometry analysis.

Duration of dexrazoxane exposure	Time (hr)	Single cells (%)	Doublets (%)	Triplets (%)	Quadruplets (%)	Quintuplets (%)
Exposed daily	0	86.1	10.8	2.2	0.0	0.9
	24	93.6	6.0	0.4	0.0	0.0
	48	94.4	5.1	0.4	0.0	0.0
	96	99.0	1.0	0.0	0.0	0.0
	168	99.5	0.5	0.0	0.0	0.0
	216	100.0	0.0	0.0	0.0	0.0

Table 3.7. Cell cycle distribution of K562 cells continuously exposed to ICRF-187.

Duration of dexrazoxane exposure	Time (hr)[a]	Cell cycle distribution (%)[b]					
		sub G1	2N	4N	8N	16N	32N
Exposed daily	0	0.0	54.2	40.7	4.5	0.5	0.1
	24	0.0	62.5	36.3	1.2	0.0	0.0
	48	0.0	39.3	52.6	8.0	0.1	0.0
	96	9.3	44.5	27.6	10.7	7.7	0.2
	168	15.9	40.0	21.7	16.0	6.2	0.3
	216	11.4	42.8	25.6	11.5	6.8	1.9

[a] Duration of exposure of cells to the dexrazoxane

[b] The cell cycle distribution was calculated by computer analysis from red (DNA) fluorescence histograms displayed in Fig. 3.11. The number of cells residing within each successive ploidy phase was approximated by first, assuming non-definable S phases and second, dividing the number of counted cells between successive valley region midpoints by the total overall number of cells analyzed.

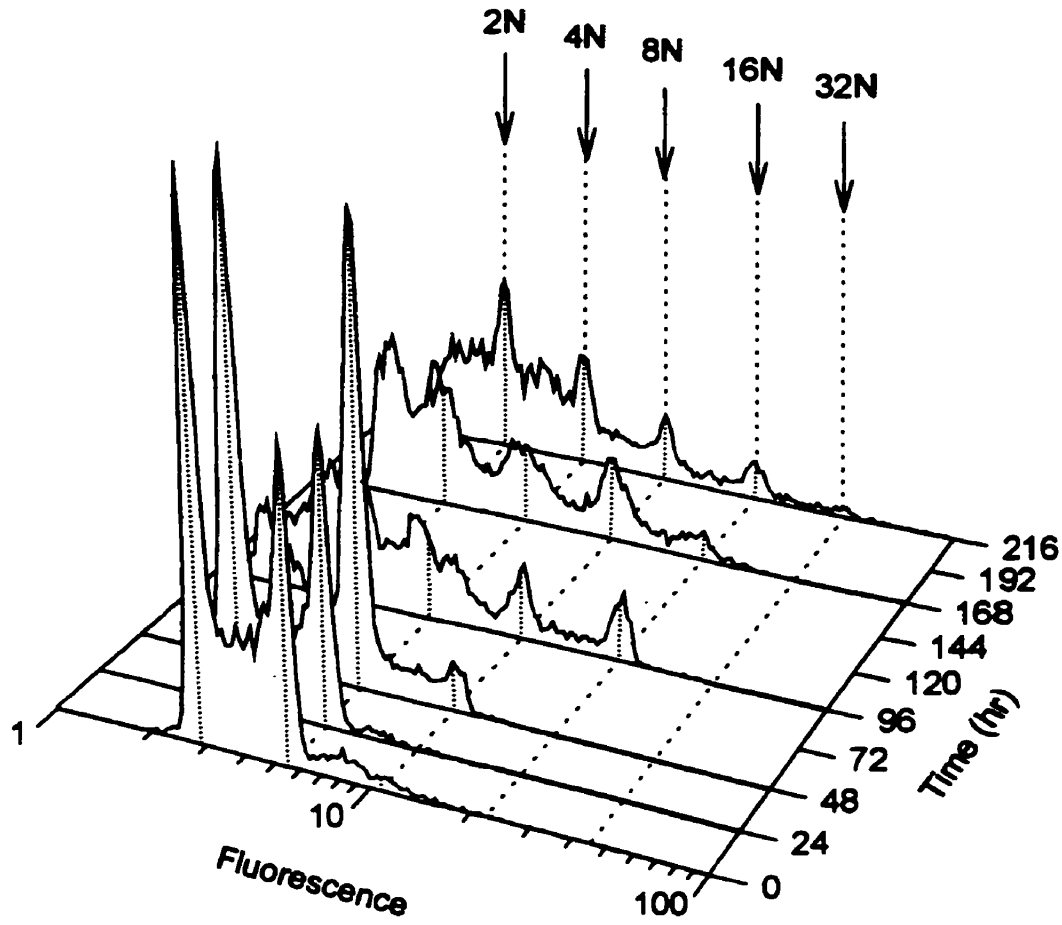

Fig. 3.11. Cell cycle analysis of K562 cells exposed daily to dexrazoxane with media replacement. Cells were taken directly from suspension cultures at the indicated times, stained with propidium iodide and analyzed by flow cytometry as described in Section 3.3.2.5. Shown here is integrated red fluorescence on a logarithmic scale, reflective of increasing DNA content vs. the number of cells. The leftmost peak in the control (0 hr) culture represents G0/G1 (2N) cells. Cells with twice the fluorescence of G0/G1 cells represent the G2/M cells with tetraploid (4N) levels of DNA. At subsequent times, higher multiples of the G0/G1 peak can be seen, representative of higher ploidy levels (8N, 16N, 32N respectively). A total of 10,000 cells were analyzed per time interval.

3.4 Examination of differentiation in dexrazoxane-treated K562 cells

3.4.1 Introduction

It has been well established that many compounds including topoisomerase II inhibitors are capable of inducing the expression of erythroid-like features in K562 cells [120]. One of the most common means of identifying this progression is to monitor the production of hemoglobin, using a benzidine stain to obtain population percentages [65,72,73,71], or to quantitate actual hemoglobin levels spectrophotometrically [70,65,71]. To this effect it was first examined whether dexrazoxane was capable of inducing the production of hemoglobin in K562 cells. Second, the relationship between dexrazoxane concentration and hemoglobin expression was further investigated in combination with a cell counting analysis of cytotoxicity. Third, the effect of other bisdioxopiperazines, etoposide, and other known differentiation inducing compounds (DMSO and hemin, Fig. 3.12) on the growth and expression of hemoglobin in K562 cells was examined. And finally, using a flow cytometry immunofluorescence analysis the simultaneous expression of erythroid and megakaryocyte antigens was examined.

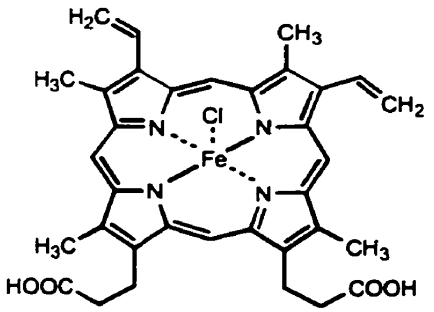

Hemin
M_w = 651.95 g/mol

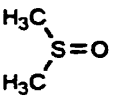

Dimethyl sulfoxide (DMSO)
M_w = 78.14 g/mol

Fig. 3.12. Chemical structure of hemin and DMSO.

3.4.2 Materials and Methods

3.4.2.1 Materials

3.4.2.1.1 Drugs, chemicals, reagents, and monoclonal antibodies

Dexrazoxane (Zinecard®, dexrazoxane), and ADR-925 were gifts of Pharmacia & Upjohn (Columbus, OH, U.S.A.). Etoposide was obtained from Sigma Chemical Co. (cat No. E-1383), ICRF-193 and ICRF-154 were synthesized previously in our laboratory. DMSO used to dissolve drugs, 99.5% cat. No. D-5879), trypan blue dye (cat. No. T-6146), paraformaldehyde (cat. No. P-6148), benzidine dihydrochloride (cat. No. B-0386), were obtained from Sigma Chemical Co. (St. Louis, MO, U.S.A.). Acetic acid (1 N, cat. No. 31,859-0), ammonium hydroxide (4.96 N, cat. No. 31,861-2), and hydrogen peroxide (30%, cat. No. 21,676-3) were obtained from Aldrich Chemical Co. (Milwaukee, WN, U.S.A.). Dulbecco's phosphate buffered saline (PBS, cat. No. D-5652), DMEM (cat. No. 12800-017), and fetal bovine serum (FCS, cat. No. 26140-079) were obtained from Gibco-BRL, Life Technologies Inc. (Burlington, ON). Hemin (cat. No. 2203) was obtained from Eastman Kodak Co. (Rochester, NY, U.S.A.). Isoton II Coulter balanced electrolyte solution (cat. No. PN 8546719) was obtained from Beckman Coulter Inc. (Burlington, ON). Sodium chloride (NaCl, cat. No. AC-8304) was obtained from Anachemia Ltd. (Toronto, ON). Na_2EDTA (99.5%, cat. No. 10093) was obtained from BDH Chemicals Ltd. (Toronto, ON).

All monoclonal antibodies (mAb) used to assess maturation level of K562 cells were mouse IgG1 isotypes, obtained from Coulter-Immunotech (Burlington, ON), and stored at 2-8°C. The 11E4B7.6 (KC16) mAb (cat. No. IM2212) conjugated to fluorescein-

isothiocyanate (FITC) was specific for glycophorin A, a major transmembrane sialoglycoprotein expressed on red blood cells and erythroid precursors. The P2 mAb (cat. No. IM1416) conjugated to phycoerythrin (PE) was specific for CD41 or the gpIIb component of the gpIIb/IIIa complex present on platelets and early promegakaryoblasts [36]. The 679.1Mc7 monoclonal antibodies (cat. No. IM1203) served as isotype control (IgG1-FITC / IgG1-PE) possessing irrelevant specificity.

3.4.2.1.2 Preparation of drugs and reagents

Dexrazoxane (M_w = 268.28 g/mol) and ADR-925 (M_w = 302.3 g/mol) were dissolved in cell culture medium (DMEM/FCS) and filter sterilized through a 0.2 μm acetate filter. Etoposide (M_w = 588.6 g/mol), ICRF-193 (M_w = 282.3 g/mol), ICRF-154 (M_w = 254.25 g/mol) were dissolved in 99.5% DMSO by brief sonication and heating in a 37°C water bath and subsequently added to cell cultures at 0.5% (v/v) DMSO. DMSO was also examined by itself as a possible inducer of differentiation at a concentration of 1.5% (v/v) in DMEM/FCS. Hemin (M_w = 651.95 g/mol) was prepared as a stock solution, dissolved in 0.134 M ammonium hydroxide and filtered sterilized through a 0.2 μm acetate filter. Trypan blue dye (0.6% w/v) was prepared by dissolving 0.6 g of dye in ddH_2O containing 150 mM NaCl and 1 mM Na_2EDTA. A 2% (w/v) solution of paraformaldehyde was prepared in PBS (pH 7.2) by heating and stirring, followed subsequent cooling to room temperature.

3.4.2.2 Assessment of hemoglobin production

3.4.2.2.1 Benzidine staining assay for hemoglobin expression

The percentage of cells containing hemoglobin was estimated by staining with benzidine [70]. A stock solution of 0.2% (w/v) benzidine dihydrochloride in 0.5 M acetic acid was prepared, and was stable for months at 4°C. For each estimation a fresh 0.4% (v/v) staining solution of 30% (v/v) hydrogen peroxide in the benzidine stock solution was prepared before use. Next, a one-tenth volume of the staining solution was added to the cell suspension to be tested, or 10 μL for every 100 μL cell suspension in DMEM/FCS. The mixture was then examined microscopically under a hemacytometer chamber after 5 min under bright-field conditions. At least 500 cells of normal size or larger were counted per sample using a 40X objective lens for an accurate estimation of the number of benzidine-positive (blue) cells present.

3.4.2.2.2 Spectrophotometric assay for hemoglobin levels

The absolute hemoglobin content in K562 cells was assessed by aseptically removing $1x10^7$ cells from culture and then washing twice with PBS by centrifugation at 250 *g* for 12 min. Washed cell pellets were then resuspended in 0.2 mL PBS, lyzed by a minimum of 5-10 cycles of freeze-thawing between –80°C and 37°C, and centrifuged at 16,000 *g* for 1-1½ hr so as to remove cell debris from analysis. The absorbance spectrum of 150 μL of supernatant was then determined on the Cary 100 spectrophotometer between 350-550 nm by the addition to 450 μL of PBS, previously blanked. The instrument

parameters used included: 15.0 nm/min scan rate, 0.5 nm data interval, 2.0 sec average time, double beam mode, and baseline correction.

The spectral absorbance peak at 415 nm was previously confirmed to be representative of hemoglobin by comparing the 415/450 nm absorbance ratio of samples isolated from K562 and neonatal rat red blood cells to known literature values [71]. Spectral data of each determination was saved in a **.CSW* format, imported into SigmaPlot, and displayed as 2 separate distributions, plot 1: 374-459 nm (the isolated absorbance peak), plot 2: 350-373 and 460-550 nm. Background absorbance at 415 nm was empirically calculated from a 2nd order linear regression equation ($y = Ax^2 + Bx + C$) plotted to join adjacent sections of plot 2. Absolute hemoglobin content was then quantified at 415 nm in units of pg/cell after subtraction of the calculated background absorbance assuming a molar extinction coefficient (ε) of 125,000 $M^{-1}cm^{-1}$, path length (b) of 1 cm, and the molecular weight (M_w) of hemoglobin as being 16,000 g/mol [25,26,70]. The equation used to arrive at this determination, and a sample calculation is as follows:

Table 3.8. Calculation of absolute hemoglobin content level in K562 cells.

Total no. cells sampled	Volume of PBS resuspended in (L), converted from μL	Dilution ratio in cuvette (μL/μL)	Peak absorbance at 415 nm	Calculated background absorbance at 415 nm	True absorbance (Peak – Calc.)
7.426E+06	1.826E-04	550 / 150	0.197	0.108	0.089

Beer's Law: $A = \varepsilon bc$ (where c = [hemoglobin] in this case)

$$[\text{Hemoglobin}] = \frac{\text{True Abs}}{\varepsilon b} \times \text{Dilution ratio} \times M_w \times \text{Vol. PBS resuspended in} \times \frac{1}{\text{Total no. cells}}$$

$$[\text{Hemoglobin}] = \frac{0.089}{125000\ M^{-1}cm^{-1}\ (1\ cm)} \times \frac{550}{150} \times 16000\ g/mol \times 1.826E\text{-}04\ L \times \frac{1}{7.426E+06}$$

$$= 1.0 \times 10^{-12}\ g/cell$$

$$= 1.0\ pg/cell$$

3.4.2.3 Determination of relative positivity and absolute content levels of hemoglobin expression after exposure to dexrazoxane for various periods of time

The objectives of these experiments were to examine the effect of various periods of dexrazoxane exposure on hemoglobin expression levels in K562 cells. Exponentially growing K562 cells were diluted into 2 separate T-75 flasks at starting cell densities of $0.8x10^6$ cells/mL in DMEM/FCS followed by the addition of a requisite stock solution of dexrazoxane at <10% (v/v) to produce a final concentration of 100 μM. A concentration of 100 μM dexrazoxane was adopted, as previously mentioned due to its effectiveness of remaining in unhydrolyzed, topoisomerase II inhibitory form in culture for long periods of time [72]. Cells in these 2 cultures were aseptically removed daily, centrifuged at 250 *g* for 12 min and resuspended in an appropriate volume of ~80% fresh DMEM/FCS in an attempt to maintain cell densities approximately equivalent to that of before centrifugation or sampling. This was followed by the subsequent re-addition of dexrazoxane, administered to the same concentration of 100 μM, and in the same fashion as before. At each 24 hr time interval $\sim 1x10^7$ cells were removed from the first culture, followed by the determination of absolute hemoglobin content level, as described in Section 3.4.2.2.2. At indicated time intervals of 24, 48, 120, 168 hr of continuous exposure, cells were removed from the second culture and seeded into T-75 flasks in fresh medium at cell densities of $0.1\text{-}0.2 \times 10^6$ cells/mL, total volume 20 mL. These separate cultures were allowed to grow

without daily media changing, with the exception of cells removed at the 24 and 48 hr intervals of the experiment. Cells removed and re-seeded at these time periods eventually grew to a state just below maximum cell density (~$1x10^6$ cells/mL) at 96 and 168 hr, respectively at which time they were diluted again to $0.2x10^6$ cell/mL.

Cell densities were assessed daily by counting on a model Z_f Coulter counter with a threshold setting of 7, 100 μm aperture tube (1/amp. = 2, 1/ap.curr. = 8, diameter cutoff ≅ 8.7 μm). Final growth curves and doubling rates for cultures in which media was changed were determined after normalization for slight changes in cell densities and volumes, as previously described (Section 3.2.2.2.1). Cell viability was judged under a hemacytometer chamber by the ability of cells of normal size and larger to exclude 0.6% (w/v) trypan blue dye. The relative percentage of cells expressing hemoglobin was assessed by benzidine-positivity as previously described (Section 3.4.2.2.1). Finally, photographic images were taken after various periods of dexrazoxane exposure under a 10X and 40X objective lens using a Nikon camera with Kodak 400 color film.

3.4.2.4 Relating dexrazoxane-induced growth inhibition of K562 cells to a concentration dependency for hemoglobin expression

The results of the previous experiment demonstrated that dexrazoxane, a known topoisomerase II inhibitory agent was able to induce hemoglobin synthesis in K562 cells. The purpose of the following experiment was two-fold. First, the objective was to establish whether a dexrazoxane concentration dependency relationship existed with respect to hemoglobin expression. And second, to attempt to correlate this relationship, in

the same experiment with the growth inhibitory concentration (IC_{50}) of dexrazoxane in K562 cells, which is reflective of topoisomerase II inhibition [72].

The primary difficulty in the design of this experiment centered around overcoming the eventual cytotoxic effect of dexrazoxane (see Section 3.2.3.1), yet still obtaining enough cells overall (~0.5-1x10^7 cells) after 72 hr, at each tested drug concentration to properly assess absolute hemoglobin content. One of two options presented themselves: either seed for each tested dexrazoxane concentration at the same cell density but to different overall volumes, or seed the cells initially at a range of cell densities at much lower constant volumes. Although, the former protocol outlining the seeding of cells at the same cell density is usually the ideal preferred method, the latter method was chosen for a variety of reasons. In particular, extraordinary amounts of dexrazoxane would have been required in the first protocol for obtaining high drug concentrations in large culture volumes. As well, the second protocol seemed more realistic given the fact that we had previously demonstrated, by benzidine-positive staining that relative hemoglobin expression was not dependent on the initial seeded cell density but rather on the consistency of dexrazoxane exposures (data not shown).

Utilizing previously obtained 72 hr dexrazoxane cytotoxicity analysis data (Section 3.2.3.3) as a template, the factor by which cell density would increase from the same initial levels to a period of 72 hr after exposure, for a range of dexrazoxane concentrations was determined. For example, control 0 μM dexrazoxane-treated cells increased by 16-fold in 72 hr (consistent with their doubling time of 18 hr), 10 μM dexrazoxane-treated cells by 13-fold, 100 μM by 3-fold, 1000 μM by 1.5-fold, etc. Although cells subjected to high dexrazoxane concentrations would only marginally increase in cell number over 72 hr, it

was decided not to seed these cells at densities above $0.5x10^6$ cells/mL. The premise was that this many cells in culture would begin to deplete glucose levels before 72 hr, thus playing an undesirable possible role in influencing either cell kill or hemoglobin production.

In brief, for dexrazoxane concentrations of 0-5 μM cells were seeded at $0.6x10^5$ cells/mL, for 10 and 30 μM at $0.75x10^5$ and $1.75x10^5$ cells/mL respectively, and for concentrations of 100-5000 μM at $3.0x10^5$ cells/mL. All cells were seeded accordingly as single determinations to 14 mL in T-25 flasks, followed by the addition of 1 mL of the requisite stock solution of dexrazoxane to produce the desired final concentration. Cells were then cultured, as before for the duration of 72 hr, without any changing of media. After this period of time cell densities were determined on a model Z_f Coulter counter using a high threshold setting of 20, 100 μm aperture tube (1/amp = 2, 1/ap.curr = 8, diameter cutoff ≅ 11.9 μm) in order achieve an accurate determination of the number of actual whole cells. Growth inhibition analysis and IC_{50} values were determined by plotting the factor of increase in cell density or C/C_o (i.e. final cell densities (C) relative to initial seeded densities (C_o)) versus the range of dexrazoxane concentrations tested. From the remainder of cells in each culture flask were resolved both the relative expression of hemoglobin by benzidine staining (Section 3.4.2.2.1), and the absolute hemoglobin content level spectrophotometrically (Section 3.4.2.2.2).

Non-linear, least squares fitting of the (i) factor of cell density increase, and level of hemoglobin expression by (ii) benzidine-positivity and (iii) absolute content from absorbance at 415 nm versus dexrazoxane concentration was performed using a four-parameter logistic equation, $y = (a-d)/(1+(x/c)^b)+d$ in SigmaPlot (Jandel Corp.,

San Rafael CA). In this equation y is either (i), (ii), or (iii), x is the concentration of dexrazoxane, c is median inhibitory concentration expressed terms known as IC_{50} in the case of (i), or DC_{50} in the cases of (ii) or (iii), and b is a Hill-type exponential factor. In the determination of IC_{50}, a is the maximal value of (i) and d is the minimal value at the highest drug concentration. In the determination of DC_{50} using either (ii) or (iii) values, a is the minimal value, and d is the maximal value at the highest drug concentration. Values of IC_{50} and DC_{50} represent concentrations of dexrazoxane at which 50% growth inhibition and 50% differentiation occurs, respectively.

3.4.2.5 Determination of relative positivity of hemoglobin expression after exposure to ADR-925, ICRF-193, ICRF-154, etoposide and other known inducers of K562 differentiation

The purpose of the following experiments were to examine the possible induction of hemoglobin expression in K562 cells by a variety of other agents besides dexrazoxane, including the bisdioxopiperazines ADR-925, ICRF-193, ICRF-154, as well etoposide, DMSO, and hemin. Growth inhibition experiments conducted earlier by MTS analysis (Fig. 3.7) allowed for the determination of appropriate concentrations of ICRF-193, ICRF-154, ADR-925, and etoposide to assay for hemoglobin expression. Although sub-cytotoxic concentrations of etoposide [3,45], and dexrazoxane (Section 3.4.2.4) have previously been shown to be capable of inducing hemoglobin expression, it was believed that concentrations within the range of the respective IC_{50} values of the above mentioned agents would optimally induce a high level of hemoglobin expression.

Exponentially growing K562 cells were diluted to starting cell densities of 0.2×10^6 cells/mL in separate T-25 flasks and exposed daily with media replacement to either 5 μM

ICRF-193, 100 μM ICRF-154, 10 μM etoposide, or 100 μM dexrazoxane, administered from stock solutions, prepared as outlined in Section 3.4.2.1.2. The hydrolyzed form of dexrazoxane, ADR-925 was previously shown not to induce cytotoxic effects below concentrations of 1000 μM (Fig. 3.7b). Consequently, a separate culture of cells were exposed once to 100 μM ADR-925, an equivalent concentration to dexrazoxane. Additionally, cell cultures were exposed once to either 1.5% (v/v) DMSO or 30 μM hemin, prepared as described in Section 3.4.2.1.2. These two agents differed from the previously mentioned compounds in that they are not inhibitors of topoisomerase II, but have been shown to be capable of inducing of megakaryocyte and erythroid-like differentiation in K562 cells, respectively at these concentrations [11,25,60]. Cell densities, viability, and hemoglobin expression through benzidine-positive staining were conducted as described in the preceding section for all prepared cultures (Section 3.4.2.3). Final growth curves and doubling rates for these cultures were determined after normalization for slight changes in cell densities and volumes, as previously described (Section 3.2.2.2.1).

3.4.2.6 Flow cytometry analysis of megakaryocyte and erythroid surface markers after immunofluorescence labeling

Exponentially growing cultures were diluted to starting cell densities of $5x10^5$ cells/mL in T-75 flasks followed by the addition of 1-2 mL of the requisite stock solution of dexrazoxane to produce a final concentration of 100 μM (total volume of 15-40 mL). Separate cultures were prepared on subsequent days so has to have a range of treated cells (0, 24, 48, 96, 120 hr) ready for analysis on the same day. On a daily basis, cells were centrifuged at 250 *g* for 10 min, resuspended in ~80% fresh DMEM/FCS followed by the

subsequent re-addition of dexrazoxane administered to the same concentration of 100 μM, and in the same fashion as before.

To assess megakaryocytic and erythroid differentiation, cell surface expression of glycoprotein IIb/IIIa (CD41) and glycophorin A, respectively were detected by indirect immunofluorescence using flow cytometry. On the day of analysis cell densities were determined on a model Z_f Coulter counter with a threshold setting of 20, 100 μm aperture tube (1/amp = 2, 1/ap.curr. = 8, diameter cutoff ≅ 11.9 μm). Next, ~$5x10^5$ cells were removed from each culture in duplicate (1 for isotypic control mAb and 1 for test mAb), centrifuged for 6 min at 250 *g* in microcentrifuge tubes, and then gently resuspended in 150 μL of DMEM/FCS. To each control tube was added 20 μL of the isotypic control 679.1Mc7 mAb (IgG1-FITC / IgG1-PE), and to the other tubes was added 20 μL of P2-PE mAb (anti-CD41), and 20 μL of 11E4B7.6 (KC16)-FITC mAb (anti-GlyA). Each of the preceding samples were prepared in turn then lightly vortexed, and incubated on ice for 45 min. Samples were then diluted to 2 mL with cold buffered DMEM/FCS, pelletted by centrifugation for 6 min at 250 *g*. This was followed by the removal of supernatants in turn, the addition of 350 μL of 2% (w/v) freshly prepared paraformaldehyde fixative in PBS, an immediate gentle vortexing, and storage on ice wrapped in aluminum foil until analyzed.

Two-color analysis was conducted by Dr. Edward Rector on a highly modified EPICS V multiparameter flow cytometer (Coulter electronics, Hialeah, FL, U.S.A.) in the Department of Immunology (University of Manitoba, Winnipeg, MB). The instrument was tuned to collect integrated green (FITC) fluorescence from ~515-545 nm, and integrated red (PE) fluorescence from ~570-580 nm using 3.5-decade logarithmic

amplifiers. Bivariate flow cytometry data were separated into four regions (I-IV) for untreated and dexrazoxane-treated samples. Region I corresponded to cells which bound anti-CD41 but not anti-GlyA; Region II to cells which bound both anti-CD41 and anti-GlyA; Region III to cells which bound neither anti-CD41 or anti-GlyA; and Region IV to cells which bound anti-GlyA but not anti-CD41. The distribution obtained using the control primary mAbs, for each analyzed time interval in turn was first adjusted to match the distribution using the test mAbs in Region III, considered to represent non-specific binding by setting the cell count in this region to 1% of the total cell count. The percent increase in specific fluorescence was derived from the difference between the two distributions, the distribution using the test mAbs (total fluorescence) and the distribution using the control mAbs of the same Ig subclass (fluorescence due to Fc receptor binding and other nonspecific fluorescence). This allowed for the determination of the percentage of doubly-positive cells (Region II), as well as the percentage of singly-positive cells for megakaryocyte and erythroid marker expression in Region I and IV, respectively.

3.4.3 Results

3.4.3.1 Hemoglobin expression levels in dexrazoxane exposed K562 cells

Initially, it was noticed that 1 or 2 exposures to dexrazoxane was enough to induce a change in benzidine-positivity which increased in parallel to cells continuously exposed to dexrazoxane over the first 120 hr (Fig. 3.13c), with a minimal loss of viability (Fig. 3.13b). However, as cell numbers proliferated exponentially upon transfer to fresh medium without dexrazoxane (Fig. 3.13a) the level of staining diminished back to pre-treatment levels of 0.3-0.5% staining within a few days (Fig. 3.13c). Daily exposure of K562 cells to dexrazoxane produced increased levels of benzidine-positive staining (expressed as a percentage of the population) which eventually plateaued at ~40% after 240 hr (Fig. 3.13c). In accordance with this result though, the actual number of viable benzidine-stained cells (as determined from combining Fig. 3.13a and 3.13b), remained fairly constant after approximately 120 hr (Fig. 3.13d). This suggests, in contrast to what is inferred by Fig. 3.13c that dexrazoxane commits K562 cells to irreversibly differentiate towards an erythroid-like lineage irrespective of the duration of exposure or the growth rate of the culture.

As demonstrated in Fig. 3.13a, and as shown previously (Fig. 3.5a) daily exposure of K562 cells to dexrazoxane ensures that cell division is completely halted. Growth rates and doubling times of cells exposed to dexrazoxane for various periods of time are displayed in Table 3.9. These values were computed using the single exponential rise equation $C = C_o e^{kt}$, as previously explained (Section 3.2.2.2.2). Growth curves displayed in Fig. 3.13a suggest that the number of dexrazoxane exposures correlates with the

duration of a partial lag phase of growth. When these cultures, removed after 24, 48, 120, and 168 hr of dexrazoxane exposure were allowed to continue to grow in the absence of drug, cell growth was observed to eventually recover to a state resembling pre-treatment conditions (partially shown in Table 3.9). After various periods of dexrazoxane exposure percent viability diminished at a rate that was comparable, within reason to previous assessments (Fig 3.13b and 3.5b). The results displayed here (Fig. 3.13b) suggest that if media is replaced with daily dexrazoxane exposure then the viability of the culture does not decline quite as readily, compared to non-replacement conditions (Fig. 3.5b). Any observed variance in viability between separately conducted experiments may be attributable to slightly different growth conditions, culture volumes, or to the centrifugation process incurred during media replacement which may have inadvertently washed away some non-viable cells.

The benzidine staining observed was not restricted solely to those cells in the population which continued to enlarge in size. The degree of staining was differential, in that some cells stained darker that others (Fig. 3.14a and 3.14c). This observation of hemoglobin production was not consistently correlated with cell size. Some cells would appear identical, for all purposes (Fig. 3.14a and 3.14b) with the exception that some would stain for hemoglobin, whereas others would not. The staining of hemoglobin seemed as well to be localized around lobated regions in enlarged cells, and throughout the cytoplasm in smaller cells. Finally, some enlarged cells possessed no such lobular regions or hemoglobin staining (Fig. 3.14d). These particular cells were later confirmed to be apoptotic as seen by combining benzidine staining with DNA-binding fluorescent dyes (Fig. 3.22). Together these results suggest that the role of topoisomerase II inhibition with

respect to differentiation induction may be indirect, in that a consistent correlation between cell enlargement and hemoglobin production was not observed.

Although on a per cell basis the expression of hemoglobin was not consistent, a correlation did exist between the level of absolute hemoglobin content and the number of cell cyclings or length of growth. Absolute hemoglobin content level, as quantitated spectrophotometrically from spectra such as Fig. 3.15, showed that on average, hemoglobin content increased 10.3-fold after 120 hr of dexrazoxane exposure, from 0.89 ± 0.29 pg/cell to 9.2 pg/cell (Fig. 3.16). Standard error values (N = 5) were only determined for control samples. When analyzed by statistical linear regression analysis, a highly significant ($p < 0.001$) relationship was identified between the duration of dexrazoxane exposure and the increase in absolute hemoglobin content (Fig. 3.16). This relationship further suggests a cell cycling dependency or regulatory process with respect to hemoglobin production.

Table 3.9. Growth rates and doubling times of K562 cells exposed to dexrazoxane for various periods of time.

Duration of dexrazoxane exposure	κ (hr^{-1})	S.E.	C.V. (%)	t (hr)
None	3.54E-02	1.04E-03	2.9	20
0-24 hr	2.82E-02	1.36E-03	4.8	25
0-48 hr	3.19E-02	2.23E-03	7.0	22
0-120 hr	5.20E-03	6.14E-04	11.8	133
0-168 hr	7.41E-03	5.18E-04	7.0	94

Fig. 3.13. Effect of dexrazoxane on the fraction of hemoglobin containing K562 cells. K562 cells ($0.8x10^6$ cells/mL) were treated daily to 100 μM dexrazoxane (●) with media replacement. Portions of cells were transferred to medium without dexrazoxane after 24 hr (▽), 48 hr (■), 120 hr (◇), and 168 hr (▲), and were grown in parallel to control untreated cells (○). On a daily basis samples were removed and (a) cell densities were determined on a Coulter counter (threshold of 7, 100 μm aperture, diameter cutoff ≅ 8.7 μm) followed by normalization. (b) Cell viability was assessed by trypan blue dye exclusion analysis. (c) K562 differentiation was assessed by benzidine-positive staining of hemoglobin containing cell. (d) The actual number of viable benzidine-stained cells was determined by combining plots (a) and (c).

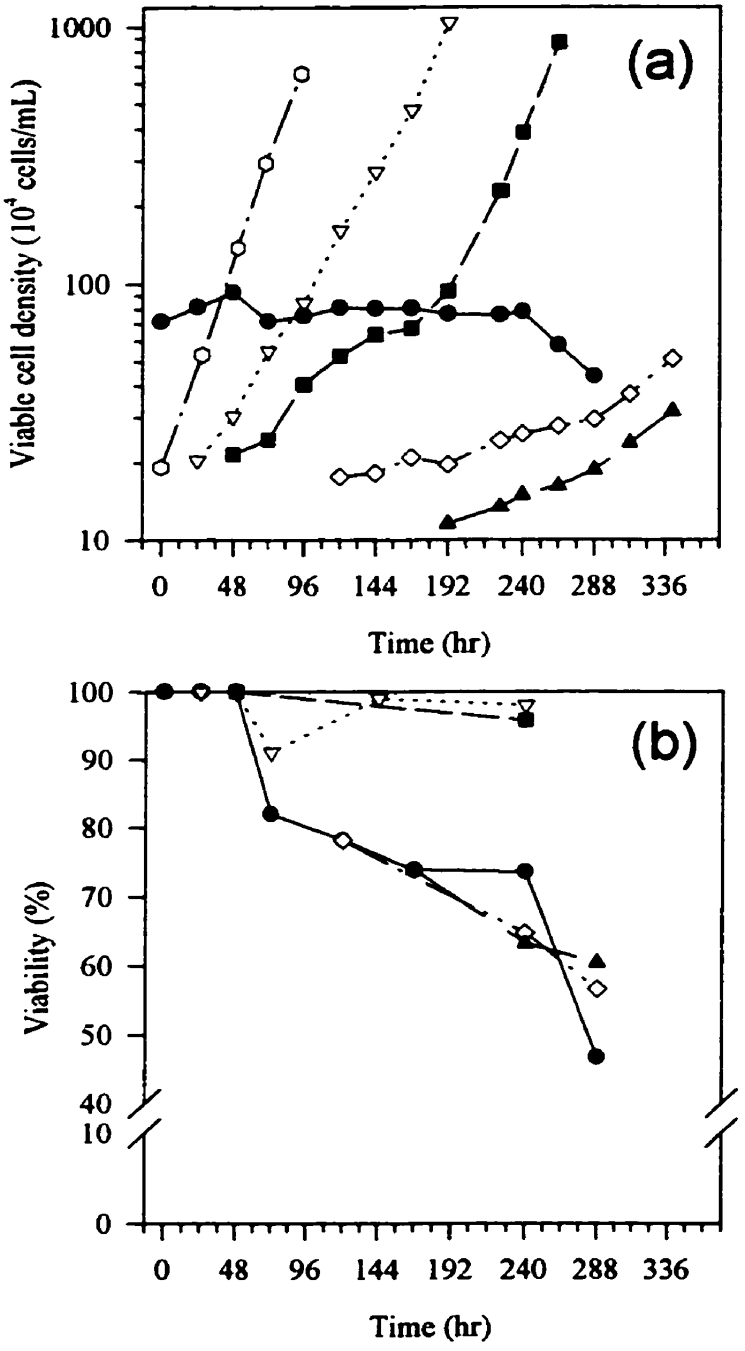

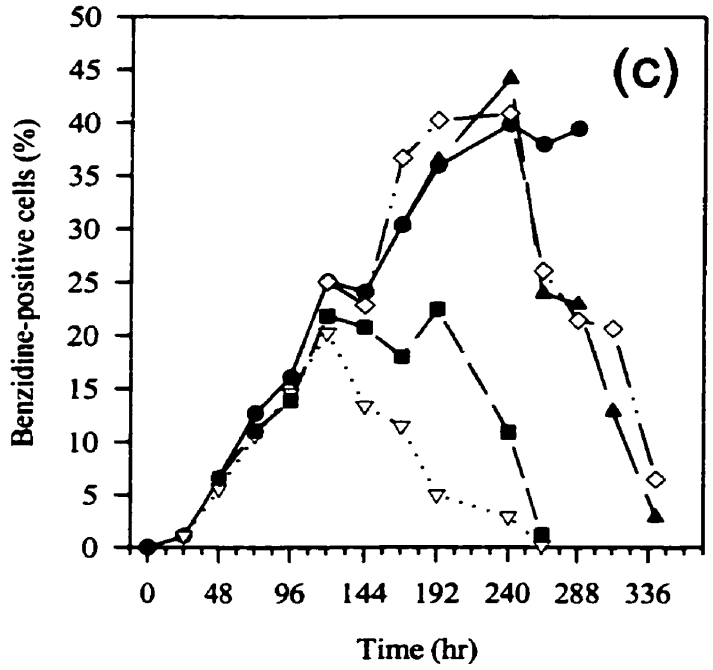
(c)
Benzidine-positive cells (%)
50
45
40
35
30
25
20
15
10
5
0
0
48
96
144
192
240
288
336
Time (hr)

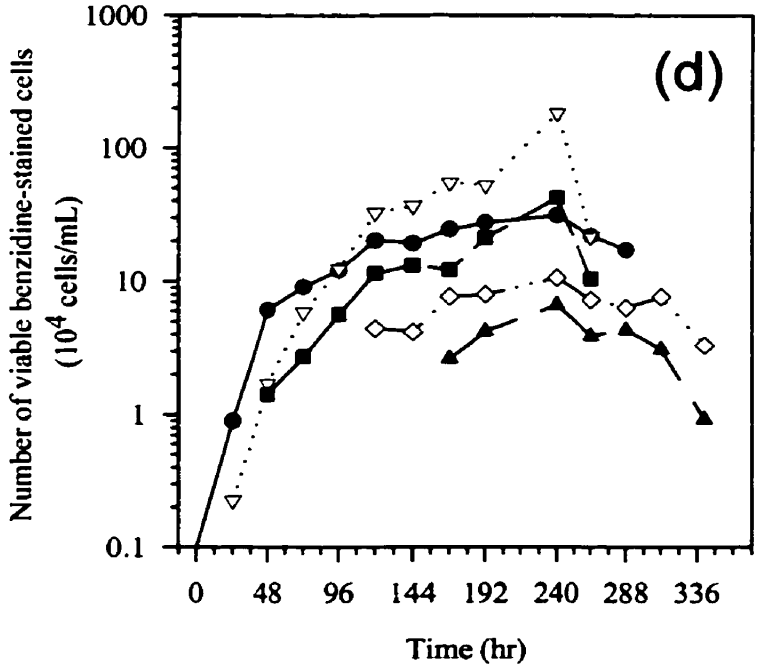
(d)
Number of viable benzidine-stained cells
(10^4 cells/mL)
1000
100
10
1
0.1
0
48
96
144
192
240
288
336
Time (hr)

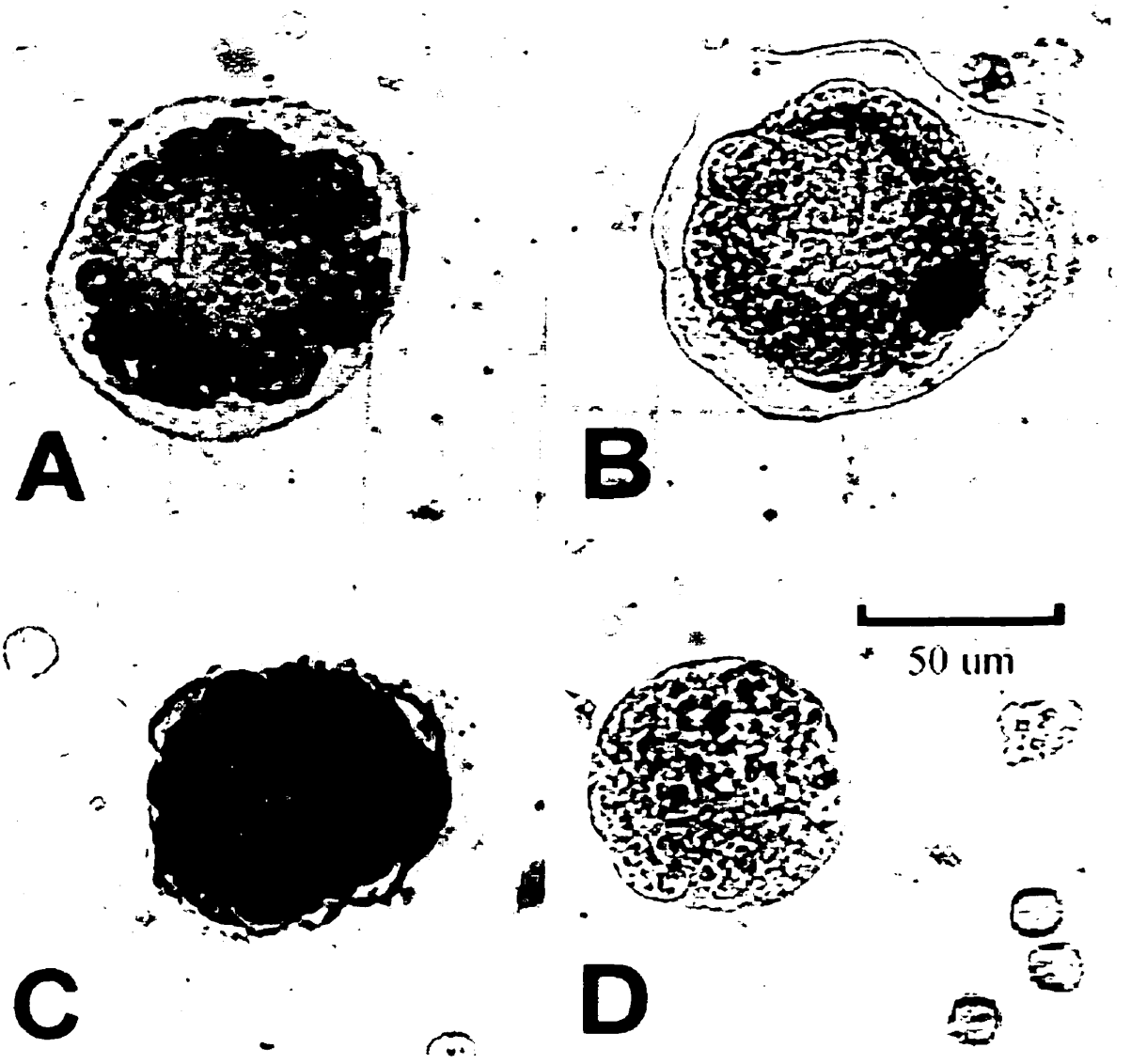

Fig. 3.14. Bright-field photomicrographs of benzidine-stained K562 cells after 240 hr (10 days) of daily exposure to dexrazoxane. After 240 hr of dexrazoxane exposure the diameter of some cells approached 100 μm, as viewed under a 40X objective lens. This corresponded to a 230-fold increase in volume as compared to the mean cell volume (Fig. 3.9) of control untreated cells (*bottom right, inset*). At each examined interval of dexrazoxane exposure the degree of benzidine-positivity differed. As some cells would stain for hemoglobin (A) others would not (B) and (D). In addition, the degree of staining differed between cells, as can be seen by comparing (A) and (C). Furthermore, cell size and morphology did not necessarily predispose positive-staining for hemoglobin. This can be seen by a comparison of some cells which possessed what looked to be lobular regions around the periphery of the cell, (A) and (B).

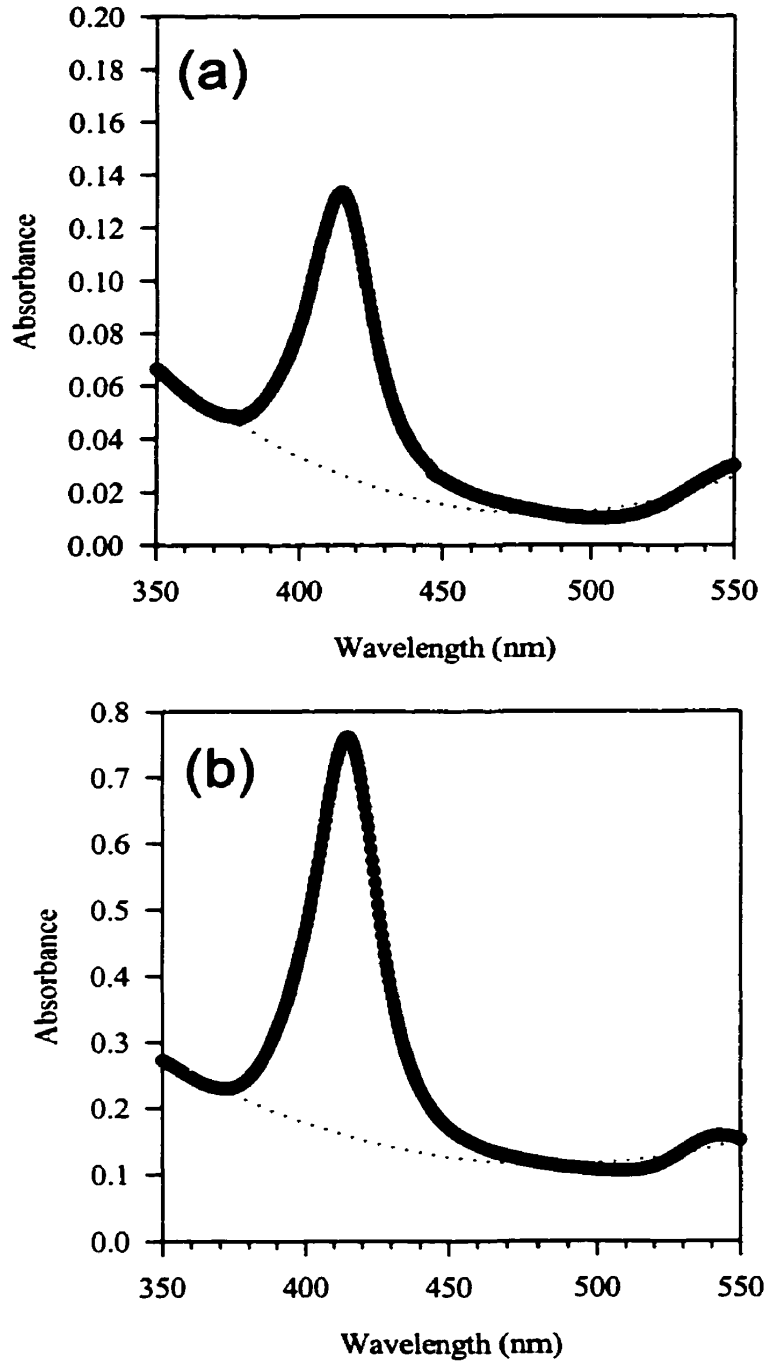

Fig. 3.15. Spectral properties of human hemoglobin from K562 cells. Absolute hemoglobin content of ~0.8×10^7 K562 cells was analyzed after (a) 0 hr and (b) 96 hr of daily exposure to dexrazoxane with media replacement. Both spectra reveal absorbance peaks at 415 and 541 nm characteristic of HbO_2. True absorbance at 415 nm was determined by subtraction of an empirically calculated background absorbance (using a quadratic equation), from the overall peak absorbance.

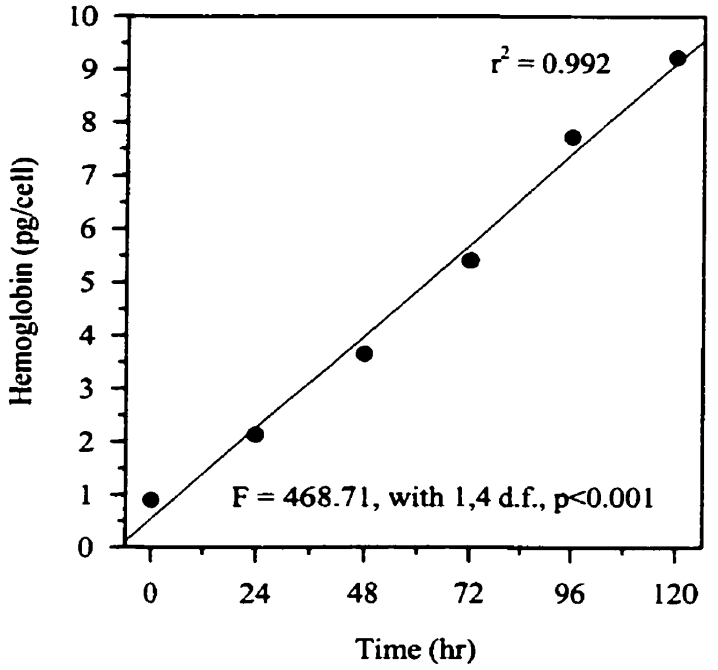

Fig. 3.16. Evaluation of absolute hemoglobin content in K562 cells exposed continuous to dexrazoxane. K562 cells were exposed daily to 100 μM dexrazoxane with media replacement. At indicated periods of time cell densities were determined on a Coulter counter (threshold of 7, 100 μm aperture, diameter cutoff ≅ 8.7μm) and ~$0.8x10^7$ cells were removed, washed with PBS and lyzed through freeze-thawing. Hemoglobin content levels were determined spectrophotometrically on cell lysate supernatants by absorbance measurement at 415 nm and subtraction from an empirically calculated background absorbance assuming a molar extinction coefficient of 125,000 $M^{-1}cm^{-1}$ and M_W of 16,000 g/mol. As demonstrated by statistical linear regression analysis a highly significant relationship ($p<0.001$) was identified.

3.4.3.2 Dexrazoxane dose response curves with respect to growth inhibition and hemoglobin expression

Dependent variables displayed in Fig. 3.17 were the result of single determinations. The calculated IC_{50} value of 13.8 ± 1.3 μM by the method used herein is in strong agreement with previously determined dexrazoxane IC_{50} values by such methods as MTS and cell counting analysis (Table 3.5), whereby observed cytotoxicities can be related to the inhibition of topoisomerase II [72]. The concentration of dexrazoxane at which 50% erythroid-like differentiation occurs, as determined by the level of hemoglobin expression was termed DC_{50}. By drawing comparisons to corresponding IC_{50} values (Fig. 3.17c), DC_{50} values were used only in the context of this thesis in an attempt to correlate a relationship between hemoglobin production and the catalytic inhibition of topoisomerase II by dexrazoxane. Open circle data points displayed after 1000 μM dexrazoxane by benzidine-staining analysis (Fig. 3.17a), and after 100 μM dexrazoxane by spectrophotometric analysis (Fig. 3.17b) were excluded from the determination of DC_{50} values. At extremely high dexrazoxane concentrations representative high levels of hemoglobin expression were not seen. This was possibly due to a leakage of hemoglobin from these cells as the chelation of divalent cations by the hydrolyzed product of dexrazoxane induced a high level of cytotoxicity. In spite of these complications, DC_{50} values of 90.5 ± 11.3 μM and 12.2 ± 31.6 μM dexrazoxane were approximated from benzidine-staining and spectral hemoglobin analyzes, respectively. The dose-response curve from benzidine-staining (Fig. 3.17a) appeared to lag, as compared to spectral hemoglobin analysis (Fig. 3.17b) thus resulting in a higher DC_{50} value. This result was in part attributable to the accuracy in scoring intact benzidine-positive cells amongst a highly fragmented cell

population, and the difficulty in detecting faintly stained cells with extremely low hemoglobin expression levels. Overall, the above results suggest the existence of an dexrazoxane dose-dependency effect with respect to hemoglobin expression which may directly correlate to its method of action in terms of topoisomerase II inhibition.

3.4.3.3 Hemoglobin expression levels after exposure to other bisdioxopiperzines, etoposide, and known inducers of K562 differentiation

The effects caused by dexrazoxane on K562 cells in terms of proliferation, viability and benzidine-positivity were additionally compared to those caused by other topoisomerase II inhibitors and known inducers of differentiation. Exposure of K562 cells to 100 μM ADR-925, the non-topoisomerase II inhibitory hydrolyzed form of dexrazoxane [72], resulted in a form of cell proliferation comparable to untreated cells (Fig. 3.18a). In contrast to its unhydrolyzed form, ADR-925 did not effect cell morphology or cell size, and hemoglobin production was not induced (Fig. 3.18c). Other compounds similar in structure to dexrazoxane were also tested, which included ICRF-193 and ICRF-154. Previously, it has been shown that of these non-cleavable complex forming topoisomerase II inhibitors, ICRF-193 is the strongest and most potent [72,73]. Slightly cytotoxic concentrations of these compounds were chosen after MTS cytotoxicity analysis (Fig. 3.7) on the premise that higher benzidine-positivity levels would result in a similar manner as had occurred at such concentrations of dexrazoxane. As a consequence, both agents displayed similar morphological changes in the cells, as previously mentioned with respect to dexrazoxane exposure. Exposure to 5 μM ICRF-193 resulted in a significant inhibition of cell division (Fig. 3.18a). This was accompanied by a level of benzidine-positivity of

~15% after 96 hr compared to ~24% with dexrazoxane (Fig. 3.18c). Cell proliferation in the presence of ICRF-154 increased marginally over the same period of time, accompanied by an increase in benzidine-positivity of only ~4%. The closed-clamp topoisomerase II inhibitor etoposide, which generates DNA strand breaks through its mode of topoisomerase II inhibition [74] was shown to decrease cell number more readily than any of the other agents when used at a similarly chosen cytotoxic concentration of 10 μM (Fig. 3.18a). The observed changes in morphology and levels of benzidine-positivity attained were strikingly similar to those induced by dexrazoxane, and consistent with previously used concentrations [45].

DMSO was used as a negative control for the induction of erythroid differentiation. When exposed to 1.5% (v/v) DMSO K562 cells have been shown to produce some antigenic determinants of megakaryocytes while decreasing the production of hemoglobin and other erythroid markers [11]. Proliferation and benzidine-positivity remained indistinguishable from control cells (Fig. 3.18a, c), although a partial reduction in cell size was observed. Exposure of K562 cells to 30 μM hemin, a known effective non-topoisomerase II, non-commitment inducer of erythroid-like differentiation [9,19,26] resulted in a partial inhibition of proliferation (Fig. 3.18a), some cellular fragmentation, and a marginal increase in cell size. Upon exposure to hemin benzidine-positivity increased to ~12% by 100 hr (Fig. 3.18c), as similarly seen elsewhere [19,25,45,60]. However, repeated trials of hemin exposure revealed benzidine-positivity increments to ~5-8%, accompanied by a more attenuated inhibition of cell division. Cell viability declined at a relatively equivalent rate in all instances in which cells were exposed to agents of known topoisomerase II inhibitory function (Fig. 3.18b).

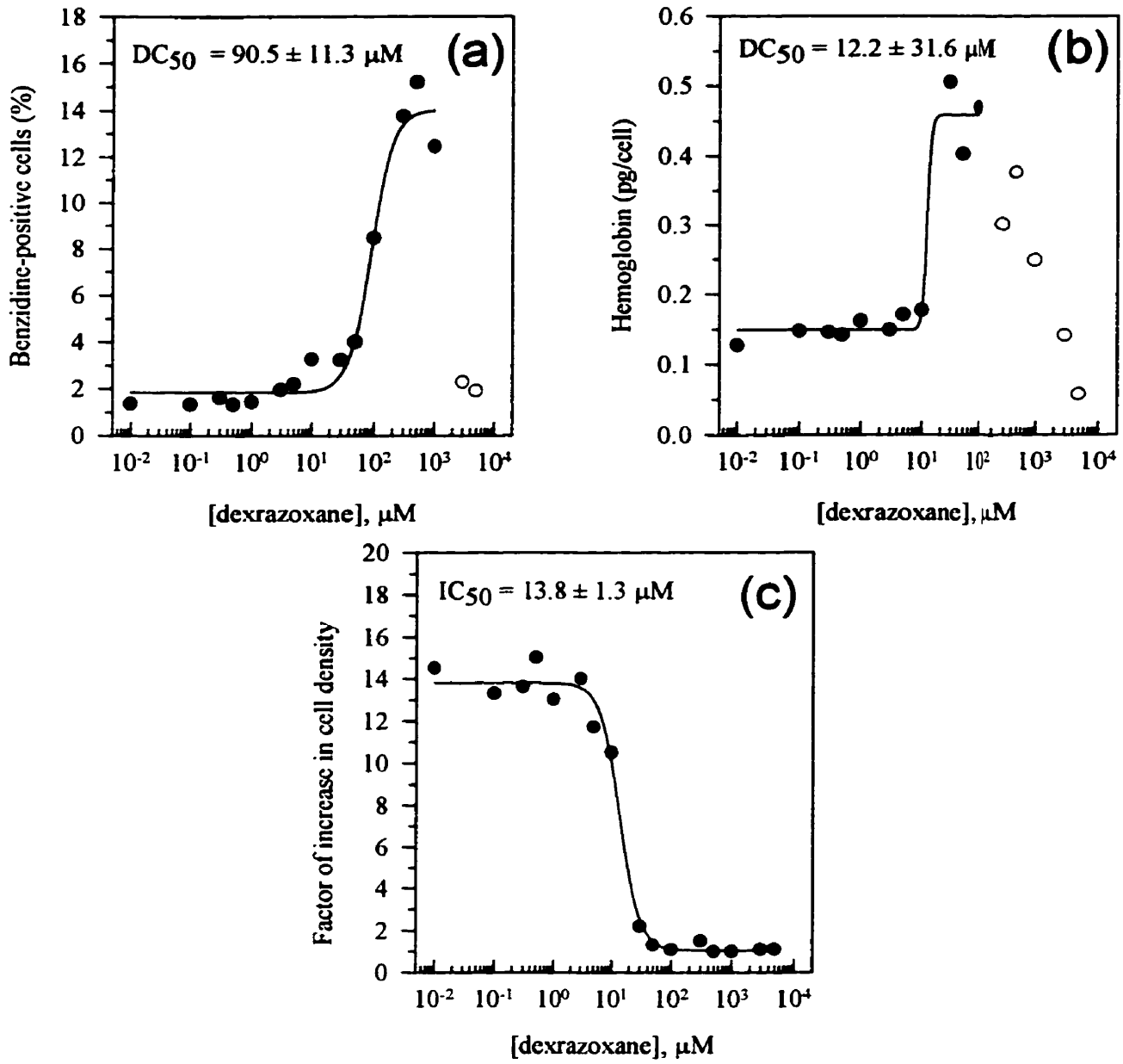

Fig. 3.17. Concentration dependency of dexrazoxane induced erythroid-like differentiation of K562 cells. K562 cells (0.6-3.0x10^5 cells/mL) were grown in T-25 flasks and exposed once to various concentrations of dexrazoxane. After 72 hr of exposure differentiation was assessed by (a) benzidine staining, and (b) spectrophotometric quantitation of hemoglobin levels. DC_{50} values are reflective of dexrazoxane concentrations at which 50% differentiation has occurred relative to the duration of exposure. Open circle data points (O) were not used in the determination of these values, by a 4-parameter logistic equation as it was believed that chelation of divalent cations lead to the reduced hemoglobin accumulation at these concentrations. (c) A dexrazoxane dose response curve was constructed, using the factor of cell density increase from Coulter counter analysis (threshold of 20, 100 μm aperture, diameter cutoff ≅ 11.9 μm). IC_{50} is reflective of the dexrazoxane concentration required to inhibit the growth of cells by 50%.

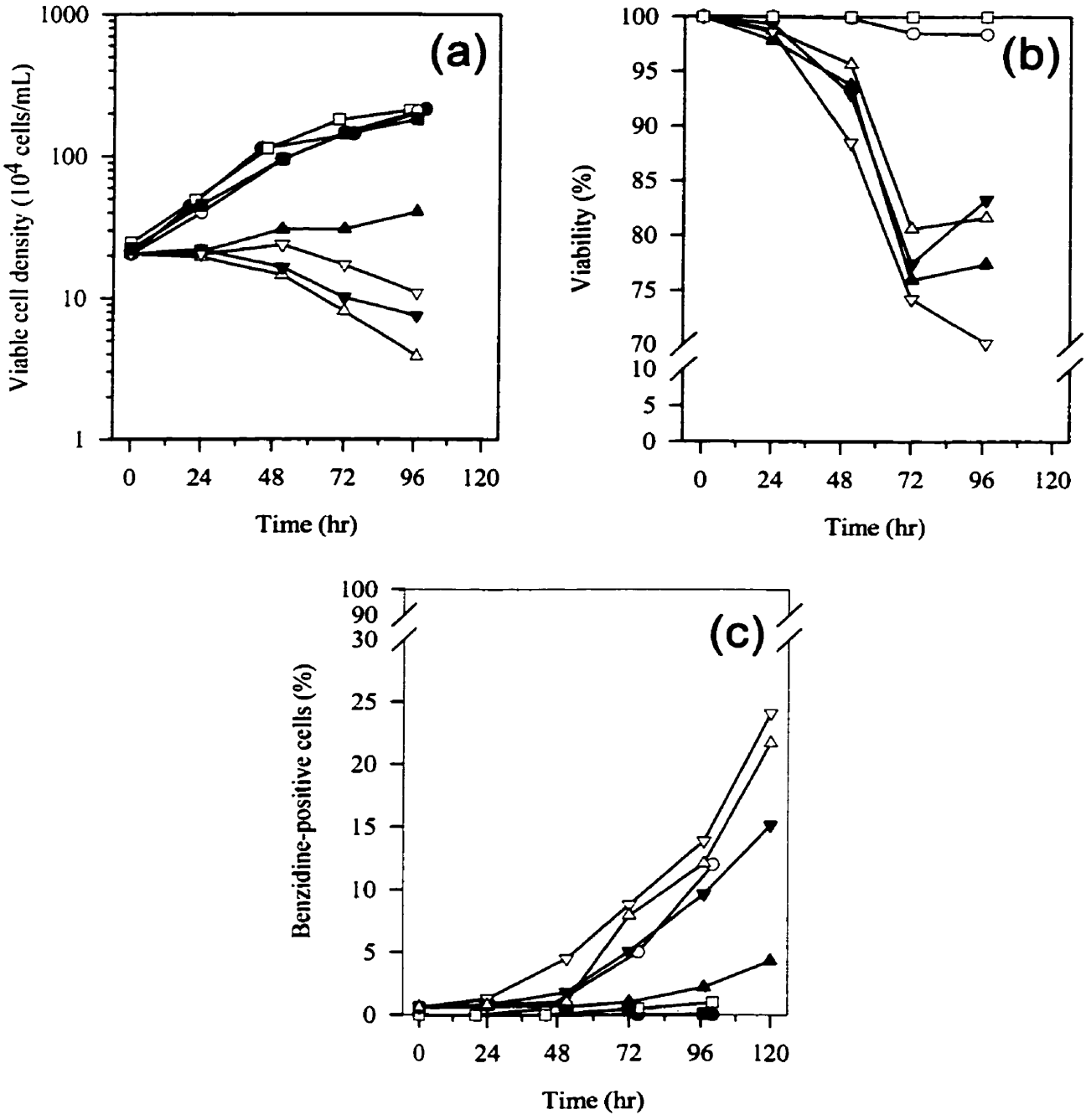

Fig. 3.18. Effects of various agents on hemoglobin production in K562 cells. Untreated cells (●) were seeded at 2.1×10^5 cells/mL and treated once with 30 μM hemin (○), 1.5% DMSO (□), or 100 μM ADR-925 (■). Other cells were treated daily with 100 μM dexrazoxane (▽), 5 μM ICRF-193 (▼), 50 μM ICRF-154 (▲), or 10 μM etoposide (△) with media replacement. At indicated times, samples were removed and (a) cell densities were determined on a Coulter counter (threshold of 20, 100 μm aperture, diameter cutoff ≅ 11.9 μm); (b) viability by trypan blue dye exclusion analysis; and (c) cell differentiation by benzidine staining for hemoglobin expression.

3.4.3.4 Flow cytometry immunofluorescence analysis of megakaryocyte and erythroid antigen expression

Megakaryocytic and erythroid specific monoclonal antibodies were used to study the induction of differentiation of K562 cell cultures in the presence of dexrazoxane (Fig. 3.19). When compared to the non-specific binding of isotypic control mAbs, untreated K562 cells stained with anti-CD41 mAb were shown to be unreactive (Fig. 3.19a and 3.19b). A marginal difference in the percentage of positive cells in region IV of 0.13% indicated that perhaps a very small fraction of these untreated cells constitutively expressed the erythroid marker, glycophorin A, in direct correlation with previous results of <1% benzidine-positive staining (Fig. 3.13 and 3.18). Dexrazoxane treatment greatly increased the number of glycophorin A-specific cells after 96 hr of dexrazoxane exposure as seen by the relative number of fluorescent-stained cells depicted in region IV of Fig. 3.19d. Correspondingly, as shown in Table 3.10 the percentage of glycophorin A-positive cells increased 85-fold relative to isotypic controls from 0.13-11.00% by 96 hr. In contrast, the percentage of cells staining for expression of the gpIIb/IIIa megakaryocytic antigen, either alone (region I) or in combination with glycophorin A (region II) remained unchanged over the entire treatment period (Table 3.10). Only a small insignificant 0.07% increase of megakaryocytic expression was identified in region I after 96 hr of exposure, which in all likelihood could be attributed to cell clumping. When the above experiment was repeated at a later date very similar results were seen (data not shown). Overall these results suggest that although K562 cells differentiate in the presence of dexrazoxane in an erythroid-like fashion, they do so in the absence of an increase in megakaryocytic features.

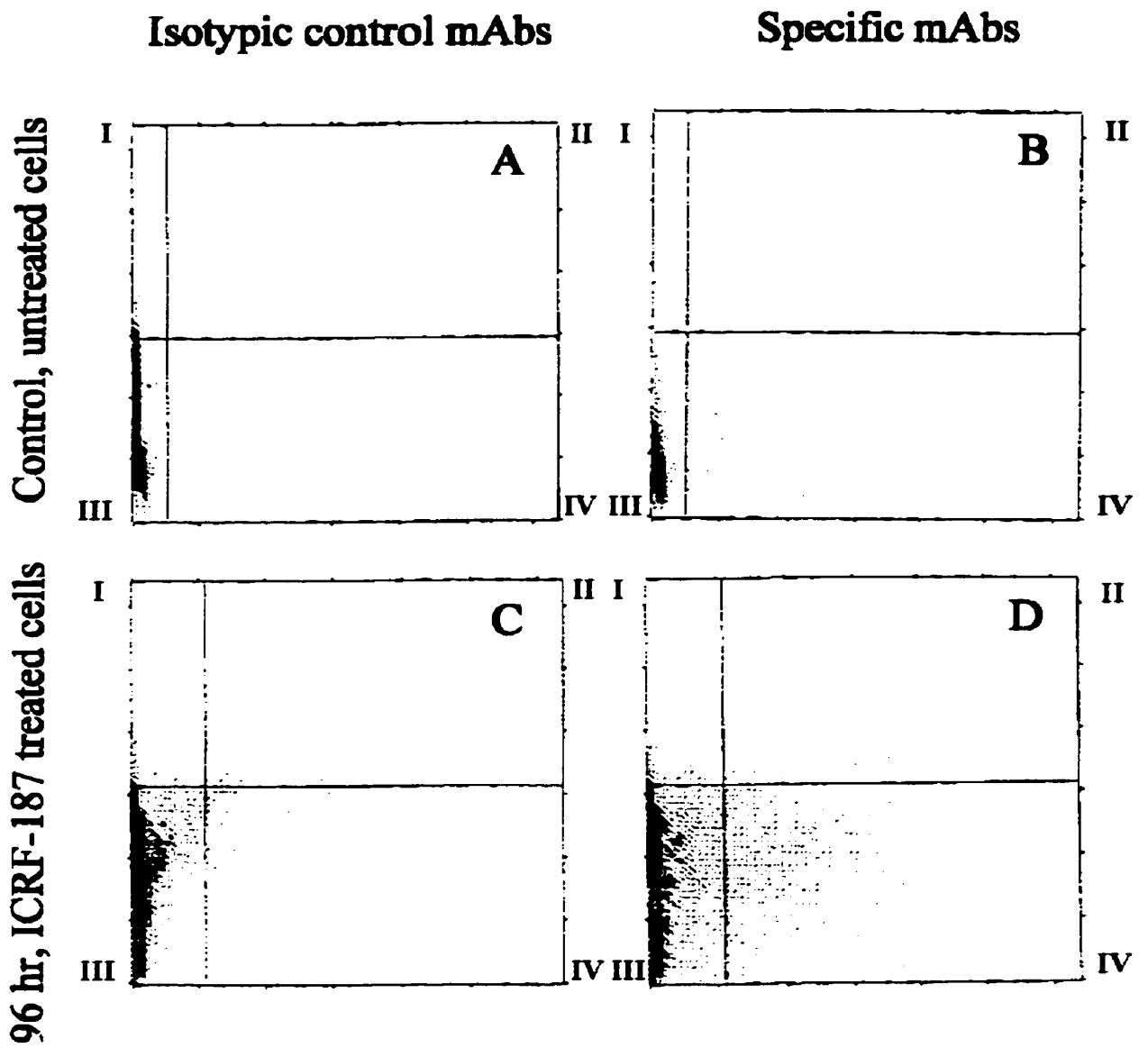

Fig. 3.19. Flow cytometry analysis of glycophorin A and gpIIb/IIIa antigens on single K562 cells with exposure to dexrazoxane. Untreated K562 cells (A and B) were exposed daily to 100 μM dexrazoxane with media replacement for 96 hr (C and D). Cells were analyzed with specific primary antibodies (11E4B7.6 for glycophorin A and P2 for gpIIb/IIIa in B and D) or with control primary antibodies (nonimmune IgG1-FITC / IgG1-PE in place of both specific antibodies in A and C). Displayed horizontally is log green fluorescence, detecting FITC-conjugated anti-IgG1 binding 11E4B7.6. Displayed vertically is log red fluorescence, detecting phycoerythrin-conjugated anti-IgG1 binding P2. Each bivariate determination has been divided into regions I-IV as follows: I, binding P2 only; II, binding both 11E4B7.6 and P2, III, binding neither primary antibody; and IV, binding 11E4B7.6 only.

Table 3.10. Percent increase of fluorescence in lineage-specific mAb staining on K562 cells after various periods of dexrazoxane exposure.

Antibody	Region	Duration of dexrazoxane exposure (hr)*				
		0	24	48	96	120
anti-CD41	I	0.00	0.00	0.02	0.07	0.00
anti-Glycophorin A	IV	0.13	0.47	6.05	11.10	6.05
both	II	0.00	0.00	0.04	0.03	0.14
neither	III	-	-	-	-	-

* The percentage increase in specific fluorescence was derived from the difference between the distribution using the lineage-specific mAbs and the distribution using the isotypic control mAbs of the same Ig subclass for each analyzed time interval in turn.

3.5 Examination of apoptosis in K562 cells treated with dexrazoxane and other topoisomerase II inhibitors

3.5.1 Introduction

Accumulating evidence suggest that the regulation of a cell commitment to death is an essential component of malignant cells sensitivity to chemotherapeutic agents [53]. Taking into account the aforementioned observations of K562 erythroid-like differentiation induced by dexrazoxane it is important to consider that these results may have been a first level response to topoisomerase II inhibition. The observed eventual fragmentation of cells may likely have been attributed to a form of cell death known as apoptosis. The lack of spontaneous cell death upon dexrazoxane exposure, as will be discussed further may simply have been due to the length of the cell commitment process and/or the degree of sensitivity inherent to K562 cells.

In the following section, attributes of apoptotic induction by dexrazoxane, and to a lesser extent ICRF-193 and etoposide were investigated. Cell death can commonly occur by two basically different processes, apoptosis or necrosis. As mentioned previously, apoptosis is an intrinsically controlled process in which a cell actually commits suicide in response to particular modifications in its environment [75]. The process of apoptosis is defined morphologically by cell shrinkage, as water is extruded in an energy dependent manner requiring intact mitochondria. This is followed by nuclear condensation of chromatin into a specific pattern, endonuclease-mediated cleavage of cellular DNA, release of apoptotic bodies, and the eventual lysis of the plasma membrane [55]. In contrast, necrosis is considered a passive uncontrolled phenomenon. This process is characterized by a destructive series of events which include swelling of the cell and mitochondria,

nonspecific degradation of DNA, and the immediate loss of plasma membrane integrity [75,76].

Over the course of this study the induction of apoptosis was quantified by a number of different methods. An analysis of internucleosomal DNA fragmentation by agarose gel electrophoresis provided a convenient marker for identifying the progression of apoptosis. The use of fluorescence DNA-binding dyes allowed for the direct examination of cells in order to identify morphological characteristics of apoptosis and necrosis, and to quantify their proportion over the course of the treatment period. Finally, flow cytometry was used for two purposes. First, the detection of the light-scattering properties of cells allowed for quantitation of changes in cell size and granularity that occur during apoptosis when water is lost. And second, flow cytometry permitted the detection of apoptotic bodies that contained sub-diploid (sub-G0/G1) amounts of DNA after staining with propidium iodide, a DNA-binding fluorophore.

3.5.2 Materials and Methods

3.5.2.1 Materials

Dexrazoxane (Zinecard®, dexrazoxane) was a gift of Pharmacia & Upjohn (Columbus, OH, U.S.A.). Etoposide (cat No. E-1383) and camptothecin (cat No. C-9911), were obtained from Sigma Chemical Co. ICRF-193 was synthesized previously in our laboratory. DMSO (99.5%, cat. No. D-5879), benzidine dihydrochloride (cat. No. B-0386), ethidium bromide (95%, cat No. E-8751), acridine orange (cat No. A-6014), bromophenol blue sodium salt (cat. No. B-8026), proteinase K (stored at –20°C, cat. No. P-

2308), RNase A (stored at –20°C, cat. No. R-5503), N-lauryl sarcosine (sarkosyl, cat. No. L-5125), Tris-base (reagent grade, cat. No. T-1503), Lambda BstE II digest molecular weight markers (cat. No. D-9793), propidium iodide (cat. No. P-4170), and 8-hydroxyquinoline (cat. No. H-6878), were obtained from Sigma Chemical Co. (St. Louis, MO, U.S.A.). Triton X-100 (cat. No. X198-5), and iso-amyl alcohol (cat. No. 9038) were obtained from J.T. Baker Chemical Co. (Phillipsburg, NJ, U.S.A.). Hydrogen peroxide (30% v/v, cat. No. 21,676-3) was obtained from Aldrich Chemical Co. (Milwaukee, WN, U.S.A.). Dulbecco's phosphate buffered saline (PBS, cat. No. D-5652), DMEM (cat. No. 12800-017), fetal bovine serum (FCS, cat. No. 26140-079), and agarose (ULTRAPURE, cat. No. 15510-019 were obtained from Gibco-BRL, Life Technologies Inc. (Burlington, ON). Cover glass slips (22x22 mm, no. 1½, cat. No. 12-541B), glass slides (75x25 mm, cat. No. 12-550A), and sodium acetate (cat. No. S-209B) were obtained from Fisher Scientific (Fairlawn, NJ, U.S.A.). Isoton II Coulter balanced electrolyte solution (cat. No. PN 8546719) was obtained from Beckman Coulter Inc. (Burlington, ON). Glacial acetic acid (3 N, cat. No. 2501), phenol loose crystals (cat. No. UN1671), and chloroform (cat. No. 4440) were obtained from Mallinckrodt Specialty Chemicals Co. (Paris, KT, U.S.A.). Hydrochloric acid (11.6 M HCl, cat. No. C9800-10) was obtained from Baxter Corp. (Toronto, ON). Sodium chloride (NaCl, cat. No. AC-8304), and boric acid (cat. No. AC-1308) were obtained from Anachemia Ltd. (Toronto, ON). Sucrose (cat. No. B10274), and Na_2EDTA (99.5%, cat. No. 10093) were obtained from BDH Chemicals Ltd. (Toronto, ON).

3.5.2.2 Drug treatments

Characteristics of apoptosis in K562 cells exposed to dexrazoxane were examined by use of DNA fluorescent stains, agarose gel electrophoresis, and flow cytometry. Cells exposed either to ICRF-193 or etoposide were examined only for attributes of DNA fragmentation by agarose gel electrophoresis. Dexrazoxane was dissolved in DMEM/FCS and filter sterilized through a 0.2 μm acetate filter. Etoposide, and ICRF-193 were dissolved in 99.5% DMSO by brief sonication and heating in a 37°C water bath.

Exponentially growing K562 cells were diluted to starting cell densities of $5x10^5$ cells/mL in DMEM/FCS followed by the addition of a requisite stock solution of dexrazoxane at <10% (v/v) to produce a final concentration of 100 μM (total volume of 15-40 mL). Similarly, ICRF-193 and etoposide were added to separate cultures of identical volumes from prepared stock solutions such that final concentrations would be 5 and 10 μM, respectively. The amount of contributing DMSO, within which these drugs were dissolved was kept constant at 0.5% (v/v). On a daily basis, cells were centrifuged at 250 *g* for 12 min and resuspended in an appropriate volume of ~80% fresh DMEM/FCS in an attempt to maintain cell densities approximately equivalent to that of before centrifugation or sampling. This was followed by the subsequent re-addition of dexrazoxane, ICRF-193, or etoposide, administered to the same concentrations and in the same fashion as before. Cell densities were monitored daily by counting on a model Z_f Coulter counter with a threshold setting of 20, 100 μm aperture tube (1/amp. = 2, 1/ap.curr. = 8, diameter cutoff ≅ 11.9 μm).

3.5.2.3 Quantitation of apoptosis and cell viability using fluorescent dyes

The following protocol was utilized so as to visualize, photograph, and count cells with aberrant chromatin organization and other morphological features characteristic of apoptosis and necrosis after the introduction of fluorescent DNA-binding dyes [75,77].

3.5.2.3.1 Preparation of working dye solution, controls, and samples

Working dye solution: A working dye solution of ethidium bromide/acridine orange (100 μg/mL) was prepared by adding 5 μL acridine orange (10 mg/mL) and 5 μL ethidium bromide (10 mg/mL) to 490 μL of PBS and was stored at 4°C.

Benzidine stock solution: A stock solution of 0.2% (w/v) benzidine dihydrochloride in 0.5 M acetic acid was prepared, and was stable for months at 4°C. For each estimation a fresh 0.4% (v/v) staining solution of 30% (v/v) hydrogen peroxide in the benzidine stock solution was prepared before use.

Apoptotic and necrotic controls: Apoptotic control samples were prepared by exposing both K562 and CHO cells twice to 10 μM camptothecin at 0, 24 hr. A camptothecin stock solution of 2000 μM was prepared by dissolving in 99.5% DMSO followed by the addition of 50 μL to 9950 μL culture volumes in T-25 flasks at 0.5% (v/v). At the time of initial exposure K562 cell density was approximately $5x10^5$ cells/mL, and the CHO culture was approximately half-confluent (i.e. $5x10^6$ cells). Necrotic controls were prepared by resuspending ~$5x10^6$ exponentially growing K562 cells in 4 mL of cold 70% (v/v) ethanol overnight at – 20°C.

Sample preparation: In brief, cells were collected after different periods of dexrazoxane exposure, or from prepared control samples and pelleted by centrifugation at 250 *g* for 6 min to ~$1x10^6$ cells/mL. Then 4 μL of the working dye solution was added to 100 μL of cell suspension, mounted on a glass cover slide, and examined under a 40X objective lens by fluorescence microscopy employing an XF-19 filter set (Omega Optical, Brattleboro, VT, U.S.A.).

The optimal procedure for sample mounting first involved the application of tiny droplets of Vaseline onto the four corners of the glass cover slip. This was followed by the addition of 10 μL of the sample onto the middle of the cover slip, cautiously lowering the glass cover slide onto the cover slip at a 45° angle, then turning the entire preparation right-side up and applying light even streaks of nail polish along the edges of the glass cover slip to prevent premature evaporation.

In order to examine whether hemoglobin was expressed in cells displaying characteristic features of apoptosis the benzidine-staining assay and the following method of apoptosis identification were combined. After 96 and 168 hr of daily exposure to dexrazoxane K562 cell samples were collected and concentrated as described above. To 100 μL of cell suspension was added 10 μL of benzidine stock solution. This was followed by the addition of either 4 μL of acridine orange (10 mg/mL), or 4 μL of working dye solution, with the former producing the best fluorescence clarity. Samples were mounted onto glass cover slips, as previously described and examined under a 40X objective by fluorescence and bright-field microscopy with the same filter sets as before.

3.5.2.3.2 Criteria and method of apoptosis and viability quantitation

The premise behind the use of such fluorescent dyes is as follows. Acridine orange (AO) is membrane permeable dye taken up by cells which may or may not possess an intact membrane, causing them to appear green after intercalation into double-stranded DNA. In addition, acridine orange binds to RNA and single-stranded DNA staining red-orange. Ethidium bromide (EB) is a membrane impermeable dye which enters only cells possessing damaged outer membranes, and causes them to appear orange after intercalation into double-stranded DNA, thus overwhelming acridine orange fluorescence. The integrity of the membrane and hence viability of the cell was therefore determined by the color of the chromatin, green for viable, orange for non-viable.

Discernment between apoptotic and non-apoptotic cells was based on the morphology of cellular chromatin. Apoptotic cells were identified by the presence of condensed fragmented nuclei, slight cytoplasmic shrinkage in some cases, and extremely bright condensed chromatin spread around the periphery of the nucleus or present as groups of bright featureless spherical beads [75]. Late stage chromatin-free apoptotic cells, which had totally lost their DNA content were identified by very weak green-orange staining. Non-apoptotic cells exhibited a diffuse fluorescence in nuclear region and an ordered form of chromatin condensation, consistent with normal cell division.

A minimum of 600 total cells were counted by fluorescence microscopy per sample such that only those cells of normal cell size and above were included. Based on the various morphological appearances, chromatin structures, and membrane integrity observed the percentage of each cell type was determined with respect to the total number of cells counted (i.e. %VNA = number of VNA cells / total cell count x 100%). Initially,

the number of cells of each of the following four cellular states were counted: (i) VNA, viable cells with green non-apoptotic chromatin/nuclei and diffuse fluorescence intensity; (ii) VA, viable cells with green apoptotic chromatin/nuclei; (iii) NEC, necrotic or non-viable cells with orange normal chromatin/nuclei and diffuse fluorescence; (iv) NVA, non-viable cells with orange apoptotic chromatin/nuclei. Subsequently, the total percentage of the following general states were determined by combining the above mentioned percentages: apoptotic cells by combining (ii) and (iv); non-apoptotic cells from (i) and (iii); viable cells from (i) and (ii); non-viable cells from (iii) and (iv). Photographs of cells were taken using a Nikon camera mounted on a photomicroscope with epifluorescence attachment. Kodak Ektachrome (Elitechrom) 400 daylight color slide film was used with the following settings under a 40X objective lens: shutter control on, step setting of +1, set time of 4 sec, actual exposure time ~10 sec.

3.5.2.4 Detection of internucleosomal fragmentation of genomic DNA by agarose gel electrophoresis

3.5.2.4.1 Extraction and precipitation of genomic DNA

Lysis buffer: This solution contained 50 mM Tris-base (M_w = 121.1g/mol), 10 mM Na_2EDTA (M_w = 372.24g/mol), and 0.5% (w/v) N-lauryl sarcosine (sarkosyl) dissolved in ddH_2O and was stored at 4°C. Just prior to use, 1 mg of proteinase K was added to 1 mL of this solution to produce a concentration of 0.5 mg/mL proteinase K in lysis buffer.

DNase-free RNase A: It was necessary to ensure that prepared solutions of RNase A (0.5 mg/mL) were free of contaminating DNA digestive nuclease enzymes. This was achieved

by dissolving 0.5 mg RNase A in 1 mL lysis buffer, followed by boiling for 5 min in a beaker of ddH_2O for 5 min.

Buffering phenol and preparation of 25:24:1 phenol/chloroform/isoamyl alcohol: Into a 200 mL glass beaker containing a stir bar and 0.1 g of 8-hydroxyquinoline was added 100 mL of liquefied phenol (melted in a water bath at 65°C). Next, 100 mL of 50 mM Tris-base (unadjusted pH ~10.5) was added, the beaker was covered with aluminum foil, and stirred for 10 min at low speed in the fume hood. After the phases were allowed to separate at room temperature the aqueous phase was decanted as waste, followed by the addition of 100 mL of 50 mM Tris-HCl (pH 8.0). These last few steps were repeated twice with successive stirring, decanting, and addition of 100 mL of 50 mM Tris-HCl. Finally, 50 mL of 50 mM Tris-HCl was kept on top of the buffered phenol, and the entire mixture was transferred to a brown glass bottle, wrapped in aluminum foil, and was stored at 4°C. For use in DNA purification, 25 volumes of phenol was mixed with 24 volumes of chloroform, and 1 volume of isoamyl alcohol (25:24:1).

TE Buffer: This solution contained 10 mM Tris-base and 1 mM Na_2EDTA, titrated to a pH 8.0 with concentrated HCl, and stored at 4°C.

At specified intervals following treatment with dexrazoxane, ICRF-193, or etoposide, ~$6x10^6$ cells were pelleted and washed twice with PBS by centrifugation at 250 *g* for 12 min. Cell pellets were then resuspended in 400 µL of lysis buffer (10 mM Na_2EDTA, 50 mM Tris-base, pH 8, 0.5% (w/v) sodium lauryl sarcosine, 0.5 mg/mL proteinase K) in microcentrifuge tubes and incubated for 1 hr at 50°C. This was followed by the addition of 200 µL of DNase-free RNase A (0.5 mg/mL) and an additional 1 hr of incubation at 50°C. Next, genomic DNA was extracted by adding 600 µL of

phenol/chloroform/isoamyl alcohol (25/24/1), inverting gently several times, centrifuging 5 min at 11,000 *g* to ensure optimal separation of organic/aqueous phases, and careful removal and transfer of ~400 µL of the aqueous phase to a separate microcentrifuge tube. If any white precipitate was transferred, subsequent extractions were performed in an identical manner. This was followed by the addition of $1/10^{th}$ volume of 3 M sodium acetate (pH 5.2), 2 volumes of ice-cold 100% ethanol, brief gentle inversion, and incubation overnight at –20°C. Samples were then pelleted by cold centrifugation at 11,000 *g* for 20 min, air dried for 15-30 min, and resuspended in TE buffer (~100 µL) by gentle flicking of the tube and/or briefly heating at 65°C for 5 min.

3.5.2.4.2 Quantitation of DNA using absorption spectroscopy

In order to assess the purity and concentration of the DNA sample preparations prior to loading onto an agarose gel the absorption of each sample was measured at two different wavelengths. A_{260nm} measurements are quantitative for relatively pure nucleic acid preparations in microgram quantities. Although absorbancy readings cannot discriminate between DNA and RNA, the ratio of A_{260nm}/A_{280nm} can be used as an indicator of nucleic acid purity. For example, proteins have a peak absorption at 280 nm that will reduce the A_{260nm}/A_{280nm} ratio.

The Cary 1 UV-VIS spectrophotometer (Varian Australia Pty. Ltd.) was allowed to warm up and after selecting the Cary100 instrument type the <Simple Reads> software program was initiated under c:\CaryWinUV. On the menu bar was selected <setup>, then <Read Mode>, <User Collect>, and from the drop down menu <Read(260)/Read(280)> with <Y mode: Abs>. The above 'User Collect' statement causes the instrument to first

take a reading at 260 nm, then change to 280 nm and take a second reading. The system then divides the reading at 260 nm by the reading at 280 nm and prints the values of A_{260nm}, A_{280nm}, and A_{260nm}/A_{280nm} in the 'Report' area.

Using the above procedure 490 μL of TE buffer was first placed in a cuvette and an initial reading was taken. Then 10 μL of sample DNA was added followed by a brief mixing with a Pasteur pipet, and then another reading was taken. Afterwards the program displayed the value of the ratio A_{260nm}/A_{280nm}. Ratio values which lied between 1.8-1.9 indicated highly purified preparations of DNA, and values significantly lower than these indicated protein and/or phenol contamination resulting from poor extraction, and raised the possibility that DNA band smearing would occur upon electrophoresis. The amount of DNA present in each sample was determined from only the corrected A_{260nm} values (i.e. A_{260nm} (sample) - A_{260nm} (blank)), whereby a final A_{260nm} value of 1.0 indicates 50 μg/mL of double-stranded DNA. A sample calculation of determining the amount of DNA is as follows, based on the above protocol:

corrected A_{260nm} = 0.2772
Dilution in cuvette = 10 μL sample + 490 μL TE buffer = 10 μL / 500 μL dilution
Original volume of stock sample in microcentrifuge tube = 100 μL = 0.1 mL

$$[DNA]_{stock} = 0.2772 \times 50\ \mu g/mL \times \frac{500\ \mu L}{10\ \mu L} = 693\ \mu g/mL \times 0.1\ mL = 69.3\ \mu g$$

3.5.2.4.3 Agarose gel electrophoresis

10x TBE stock buffer: A 1 L volume of Tris-boric acid- Na_2EDTA buffer was prepared ten times concentrated in ddH_2O containing: 1M Tris-base (M_w = 121.10 g/mol), 1M boric acid (M_w = 61.80 g/mol), 20 mM Na_2EDTA (M_w = 372.24 g/mol), with pH adjusted to 8.3 at room temperature with 5 M NaOH (*aq*), and stored at 4°C.

Ethidium bromide stock solution (10 mg/mL): This solution was prepared by dissolving 0.01 g ethidium bromide in 1 mL ddH_2O, and was stored at 4°C in a microcentrifuge tube for no longer than one month.

Running buffer: The running buffer was prepared fresh by a ten times dilution of 100 mL of TBE stock buffer in 900 mL ddH_2O. After 100 mL of this solution was used to dissolve 2 g of agarose, 18 µL of ethidium bromide (10 mg/mL) was added to the remaining 900 mL, and subsequently poured into electrophoresis chamber to a level of 0.5 cm above a prepared agarose gel.

Loading buffer: A sucrose-based loading buffer was prepared as opposed to a glycerol based loading buffer for the reason that sucrose has a much higher molecular weight and would ensure that samples would completely fall to the bottom of gel wells. Additionally, in TBE gels glycerol emphasizes the smiling of DNA bands and interacts with borate which may alter the local pH. This buffer contained 0.1 M Na_2EDTA (M_w = 372.24 g/mol), 0.25% (w/v) bromophenol blue (as a tracking dye), and 40% (w/v) sucrose, titrated to a pH of 8.0 and was stored at -20°C.

Agarose gel casting and preparation: A 2% (w/v) agarose gel was prepared by weighing 2 g of agarose in a beaker and adding 100 mL of running buffer, devoid of ethidium bromide. An agarose concentration of 2% (w/v) was chosen to allow for the highest possible resolution of DNA fragments less than 1 kb, consistent with internucleosomal DNA laddering. The mixture was heated on a hot plate and stirred constantly with a magnetic stirrer until the boiling point. This was followed by cooling to 60°C, addition of 2 μL ethidium bromide (10 mg/mL), stirring, and pouring into a leveled gel caster tray (15x7 cm), with the 20-tooth well comb in place. Ethidium bromide which intercalates between DNA bases was placed into the agarose itself so as to allow for examination under UV at different stages of band migration. All of the air bubbles in the gel were subsequently moved to the sides with a Pasteur pipet and the gel was left to set for at least 60 min.

Preparation of DNA samples for loading and electrophoresis: DNA samples were prepared by adding to a microcentrifuge tube a volume corresponding to 4 μg of DNA, 4 μL of loading buffer, and TE buffer to bring the total volume to 24 μL. Lambda BstE II digest molecular weight markers (559 μg/mL) were prepared in an identical fashion, except that only 0.9 μL (i.e. 0.5 μg) of DNA was used.

Running the gel: After the gel was set, the comb was removed, and the gel was transferred into the electrophoresis chamber (Sub-Cell GT Agarose Gel Electrophoresis System, Bio-Rad Laboratories Inc., Hercules, California, U.S.A.). Running buffer containing ethidium bromide was poured into the chamber until it was level at about 0.5 cm above the gel surface, making sure no air pockets were trapped within the wells. The 24 μL prepared DNA samples were delivered to every well, in series. The chamber was covered with the

lid attaching electrodes in the proper orientation (black negative potential electrode on the loading wells side). A 50 V potential was slowly applied and the gel was run for approximately 2 hr. The gel was examined under UV light on a VWR, bench transilluminator (model M-20E) using a single 302 nm ultraviolet wavelength. In an attempt to obtain better contrast gels were destained in 1 L of ddH_2O for ~2-4 hr while being shaken, but to no avail.

Gel photography: A Polaroid direct screen instant camera DS34, with ISO3000, type 667 Polaroid film was used to photograph the gel under UV trans-illumination. Typical conditions for photography were as follows: 1/8 s exposure and 5.6 f-stop, 30 s development time.

3.5.2.5 Detection of apoptosis using flow cytometry

Preparation of dexrazoxane treated cell samples for analysis of apoptotic features using flow cytometry was conducted in conjunction with cell cycle progression analysis, as explicitly described in Section 3.3.2.5. In brief, at each specified time interval ~$8x10^6$ cells were fixed as single cell suspensions in 4.5 mL of 70% (v/v) cold ethanol overnight at -20°C. Samples were subsequently washed with PBS, resuspended in 1 mL of a 0.1% (v/v) Triton X-100 solution containing 0.02 mg/mL propidium iodide and 0.1 mg/mL DNase-free RNase A, followed by incubation for 15 min at 37°C. Cells were then examined for features of apoptosis through an analysis of DNA content and light scattering properties. Analysis was carried out on a highly modified EPICS V multiparameter flow cytometer (Coulter electronics, Hialeah, FL, U.S.A.) with an argon laser tuned to 488 nm. This was followed by the collection of red fluorescence emissions at 630 nm using 3.5

decade logarithmic amplifiers over a span of 256 channels of increasing fluorescence intensity, directly proportional to DNA ploidy level.

Collected light intensity data was processed using specialized analytical software in order to produce bivariate light scattering histograms. DNA content frequency histograms were generated as described in Section 3.3.2.5 from collected raw data of the number of cells that fell within increasing channels of fluorescence, representative of DNA content. The relative percentage of cells residing within each discrete ploidy level was determined empirically from the collected raw data by first counting, and then dividing the number of cells between two midpoints of successive valley regions by the total number of cells counted overall, assuming non-definable S phases.

3.5.3 Results

3.5.3.1 Cell viability and nuclear morphology

K562 cells exposed daily to 100 μM dexrazoxane were sampled daily, stained with ethidium bromide/acridine orange, and examined using fluorescence microscopy in order to identify and count cells with aberrant chromatin organization (Section 3.5.2.3). After 48 hr of dexrazoxane exposure the percentage of viable and non-viable apoptotic cells began to increase, and by 120 hr non-viable apoptotic cells represented nearly 50% of the population (Fig. 3.20a). These increases were paralleled by a significant decrease, to 20% by 120 hr in the percentage of viable non-apoptotic cells and a slight increase, from 3.7-13.7% in the proportion of necrotic cells. Overall, the percentage of apoptotic cells (viable and non-viable) increased dramatically after 48 hr, reaching 75% by 120 hr (Fig. 3.20b).

Correspondingly, the overall viability of the population fell to a level of 50% by 120 hr (Fig. 3.20b), which correlates fairly well with previously determined trypan blue viability percentages (Fig. 3.5b). However, the difference between the percentage of apoptotic cells and non-viable cells after extended periods of dexrazoxane exposure suggests that viable apoptotic cells may still be progressing through earlier stages of apoptosis when the integrity of the plasma membrane is still well preserved.

Apoptotic cells (VA, green; NVA, orange) were identified by the presence of condensed fragmented nuclei, slight cytoplasmic shrinkage, and extremely bright condensed chromatin spread as crescents around the periphery of the nucleus or as groups of bright featureless spherical beads (Fig. 3.21, *arrow #1*). Late stage apoptotic cells, which had totally lost their DNA content exhibited a very weak green-orange staining (Fig. 3.21, *arrow #4*). As cells became enlarged with extended periods of dexrazoxane exposure, some cells exhibited apoptotic features while other did not. Non-apoptotic cells (VNA, green; NEC, orange) appeared in some cases to be undergoing mitosis in the absence of cytokinesis, as identified by the presence of multiple nuclear lobes (Fig. 3.21, *arrow #2*). These cells exhibited varying degrees of chromatin condensation in their lobes, not as bright in fluorescence as apoptotic cells, as well as features of nuclear compaction with continued cell cycling. Extreme care had to be taken to distinguish the chromatin pattern of these cells from that of in apoptotic cells. After longer periods of dexrazoxane exposure, DNA containing membrane-bound structures known as apoptotic bodies were presumably released as a result of cellular degeneration (Fig. 3.21, *arrow #3*).

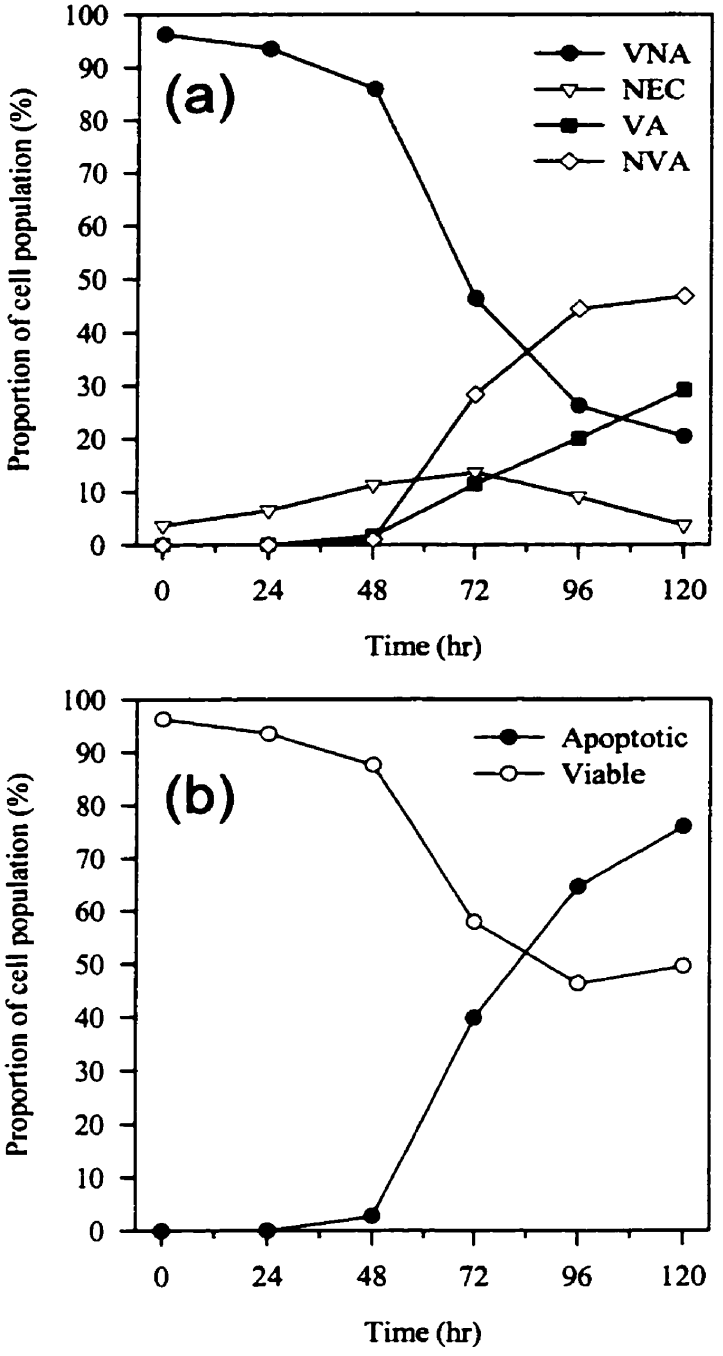

Fig. 3.20. Evolution in the percentage of various morphologically identifiable cellular states after daily exposure to dexrazoxane. K562 cells seeded at $5x10^5$ cells/mL were exposed daily to 100 μM dexrazoxane with media replacement. (a) Cells were stained with acridine orange and ethidium bromide, and upon counting a minimum of 600 cells the percentage of viable non-apoptotic (VNA), necrotic (NEC), viable apoptotic (VA), and non-viable apoptotic (NVA) were determined as previously described (Section 3.5.2.3). (b) The unification of the percentages of some of these states permitted a determination of the overall change in the percentage of apoptotic and viable cells with time.

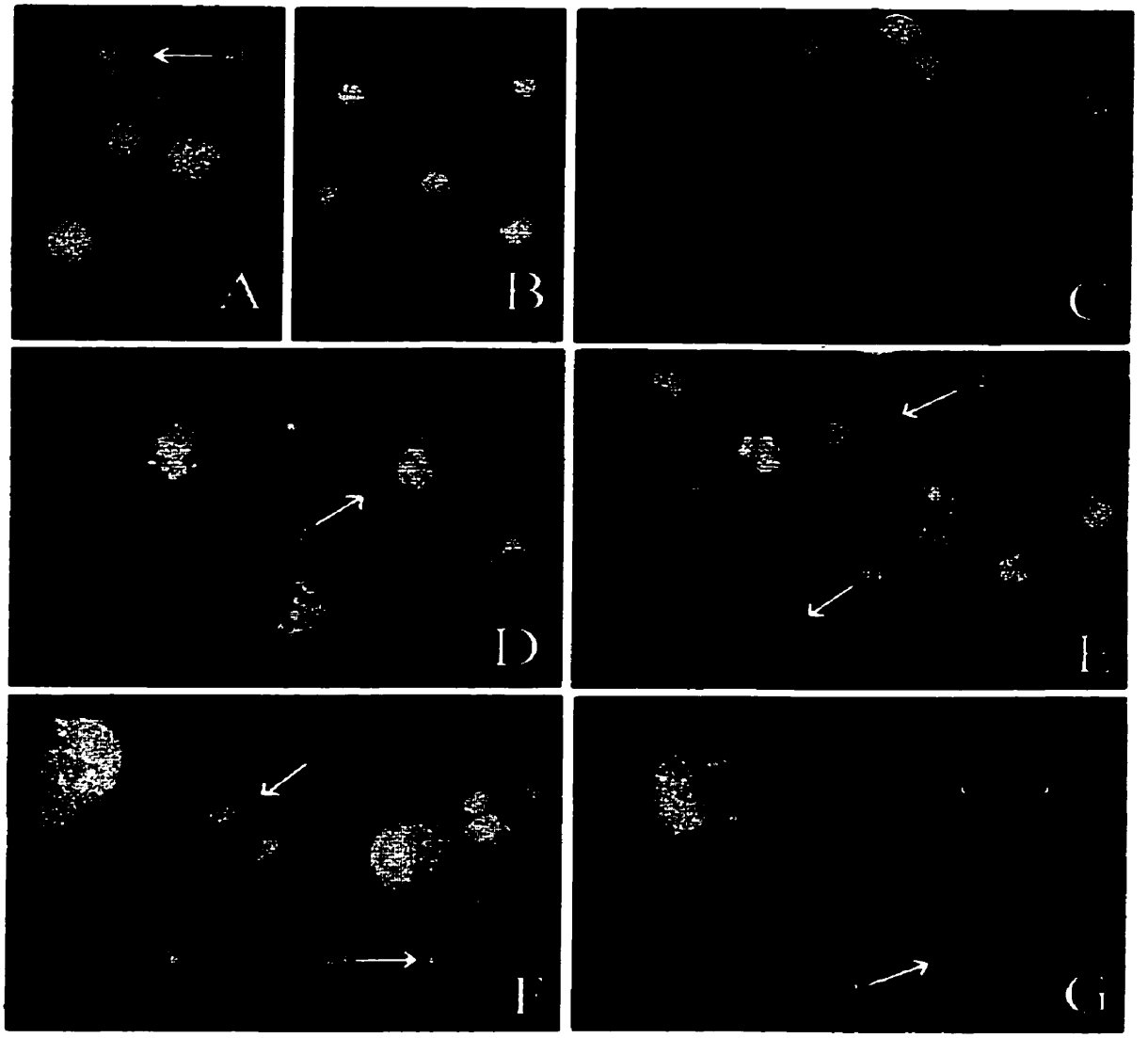

Fig. 3.21. Fluorescent photomicrographs of dexrazoxane-treated K562 cells stained with acridine orange and ethidium bromide and viewed using epi-illumination. Apoptotic (A) and necrotic (B) controls were prepared by a 48 hr daily exposure to 10 μM camptothecin and overnight exposure to 70% ethanol, respectively. Exponentially growing cells (C) were exposed daily to dexrazoxane for 48 hr (D), 72 hr (E), 96 hr (F), and 120 hr (G) and subsequently examined and characterized as described (Section 3.5.2.3). As viewed under a 40X objective lens, apoptotic cells were identified by fragmented nuclei, and bright, uniformly fluorescent spherical beads of condensed chromatin spread around the periphery of the nucleus (*arrows #1*). Non-apoptotic cells undergoing mitosis in the absence of cytokinesis were identified by the presence of multiple nuclear lobes, and varying degrees of fluorescent staining chromatin, as well as nuclear compaction (*arrows #2*). Also identified were the progressive appearance of apoptotic bodies (*arrow #3*), and late stage chromatin-free cells (*arrow #4*).

Cells were stained with both benzidine/hydrogen peroxide and ethidium bromide/acridine orange so as to examine the corresponding cell morphology and chromatin pattern in hemoglobin containing cells (Fig. 3.22). Benzidine-positive, hemoglobin containing cells were identified, as previously described by a blue appearance under a 40X objective lens by bright-field microscopy. Using fluorescence microscopy the corresponding images of over 30 of these cells were viewed. In all cases, the chromatin pattern exhibited by hemoglobin containing cells did not resemble features considered to be apoptotic. Although enlarged cells expressing hemoglobin generally contained multiple nuclear lobes (Fig. 3.22A and 3.22B) the reverse was not necessary true (Fig. 3.22C and 3.22D). For the most part, fluorescent staining appeared slightly dull, either orange or green-orange in color perhaps due to some competition with the benzidine/hydrogen peroxide. It is possible that cells containing hemoglobin progressively lose their hemoglobin and die by apoptosis as they enter the later stages of differentiation [53]. However, the previously observed presence of a consistent actual number of benzidine-stained cells after longer periods of dexrazoxane exposure (Fig. 3.13d) suggests that apoptosis may not necessarily be the end point in these particular cells. It is plausible, as suggested elsewhere that the processes of differentiation and apoptosis may be occurring simultaneously but separately upon induction [15,41,78].

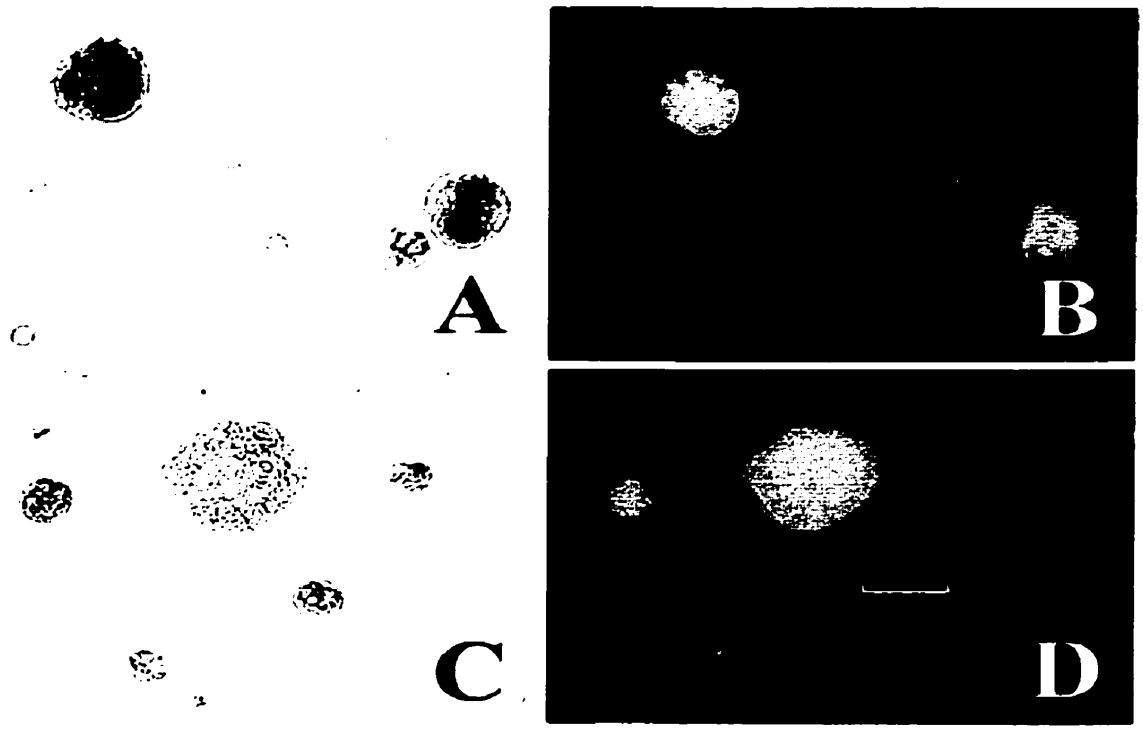

Fig. 3.22. Fluorescent and bright-field photomicrograph pairs of hemoglobin containing dexrazoxane-treated K562 cells. K562 cells exposed daily to 100 μM dexrazoxane for 96 hr were stained with both benzidine/hydrogen peroxide and ethidium bromide/acridine orange and viewed under fluorescent and bright-field conditions through a 40X objective lens. Enlarged hemoglobin containing cells (A) possessed multiple nuclear lobes and no concomitant apoptotic chromatin patterns (B). Cells which did not contain hemoglobin expressed chromatin patterns consistent with either apoptosis (C and D), or a relatively normal continued cell cycling in the absence of cell division resulting in multiple nuclear lobes (data not shown).

3.5.3.2 Internucleosomal DNA fragmentation

DNA was extracted from K562 cells treated with dexrazoxane after various periods of time. Agarose gel electrophoresis revealed a progressive appearance of a ladder-like pattern of DNA fragments after extended periods of growth (Fig. 3.23 lanes 2-6). This pattern was consistent with an endonuclease-mediated cleavage of corresponding lengths of DNA (~180-200 base pairs) between nucleosomes subsequent to the induction of apoptosis [53,76,79-81]. In more apoptotic sensitive HL-60 cells, others have reported discrete ~50 and ~300 kb DNA fragments present upon agarose gel electrophoresis [59]. It has been postulated that a 50-kb fragmentation pattern reflects chromatin loop organization, whereas a 180-300-kb periodicity results from the cleavage of bundles of these loops in higher-order chromatin structures, possibly due to the direct involvement or association with topoisomerase II [59]. In addition, the smeared appearance of the DNA fragmentation ladder has been cited as probably being due to a combination of apoptosis and secondary necrosis, the slow kinetics of apoptotic induction in these inherently apoptotic resistant cells [56,61,76,82], or a partial inhibition of endonuclease resulting in more single-stranded DNA breaks than double-stranded ones [18]. The observed fragmentation beginning after 48 hr of growth in the presence of dexrazoxane (Fig. 3.23) complements the observed appearance of sub-diploid cells by flow cytometry (Fig. 3.11), and the morphological breakdown of these cells (Fig. 3.21).

DNA extracted from cells exposed to other topoisomerase II inhibitory agents revealed similar effects. Exposure to 5 μM ICRF-193 resulted in similar patterns of fragmentation indistinguishable from that of dexrazoxane (Fig. 3.23 lanes 7,8). Although exposure to 10 μM etoposide also resulted in a laddering effect, it began to appear more

gradually than dexrazoxane or ICRF-193 (Fig. 3.23 lanes 9,10). This result suggests that the formation of the topoisomerase II-DNA cleavable complex by etoposide may somehow delay the onset of apoptosis in K562 cells longer than the non-cleavable complex-forming inhibitors dexrazoxane and ICRF-193, perhaps through the prevention of continued cell cycling. This is not without reason given that in thymocytes Sun *et al.* [83] confirmed that during etoposide-induced apoptosis, critical alterations in nuclear chromatin are seen at an earlier stage than DNA fragmentation caused by endonuclease-mediated cleavage.

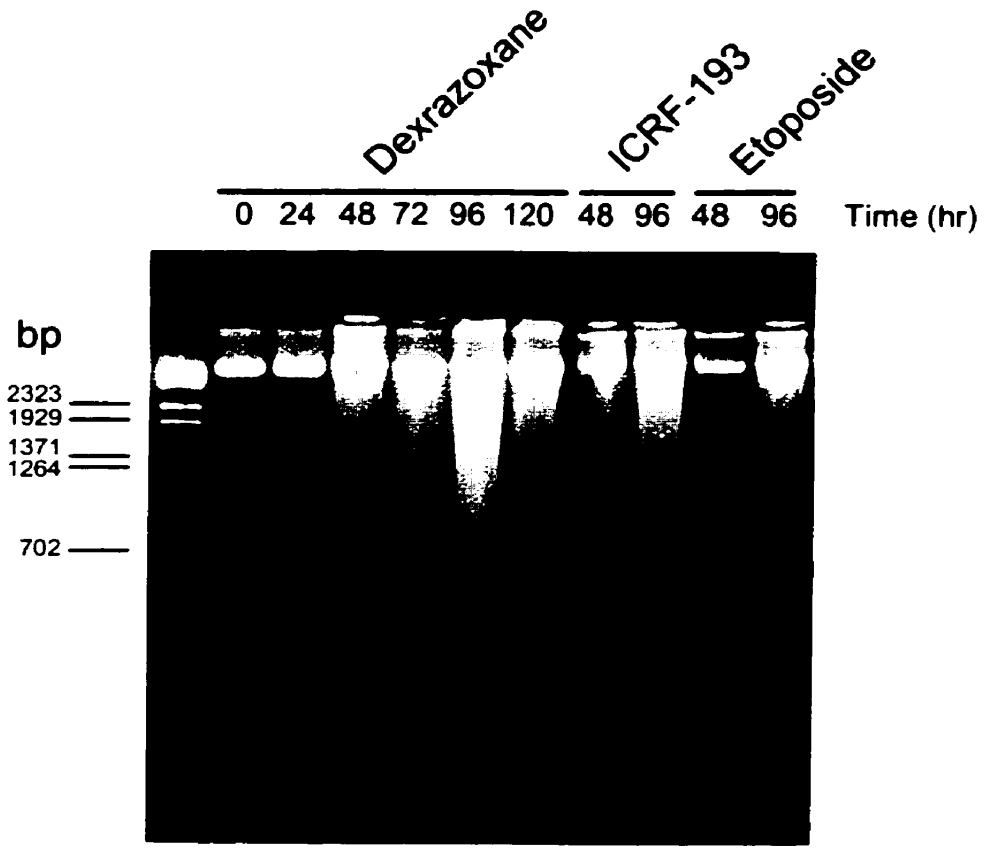

Fig. 3.23. Agarose gel electrophoresis of DNA extracted from K562 cells exposed to various topoisomerase II inhibitory agents. At indicated times of daily exposure to 100 μM dexrazoxane (0, 24, 48, 72, 96, 120 hr: *lanes 2-7*), 5 μM ICRF-193 (48, 96 hr: *lanes 8,9*), and 10 μM etoposide (48, 96 hr: *lanes 10,11*) DNA was extracted from removed cell samples as described in Section 3.5.2.4 and analyzed on a 2% (w/v) agarose gel containing 0.2 μg/mL ethidium bromide, and run at 50V for 2 hr. The lowest bands on the Lambda BstE II digest molecular weight marker lane (*lane 1*) represent DNA with a molecular weight equivalent of 2323, 1929, 1371, 1264, and 702 base pairs, respectively. Note the typical "ladder" pattern of DNA fragments of the size equivalent to single nucleosomes or oligonucleosomes. This pattern is characteristic of the DNA in apoptotic cells.

3.5.3.3 Reduced DNA content of sub-diploid apoptotic bodies

The detection of cells with diminished DNA content by flow cytometry, lower than that of G1 cells (i.e. sub-diploid) has been considered by many to be a marker of cell death by apoptosis [77,82]. After 48 hr of continuous dexrazoxane exposure a sub-G1 peak began to appear in DNA frequency histograms (Fig. 3.11), reflective of apoptotic bodies or fragments of the cell interior containing reduced levels of DNA. As more cells progressively became apoptotic the fraction of these DNA containing apoptotic bodies and other particulates in the population dramatically increased, as seen at subsequently analyzed time periods (Fig. 3.11). Although this data was collected in a gated form to exclude some small particulates, the relative fraction of the population that these cells represented was approximated from the raw data and displayed in Table 3.7. Between 48 hr and 168 hr of dexrazoxane exposure the percentage of sub-diploid cells increased from 0.02% to at least 15.85%. The observed reduction in DNA content of apoptotic cells may be a consequence of a partial cellular loss of DNA prior to analysis, resulting from the activation of endogenous endonucleases and the subsequent diffusion of lower molecular weight DNA from the cells [77]. Specifically, following fixation free single nucleosomes or small oligonucleosomes may diffuse out of the cell, leaving only small fragments of DNA loops still attached to the nuclear matrix in the cell.

3.5.3.4 Altered light-scattering properties with the induction of apoptosis

Cell shrinkage through loss of water is a hallmark of apoptosis, and this change in cell size and granularity can be readily detected by measuring the light-scattering properties of cells using flow cytometry. As mentioned earlier, the intensity of light scattered in the forward direction generally correlates with cell size, and the intensity of light scattered at right angles to the laser beam correlates with granularity and the ability of intracellular structures to reflect light [82]. Displayed in Fig. 3.24 are bivariate light scattering histograms of data collected from control untreated cells (A), and cells exposed daily to dexrazoxane for 216 hr (B). The most evident change in the light-scattering properties of dexrazoxane-treated cells was that after 48 hr of exposure an increasing number of cells displayed reduced forward angle light scattering properties (Fig. 3.24b). This can be seen by the dense accumulation of cells in the bottom left-hand corner of the histogram for 216 hr dexrazoxane-treated cells (Fig. 3.24b). It is believed by many observers than this dense accumulation is representative of the appearance of apoptotic bodies as separate particles with low light-scattering properties [77]. Additionally, it was observed that by 216 hr of dexrazoxane exposure a minor increase in right angle light scattering had occurred, as compared to control cells. This result most likely reflects the condensation of chromatin and fragmentation of nuclei [77]. Concomitant with the appearance of cells with reduced light scatter properties, cells were also identified after extended periods of dexrazoxane exposure to exhibit increased forward and right angle light scattering properties, representative of being significantly larger and more granular. As demonstrated earlier, with respect to dexrazoxane-treated CHO cells (Fig. 2.21) using a process known as backgating (Section 2.7.4) it extremely likely that these particular

enlarged cells represent the portion of the population possessing a much higher DNA ploidy content.

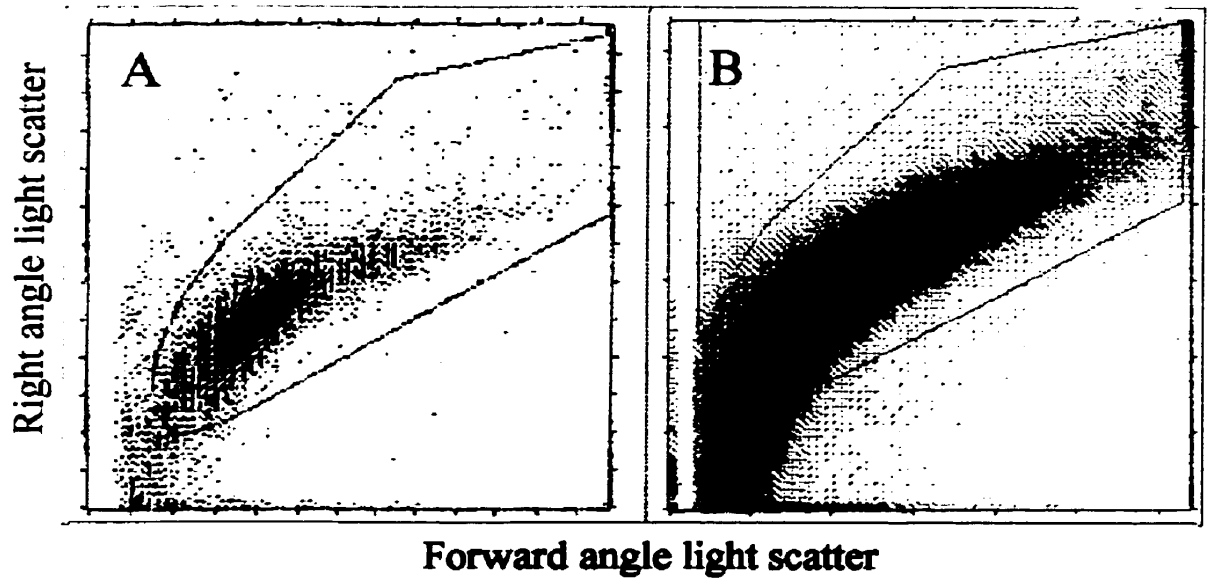

Fig. 3.24. Alterations in light scattering properties of dexrazoxane-treated K562 cells. Shown here are the full spectra of light scattering data collected from (A) control untreated cells, and (B) cells exposed daily to 100 μM dexrazoxane with media replacement for 216 hr. K562 cells exposed to dexrazoxane for extended periods of time revealed alterations in the intensity of light scattering properties, respective of apoptosis. Although forward angle light scattering (*x-axis*) did increase with time, as some cells increased in size the intense proportion of cells in the lower left corner after 216 hr (B) is reflective of a high degree of cell fragmentation and the formation of apoptotic bodies. This was paralleled by an increase in right angle light scatter (*y-axis*), reflective of an increase in cell granularity.

3.6 Discussion

The homeostatic control of many hematopoietic cells is regulated by a number of processes that include cell proliferation, differentiation, and cell death [15,41]. Partial differentiation of various human and rodent leukemic cell lines have been found to be induced by a number of known topoisomerase II inhibitors [3,44-48]. In addition, other known differentiation-inducing drugs such as phorbol esters, and retinoic acid have been shown to be associated with a reduction of topoisomerase II activity [46,50,51], and an increase in protein-associated DNA strand breaks, respectively [52]. Consequently, many leukemic cell lines induced to differentiate may be predisposed to eventually reach a terminal endpoint of cell death by apoptosis [15,53]. Currently, there exists no single theory to explain how topoisomerase II inhibition leads to either cell cycle arrest, differentiation, and/or apoptosis. Although this remains an area of much discussion and uncertainty it is known that the induction of these processes depend upon the type of inducer or topoisomerase II inhibitor used, the degree of incurred DNA damage, the intensity and/or frequency of treatment, the cell line, the stage of differentiation, as well as other environmental signals which together or separately determine whether features of lineage-specific differentiation, apoptosis, and/or cell cycle arrest will be identified [53,55].

In light of such complications, there exist interesting parallels between the processes of drug-induced apoptosis and drug-induced differentiation. In some cell lines a pre-commitment period is necessary before apoptosis is initiated [55]. These types of commitment kinetics have been observed with many drugs that stimulate differentiation in leukemic cells. In some cases, the actual removal of the drug stimulus before the

completion of this period does not engage the programmed terminal endpoint of cell death. Correspondingly, the length of the pre-commitment time for apoptosis to be triggered has been related to the mitotic cycle time and differentiation status of a cell line [55], whereby certain cells may respond within a few hours to the apoptotic stimulus and others would require a much longer period of time.

The induction of cleavable complexes between topoisomerase II and DNA by some inhibitors, together with a reduction in proliferative potential may be enough to trigger an adaptive response which engages a program of terminal differentiation [55]. However, in light of the mechanism of action of other topoisomerase inhibitors, the formation of the cleavable complex may not be essential to the process of differentiation. Agents such as aclarubicin, and ICRF-193 which inhibit topoisomerase II without the formation of the cleavable complex have likewise been shown to induce differentiation in such cell lines as K562 [3] and U937 [49], respectively. With observations such as these it appears that the induction of differentiation and apoptosis may not be reliant on the actual formation of a cleavable-complex but rather on a number of other possible downstream factors which play a role in these processes.

In the present study, the induction of K562 differentiation and apoptosis upon exposure to dexrazoxane, a non-cleavable complex forming topoisomerase II inhibitor was investigated. By monitoring the expression of hemoglobin, the ability of other bisdioxopiperazines including ICRF-154 and ICRF-193 to induce erythroid-like differentiation of K562 cells was contrasted to that of other agents such as hemin, DMSO, and the topoisomerase II poison, etoposide. As discussed below, parallels between the induced processes of differentiation and apoptosis were made as to the conditions of

exposure these cells were subjected to. Furthermore, alterations in cell size, chromatin, and DNA ploidy upon exposure to dexrazoxane provided insight into the role of topoisomerase II inhibition during the process of erythroid and/or megakaryocyte differentiation, as well as apoptosis induction.

3.6.1 Cytotoxicity analysis of the bisdioxopiperazines and other topoisomerase II inhibitory compounds

The cytotoxicity of the bisdioxopiperazines and other agents towards K562 cells are discussed in the following section. It has been previously demonstrated that the cytotoxicity of the bisdioxopiperazines toward CHO and mouse-L cells is highly correlated with their ability to inhibit the catalytic activity of topoisomerase II, presumably in a structurally dependent manner [72]. This inhibition has been shown to occur without promoting the formation or stabilization of the covalent topoisomerase II-DNA intermediate [73], unlike other topoisomerase II inhibitors such as etoposide (etoposide), and doxorubicin [74].

A 72 hr growth period in the presence of these compounds was adopted on the premise that the cytotoxicity profile would be more prominent after at least four rounds of cell cycling had occurred (doubling time ~18 hr). The most toxic of the general ICRF-series analogs (Table 3.5) was shown to be ICRF-193 (0.541 ± 0.052 μM) which appeared to be only 38 times as toxic as the next bisdioxopiperazine, dexrazoxane (20.3 ± 1.9 μM), followed by ICRF-154 (33.5 ± 3.9 μM). As expected, of the cleavable complex-forming topoisomerase II poisons investigated all were able to induce a considerable cytotoxic effect at low drug concentrations. The corresponding IC_{50} values for etoposide and

doxorubicin were 0.71 ± 0.12 μM and 0.073 ± 0.013 μM, respectively (Table 3.5). Cytotoxicity in the presence of ADR-925, the fully hydrolyzed product of dexrazoxane was not seen until exceedingly high concentrations were achieved (IC_{50} = 1229 ± 20.2 μM). Since ADR-925 is a polar charged molecule it is unlikely that it was able to permeate the cell membrane as effectively as dexrazoxane. In addition, ADR-925 has been previously demonstrated to possess no measurable inhibitory activity toward DNA topoisomerase II or cytotoxicity toward CHO cells [72]. The observed cytotoxicity at high dexrazoxane and ADR-925 concentrations is believed to be due to the chelation of free calcium and magnesium ions from the growth medium by ADR-925 [84].

The dexrazoxane cytotoxicity profile generated by MTS analysis after 72 hr of growth differed from the profiles of the other agents tested in that it was clearly biphasic and sigmoidal in nature (Fig. 3.7a). Data from only the first phase was used in the determination of a dexrazoxane IC_{50} value of 20.3 ± 1.9 μM. In contrast, cell counting analysis of dexrazoxane-mediated cytotoxicity by either of the two methods used produced monophasic dose-response curves (Fig. 3.8) and comparable IC_{50} values to MTS analysis (Table 3.5). Although similar IC_{50} values were determined by all methods of analysis there clearly existed a discrepancy between the actual number of cells and the level of formazan production, reflective in the shapes of the respective cytotoxicity profiles. Although a very few number of cells remained after 72 hr exposure to high concentrations of dexrazoxane (above the IC_{50} value) these cells seemed to possess an enhanced ability to reduce MTS to formazan. Microscopic examination revealed the presence of enlarged cells at these concentrations of dexrazoxane accompanied by many cellular fragments and particulates, implicative of drug-induced apoptotic cell death.

As suggested previously, with respect to dexrazoxane-mediated cytotoxicity in CHO cells (Section 2.11.1) dexrazoxane induces a level of cell cycle phase alteration and increased cell size which, may significantly influence mitochondrial number and/or function and, consequently the level of MTS reduction to formazan. Therefore, the second phase on the MTS biphasic sigmoidal dose-response curve (Fig. 3.7) may be representative of a small portion of the cell population possessing high mitochondrial reductase potential and the ability to survive at high dexrazoxane concentrations up to the point at which divalent cations are chelated from the surrounding medium and cell death ensues. A result such as this may constitute an important bias in analyzing the cytotoxic effects of many such agents which, could lead to a considerable underestimation of their growth-inhibiting activity. At this time it is not known precisely why exposure to ICRF-193 or ICRF-154 did not result in the formation of a definitive biphasic curve, especially since the former compound has been proven to be a stronger catalytic inhibitor of topoisomerase II than dexrazoxane [72]. The possibility remains though that any number of factors could play a role in observing such an effect including solubility, lipophilicity, duration of growth, the number of cell cycles completed, and/or the degree of cell cycle alteration incurred.

3.6.2 Erythroid-like differentiation versus apoptosis induction

It has often been stated that drugs capable of promoting terminal differentiation of leukemia cells, such as the topoisomerase II inhibitors do so at concentrations which are marginally below levels that produce cytodestruction [3,56]. The use of sub-cytotoxic concentrations has been cited as causing only transient cell cycle arrest in some cell lines, with limited cytotoxicity. However, in the presence of higher drug concentrations

differentiation could simply be a first level response that consequently induces apoptosis through a more progressive S or G2 arrest, or directly without any cell progression to G2 [53,56].

In this study, the exposure of K562 cells to slightly cytotoxic concentrations of the topoisomerase II-inhibitory drug dexrazoxane resulted in an induced expression of hemoglobin, an erythroid differentiation marker as monitored spectrophotometrically and by benzidine-positive staining (Fig. 3.16 and 3.13). The attainment of a mean hemoglobin content level of 9 pg/cell in a significantly linear fashion ($p < 0.001$) was not only comparable to that caused by other differentiation-inducing agents such as hemin [19], but also suggested a cell cycle dependency in terms of regulated expression. Hemoglobin expression was additionally paralleled by a diminished proliferative capacity (Fig. 3.13a), a slight accentuation in mean DNA and protein levels over the first 48 hr (Fig. 3.10), and the continued cycling of some cells onto higher ploidy levels ranging from 2-32 N (Fig. 3.11) as their respective cell size increased to volumes 230-fold larger than normal (Fig. 3.9 and 3.14).

Exposure of K562 cells to other bisdioxopiperazines, such as ICRF-193 and ICRF-154, as well as etoposide all resulted in increases of benzidine-positivity, changes in morphology and reductions in proliferative capacity, comparable but slightly less accentuated than that caused by dexrazoxane (Fig. 3.18). The reason for this discrepancy can possibly be attributed to the concentration of each agent chosen for examination. Dose-response curves with respect to growth inhibition and hemoglobin expression upon dexrazoxane exposure suggested a correlation between higher topoisomerase II-inhibitory concentrations of such agents and the level of inducible hemoglobin expression (Fig. 3.17).

Further support of the involvement of topoisomerase II inhibition during differentiation was provided by the fact that ADR-925, the hydrolyzed non-topoisomerase II inhibitory form of dexrazoxane [72] did not cause any increase in the level of hemoglobin expression in K562 cells (Fig. 3.18). These results when taken together indicate a clear association between topoisomerase II inhibition and the induction of hemoglobin production in K562 leukemic cells. Therefore, the bisdioxopiperazines dexrazoxane, ICRF-193, and ICRF-154 should be included amongst other well known topoisomerase II inhibitors such as amsacrine, doxorubicin, teniposide, and etoposide which have previously been shown to induce the expression of erythroid-like characteristics in K562 cells [3,45].

The expression of hemoglobin arising from the inhibition of topoisomerase II by the above mentioned agents was the most evident change that occurred in the K562 cells over the first few days of exposure, accompanied as well by a partial increase in cell size. However as eluded to previously, early stage differentiating cells may undergo a state of "priming", during which the synthesis and/or activation and accumulation of apoptotic effectors may occur [85]. Recent investigations though have revealed that the K562 cell line, derived from a patient with CML expresses a number of gene products attributing them with an enhanced survival capacity or refractoriness to drug-induced apoptosis, no matter how novel the drug is or its ability to induce protein-linked DNA strand breaks [3,55]. Moreover, the regulation of these signals are generally associated with a poor prognosis in myelogenic leukemia patients, resulting in a malignant transformation [17]. This inherent apoptotic resistance is presumed to possibly occur through the regulated expression of such gene products as tyrosine kinase from *bcr-abl* [15,18,44,48], the apoptotic suppressor gene *bcl-X* [41] or *bcl-*X_L [15,16], and to a lesser extent proto-onco

genes such as c-*fos* and c-*jun* [61,86]. Regulation of a number of these gene products may ultimately correlate with the ability, and/or direction to which the K562 cell line differentiates as is the case with *bcl-*X_L [41], a presumed channel protein thought to regulate the transport of ions and other differentiation/apoptosis-related signals across the outer mitochondrial membrane [87]. Concurrently or individually, *bcr-abl* and *bcl-*X_L expression is believed to block diverse upstream apoptotic stimuli by preventing the accumulation of cytochrome c (*cyt c*). As a result this inhibits other pre-apoptotic mitochondrial events, the activation of downstream caspases, in particular caspase-3 and the execution of apoptosis [87].

Many cell lines seem to differ in the length of the pre-commitment period following topoisomerase II inhibition until which the process of apoptosis is engaged. Upon exposure to high concentrations of etoposide many cell lines such as HL-60 [53,56,61] reveal signs of apoptosis almost immediately upon the formation of cleavable complexes. However, with K562 cells the same concentrations reportedly result in the induction of significant levels of differentiation without any immediate notable effect on viability [3]. In light of the following results, the absence of immediate apoptosis in K562 cells after cytotoxic-drug exposure does not necessarily preclude its eventual development. With respect to the various topoisomerase II inhibitory agents investigated, the positive expression of hemoglobin was paralleled as well by the delayed induction of programmed cell death. This was in agreement with what was reported by Synold *et al.* [88] that prolonged exposure to clinically achievable concentrations of dexrazoxane is cytotoxic to human leukemic cells. In the case of our investigation apoptosis was observed in these cells after 48 hr of exposure by the appearance of a DNA ladder pattern on a agarose gel

(Fig. 3.23), consistent with internucleosomal DNA fragmentation. Induction of apoptosis in dexrazoxane-treated cells was further confirmed by a proportional increase in the population of cells expressing nuclear morphologies and chromatin organization in accordance with apoptosis (Fig. 3.21). Cell cycle analysis further revealed a significant increase in sub-diploid cells after 48 hr, representative of late-stage apoptotic bodies (Fig. 3.11 and 3.24). Although the initiation of an apoptotic signaling pathway may have occurred after preliminary drug exposure, identifiable characteristics were not evident until after 48 hr of growth. Even in the case of etoposide, as noted elsewhere [56], a pattern of DNA laddering was not seen until this time period.

Perhaps further investigation into the gradual alterations in the activity, level, or phosphorylation states of topoisomerase II will provide insight into the slow development of apoptosis [3,50,89]. Even still, maybe the events causing internucleosomal DNA fragmentation occur at a stage of apoptosis much later than those events involved in the initial drug-target interactions [55,59,61,90]. Accumulating evidence to this effect has suggested that during apoptosis, changes in nuclear morphology are more closely related with the onset of a higher-order chromatin fragmentation which has been shown to precede [83] or occur in the absence [91] of internucleosomal DNA cleavage.

Apoptosis is indeed the mode of death common to differentiated cells at the end of their life span [46,85]. Whether this statement applies to such partially differentiated cell lines as K562 remains to be proven. Differentiation of K562 cells has been citied as occuring neither normally or to completeness [8,21]. Likewise, this study has shown that after extended periods of dexrazoxane exposure, large, viable, polyploid cells remain in culture irrespective of the presence of apoptotic features or the expression of hemoglobin.

This suggests possible differences amongst the population of K562 cells in their sensitivity to, or ability to detect topoisomerase II inhibition. To this effect, others have made similar observations that only subsets of differentiated cells will undergo apoptosis relatively early after the induction of differentiation [85]. Although the processes of apoptosis and hematopoietic cell differentiation are strongly suggested to be regulated separately [41,78] and proceed simultaneously [15] they are not mutually exclusive in entirety [92].

Topoisomerase II inhibitor-induced differentiation is commonly perceived as an irreversible process that rarely results in the achievement of fully mature lineage-specific state [3]. With respect to K562 cells, it appeared as if initial exposures to dexrazoxane committed some cells to undergo differentiation and apoptosis, but that continuous exposure would ensure a greater population-wide commitment with time. Preliminary experiments revealed that 1-2 exposures of topoisomerase II inhibitory agents was not sufficient enough to completely inhibit cell division or induce a cell cycle arrest in the entire cell population (Fig. 3.5 and 3.13a). This result was in contrast to what had been previously identified in other cell lines [73,93-96], as well as in CHO cells (Section 2.4). Therefore in an effort to effectively halt further cell division and as well maintain a highly differentiated state a continuous daily drug exposure protocol was adopted.

Upon daily exposure to the bisdioxopiperazines K562 cell division was substantially inhibited resulting in the apparent prolongment and continuation of erythroid-like differentiation (Fig. 3.13 and 3.18). However, 1-2 exposures to dexrazoxane appeared to likewise induce an increase in the percentage of cells expressing hemoglobin, which at first was thought to exclude the need for a consistent presence of topoisomerase II inhibitory drug dexrazoxane (Fig. 3.13c). Closer analysis revealed instead that the actual

number of hemoglobin-stained cells remained constant in the population, despite the number of dexrazoxane exposures (Fig. 3.13d). Clearly, these results indicated that only a fraction of the actual initial number of cells in the population are capable of undergoing differentiation upon initial exposure. However, a continuous dexrazoxane exposure increases not only the likelihood of drug-induced apoptosis and the sustained inhibition of cell proliferation, but an increase in the apparent percentage of cells expressing hemoglobin, as fractionated apoptotic cells were excluded from analysis.

Generally, agents capable of inducing K562 cell differentiation are considered to be either commitment-inducing or non-commitment inducing [60]. Commitment refers to an irreversible process that leads to the expression of the differentiation-related phenotype, which remains after the inducer is removed. In the case of non-commitment inducers such as hemin, the phenotype such as benzidine-positivity is not permanent, and cells reverse to their normal negative state after the inducer is removed. Dexrazoxane, and presumably all of the other topoisomerase II inhibitory agents tested herein are commitment inducers of erythroid-like differentiation in K562 cells, whereby the final endpoint was not necessarily apoptosis. Cells which become positive for the expression of hemoglobin remained positive, as observed by the constant actual number of benzidine-stained cells after extended periods of time (Fig. 3.13d). Analysis of the percentage of benzidine-staining in the population should not be thought of in terms of commitment or non-commitment. Although percentages recover to pre-treatment levels after a period of time in the absence of dexrazoxane (Fig. 3.13c), it was not due to a reversible effect in the individual cells, but rather to the proliferative capacity of unaffected cells returning to normal and overtaking the population once again. The most prominent attribute which creates confusion in

comparing these effects of dexrazoxane to other commitment inducers such as Ara-C (1-β-arabinofuranosylcytosine) is that the former induces apoptosis and a change in viability, whereas the latter does not [60]. Therefore in some reports it is common to identify the use of a population-wide percent change in benzidine-staining rather that the actual number of stained cells for classifying commitment versus non-commitment in cases where the inducer inhibits cell growth without effecting viability [60].

3.6.3 Polyploidization through continued cell cycling

As reported earlier, K562 cells seemingly exhibited a significant tendency for continuing to proliferate in the presence of topoisomerase II inhibitory agents. Upon daily exposure to dexrazoxane sustained cell division was inhibited at the expense of apoptosis induction. This was superceded by the appearance of some cells with enormous sizes, and multiple nuclear lobes (Fig. 3.21), complemented by identifiable ploidy content in the range of 8-32N (Fig. 3.11). As noted previously, in the case of other topoisomerase II-reactive drugs such as etoposide, the fraction of K562 cells undergoing apoptosis increases regularly with drug doses [56] as cells become held up in G2/M [45,68,97]. In addition, topoisomerase I and II inhibitory drugs administered at concentrations close to their IC_{50} values have been shown to induce S or G2 arrest, in a cell line dependent manner [15,98]. In light of these observations it is interesting to speculate on why in the presence of dexrazoxane that some cells continue to cycle onto higher ploidy levels while others either do not, or become increasingly more susceptible to apoptosis.

Continued cell cycling in the absence of cell division may directly be related to the mechanism of topoisomerase II inhibition. Many of the bisdioxopiperazines, including

dexrazoxane have been reported to inhibit the catalytic activity of topoisomerase II without stabilizing the topoisomerase II-DNA covalent complex and without causing primary DNA strand breakage [73,99]. As a result, cells may consequently be able to progress through the topoisomerase II-dependent G2 checkpoint control mechanism [100] which normally blocks cell cycling until the detected DNA damage is repaired [47,68,95]. Perhaps as well, K562 cells lack the capability of arresting fully at the G1-checkpoint control, due to a lack or mutation of the p53 tumor suppressor gene [47,53,56]. Both of these possibilities could allow for the K562 cell population to recover more quickly. In comparison, a number of cell lines have been shown to be capable of slowing down their progression along the cell cycle, repair DNA damage, and continue to progress again along the cell cycle [47,56,97].

The identified changes in nuclear size and shape, with respect to chromatin reorganization may also be associated with the differentiation process of hematopoietic cell lines [3]. Others have cited differentiation to be a consequence of an unbalanced cell growth defined by abnormally high ratios of cell mass to DNA content which can then lead to apoptosis [49]. In general though, the accumulation of cells into G1, S or G2 as a consequence of topoisomerase II inhibition depends specifically on the cell line being studied and the drug doses being applied [56,68,95,101]. Here, we have identified a correlation between increasing K562 cell size and higher ploidy content levels with extended periods of dexrazoxane exposure. The fact that there did not seem to be an overall progression of the population towards a single high ploidy content level is suggestive of a differential ability of the cells to continue to cycle. Some cells may have ceased to cycle at 2N, 4N or intermediate ploidy ranges, while others may have continued onto higher levels, identified by the continuum of S-phase(s).

Polyploidization, or incomplete segregation of chromosomes as a consequence of topoisomerase II inhibition has been well demonstrated in a number of cell lines [68,73,95,96,102-104]. Exposure to such agents as dexrazoxane or ICRF-193 has been shown in CHO [95,96,103], HeLa [96,103], epithelial [102], and human leukemia and lymphocytic cells [95] to interfere with the normal functions of topoisomerase II, thus effecting the mitotic processes of spindle apparatus reorganization, disassembly and reassembly of the nuclear envelopes, incomplete segregation of chromosomes, as well as resulting in the development of multilobed nuclei [68,103]. As a consequence, cells continue through further rounds of cell cycling in the absence of cell division, becoming polyploid and losing viability. Although topoisomerase II plays a role in the continuation of such genetic processes as replication and transcription, it has been suggested to simply complement the functional ability of topoisomerase I in controlling torsional strain during these processes [103]. The essential roles of topoisomerase II have thusly been attributed to its functions in decatenating intertwined replicated chromosomes and facilitating the segregation of chromosomes [64,103].

3.6.4 Expression of erythroid versus megakaryocyte characteristics upon dexrazoxane exposure

It has been reported that K562 cells can be induced to differentiate along either erythroid or megakaryocytic lineages by a variety of inducers [6,13,14,20,40,41,105] and that the process of differentiation may occur in a non-specific fashion [12]. In other words, although many different inducers have been shown to modify the K562 phenotype, none of them leads to the expression of antigenic determinants of a single-cell lineage alone [14]. Various reports have described a putative relationship between erythropoiesis and megakaryocytopoiesis [105,106]. As well, some leukemic cell lines such as LAMA-84, Dami, and HEL constitutively express markers of both lineages, suggesting that common factors may control or allow the expression of markers of both lineages in some circumstances [32,105]. Anthanasiou *et al.* [105] have identified that the ETS family of transcription factors, in particular FLI-1/ERGB, plays a role in controlling megakaryocytic differentiation and gene expression as well as controlling multiple developmentally regulated hematopoietic genes such as hemoglobin in K562 cells. Furthermore, Rowley *et al.* [13] demonstrated clearly, that single K562 cells can express, and are inducible for both erythroid and megakaryocytic expression antigens.

Although many topoisomerase II inhibitors are capable of inducing differentiation in many leukemic cell lines, research conducted in this field, with respect to K562 induced differentiation has been mainly concentrated on examining changes in erythroid-like features [3,15,45]. We have observed that when K562 cells are exposed to dexrazoxane, megakaryocytic-like features have appeared such as: a reduction in growth potential, an increase in cell ploidy accompanied by an increase in cell size, membrane blebbing, and the presence of identifiably large multilobed cells, similar in every way except for the

benzidine-staining of some cells for hemoglobin expression. To our knowledge, when these features were identified in cases involving topoisomerase II-inhibitor induced K562 erythroid-like differentiation, an extensive analysis, if any, of a simultaneous expression of specific megakaryocytic features was not adequately examined [14,45,60,98,107]. This therefore poses the question as to whether megakaryocyte differentiation can be induced by topoisomerase II inhibitors, such as dexrazoxane concomitant with erythroid-like differentiation.

Through the use of immunofluorescence flow cytometry analysis we have demonstrated that dexrazoxane-induced K562 differentiation proceeds in a relatively coordinated manner towards an erythroid lineage alone. The percentage of cells expressing the erythroid antigen glycophorin A increased with extended periods of dexrazoxane exposure (Table 3.10), thus complementing our previous data of an observed similar trend in accentuated hemoglobin expression levels in these cells (Fig. 3.16). The absence of any significant determinant expression of the platelet/megakaryocyte marker gpIIb/IIIa (CD41) on K562 cells after extensive treatment suggests that dexrazoxane-induced differentiation does not proceed towards the megakaryocytic lineage, in spite of an observed characteristic increase in DNA ploidy. Perhaps a complex set of signaling events exist, which follows topoisomerase II inhibition to allow exclusively for an increased transcription/translation of erythroid markers while suppressing the expression of megakaryocytic markers such as gpIIb/IIIa. Some researchers have gone so far as to show that the *bcl-X* apoptosis suppressor gene is overexpressed during K562 megakaryocyte differentiation and downregulated during erythroid differentiation [15,41].

In contrast to what some have reported [14,32,105], we did not detect any expression of the gpIIb/IIIa complex in untreated K562 cells. Usually, as is the case during phorbol ester induced K562 megakaryocyte differentiation, the expression of gpIIb/IIIa or other markers such as platelet peroxidase becomes upregulated, paralleled with a downregulation in the expression of erythroid markers [12,32,40,42]. From our observations there exist a few possibilities as to why we did not first, detect gpIIb/IIIa expression at the onset of the experiment and second, observe a comparative downregulation in gpIIb/IIIa with upregulated erythroid-like expression.

To begin with, gpIIb/IIIa expression is considered by many to be an early antigenic determinant of megakaryocyte maturation [39,106,108], preceded only slightly by the appearance of platelet peroxidase activity in the nuclear envelope and strands of the rough endoplasmic reticulum [32,40]. Some authors have demonstrated the elementary expression of both gpIIb and gpIIIa in untreated K562 cells [39], and have used such monoclonal antibodies as P2 [12,60], J2 [12], and J15 [108] to detect an increased expression of this complex from 8% to 87% upon phorbol dibutyrate induced differentiation [12]. Others believe that in K562 cells gpIIIa synthesis does not require concomitant gpIIb synthesis [109], and that only the former increases in expression upon treatment with phorbol esters [12,32,109]. Consequently, these authors detected large increases in gpIIIa expression, while detecting gpIIb/IIIa complex increases of only 5% to 8% [17,32]. Although either of these explanations may be true, it is believed that we should have detected some expression of the gpIIb/IIIa complex in untreated cells using the P2 mAb, even if the level of expression did not increase with dexrazoxane exposure, provided that the K562 clone we were using was the same as used by other such

researchers. Gewirtz *et al.* [39] attributed their failure to detect gpIIb/IIIa on untreated K562 cells due to a highly restrictive antigenic recognition. They claimed that glycoproteins such as gpIIb/IIIa on K562 cells may be assembled differently and have altered patterns of glycosylation which would make them unrecognizable to a mAb such as P2 raised against the normal complex [39]. The amount of specific mAb used in accordance with Coulter-Immunotech guidelines, was obviously sufficient enough to generate non-specific binding. Therefore, any desired specific binding not obtained could be attributed to such reasons as raised by Gewirtz *et al.* [39], or quite simply that the complex was indeed not present on the cells.

In summary, we have shown that the non-cleavable complex forming topoisomerase II inhibitors known as the bisdioxopiperazines, specifically dexrazoxane, are able to induce erythroid-like properties in K562 cells. The fact that the differentiation process was paralleled by the eventual development of apoptosis, irrespective of the mechanism of topoisomerase II inhibition is of significance given that these cells possess inherent anti-apoptotic properties [56,61,76,82]. Exposure to dexrazoxane additionally resulted in the continuation of cell cycling to higher ploidy levels in the absence of further cell division. This was proposed to be a consequence of the mechanism of dexrazoxane-induced topoisomerase II inhibition and the absence or mutation of mitotic checkpoint controls, rather than the concurrent differentiation towards a megakaryocytic lineage. Although the development of polyploid erythroid-like cells by dexrazoxane appears to be an unusual phenomenon, it does not necessarily preclude further investigation of its ability to induce differentiation in other leukemic cell lines. Perhaps this form of induced tumor cell differentiation in combination with other agents such as cytokines may create new

therapeutic strategies towards the effective treatment of leukemia. Furthermore, a better understanding of apoptotic resistance mechanisms in K562 and other leukemic cells may be obtained by virtue of the non-cleavable complex-forming topoisomerase II inhibition mechanism of the bisdioxopiperazines.

3.7 References

1. Abbas, A.K., Lichtman, A.H., and Pober, J.S. Cells and tissues of the immune system. In: Cellular and molecular immunology., pp. 14-30, Philadelphia: W.B. Saunders Company. 1994.

2. Sachs, L. The control of hematopoiesis and leukemia: from basic biology to the clinic. *Proc. Natl. Acad. Sci.U.S.A.*, **93**: 4742-4749, 1996.

3. Larsen, A.K. Involvement of DNA topoisomerases and DNA topoisomerase inhibitors in the induction of leukemia cell differentiation. *Ann. Oncol.*, **5**: 679-688, 1994.

4. Horton, M., Cedar, S., and Edwards, P.A.W. Cell surface changes during erythroid differentiation in the K562 cell line. In: G. Stamatoyannopoulos and A.W. Nienhuis (eds.), Hemoglobins in development and differentiation., pp. 473-485, New York: Alan R.Liss, Inc. 1981.

5. Lozzio, B.B. and Lozzio, C.B. Properties and usefulness of the original K-562 human myelogenous leukemia cell line. *Leuk. Res.*, **3**: 363-370, 1979.

6. Lozzio, B.B. and Lozzio, C.B. Human chronic myelogenous leukemia cell-line with positive Philadelphia chromosome. *Blood*, **45**: 321-334, 1975.

7. McKenna, S.L. and Cotter, T.G. Functional aspects of apoptosis in hematopoiesis and consequences of failure. *Adv. Cancer Res.*, **71**: 121-164, 1997.

8. Hoffman, R., Murnane, M.J., Burger, D., Tonkonow, B.L., Idrahim, N., Elder, J.T., Mazur, E.M., Scarpa, A., Diamond, A., Bruno, E., Evere, R.D., Orget, B.G., and Enz Jr, E.J. Characterization of a human leukemic cell line. In: G. Stamatoyannopoulos and A.W. Nienhuis (eds.), Hemoglobins in development and differentiation., pp. 487-506, New York: Alan R.Liss, Inc. 1981.

9. Villeval, J.L., Pelicci, P.G., Tabilio, A., Titeux, M., Henri, A., Houesche, F., Thomopoulos, P., Vainchenker, W., Garbaz, M., Rochant, H., Breton-Gorius, J., Edwards, P.A., and Testa, U. Erythroid properties of K562 cells. Effect of hemin, butyrate and TPA induction. *Exp. Cell Res.*, **146**: 428-435, 1983.

10. Andersson, L.C., Nilsson, K., and Gahmberg, C.G. K562--a human erythroleukemic cell line. *Int. J. Cancer*, **23**: 143-147, 1979.

11. Sutherland, J.A., Turner, A.R., Mannoni, P., McGann, L.E., and Turc, J.M. Differentiation of K562 leukemia cells along erythroid, macrophage, and megakaryocyte lineages. *J. Biol. Response Mod.*, **5**: 250-262, 1986.

12. Leary, J.F., Ohlsson-Wilhelm, B.M., Giuliano, R., LaBella, S., Farley, B., and Rowley, P.T. Multipotent human hematopoietic cell line K562: lineage-specific constitutive and inducible antigens. *Leuk. Res.*, **11**: 807-815, 1987.

13. Rowley, P.T., Farley, B.A., LaBella, S., Giuliano, R., and Leary, J.F. Single K562 human leukemia cells express and are inducible for both erythroid and megakaryocytic antigens. *Int. J. Cell Cloning.*, **10**: 232-240, 1992.

14. Tabilio, A., Pelicci, P.G., Vinci, G., Mannoni, P., Civin, C.I., Vainchenker, W., Testa, U., Lipinski, M., Rochant, H., and Breton-Gorius, J. Myeloid and megakaryocytic properties of K-562 cell lines. *Cancer Res.*, **43**: 4569-4574, 1983.

15. Benito, A., Silva, M., Grillot, D., Nunez, G., and Fernandez-Luna, J.L. Apoptosis induced by erythroid differentiation of human leukemia cell lines is inhibited by Bcl-XL. *Blood*, **87**: 3837-3843, 1996.

16. Boise, L.H., Gonzalez-Garcia, M., Postema, C.E., Ding, L., Lindsten, T., Turka, L.A., Mao, X., Nunez, G., and Thompson, C.B. bcl-x, a bcl-2-related gene that functions as a dominant regulator of apoptotic cell death. *Cell*, **74**: 597-608, 1993.

17. Smith, B.D., Bambach, B.J., Vala, M.S., Barber, J.P., Enger, C., Brodsky, R.A., Burke, P.J., Gore, S.D., and Jones, R.J. Inhibited apoptosis and drug resistance in acute myeloid leukaemia. *Br. J. Haematol.*, **102**: 1042-1049, 1998.

18. McGahon, A., Bissonnette, R., Schmitt, M., Cotter, K.M., Green, D.R., and Cotter, T.G. BCR-ABL maintains resistance of chronic myelogenous leukemia cells to apoptotic cell death [published erratum appears in Blood 1994 Jun 15;83(12):3835]. *Blood*, **83**: 1179-1187, 1994.

19. Dean, A., Erard, F., Schneider, A.P., and Schechter, A.N. Induction of hemoglobin accumulation in human K562 cells by hemin is reversible. *Science*, **212**: 459-461, 1981.

20. Andersson, L.C., Jokinen, M., and Gahmberg, C.G. Induction of erythroid differentiation in the human leukemia cell line K562. *Nature*, **278**: 364-365, 1979.

21. Benz, E.J.J., Murnane, M.J., Tonkonow, B.L., Berman, B.W., Mazur, E.M., Cavallesco, C., Jenko, T., Snyder, E.L., Forget, B.G., and Hoffman, R. Embryonic-fetal erythroid characteristics of a human leukemic cell line. *Proc. Natl. Acad. Sci.U.S.A.*, **77**: 3509-3513, 1980.

22. Rutherford, T.R., Clegg, J.B., and Weatherall, D.J. K562 human leukaemic cells synthesise embryonic haemoglobin in response to haemin. *Nature*, **280**: 164-165, 1979.

23. Rutherford, T., Clegg, J.B., Higgs, D.R., Jones, R.W., Thompson, J., and Weatherall, D.J. K562 human leukemic cells: A model system for the study of hemoglobin switching? In: G. Stamatoyannopoulos and A.W. Nienhuis (eds.), Hemoglobins in development and differentiation., pp. 459-472, New York: Alan R.Liss, Inc. 1981.

24. Vainchenker, W., Guerrasio, A., Tetsa, U., Titeux, M., Guichard, J., Beuzard, Y., Rosa, J., and Breton-Gorius, J. Multipotential capacities of differentiation and hemoglobin pattern of K562 cell line. In: G. Stamatoyannopoulos and A.W. Nienhuis (eds.), Hemoglobins in development and differentiation., pp. 507-518, New York: Alan R.Liss, Inc. 1981.

25. Cioe, L., McNab, A., Hubbell, H.R., Meo, P., Curtis, P., and Rovera, G. Differential expression of the globin genes in human leukemia K562(S) cells induced to differentiate by hemin or butyric acid. *Cancer Res.*, **41**: 237-243, 1981.

26. Orkin, S.H., Harosi, F.I., and Leder, P. Differentiation in erythroleukemic cells and their somatic hybrids. *Proc. Natl. Acad. Sci.U.S.A.*, **72**: 98-102, 1975.

27. Gewirtz, A.M. Megakaryocytopoiesis: the state of the art. *Thromb. Haemost.*, **74**: 204-209, 1995.

28. Mazur, E.M. Megakaryocytopoiesis and platelet production: a review. *Exp. Hematol.*, **15**: 340-350, 1987.

29. Avraham, H. Regulation of megakaryocytopoiesis. *Stem.Cells (Dayt.)*, **11**: 499-510, 1993.

30. Alberts, B., Bray, D., Lewis, J., Raff, M., Roberts, K., and Watson, J.D. Differentiated cells and the maintenance of tissues. In: AnonymousMolecular Biology of the Cell., pp. 973-984, New York, N.Y.: Garland Publishing, Inc. 1989.

31. Baatout, S. The importance of cytoskeleton proteins in megakaryocyte spreading and platelet formation. *Blood Rev.*, **10**: 17-19, 1996.

32. Alitalo, R. Induced differentiation of K562 leukemia cells: a model for studies of gene expression in early megakaryoblasts. *Leuk. Res.*, **14**: 501-514, 1990.

33. Erusalimsky, J.D. and Martin, J.F. The regulation of megakaryocyte polyploidization and its implications for coronary artery occlusion. *Eur. J. Clin.Invest.*, **23**: 1-9, 1993.

34. Lund, J.E. and Brown, P.K. Hypersegmented megakaryocytes and megakaryocytes with multiple separate nuclei in dogs treated with PNU-100592, an oxazolidinone antibiotic. *Toxicol. Pathol*, **25**: 339-343, 1997.

35. Mazur, E.M. and Hoffman, R. Human megakaryocyte progenitors. In: D.W. Golde (ed.), Hematopoiesis, pp. 133-149, New York: Churchill Livingstone Inc. 1984.

36. Kanz, L., Lohr, G.W., and Fauser, A.A. Human megakaryocytic progenitor cells. *Klin. Wochenschr.*, **65**: 297-307, 1987.

37. Sullivan, D.M., Latham, M.D., Rowe, T.C., and Ross, W.E. Purification and characterization of an altered topoisomerase II from a drug-resistant Chinese hamster ovary cell line. *Biochemistry*, **28**: 5680-5687, 1989.

38. Vainchenker, W., Testa, U., Guichard, J., Titeux, M., and Breton-Gorius, J. Heterogeneity in the cellular commitment of a human leukemic cell line: K562. *Blood Cells*, **7** : 357-375, 1981.

39. Gewirtz, A.M., Burger, D., Rado, T.A., Benz, E.J.J., and Hoffman, R. Constitutive expression of platelet glycoproteins by the human leukemia cell line K562. *Blood*, **60**: 785-789, 1982.

40. Tetteroo, P.A., Massaro, F., Mulder, A., Schreuder-van, G.R., and von dem Borne AE Megakaryoblastic differentiation of proerythroblastic K562 cell-line cells. *Leuk. Res.*, **8**: 197-206, 1984.

41. Terui, Y., Furukawa, Y., Kikuchi, J., Iwase, S., Hatake, K., and Miura, Y. Bcl-x is a regulatory factor of apoptosis and differentiation in megakaryocytic lineage cells. *Exp. Hematol.*, **26**: 236-244, 1998.

42. Butler, T.M., Ziemiecki, A., and Friis, R.R. Megakaryocytic differentiation of K562 cells is associated with changes in the cytoskeletal organization and the pattern of chromatographically distinct forms of phosphotyrosyl-specific protein phosphatases. *Cancer Res.*, **50**: 6323-6329, 1990.

43. Sahyoun, N., Wolf, M., Besterman, J., Hsieh, T., Sander, M., LeVine, H., Chang, K.J., and Cuatrecasas, P. Protein kinase C phosphorylates topoisomerase II: topoisomerase activation and its possible role in phorbol ester-induced differentiation of HL-60 cells. *Proc. Natl. Acad. Sci.U.S.A.*, **83**: 1603-1607, 1986.

44. Ritke, M.K. and Yalowich, J.C. Altered gene expression in human leukemia K562 cells selected for resistance to etoposide. *Biochem. Pharm.*, **46**: 2007-2020, 1993.

45. Constantinou, A., Grdina, D., Kiguchi, K., and Huberman, E. The effect of topoisomerase inhibitors on the expression of differentiation markers and cell cycle progression in human K-562 leukemia cells. *Exp. Cell Res.*, **203**: 100-106, 1992.

46. Zwelling, L.A., Hinds, M., Chan, D., Altschuler, E., Mayes, J., and Zipf, T.F. Phorbol ester effects on topoisomerase II activity and gene expression in HL-60 human leukemia cells with different proclivities toward monocytoid differentiation. *Cancer Res.*, **50**: 7116-7122, 1990.

47. O'Connor, P.M. and Kohn, K.W. A fundamental role for cell cycle regulation in the chemosensitivity of cancer cells? *Semin. Cancer Biol.*, **3**: 409-416, 1992.

48. Evans, C.A., Owen-Lynch, P.J., Whetton, A.D., and Dive, C. Activation of the Abelson tyrosine kinase activity is associated with suppression of apoptosis in hemopoietic cells. *Cancer Res.*, **53**: 1735-1738, 1993.

49. Perez, C., Vilaboa, N.E., Garcia-Bermejo, L., de, B.E., Creighton, A.M., and Aller, P. Differentiation of U-937 promonocytic cells by etoposide and ICRF-193, two antitumour DNA topoisomerase II inhibitors with different mechanisms of action. *J. Cell Sci.*, **110**: 337-343, 1997.

50. Constantinou, A., Henning-Chubb, C., and Huberman, E. Novobiocin- and phorbol-12-myristate-13-acetate-induced differentiation of human leukemia cells associated with a reduction in topoisomerase II activity. *Cancer Res.*, **49**: 1110-1117, 1989.

51. Zwelling, L.A., Chan, D., Hinds, M., Mayes, J., Silberman, L.E., and Blick, M. Effect of phorbol ester treatment on drug-induced, topoisomerase II- mediated DNA cleavage in human leukemia cells. *Cancer Res.*, **48**: 6625-6633, 1988.

52. Francis, G.E., Berney, J.J., North, P.S., Khan, Z., Wilson, E.L., Jacobs, P., and Ali, M. Evidence for the involvement of DNA topoisomerase II in neutrophil-granulocyte differentiation. *Leukemia*, **1**: 653-659, 1987.

53. Solary, E., Bertrand, R., and Pommier, Y. Apoptosis induced by DNA topoisomerase I and II inhibitors in human leukemic HL-60 cells. *Leuk. Lymphoma.*, **15**: 21-32, 1994.

54. Heck, M.M. and Earnshaw, W.C. Topoisomerase II: A specific marker for cell proliferation. *J. Cell Biol.*, **103**: 2569-2581, 1986.

55. Dive, C. and Hickman, J.A. Drug-target interactions: only the first step in the commitment to a programmed cell death? *Br. J. Cancer*, **64**: 192-196, 1991.

56. Dubrez, L., Goldwasser, F., Genne, P., Pommier, Y., and Solary, E. The role of cell cycle regulation and apoptosis triggering in determining the sensitivity of leukemic cells to topoisomerase I and II inhibitors. *Leukemia*, **9**: 1013-1024, 1995.

57. Kaufmann, S.H. Cell death by topoisomerase-targeted drugs: more questions than answers. *Biochem. Biophys. Acta.*, **1400**: 195-211, 1998.

58. Sugimoto, K., Yamada, K., Egashira, M., Yazaki, Y., Hirai, H., Kikuchi, A., and Oshimi, K. Temporal and spatial distribution of DNA topoisomerase II alters during proliferation, differentiation, and apoptosis in HL-60 cells. *Blood*, **91**: 1407-1417, 1998.

59. Beere, H.M., Chresta, C.M., and Hickman, J.A. Selective inhibition of topoisomerase II by ICRF-193 does not support a role for topoisomerase II activity in the fragmentation of chromatin during apoptosis of human leukemia cells. *Mol. Pharmacol.*, **49**: 842-851, 1996.

60. Yumoto, Y., Tashima, M., Kato, Y., Ueda, T., Okuda, T., Ogawa, K., and Sawada, H. Effect of second-messenger modulators in K-562 cell differentiation: dual action of calcium/phospholipid-dependent protein kinase in the process of differentiation. *J. Cell Physiol.*, **143**: 243-250, 1990.

61. Ritke, M.K., Rusnak, J.M., Lazo, J.S., Allan, W.P., Dive, C., Heer, S., and Yalowich, J.C. Differential induction of etoposide-mediated apoptosis in human leukemia HL-60 and K562 cells. *Mol. Pharmacol.*, **46**: 605-611, 1994.

62. Sachs, L. and Lotem, J. Control of programmed cell death in normal and leukemic cells: new implications for therapy. *Blood*, **82**: 15-21, 1993.

63. Ray, S., Bullock, G., Nunez, G., Tang, C., Ibrado, A.M., Huang, Y., and Bhalla, K. Enforced expression of Bcl-XS induces differentiation and sensitizes chronic myelogenous leukemia-blast crisis K562 cells to 1-beta-D- arabinofuranosylcytosine-mediated differentiation and apoptosis. *Cell Growth Differ.*, **7**: 1617-1623, 1996.

64. Anderson, H.J. and Roberge, M. DNA topoisomerase II: a review of its involvement in chromosome structure, DNA replication, transcription and mitosis. *Cell Biol. Int. Rep.*, **16**: 717-724, 1992.

65. Hasinoff, B.B. Pharmacodynamics of the hydrolysis-activation of the cardioprotective agent (+)-1,2-bis(3,5-dioxopiperazinyl-1-yl)propane. *J. Pharm. Sci.*, **83**: 64-67, 1994.

66. Barltrop, J.A. 5-(3-carboxymethoxyphenyl)-2-(4,5-dimethylthiazolyl)-3-(4-sulfophenyl) tetrazolium, inner salt (MTS) and related analogs of 3-(4,5-dimethylthiazolyl)-2,5-diphenyltetrazolium bromide (MTT) reducing purple water-soluble formazans as cell viability indicators. *Bioorg. & Med. Chem. Lett.*, **1**: 611, 1991.

67. Pagliacci, M.C., Spinozzi, F., Migliorati, G., Fumi, G., Smacchia, M., Grignani, F., Riccardi, C., and Nicoletti, I. Genistein inhibits tumour cell growth *in vitro* but enhances mitochondrial reduction of tetrazolium salts: A further pitfall in the use of the MTT assay for evaluating cell growth and survival. *Eur. J. Cancer*, **29A**: 1573-1577, 1993.

68. Gorbsky, G.J. Cell cycle progression and chromosome segregation in mammalian cells cultured in the presence of the topoisomerase II inhibitors ICRF-187 [(+)-1,2-bis(3,5-dioxopiperazinyl-1-yl)propane; ADR-529] and ICRF-159 (Razoxane). *Cancer Res.*, **54**: 1042-1048, 1994.

69. Scher, W. and Friend, C. Breakage of DNA and alterations in folded genomes by inducers of differentiation in Friend erythroleukemic cells. *Cancer Res.*, **38**: 841-849, 1978.

70. Gopalakrishnan, T.V. and Anderson, W.F. Mouse erythroleukemia cells. *Methods Enzymol.*, **58:506-11**: 506-511, 1979.

71. Antonini, E. and Brunori, M. Hemoglobin and myoglobin in their reactions with ligands. London: North-Holland Publishing Co., 1971.

72. Hasinoff, B.B., Kuschak, T.I., Yalowich, J.C., and Creighton, A.M. A QSAR study comparing the cytotoxicity and DNA topoisomerase II inhibitory effects of bisdioxopiperazine analogs of ICRF-187 (dexrazoxane). *Biochem. Pharm.*, **50**: 953-958, 1995.

73. Ishida, R., Miki, T., Narita, T., Yui, R., Sato, M., Utsumi, K.R., Tanabe, K., and Andoh, T. Inhibition of intracellular topoisomerase II by antitumor bis(2,6-dioxopiperazine) derivatives: mode of cell growth inhibition distinct from that of cleavable complex-forming type inhibitors. *Cancer Res.*, **51**: 4909-4916, 1991.

74. Corbett, A.H. and Osheroff, N. When good enzymes go bad: conversion of topoisomerase II to a cellular toxin by antineoplastic drugs. *Chem. Res. Toxicol.*, **6**: 585-597, 1993.

75. Mercille, S. and Massie, B. Induction of apoptosis in nutrient-deprived cultures of hybridoma and myeloma cells. *Biotechnology and Bioengineering*, **44**: 1140-1154, 1994.

76. Tepper, C.G. and Studzinski, G.P. Resistance of mitochondrial DNA to degradation characterizes the apoptotic but not the necrotic mode of human leukemia cell death. *J. Cell Biochem.*, **52**: 352-361, 1993.

77. Darzynkiewicz, Z., Bruno, S., Del, B.G., Gorczyca, W., Hotz, M.A., Lassota, P., and Traganos, F. Features of apoptotic cells measured by flow cytometry. *Cytometry*, **13**: 795-808, 1992.

78. Terui, Y., Furukawa, Y., Sakoe, K., Ohta, M., and Saito, M. Expression of differentiation-related phenotypes and apoptosis are independently regulated during myeloid cell differentiation. *J. Biochem.(Tokyo.)*, **117**: 77-84, 1995.

79. Singh, R.P., Al-Rubeai, M., Gregory, C.D., and Emery, A.N. Cell death in bioreactors: A role for apoptosis. *Biotechnology and Bioengineering*, **44**: 720-726, 1994.

80. Chau, Y.P., Shiah, S.G., Don, M.J., and Kuo, M.L. Involvement of hydrogen peroxide in topoisomerase inhibitor beta- lapachone-induced apoptosis and differentiation in human leukemia cells. *Free Radic. Biol. Med.*, **24**: 660-670, 1998.

81. Khelifa, T. and Beck, W.T. Merbarone, a catalytic inhibitor of DNA topoisomerase II, induces apoptosis in CEM cells through activation of ICE/CED-3-like protease. *Mol. Pharmacol.*, **55**: 548-556, 1999.

82. Gorman, A.M., Samali, A., McGowan, A.J., and Cotter, T.G. Use of flow cytometry techniques in studying mechanisms of apoptosis in leukemic cells. *Cytometry*, **29**: 97-105, 1997.

83. Sun, X.M., Snowden, R., Dinsdale, D., Ormerod, M., and Cohen, G.M. Changes in nuclear chromatin precede internucleosomal DNA cleavage in the induction of apoptosis by etoposide. *Biochem. Pharm.*, **2**: 187-195, 1993.

84. Huang, Z.-X., May, P.M., Quinlan, K.M., Williams, D.R., and Creighton, A.M. Metal binding by pharmaceuticals. Part 2. Interactions of Ca(II), Cu(II), Fe(II), Mg(II), Mn(II) and Zn(II) with the intracellular hydrolysis products of the anti-tumour agent ICRF-159 and its inactive homologue ICRF-192. *Agents Actions*, **12**: 536-542, 1982.

85. Bhatia, U., Traganos, F., and Darzynkiewicz, Z. Induction of cell differentiation potentiates apoptosis triggered by prior exposure to DNA-damaging drugs. *Cell Growth Differ.*, **6**: 937-944, 1995.

86. Rubin, E., Kharbanda, S., Gunji, H., and Kufe, D. Activation of the c-jun protooncogene in human myeloid leukemia cells treated with etoposide. *Mol. Pharmacol.*, **39**: 697-701, 1991.

87. Amarante-Mendes, G.P., Naekyung, K.C., Liu, L., Huang, Y., Perkins, C.L., Green, D.R., and Bhalla, K. Bcr-Abl exerts its antiapoptotic effect against diverse apoptotic stimuli through blockage of mitochondrial release of cytochrome C and activation of caspase-3. *Blood*, **91**: 1700-1705, 1998.

88. Synold, T.W., Tetef, M.L., and Doroshow, J.H. Antineoplastic activity of continuous exposure to dexrazoxane: potential new role as a novel topoisomerase II inhibitor. *Semin. Oncol.*, **25**: 93-99, 1998.

89. Ritke, M.K., Roberts, D., Allan, W.P., Raymond, J., Bergoltz, V.V., and Yalowich, J.C. Altered stability of etoposide-induced topoisomerase II-DNA complexes in resistant human leukaemia K562 cells. *Br. J. Cancer*, **69**: 687-697, 1994.

90. Fisher, T.C., Milner, A.E., Gregory, C.D., Jackman, A.L., Aherne, G.W., Hartley, J.A., Dive, C., and Hickman, J.A. bcl-2 modulation of apoptosis induced by anticancer drugs: resistance to thymidylate stress is independent of classical resistance pathways. *Cancer Res.*, **53**: 3321-3326, 1993.

91. Oberhammer, F., Wilson, J.W., Dive, C., Morris, I.D., Hickman, J.A., Wakeling, A.E., Walker, R.P., and Sikorska, M. Apoptotic death in epithelial cells: cleavage of DNA to 300 and/or 50 kbp fragments before or in the absence of internucleosomal fragmentation. *EMBO J.*, **12**: 3679-3684, 1993.

92. Vitale, M., Zamai, L., Falcieri, E., Zauli, G., Gobbi, P., Santi, S., Cinti, C., and Weber, G. IMP dehydrogenase inhibitor, tiazofurin, induces apoptosis in K562 human erythroleukemia cells. *Cytometry*, **30**: 61-66, 1997.

93. Hallowes, R.C., West, D.G., and Hellmann, K. Cumulative cytostatic effect of ICRF 159. *Nature*, **247**: 487-490, 1974.

94. Sehested, M., Wessel, I., Jensen, L.H., Holm, B., Oliveri, R.S., Kenwrick, S., Creighton, A.M., Nitiss, J.L., and Jensen, P.B. Chinese hamster ovary cells resistant to the topoisomerase II catalytic inhibitor ICRF-159: a Tyr49Phe mutation confers high-level resistance to bisdioxopiperazines. *Cancer Res.*, **58**: 1460-1468, 1998.

95. Traganos, F., Darzynkiewicz, Z., and Melamed, M.R. Effects of the L isomer (+)-1,2-bis(3,5-dioxopiperazine-1-yl)propane on cell survival and cell cycle progression of cultured mammalian cells. *Cancer Res.*, **41**: 4566-4576, 1981.

96. Iwai, M., Hara, A., Andoh, T., and Ishida, R. ICRF-193, a catalytic inhibitor of DNA topoisomerase II, delays the cell cycle progression from metaphase, but not from anaphase to the G1 phase in mammalian cells. *FEBS Lett.*, **406**: 267-270, 1997.

97. Tobey, R.A. Different drugs arrest cells at a number of distinct stages in G2. *Nature*, **254**: 245-247, 1975.

98. Murate, T., Saga, S., Hotta, T., Asano, H., Ito, T., Kato, K., Tsushita, K., Kinoshita, T., Ichikawa, A., and Yoshida, S. The close relationship between DNA replication and the selection of differentiation lineages of human erythroleukemia cell lines K562, HEL, and TF1 into either erythroid or megakaryocytic lineages. *Exp. Cell Res.*, **208**: 35-43, 1993.

99. Roca, J., Ishida, R., Berger, J.M., Andoh, T., and Wang, J.C. Antitumor bisdioxopiperazines inhibit yeast DNA topoisomerase II by trapping the enzyme in the form of a closed protein clamp. *Proc. Natl. Acad. Sci.U.S.A.*, **91**: 1781-1785, 1994.

100. Downes, C.S., Clarke, D.J., Mullinger, A.M., Gimenez-Abian, J.F., Creighton, A.M., and Johnson, R.T. A topoisomerase II-dependent G2 cycle checkpoint in mammalian cells/ [published erratum appears in Nature 1994 Dec 15;372(6507):710]. *Nature*, **372**: 467-470, 1994.

101. Del, B.G., Skierski, J.S., and Darzynkiewicz, Z. The concentration-dependent diversity of effects of DNA topoisomerase I and II inhibitors on the cell cycle of HL-60 cells. *Exp. Cell Res.*, **195**: 485-491, 1991.

102. Wheatley, S.P., O'Connell, C.B., and Wang, Y. Inhibition of chromosomal separation provides insights into cleavage furrow stimulation in cultured epithelial cells. *Mol. Biol. Cell*, **9**: 2173-2184, 1998.

103. Ishida, R., Sato, M., Narita, T., Utsumi, K.R., Nishimoto, T., Morita, T., Nagata, H., and Andoh, T. Inhibition of DNA topoisomerase II by ICRF-193 induces polyploidization by uncoupling chromosome dynamics from other cell cycle events. *J. Cell Biol.*, **126**: 1341-1351, 1994.

104. Clarke, D.J., Johnson, R.T., and Downes, C.S. Topoisomerase II inhibition prevents anaphase chromatid segregation in mammalian cells independently of the generation of DNA strand breaks. *J. Cell Sci.*, **105**: 563-569, 1993.

105. Athanasiou, M., Clausen, P.A., Mavrothalassitis, G.J., Zhang, X.K., Watson, D.K., and Blair, D.G. Increased expression of the ETS-related transcription factor FLI-1/ERGB correlates with and can induce the megakaryocytic phenotype. *Cell Growth Differ.*, **7**: 1525-1534, 1996.

106. Levene, R.B., Lamaziere, J.M., Broxmeyer, H.E., Lu, L., and Rabellino, E.M. Human megakaryocytes. V. Changes in the phenotypic profile of differentiating megakaryocytes. *J. Exp. Med.*, **161**: 457-474, 1985.

107. Leary, J.F., Farley, B.A., Giuliano, R., Kosciolek, B.A., La, B.S., and Rowley, P.T. Induction of megakaryocytic characteristics in human leukemic cell line K562: polyploidy, inducers, and secretion of mitogenic activity. *J. Biol. Regul. Homeost. Agents*, **1**: 73-80, 1987.

108. Vainchenker, W., Deschamps, J.F., Bastin, J.M., Guichard, J., Titeux, M., Breton-Gorius, J., and McMichael, A.J. Two monoclonal antiplatelet antibodies as markers of human megakaryocyte maturation: immunofluorescent staining and platelet peroxidase detection in megakaryocyte colonies and in in vivo cells from normal and leukemic patients. *Blood*, **59**: 514-521, 1982.

109. Silver, S.M., McDonough, M.M., Vilaire, G., and Bennett, J.S. The in vitro synthesis of polypeptides for the platelet membrane glycoproteins IIb and IIIa. *Blood*, **69**: 1031-1037, 1987.

Chapter 4 Development and characterization of a human erythroleukemic K562 cell line with acquired resistance to dexrazoxane

4.1 Introduction

Since the 1940's a number of anticancer and cytotoxic agents have been developed. The use of some of these drugs in specific combinations and dosing periods revolutionized the treatment of acute lymphoblastic leukemia (ALL), Hodgkin's and non-Hodgkin's lymphomas, and a varierty of other solid tumors [1]. However, despite these advances many patients exhibit a clinical resistance or non-responsiveness to anticancer agents at some point during the course of their disease. This observed drug resistance is an important obstacle to be overcome before effective treatment can be given. Drug resistance can either be intrinsic, or acquired at some point during the course of treatment and/or upon relapse of the disease. The Goldie-Coldman hypothesis proposed that the failure of chemotherapeutic regimens was in part due to the selection and overgrowth of drug resistant clones within a tumor, which develop by spontaneous genetic mutation and/or adaptation [2,3]. The first course of chemotherapy treatment in a patient may often result in the successful attainment of remission. However, a tiny population of drug resistant mutant cells may begin to grow exponentially while the drug sensitive population recovers. As tumor growth continues subsequent courses of chemotherapy may have no apparent effect, and patient death is inevitable [4]. The curability of many tumors is related to such factors as the type of tumor, its locale, limiting drug toxicities, tumor growth kinetics, and the mechanism(s) of drug resistance upon relapse [1].

Theoretically, there are many different ways cells can become resistant. Some of the spontaneous changes or mutations featured in drug resistance include: gene transfer,

gene amplification, gene deletion, point mutations, and transcriptional activation. These changes affect cellular drug handling by changing one or more proteins, and ultimately underlie several mechanisms of drug resistance. Such mechanisms include: (i) reduced drug delivery, (ii) decreased drug uptake, (iii) increased drug efflux, (iv) reduced metabolic drug activation, (v) increased drug inactivation, (vi) drug sequestration, (vii) increase in intracellular concentrations of target molecules, (viii) structural alterations in these target molecules, (ix) increased detoxification of cytotoxic drug, (x) increased repair of damaged target sites, and (xi) increase in normal substrate concentration to outcompete the drug for target site binding [5].

Each of the biochemical mechanisms of resistance have been characterized for a number of different drugs [5-7]. Resistance to some drugs can be conferred by more than one mechanism. On many occasions though, it has been invariably observed that tumor cells confer a simultaneous cross-resistance towards a vast number of structurally and functionally unrelated cytotoxic drugs, many of which are anticancer agents [5,8]. This phenotypic expression has been referred to as multidrug resistance (MDR) or pleiotropic resistance. The significance of multidrug resistance is that it is thought to occur mainly by the resistance mechanisms affecting drug transportation or drug detoxification.

Multidrug resistance (MDR) is clinically one of the most important modes of drug resistance whereby the acquistion of this phenotype by malignant cells has been thought to be a major factor in limiting successful chemotherapy [9]. MDR cell lines may develop cross-resistance towards a spectrum of wide ranging, structurally unrelated cytotoxic agents which include: colchicine, *Vinca* alkaloids (vincristine, vinblastine), taxol, epipodophyllotoxins (etoposide, teniposide), anthracyclines (doxorubicin, daunorubicin),

and actinomycin D [2]. The principal similarity between these drugs is that they are generally lipophilic and heterocyclic in nature [10].

The MDR phenotype has been demonstrated in a number of different drug resistant cell lines derived from several mammalian species including murine, hamster, and human [1,5]. These MDR cell lines can be selected in a single step using a cytotoxic agent, without prior mutagen treatment [2,8]. Generally, MDR cell lines display the highest degree of resistance towards the selecting agent, and lower degrees of resistance towards other compoounds. In some cases though, the MDR cell line may in fact show the greatest resistance towards a structural analogue of the selecting agent [9] and/or collateral sensitivity towards a variety of hydrophobic compounds including lidocaine, anabolic steroids and Triton X-100 [1,8].

A consistant feature of the MDR phenotype is a decreased intracellular accumulation of cytotoxic agents. Multidrug resistant cells are able to maintain lower intracellular sublethal levels of these drugs than their corresponding drug sensitive parent cells [11]. Reduced passive drug influx, increased drug efflux, and altered intracellular drug binding have all been implicated to explain this observed feature [1]. Perhaps the most consistent change associated with MDR cell is the increased expression of a 150-200 Kd transmembrane glycoprotein [8]. This glycoprotein was named P-glycoprotein (Pgp) for its association with the observed pleiotropic phenotype in MDR cells and with the apparent permeability barrier to various drugs within the MDR spectrum [4,9].

Drug-resistant cell lines can be commonly derived in the laboratory by exposure to virtually any single chemotherapeutic agent. Upon their establishment these resistant clones may exhibit cross-resistance to many structurally and functionally unrelated

compounds to which they have not yet previously been exposed [12]. The clinical perception and definition of resistance is based on the time to treatment failure, rather than tumor response to treatment [13]. Although carefully selected drug-resistant cell lines used in preclinical studies are not always good models of *in vivo* drug resistance they have expanded our knowledge of the biochemical mechanisms underlying such resistance.

Described in the following study is the isolation and preliminary characterization of a human erythroleukemic K562 cell line selected for resistance towards the non-cleavable complex-forming topoisomerase II inhibitor dexrazoxane. The first few sections of this chapter deal with describing the drugging protocol used to select a dexrazoxane-resistant cell population, followed by the isolation of single cell clones and the measurement of their respective growth rates, doubling times, and resistance factors by MTS cytotoxicity analysis. With the selection of the most ideal clone, the stability of doubling time and resistance towards dexrazoxane was monitored. The degree of cross-resistance towards other bisdioxopiperazine analogues and a few cleavable complex-forming topoisomerase II poisons was assessed by MTS cytotoxicity analysis. As a prelude to future studies of elucidating the mechanism of resistance exhibited by these cells, dexrazoxane cytotoxicity was evaluated in the presence of verapamil, a known inhibitor of multidrug resistance transmembrane efflux transporter, P-glycoprotein. And finally as a continuation, or rather extension of the work conducted in Chapter 3 with parental K562 cells, the prospect of induced erythroid-like differentiation and apoptosis were investigated to a limited extent with this newly established dexrazoxane-resistant K562 cell line.

4.2 Materials and general protocols

4.2.1 Drugs, chemicals, and reagents

Dexrazoxane (Zinecard®, ICRF-187), ADR-925, and doxorubicin were gifts of Pharmacia & Upjohn (Columbus, OH, U.S.A.). Etoposide (VP-16), was obtained from Sigma Chemical Co. (cat. No. E-1383), ICRF-193 and ICRF-154 were previously synthesized in our laboratory. DMSO used to dissolve drugs, (99.5% cat. No. D-5879), trypan blue dye (cat. No. T-6146), HEPES (cell culture grade, cat. No. H-9136), verapamil (cat. No. V-4629), benzidine dihydrochloride (cat. No. B-0386), and cell culture tested agar (cat. No. A-9915) were obtained from Sigma Chemical Co. (St. Louis, MO, U.S.A.). Acetic acid (1 N, cat. No. 31,859-0) was obtained from Aldrich Chemical Co. (Milwaukee, WN, U.S.A.). Sodium chloride (NaCl, cat. No. AC-8304) was obtained from Anachemia Ltd. (Toronto, ON). Sodium bicarbonate ($NaHCO_3$, cat. No. BP328-079) was obtained from Fisher Scientific (Fairlawn, NJ, U.S.A.). Dulbecco's phosphate buffered saline (PBS, cat. No. D-5652), Dulbecco's modified eagle medium (DMEM, cat. No. 12800-017), penicillin-streptomycin (cat. No. 25200-072), fetal bovine serum (FCS, cat. No. 26140-079), and cell culture freezing medium-DMSO (cat. No. 11101-011) were obtained from Gibco-BRL, Life Technologies Inc. (Burlington, ON). Na_2EDTA (cat. No. 10093) was obtained from BDH Chemicals Ltd. (Toronto, ON). MTS, CellTiter 96® AQ_{ueous} One Solution Reagent (cat. No. G3580) was obtained from Promega Corp. (Madison, WI, U.S.A.) and stored at –20°C protected from light. Isoton II Coulter balanced electrolyte solution (cat. No. PN 8546719) was obtained from Beckman Coulter Inc. (Burlington, ON). Carbon dioxide (standard grade) was purchased from Welder's Supply (Winnipeg,

MB). Microtitre plates 96-well (cat. No. 83.1835) and 24-well (cat. No. 83.1836), T-25cm^2 (cat. No. 83.1810.502) and T-75cm^2 (cat. No. 83.1813.502) PE green 0.2 μm vented plug capped flasks and all other plasticware were obtained from Sarstedt Inc. (St. Leonard, PQ).

4.2.2 Preparation of drugs and reagents

Dexrazoxane (M_w = 268.28 g/mol), ADR-925 (M_w = 302.3 g/mol), and verapamil (M_w = 454.6 g/mol) were dissolved in cell culture medium (DMEM/FCS) and filter sterilized through a 0.2 μm acetate filter. Etoposide (M_w = 588.6 g/mol), doxorubicin (M_w = 543.53 g/mol), ICRF-193 (M_w = 282.3 g/mol), and ICRF-154 (M_w = 254.25 g/mol) were dissolved in 99.5% DMSO by brief sonication and heating in a 37°C water bath and added to cell cultures such that DMSO concentrations did not exceed 0.5% (v/v).

4.2.3 Culturing of K562 cells

Human erythroleukemic K562 cells, donated by Dr. Jack C. Yalowich (University of Pittsburgh School of Medicine, Pittsburgh, PA, U.S.A.) were grown as suspension cultures in T-flasks in DMEM containing 20 mM HEPES, 100 units/mL penicillin G, 100 μg/mL streptomycin, 10% (v/v) fetal bovine serum in an atmosphere of 5% (v/v) CO_2 and 95% (v/v) air at 37°C (pH 7.1). Cell densities (cells/mL) in cultures were assessed from aseptically removed aliquots by the use of a model Z_f Coulter counter (Coulter Electronics, Hialeah, FL, U.S.A.), as explained in Appendix A.2.

4.2.5.1 Assessment of viability

Trypan blue dye (0.6% w/v) was prepared by dissolving 0.6 g of dye in ddH_2O containing 150 mM NaCl and 1 mM Na_2EDTA. Cell viability was assessed in a trypan blue dye exclusion analysis by diluting culture samples 1:1 with trypan blue dye. A minimum of 500 cells were counted in a hemacytometer chamber followed by the determination of the percentage non-viable (blue) cells per total number of cells counted.

4.2.5.2 Benzidine staining assay for hemoglobin expression

The percentage of cells containing hemoglobin was estimated by staining with benzidine [14]. A stock solution of 0.2% (w/v) benzidine dihydrochloride in 0.5 M acetic acid was prepared, and was stable for months at 4°C. For each estimation a fresh solution of 0.4% of 30% (v/v) H_2O_2 in the benzidine stock solution was prepared. Next, a one-tenth volume of the stain solution was added to the cell suspension to be tested or 10 μL for every 100 μL cell suspension. The mixture was then examined in a hemacytometer chamber after 5 min under bright-field light microscopy. At least 500 cells of normal size or larger were counted per sample using a 40X objective lens for an accurate estimation of the number of benzidine-positive (blue) cells present.

4.2.5.3 Normalization of cell counts from cultures in which media is replaced

Final growth curves in media replenished cultures were normalized for slight fluctuations in cell densities and volumes. In brief, normalization was achieved by multiplying in order of cell densities, by a numerical factor (±) in which the cell density

changed from its determination after centrifugation and resuspension, to the following 24 hr interval (see Section 3.2.2.2.1).

4.2.5.4 Determination of growth rates and doubling times of cultured cells

As explained earlier in Section 3.2.2.2.2 in further detail the following single exponential rise equation was used in SigmaPlot (Jandel Corp., San Rafael, CA, U.S.A.) to empirically calculate the growth rate and doubling time of cell cultures when conditions of exponential growth were evident.

$C_t = C_o e^{\kappa t}$

where, C_t = the cell density at time t (cells/mL)
C_o = the starting initial seeded cell density (cells/mL)
e = the base of the natural logarithm
κ = the growth rate constant (hr^{-1})
t = the time (hr) at which C_t is determined

4.2.4 Cryogenic freezing of cells and their recovery afterwards

Approximately $5x10^6$ cells were removed in replicate from culture and centrifuged at 250 *g* for 12 min. This was followed by the careful, separate resuspension of the cell pellets into 1 mL aliquots of cell culture freezing medium containing 5% DMSO. Cells were then placed into cryovials, set upright in a styrofoam container, and stored overnight at –80°C to allow for gradual freezing. Afterwards vials were then immersed in a liquid nitrogen dewar. When needed, cryogenic storage vials containing cells were rapidly thawed in a 37°C water bath. The cells were then aseptically removed and washed once with 15 mL of culture medium by centrifugation. Afterwards, cells were grown in T-75 flasks in 5% (v/v) CO_2 and 37°C and passed twice before use in any experiments.

4.3 Acquisition of dexrazoxane-resistance through continuous exposure

4.3.1 Introduction

Of key importance in the establishment of a stable drug resistant cell line is the ability to maintain a selection pressure so as to provide a growth advantage for single cells which sustain a desirable mutation and/or otherwise exhibit drug resistance. In the following section are outlined the sequence of observations and drugging protocols that were used to establish a dexrazoxane resistant K562 cell line, as well as the preliminary analyses conducted to confirm its resistance prior to cloning.

4.3.2 Methods

4.3.2.1 Dexrazoxane drugging protocol

K562 cells were made resistant to dexrazoxane by continually exposing the cells to a relatively high concentration of dexrazoxane, at least 5 times greater than the previously determined median growth inhibitory (IC_{50}) concentration of ~20 μM (Table 3.5). A concentration of 100 μM dexrazoxane was chosen so as to mimimize the time spent eliminating the most sensitive cells in the population while at the same time not inducing total cell kill. The drugging procedure utilized to establish a dexrazoxane-resistant cell population followed, as described below, two extensive periods of daily exposure accompanied by intermittent periods of cell recovery. Previous experiments had shown that daily exposure to 100 μM of dexrazoxane would be sufficient enough to halt further cell division (Fig. 3.6 and 3.14), as well as ensure a topoisomerase II-inhibitory

concentration of dexrazoxane [15], given that its half life at pH 7.4 of 9.3 hr [16]. However, once removed after the first few days of treatment, it was found that these cells would gradually recover to relatively normal growth rates (Fig. 3.14 and Table 3.9) and normal morphology. Therefore, it was presumed that a continuous exposure to dexrazoxane over an extensive period time would act to gradually kill off those cells unable to tolerate the drug while allowing cells with an inherent or acquired resistance to dexrazoxane to eventually form the majority of the cell population.

Exponentially growing K562 cells were diluted into T-75 flasks at 0.8×10^6 cells/mL with fresh DMEM, supplemented with 10% (v/v) fetal calf serum. This was followed by the administration of a requiste concentration of dexrazoxane at <10% (v/v), prepared as described in Section 4.2.2 such that the final concentration in culture was 100 μM. Cells were aseptically removed daily, centrifuged at 250 *g* for 12 min, and resuspended in ~80% (v/v) fresh DMEM/FCS to total volumes that allowed for the attainment of cell densities approximately equivalent to that of before centrifugation. This was followed by a subsequent exposure to 100 μM of dexrazoxane, administered in the same fashion as before. The changing of media on a daily basis not only replenished depleted nutrients but also allowed for the removal of metabolic waste and cell debris which would otherwise have unnecessarily retarded the growth of any dexrazoxane-resistant cells. In conjunction with a previous experiment the growth of these cells over a two week period was followed by cell counting on a model Z_f Coulter counter and displayed in Fig. 3.14.

After this two week period of continuous exposure to dexrazoxane, the K562 cell culture consisted mostly of enlarged cells, previously shown to be polyploid (Fig. 3.12) as

well as a great deal of cell debris and/or apoptotic bodies. Cells were then transferred to media in the absence of dexrazoxane and proceeded to double once in overall cell density over the period of one week as cells of normal size slowly began to overtake the population. At this point the entire population of cells were cryogenically frozen (see Section 4.2.4) for three weeks until they could be once again started up at the beginning of the new year (1999). Subsequently, these cells were removed from the liquid nitrogen and allowed to grow in DMEM/FCS without dexrazoxane until exponential growth ensued after the period of one week.

Once the cell population had for the most part recovered, a secondary, more extensive four week duration of dexrazoxane treatment was conducted. However, dexrazoxane was not added with fresh media everyday as before. Instead, media was changed every other day by centrifugation as dexrazoxane was added everyday so as to ensure a sustained drug concentration of ~80-150 μM. Initially, the morphological changes in the cell population were the same as before during the previous dexrazoxane treatment period. Some cells became enlarged in size and remained healthy while others disappeared from the population due to cell death. This result was a clear indication that the initial two week treatment regimen had not sufficiently established a dexrazoxane-resistant cell population of any accord. However, by the end of the third week during this secondary treatment regimen cell growth was beginning to appear normal in the presence of dexrazoxane as very few enlarged cells or little cell debris remained in culture. The population now consisted mostly of cells which appeared for all purposes normal in morphology and size when compared directly to unexposed K562 cells. These cells when viewed daily appeared to rapidly increase in number and were present in the form of

doublets or small aggregates. This result suggested that exponential growth was beginning to occur in the presence of dexrazoxane.

4.3.2.2 Preliminary analysis of growth rate and dexrazoxane cytotoxicity

In order to properly assess the extent of dexrazoxane-resistance as well as the growth rate of this new K562-derived cell population, named K562RB prior to cloning the following preliminary experiments were conducted. Exponentially growing cultures of K562 and K562RB were diluted with DMEM/FCS to starting cell densities of 0.75×10^5 cells/mL into one and two T-75 flasks, respectively. One flask containing K562RB cells served as an undrugged control whereas the other was treated daily with 100 μM of dexrazoxane accompanied by media replacement, in the same manner as before. Cell densities were determined at indicated times from removed sample aliquots on a model Z_f Coulter counter using a threshold setting of 7 (100 μm aperture tube, 1/amp. = 2, 1/ap.current = 8, diameter cutoff ≅ 8.7 μm), as explained in Appendix A.2. The relative percentage of benzidine-positive cells staining for hemoglobin expression was assessed as previously described (Section 4.2.5.2). Finally, growth rates and doubling times of all cultures were subsequently determined (Section 4.2.5.4) so as to draw comparisons to the parental K562 cell line.

Dexrazoxane cytotoxicity by cell counting analysis was assessed by diluting exponentially growing K562 and uncloned K562RB cells to cell densities of 0.6×10^5 cells/mL and 0.96×10^5 cells/mL, respectively in 6-well tissue culture plates, total volume 3.4 mL. This was followed by the addition of 0.1 mL of the requisite stock solution of dexrazoxane to produce the desired final concentration as single determinations. After

72 hr of growth at 37°C with 5% (v/v) CO_2 cell densities were determined on a model Z_f Coulter counter using a threshold setting of 20 (100 μm aperture tube, 1/amp. = 2, 1/ap.current = 8, diameter cutoff ≅ 11.9 μm). The median dexrazoxane inhibitory concentration (IC_{50}) was determined in the same fashion as previously described (Section 3.2.2.4.4) from constructed dose-response curves of cell density versus dexrazoxane concentration.

4.3.3 Results

Displayed in Fig. 4.1a are the growth curves of K562 cells and the dexrazoxane-resistant heterogeneous K562RB cell population. K562RB control cells were shown to proliferate at an exponential rate which differed from that of the parental K562 cell line (Table 4.1). Unexposed K562RB cells had a doubling time of 31 hr as compared to K562 cells which doubled every 20 hr. Upon daily exposure to dexrazoxane the growth curve and doubling rate of K562RB cells was not substantially effected. Control unexposed K562RB and dexrazoxane-exposed K562RB cells exhibited comparable levels of hemoglobin expression which were significantly higher than that of parent K562 cells (Fig. 4.1b). However, as briefly displayed in this figure benzidine-positivity gradually diminished from the K562RB culture as it continued to proliferate. One week after this experiment was conducted both of these K562RB cell cultures, exposed to dexrazoxane for a total of five and six weeks respectively stained 6% positive for hemoglobin expression. This suggested that hemoglobin containing K562RB cells were in part not dividing, as concluded earlier (see Fig. 3.14). Dexrazoxane cytotoxicity analysis of K562RB cells by cell counting (Fig. 4.2) revealed that although these cells had not yet been cloned they

exhibited a significantly high degree of dexrazoxane resistance. As determined using a three-parameter logistic equation the median growth inhibitory concentration of dexrazoxane towards K562RB cells was found to be 2040 ± 320 μM. When compared to the previously determined IC_{50} value of 17.0 ± 1.1 μM for parental K562 cells (re-plotted in Fig. 4.2 from Fig. 3.8) this was a 120-fold increase in resistance.

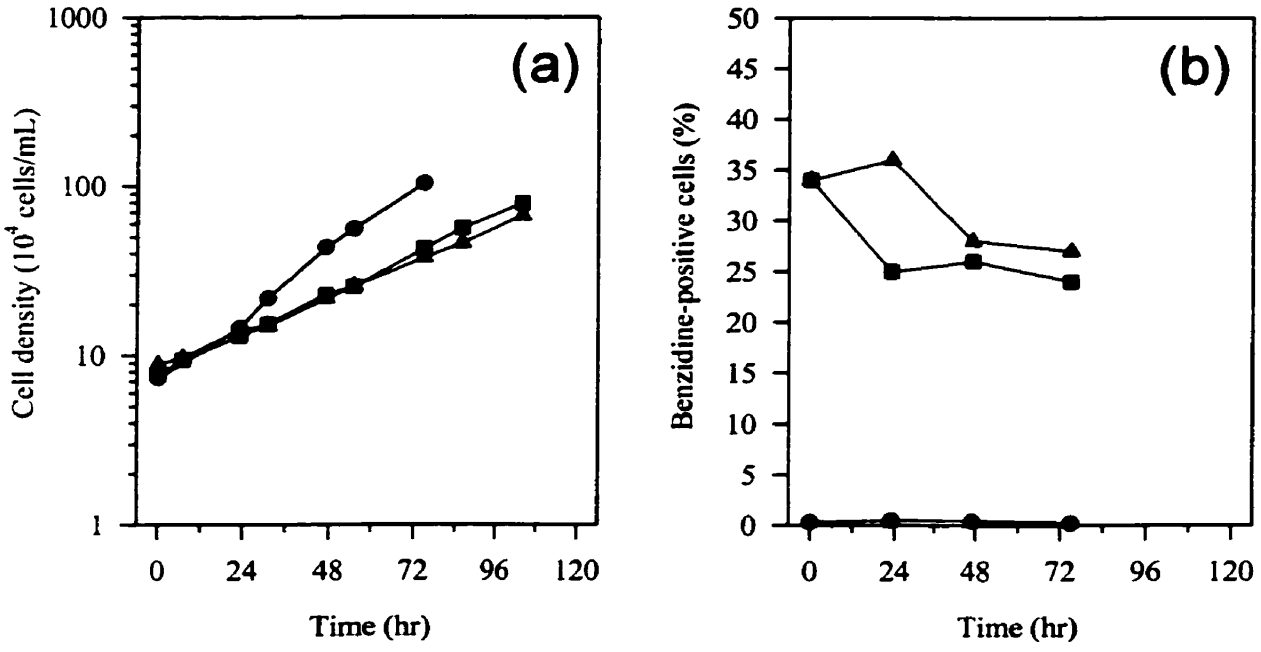

Fig. 4.1. Examination of cell growth and benzidine-positive staining in the heterogeneous dexrazoxane-resistant K562RB cell line. K562 (●) and K562RB (■) cells were seeded at 0.75×10^5 cells/mL in T-75 flasks. A separate flask of K562RB cells were treated with 100 μM dexrazoxane daily with media replacement (▲). At indicated times (a) cell densities were determined on a Coulter counter (threshold of 7, 100 μm aperture, diameter cutoff ≅ 8.7 μm) followed by normalization; and (b) relative hemoglobin expression was assessed upon benzidine staining.

Table 4.1. Growth rates and doubling times of K562 and dexrazoxane-resistant K562RB cells.

Duration of exposure	κ (hr^{-1})	S.E.	C.V. (%)	t (hr)
Unexposed control K562 cells	3.39E-02	1.56E-03	4.6	20
Unexposed K562RB cells	2.23E-02	5.30E-04	2.4	31
K562RB cells exposed daily with media replacement	1.98E-02	2.16E-04	1.1	35

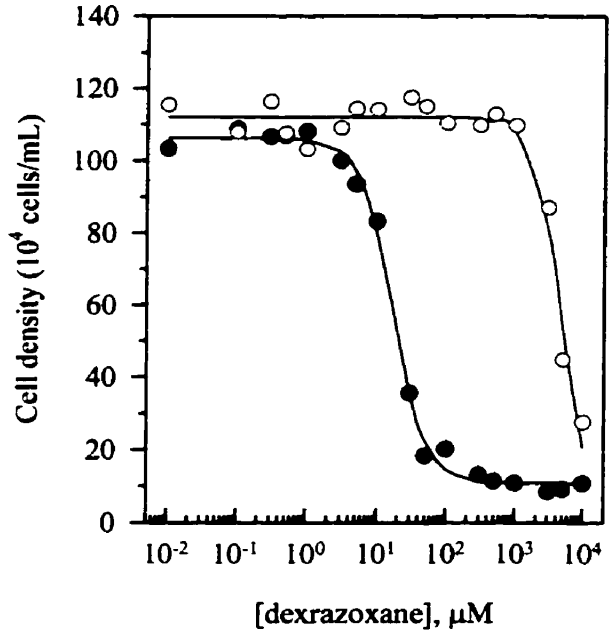

Fig. 4.2. Cell counting analysis of dexrazoxane-mediated cytotoxicity towards K562 and uncloned K562RB cells. K562 (●) and K562RB (○) cells were seeded at $0.6x10^5$ cells/mL and $0.96x10^5$ cells/mL, respectively in 6-well plates. After 72 hr of growth in the presence of various concentrations of dexrazoxane cell densities were determined on a model Z_f Coulter counter (threshold of 20, 100 μm aperture, diameter cutoff ≅ 11.9 μm). Curves represent the result of least squares non-linear regression fits of measured values to three- or four-parameter logistic equations. The lowest concentrations are the zero values, plotted for convenience on a logarithmic scale with arbitrary values. K562RB cells were 120-fold resistant, with a dexrazoxane IC_{50} value of 2040 ± 320 μM, as compared to parental cells, 17.0 ± 1.1 μM. K562 cytotoxicity data is re-plotted from Fig. 3.8.

4.4 Selection and propagation of dexrazoxane-resistant strains of K562 cells

4.4.1 Introduction

As described in the preceeding section a dexrazoxane-resistant K562 cell population had been established. However, due to the likelihood of hetereogenous dexrazoxane-resistance it was necessary to establish a series of dexrazoxane-resistant cell lines propagated from single cell clones. In the following section K562RB cells which had been exposed to dexrazoxane for a total of six weeks to establish resistance were cloned from soft agar. Upon the establishment of several viable dexrazoxane-resistant K562 cell lines the measurement of growth rates and the degree of dexrazoxane resistance by MTS cytotoxicity analysis allowed for the selection of the best cell line for future research.

4.4.2 Methods

4.4.2.1 Cloning in soft agar

Preparation and dispensing of stock agar solution: A 0.5% (w/v) stock agar solution was prepared by adding 1 g of agar powder to 30 mL of ddH_2O, autoclaving for 30 min, then cooling to 55°C in a water bath. Next, 170 mL of DMEM containing 15% (v/v) FCS was added to this solution at 55°C. Finally, 14 mL of this molten agar solution was added to each of several 100x20 mm culture dishes and allowed to gel and dry for 20 min at room temperature.

Exponentially growing K562RB cells were removed from suspension culture and prepared to a density of $0.15x10^5$ cells/mL with DMEM/FCS (15% v/v). Into six wells of a 24-well tissue culture plate was added 0.8 mL of DMEM/FCS (15% v/v). Next, the K562RB cell suspension was diluted in series 1:5 by the addition of 0.2 mL (i.e. 3000 cells) to the first well, mixing, transferring 0.2 mL to the second well and so forth with 0.2 mL discarded from the final well. Once the stock agar solution had cooled to 45°C then 1 mL was added to each well, mixed, and transferred dropwise to separate agar containing 100x20 mm culture dishes.

Culture dishes containing embedded single K562RB cells were allowed to grow at 37°C and 5% (v/v) CO_2 until visible colonies had formed containing over 100 cells/colony. After a period of 10 days of growth over 30 colonies were individually picked off using a 1000 µL pipettor tip. These were then transferred into 1 mL of DMEM/FCS (15% v/v) in separate wells of a 24-well tissue culture plate for further growth. After a 2 week period of growth the entire contents of 10 separate wells were transferred to T-25 flasks containing DMEM/FCS for further growth. Upon reaching a state of exponential growth these dexrazoxane-resistant (DZ) K562 cell clones were given the name K562/DZ with a suffix ranging from 1-10. Prior to, and after the execution of the following experiments which measured growth rates and degree of dexrazoxane cytotoxicity, approximately $5x10^6$ cells of each K562/DZ clone were cryogenically frozen for preservation, as previously described (Section 4.2.4).

4.4.2.2 Measurement of growth rates and doubling times of K562/DZ clones 1-10

Exponentially growing cultures of K562/DZ clones 1-10 were diluted with DMEM/FCS to starting cell densities of ~$0.5x10^5$ cells/mL into separate T-75 flasks and allowed to grow for up to 5 days without intervention. Cell densities were determined at indicated times from removed sample aliquots on a model Z_f Coulter counter using a threshold setting of 7 (100 μm aperture tube, 1/amp. = 2, 1/ap.current = 8, diameter cutoff ≅ 8.7 μm), as explained in Appendix A.2. The growth rates and doubling times of all cultures were subsequently determined using the single exponential rise equation, $C_t = C_o e^{kt}$ as previously described (Section 4.2.5.4).

4.4.2.3 MTS analysis of dexrazoxane cytotoxicity in K562/DZ clones 1-10

4.4.2.3.1 Seeding of microtitre plates

Exponentially growing K562/DZ clones 1-10 were diluted to one of three chosen cell densities based in part on their pre-determined rate of growth. It was previously shown through optimization of the MTS assay (Section 3.2.3.2) that a cell density of 32,000 cells/well in control columns at the stage of analysis was ideally within the range of sensitivity for accurately resolving a growth inhibition curve. Therefore, based on the different doubling times of the K562/DZ clones, cells were seeded into 96-well microtitre plates at either 2500 cells/well (K562/DZ1-6, 9), 5000 cells/well (K562/DZ7, 8), or 7000 cells/well (K561/DZ10) such that there would eventually be 32,000 cells/well in control columns after 72 hr of growth. Cells were delivered into microtitre wells at 50 μL/well in replicate (x6) between columns 2-12 and rows B-G using a multichannel pipettor.

4.4.2.3.2 Delivery of drug to microtitre plates

After the appropriate quantity of dexrazoxane was weighed and solubilized in DMEM/FCS as described in Section 4.2.2 drug stock solutions were prepared and added to microtitre plates at 40 μL/well immediately after seeding. Into all outer wells that did not contain cells (rows A and H, and column 1) was placed 100 μL of PBS for spectrophotometer blanking and/or the prevention of evaporation from inner wells containing cells and drug. To further maintain a consistent volume of 90 μL/well in all inner wells each plate was wrapped individually with Saran wrap (Dow Brands Canada Inc., Paris, ON) before placing in the incubator at 37°C with 5% (v/v) CO_2.

4.4.2.3.3 Measurement of cytotoxic effects

After 72 hr of growth in the presence of dexrazoxane, a suitable amount of the MTS one solution reagent (Promega Corp., Madison, WI, U.S.A.) was removed aseptically and placed into a sterile boat after thawing for 15 min in a 37°C water bath. Into the appropriate wells of each microtitre plate was added 10 μL of MTS reagent such that the final volume per well was 100 μL. Plates were then incubated for 3 hr at 37°C in a humidified, 5% (v/v) CO_2 atmosphere after which time a Thermomax 96-well plate reader (Molecular Devices, Menlo Park, CA, U.S.A.) was used to measure absorbance at 490 nm in the wells. Absorbance was corrected for non-specific, scattered light by subtracting the absorbance at 650 nm from the absorbance at 490 nm. Dose-response curves were subsequently constructed, and the median dexrazoxane inhibitory concentration (IC_{50}) was

determined upon non-linear least squares fitting to a four-parameter logistic equation, $Abs_{490/650} = (a-d)/(1+(x/c)^b)+d$, as previously described (Section 3.2.2.4.4).

4.4.3 Results

Displayed in Fig. 4.3 are the growth curves of dexrazoxane-resistant K562/DZ clones 1-10 which were propagated from single cell colonies of the heterogeneous K562RB cell population. All K562/DZ clones were shown to be ~100% viable by a trypan blue dye exclusion analysis (data not shown) and appeared to proliferate in an exponential fashion. The calculated growth rates and doubling times of these cell lines are displayed in Table 4.2. Overall, the majority of K562/DZ clones exhibited doubling times which were very close to that of the parent K562 cell line, previously shown to be ~19 hr (Table 3.4). The appearance of a few clones with longer doubling times permitted the classification of three relatively distinct groups of K562/DZ clones based soley on doubling time: (i) 21-24 hr (K562/DZ1-6, 9), (ii) 28-31 hr (K562/DZ7-8), and (iii) 36 hr (K562/DZ10). This slight variance in doubling time could in part account for the earlier determined mid-range doubling time of 31 hr in the original heterogeneous K562RB cell population (Table 4.1).

The individual values of the median inhibitory concentration (IC_{50}) of dexrazoxane towards each K562/DZ clone are presented in Table 4.3. Illustrated in Fig.4.4 are the cytotoxicity profiles for dexrazoxane towards each of these clones as determined by MTS analysis. Although there had appeared to be a slight variability in doubling time, the dexrazoxane IC_{50} values in all K562/DZ clones were relatively the same within experimental error. The resistance factor was calculated from the ratio of the IC_{50} value of each K562/DZ clones to the IC_{50} value of parent K562 cells, previously established as 20.3

μM by MTS analysis (Table 3.5). Overall, K562/DZ clones were shown to be ~84-110-fold resistant to dexrazoxane as compared to K562 cells. When examined microscopically after the 72 hr period of dexrazoxane exposure a few enlarged cells (<3% of the field of view) were identified only at exceedingly high dexrazoxane concentrations. Cells exhibited normal morphology at all other dexrazoxane concentrations below 5000 μM.

For the purpose of further research it was impractical to continue working with 10 dexrazoxane-resistant K562/DZ clones. Reason dictated that the K562/DZ clone of choice for future experiments should proliferate relatively rapidly and exhibit a high degree of dexrazoxane resistance. The two seemingly most rapid proliferating clones were identified as K562/DZ1 and K562/DZ5. And, of these two clones, K562/DZ1 exhibited one of the highest measured degrees of dexrazoxane resistance, preceeded only by the two slowest proliferating clones K562/DZ8 and K562/DZ10. Therefore, based on these results alone the decision was made to continue all future experiments with the use of the K562/DZ1 clone. However, it remains to shown whether any difference exists between K562/DZ1 and the other nine clones isolated.

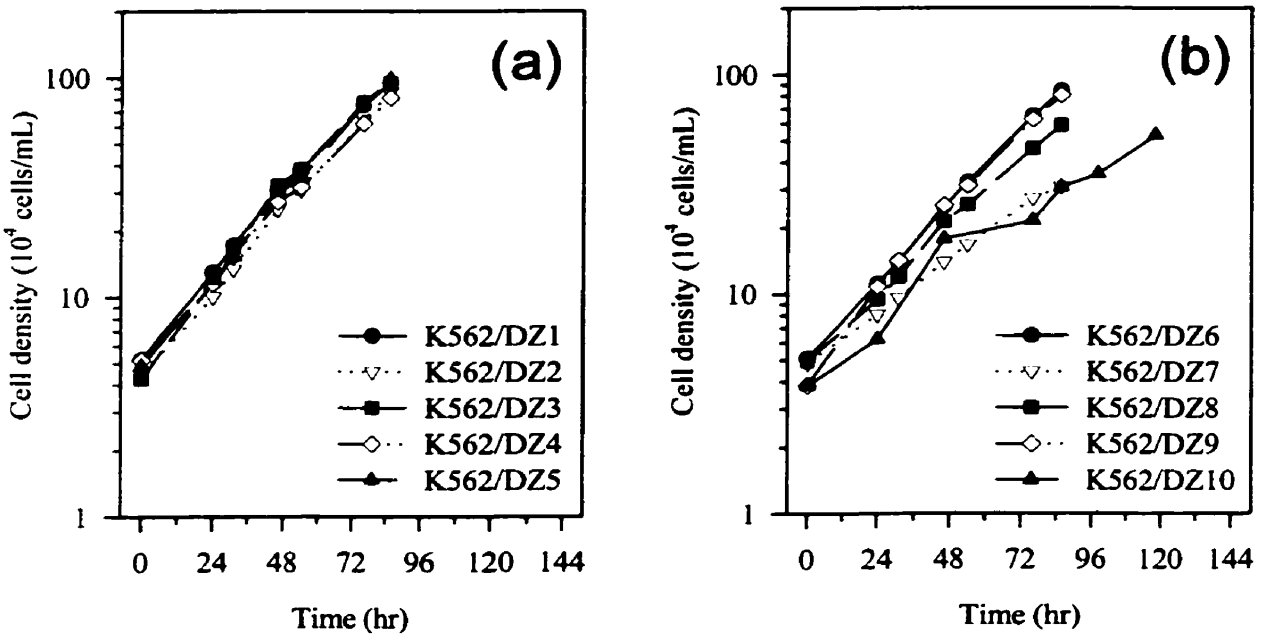

Fig. 4.3. Growth curves of dexrazoxane-resistant K562/DZ clones 1-10. K562/DZ clones (a) 1-5 and (b) 6-10 were seeded at initial cell densities of 0.5×10^5 cells/mL and allowed to grow without intervention. At indicated times samples were removed and cell densities were determined on a Coulter counter (threshold of 7, 100 μm aperture, diameter cutoff ≅ 8.7 μm).

Table 4.2. Growth rates and doubling times of dexrazoxane-resistant K562/DZ clones 1-10.

dexrazoxane-resistant clones	κ (hr^{-1})	S.E.	C.V. (%)	t (hr)
K562/DZ1	3.03E-02	1.10E-03	3.6	23
K562/DZ2	3.29E-02	7.61E-04	2.3	21
K562/DZ3	3.05E-02	1.78E-03	5.8	23
K562/DZ4	3.00E-02	7.59E-04	2.5	23
K562/DZ5	3.26E-02	1.11E-03	3.4	21
K562/DZ6	2.84E-02	1.34E-03	4.7	24
K562/DZ7	2.46E-02	1.16E-03	4.7	28
K562/DZ8	2.22E-02	2.57E-03	11.6	31
K562/DZ9	3.11E-02	9.72E-04	3.1	22
K562/DZ10	1.91E-02	1.70E-03	8.9	36

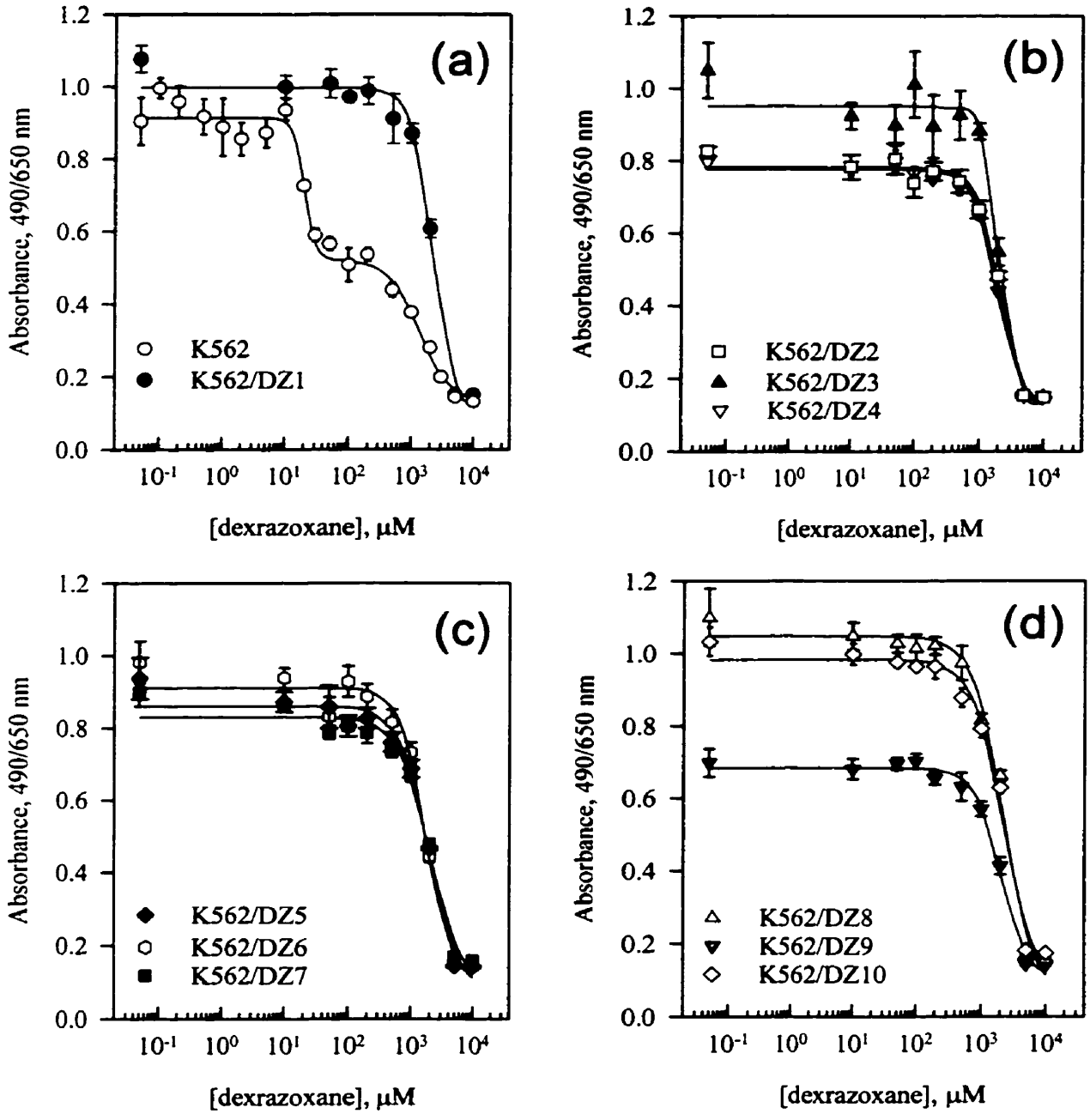

Fig. 4.4. MTS analysis of dexrazoxane-mediated growth inhibition towards dexrazoxane-resistant K562/DZ clones 1-10. K562/DZ clones (a) 1, (b) 2-4, (c) 5-7, (d) 8-10 were incubated for 72 hr in the presence of dexrazoxane. Absorbances at 490/650 nm were determined after a 3 hr incubation with MTS reagent. The curves represent the results of least squares non-linear regression fits of measured values to a four-parameter logistic equation. The error bars represent standard deviations. The lowest concentrations are the zero values, plotted for convenience on a logarithmic scale with arbitrary values. For the purpose of direct comparison the dexrazoxane cytotoxicity profile towards parent K562 cells is re-plotted here from Fig. 3.7.

Table 4.3. Cytotoxicity of dexrazoxane towards dexrazoxane-resistant K562/DZ clones 1-10 as determined by MTS analysis.

dexrazoxane-resistant clones	IC_{50}[a] (μM)	S.E. (μM)	C.V. (%)	Resistance factor[b]
K562	20.3	1.9	9.5	-
K562/DZ1	2125.0	250.0	11.8	104.6
K562/DZ2	2084.0	233.1	11.2	102.6
K562/DZ3	2003.0	193.7	9.7	98.6
K562/DZ4	1901.0	148.9	7.8	93.6
K562/DZ5	1890.0	354.0	18.7	93.0
K562/DZ6	1702.0	240.9	14.2	83.8
K562/DZ7	1980.0	415.9	21.0	97.4
K562/DZ8	2216.0	447.3	20.2	109.1
K562/DZ9	2009.0	215.3	10.7	98.9
K562/DZ10	2230.0	419.4	18.8	109.7

[a] Cytotoxicity was measured by MTS analysis with a 72 hr exposure to dexrazoxane. The IC_{50} value is the concentration of dexrazoxane at which cell growth is 50% of the maximum observed inhibition. These values were obtained by fitting absorbance measurements to a four-parameter logistic equation.

[b] The resistance factor was calculated from the ratio of the IC_{50} for K562/DZ clones 1-10 to the IC_{50} of K562 cells, determined previously (Fig. 3.8).

4.5 Retention of dexrazoxane resistance in the selected K562/DZ1 cell line and the measurement of cross-resistance towards other topoisomerase II inhibitory agents

4.5.1 Introduction

Once the dexrazoxane-resistant K562/DZ1 cell line had been established, it was important to determine whether the resistance phenotype was merely transient, eventually reverting back to normal, or whether it could be maintained for an extended period of time without the need for routine drug-challenging. Upon cryogenically freezing portions of the original K562/DZ1 cell line the remaining cells were passed regularly in the absence of drug and periodically examined, as described in the following section in terms of growth rate and stability towards dexrazoxane resistance.

Although these cells were originally selected for resistance towards dexrazoxane, the possibility remained that they additionally exhibited cross-resistance to other structurally similar analogs and/or agents targeting the same enzyme. To that effect growth inhibition experiments were conducted in the following section on K562 and K562/DZ1 cell lines to examine the degree of cytotoxicity conferred by a variety of bisdioxopiperazine analogs and other topoisomerase II-targeted drugs. If cross-resistance could be identified it was hoped that this would form an integral part of future experiments towards the elucidation of the exact mechanism of resistance acquired by K562/DZ1 cells.

4.5.2 Methods

4.5.2.1 Retention of growth rates and doubling times of K562/DZ1 cells

Exponentially growing K562/DZ1 cells were diluted with DMEM/FCS to a starting cell density of ~$0.5x10^5$ cells/mL in a T-75 flask and allowed to grow without intervention. Cell densities were determined at indicated times from removed sample aliquots on a model Z_f Coulter counter using a threshold setting of 7 (100 μm aperture tube, 1/amp. = 2, 1/ap.current = 8, diameter cutoff ≅ 8.7 μm), as explained in Appendix A.2. The growth rate and doubling time of K562/DZ1 cells were re-determined one month after its original assessment using the single exponential rise equation, $C_\tau = C_o e^{\kappa t}$ as previously described (Section 4.2.5.4).

4.5.2.2 MTS analysis of cross-resistance towards some bisdioxopiperazines and cleavable complex-forming topoisomerase II poisons in K562/DZ1 cells

4.5.2.2.1 Seeding of microtitre plates

Cytotoxicity analysis of the following topoisomerase II inhibitory agents towards K562/DZ1 cells which had been growing for two months in the absence of drug was conducted concurrently with parental K562 cells, as outlined explicitly in Section 3.2.2.4. In brief, exponentially growing cultures of K562 and K562/DZ1 cells were diluted to appropriate starting cell densities so as to seed 96-well microtitre plates at 1800 and 2300 cells/well, respectively. Based on an 18 hr and 21 hr doubling time of K562 and K562/DZ1 cells respectively, cell densities would reach an optimal 32,000 cells/well in

control columns after 72 hr of growth. For cytotoxicity analysis of drugs requiring solubilization in DMEM/FCS, 50 μL of cells were added to each well, and for drugs requiring solubilization in DMSO, 89.5 μL of cells were added in the same manner.

4.5.2.2.2 Delivery of drug to microtitre plates

After the appropriate quantity of drug was weighed and solubilized as described in Section 4.2.2 drug stock solutions were prepared and added to microtitre plates immediately after seeding to a total volume of 90 μL/well. Drugs solubilized in DMEM/FCS (dexrazoxane, ADR-925) were added at 40 μL/well, and drugs solubilized in DMSO (ICRF-154, ICRF-193, etoposide, doxorubicin) were added at 0.5 μL/well, or ~0.5% (v/v) as previously described (Section 3.2.2.4.2). Into all outer wells was placed 100 μL of PBS for spectrophotometer blanking, and each plate was subsequently wrapped with Saran wrap (Dow Brands Canada Inc., Paris, ON) before placing in the incubator at 37°C with 5% CO_2.

4.5.2.2.3 Measurement of cytotoxic effects

After 72 hr of growth the MTS one solution reagent (Promega Corp., Madison, WI, U.S.A.) was thawed for 15 min in a 37°C water bath, and aseptically placed into a sterile boat. Into the appropriate wells of each microtitre plate was added 10 μL of MTS reagent to a final volume of 100 μL/well. Plates were then incubated for 3 hr at 37°C with 5% (v/v) CO_2 after which time a Thermomax 96-well plate reader (Molecular Devices, Menlo Park, CA, U.S.A.) was used to measure absorbances at 490-650 nm in all wells. Dose-

response curves were subsequently constructed, and median inhibitory concentrations (IC_{50}) were determined as before, upon non-linear least squares fitting to the four-parameter logistic equation $Abs_{490/650} = (a - d) / (1 + (x / c)^b) + d$ explicitly described in Section 3.2.2.4.4.

4.5.3 Results

Upon its establishment after cloning, the K562/DZ1 cell line was passed for up to two months in the absence of dexrazoxane before re-evaluating by MTS analysis its resistance towards dexrazoxane. Common practice would suggest that every 2-3 months a researcher should go back to the original cell stock in liquid nitrogen storage in order to the obtain a cell line most representative of the original population. With respect to human erythroleukemic K562 cells this may be of upmost importance due to its partially differentiated state which may gradually change over time with continual passage. After a two month period of drug-free growth the doubling time of K562/DZ1 cells was found to have remained at 21 hr, as derived from the growth curve of Fig. 4.5. Although doubling time does not directly infer any relation to the stability of dexrazoxane resistance, it may be presumed that the inability to reacquire the parental doubling time of 19 hr reflects some sort of stability.

The cytotoxicity profiles for both the K562 parental and the K562/DZ1 cell line are compared in Fig. 4.6. For the purpose of a direct comparison, all of the K562 cytotoxicity data in this figure are re-plotted from earlier reported data (Fig. 3.8), although both cell lines were in fact examined concurrently. The bisphasic nature of the dexrazoxane survival curves for K562 cells was previously attributed to the high mitochondrial

reductase potential of a small number of enlarged cells able to exhibit a greater competence for reducing MTS to formazan (Section 3.6.1). The dexrazoxane cytotoxicity profile of K562/DZ1 cells after two months of growth in drug-free media appeared monophasic in nature (Fig. 4.6a), much like its previous analysis (Fig. 4.4a). The corresponding IC_{50} value for K562/DZ1 cells was found to be 2568 ± 174 μM (Table 4.4), which is very close to the previous estimation of 2125 ± 250 μM (Table 4.3). This result clearly indicates that the dexrazoxane resistance conferred by the K562/DZ1 cell line is extremely stable for at least a period of two months and may in fact last much longer without reverting.

The K562/DZ1 survival curves of other examined topoisomerase II-inhibitory agents were for the most part monophasic in nature (Fig. 4.6). The only exceptions to this trend occurred upon analysis of the bisdioxopiperazines, ICRF-193 and ICRF-154 (Fig. 4.6c, d). Due to solubility constraints, the highest concentrations of these drugs that could be tested were 50 μM and 150 μM, respectively. Although parental K562 cells exhibited measurable survival curves within the indicated range of drug concentrations, this was not true with respect to K562/DZ1 cells. As a result, ICRF-193 and ICRF-154 showed a high degree of cross-resistance giving resistance factors of at least 93- and 4.5-fold, respectively (Table 4.4) as higher concentrations were limited by the solubility of these drugs. Although ICRF-193 and ICRF-154 displayed greater if not the similar cytotoxicity towards parental K562 cells as dexrazoxane, the degree of resistance observed in K562/DZ1 cells is not without reason given that these compounds are structurally similar (Fig. 1.1) and target the same enzyme, topoisomerase II [15,17].

The fully hydrolyzed product of dexrazoxane, ADR-925 is produced with a half-time of 28 hr at pH 7.4 and 37°C [16]. In addition, ADR-925 has been previously

demonstrated to possess no measurable inhibitory activity towards DNA topoisomerase II [15]. Therefore, it was not surprising to identify relatively common cytotoxicity profiles (Fig. 4.6b) and IC_{50} values (Table 4.4) of ADR-925 towards K562 and K562/DZ1 cells. These values which were 1229 ± 202 μM and 638 ± 52 μM ADR-925, in K562 and K562/DZ1 cells respectively ideally correspond to the cytotoxicity exhibited in both cell lines at extremely high concentrations of dexrazoxane. This similarity of IC_{50} values has been previously seen in CHO and DZR cells, where upon the cytotoxicity at high concentrations of these drugs was attributed to the chelation of magnesium and calcium in the medium by ADR-925 [18].

Finally, two cleavable complex-forming topoisomerase II poisons, etoposide and doxorubicin [19] were investigated as to their degree of cross-resistance towards K562/DZ1 cells (Fig. 4.6e, f). As noted earlier in Section 3.6.1 both etoposide and doxorubicin were able to induce a considerable cytotoxic effect at low drug concentrations in the parental K562 cells. Upon analysis, K562/DZ1 cells were shown to display a moderate degree of cross-resistance towards etoposide and doxorubicin generating resistance factors of 4- and 2.4-fold, respectively (Table 4.4).

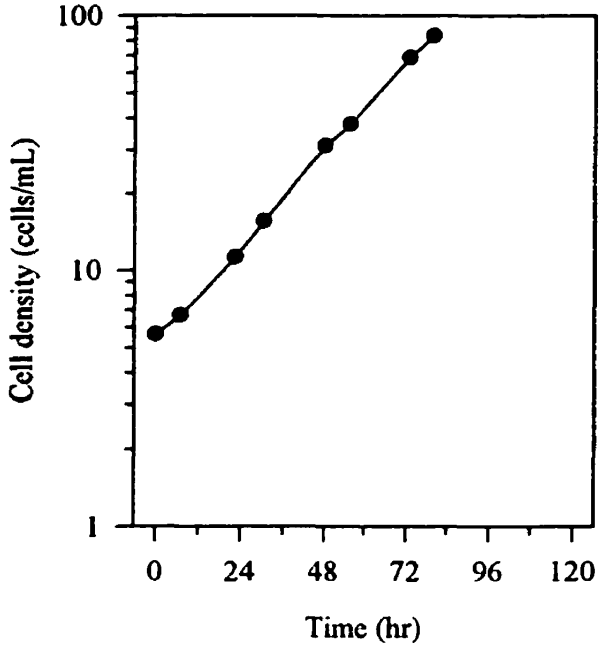

Fig. 4.5. Retention of exponential growth and doubling time in the K562/DZ1 cell line one month after first determination. K562/DZ1 cells were seeded into a T-75 flask at an initial cell density of 0.5×10^5 cells/mL and allowed to grow without intervention. At indicated times samples were removed and cell densities were determined on a Coulter counter (threshold of 7, 100 μm aperture, diameter cutoff ≅ 8.7 μm). The doubling time of K562/DZ1 cells was determined to be 21 hr, in agreement with previous assessments.

Fig. 4.6. MTS analysis of K562 and K562/DZ1 cell growth inhibition by bisdioxopiperazines and other topoisomerase II inhibitory agents. K562 (●) and K562/DZ1 (○) cells were incubated for 72 hr with (a) dexrazoxane, (b) ADR-925, (c) ICRF-193, (d) ICRF-154, (e) etoposide, and (f) doxorubicin in 96-well microtitre plates. Absorbances at 490-650 nm were determined after 3 hr of incubation with MTS reagent. The curves represent the results of least squares non-linear regression fits of measured values to a four-parameter logistic equation. The error bars represent standard deviations. The lowest concentrations are the zero values, plotted for convenience on a logarithmic scale with arbitrary values. All K562 data is re-plotted from Fig. 3.7 for comparison.

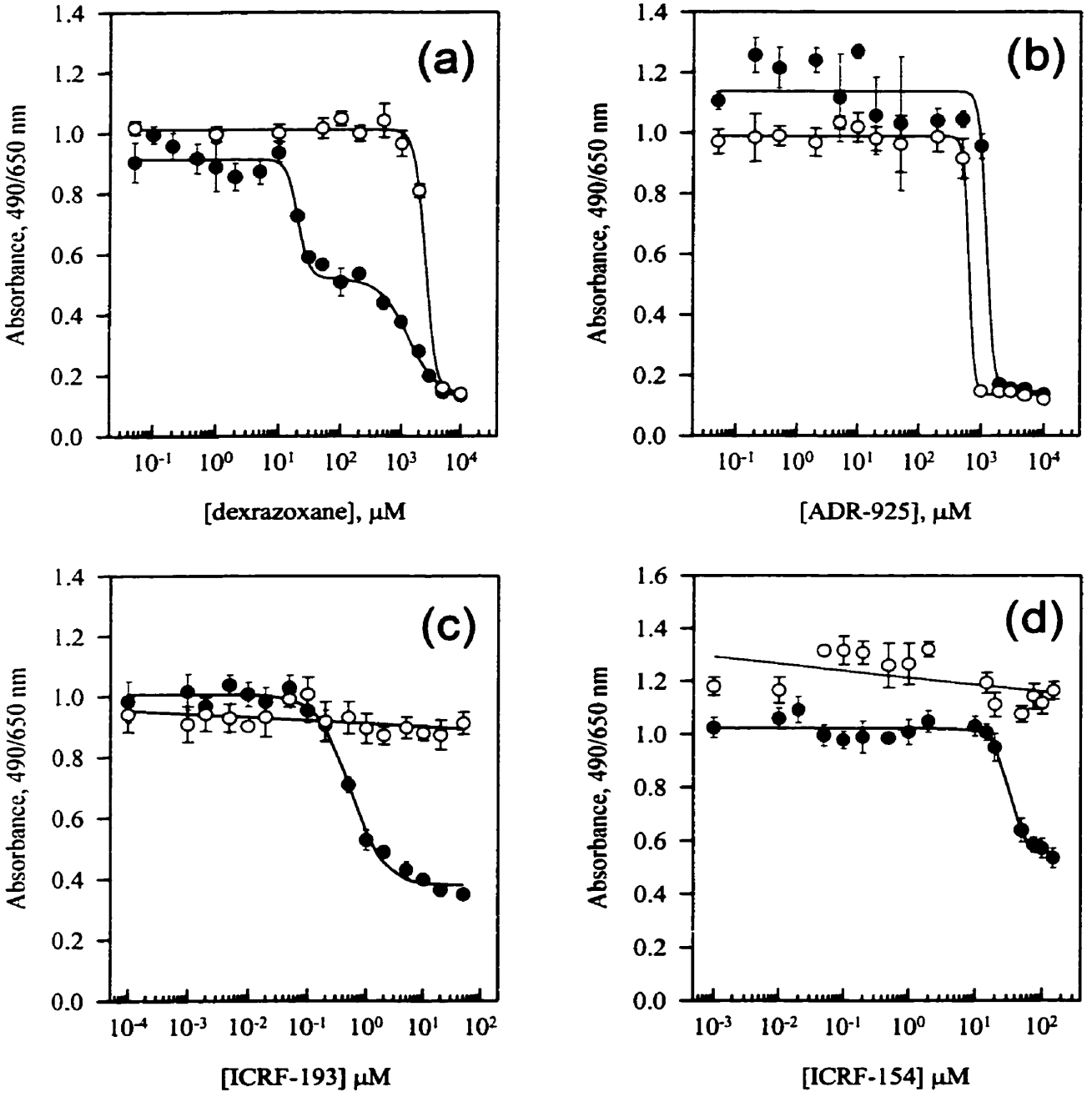

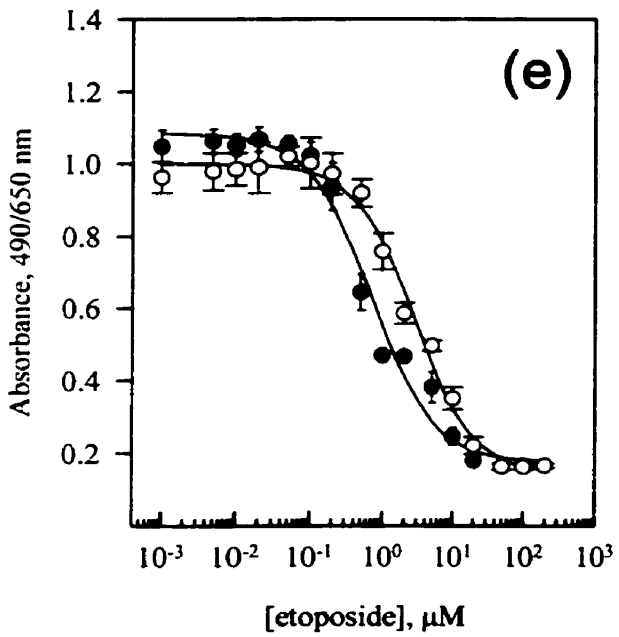
(e)
Absorbance, 490/650 nm
1.4
1.2
1.0
0.8
0.6
0.4
0.2
10^{-3} 10^{-2} 10^{-1} 10^{0} 10^{1} 10^{2} 10^{3}
[etoposide], μM

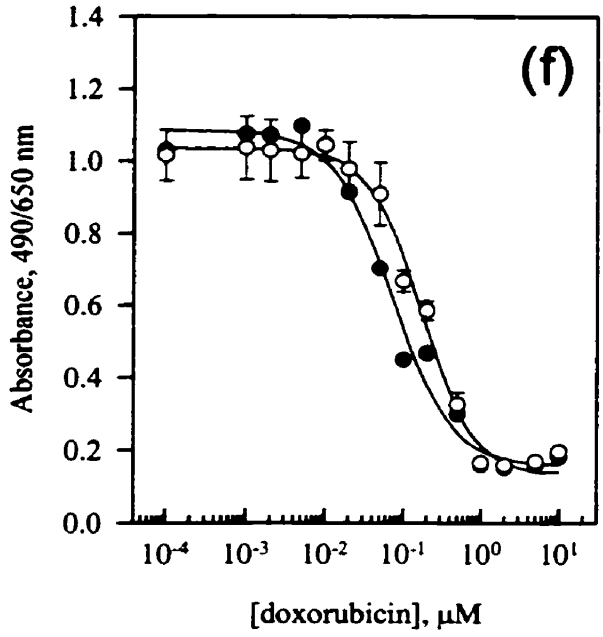
(f)
Absorbance, 490/650 nm
1.4
1.2
1.0
0.8
0.6
0.4
0.2
0.0
10^{-4} 10^{-3} 10^{-2} 10^{-1} 10^{0} 10^{1}
[doxorubicin], μM

Table 4.4. Cytotoxicity of various topoisomerase II inhibitory agents towards K562/DZ1 cells as determined by MTS analysis.

Drug	Cell line	IC_{50}[a] (μM)	S.E. (μM)	C.V. (%)	Resistance factor[b]
Non-cleavable complex-forming topoisomerase II inhibitors					
dexrazoxane	K562	20.3	1.9	9.5	-
	K562/DZ1	2568.0	173.8	6.8	126.4
ADR-925[c]	K562	1229.0	202.0	16.4	-
	K562/DZ1	638.0	52.3	8.2	1
ICRF-193	K562	0.54	0.05	9.68	-
	K562/DZ1	>50*	N/A	N/A	>93*
ICRF-154	K562	33.52	3.93	11.71	-
	K562/DZ1	>150*	N/A	N/A	>4.5*
Cleavable complex-forming topoisomerase II poisons					
etoposide	K562	0.71	0.12	17.01	-
	K562/DZ1	2.81	0.35	12.53	4.0
doxorubicin	K562	0.073	0.013	17.98	-
	K562/DZ1	0.171	0.020	11.46	2.4

[a] Cytotoxicity was measured by MTS analysis with a 72 hr exposure to the cytotoxic agent. The IC_{50} is the concentration of the agent at which cell growth is 50% of the maximum observed inhibition. Individual median inhibitory concentrations ± S.E. of the various agents were obtained by fitting absorbance data to a four-parameter logistic equation.

[b] The resistance factor was calculated from the ratio of the IC_{50} for K562/DZ1 to the IC_{50} of K562 cells, determined previously (Fig. 3.8).

[c] ADR-925, the hydrolyzed form of dexrazoxane was the only known non-topoisomerase II inhibitory agent investigated.

*These values are lower limits only from the highest concentration of drug that could be tested due to solubility constraints.

4.6 Testing for P-glycoprotein content in K562/DZ1 cells by measuring dexrazoxane resistance in the presence of verapamil

4.6.1 Introduction

P-glycoprotein (Pgp) has been revealed as an important causal molecule by which cancer cells can overcome effective chemotherapy to a wide range of structurally unrelated cytotoxic and anticancer agents. The apparent function of Pgp is that of an energy dependent efflux transporter pump which confers multidrug resistance (MDR) by maintaining reduced sublethal intracellular drug concentrations. In many tissues of the body such as in the kidney, liver, colon, and adrenal cortex [20] Pgp plays a normal physiological role of protecting cells against chemical insult [10] and clearing the body of endogenous or exogenous molecules including natural or environmental toxins, carcinogens, steroids, or other hormones [21]. The over-expression of Pgp in many types of clinical tumors has been seen not only as a prognostic indicator of the MDR phenotype, but also as an indicator of poor chemotherapeutic success, higher relapse rates, and shorter durations of remission [10,22]. For the most part Pgp expression appears to be the highest in non-dividing, differentiated cells, and lowest in rapidly dividing, less-differenttiated cells [23]. The expression of Pgp may be either constitutive in untreated tumors which are inherently unresponsive towards chemotherapy, or it may be acquired, in tumors that initially show some response to chemotherapy but then later develop MDR and relapse [1,20,23].

Chemosensitizers, also referred to as modulators are agents that inhibit the function of Pgp thus increasing the sensitivity of MDR tumor cells to cytotoxic anticancer drugs that would otherwise be ineffective [4]. The majority of these agents are apparently

substrates for the Pgp multidrug transporter which act as efflux blockers by competing with anticancer drugs for receptor binding and/or transport [10]. Other agents induce chemosensitization through alternative modes such as disturbing the membrane or inhibiting energy metabolism [21]. One such first generation chemosensitizer known as verapamil has been used to a limited extent to partially circumvent drug resistance in patients whose tumors over-express Pgp [24,25]. Verapamil is a calcium channel blocking agent able to block the efflux of toxins by Pgp. Although verapamil exhibits dose-limiting side effects and inadequate bioavailability [2,21] it has shown some value in research for identifying Pgp over-expression. In Pgp-positive tumor cells isolated from patients with end-stage myeloma, verapamil has been shown to increase the intracellular accumulation of doxorubicin and vincristine *in vitro* [25].

In the following section it was necessary to determine whether the K562/DZ1 cell line acquired its cross-resistance through the over-expression and activity of Pgp. In order to make such an assessment dexrazoxane cytotoxicity analyses were conducted in the presence of 0, 3, and 10 μM of verapamil. Thus, if K562/DZ1 cells contained elevated levels of Pgp then upon treatment with verapamil these cells would regain their sensitivity to dexrazoxane, as normally exhibited in the parent K562 cell line.

4.6.2 Methods

4.6.2.1 MTS analysis of dexrazoxane cytotoxicity towards K562 and K562/DZ1 cells in the presence of verapamil

4.6.2.1.1 Seeding of microtitre plates

Exponentially growing cultures of K562 and K562/DZ1 cells were diluted to appropriate starting cell densities so as to seed 96-well microtitre plates at 1800 and 2300 cells/well, respectively. Based on an 18 hr and 21 hr doubling time of K562 and K562/DZ1 cells respectively, cell densities would reach an optimal 32,000 cells/well in control columns after 72 hr of growth. Cells were delivered into microtitre wells at 30 μL/well in replicate (x6) between columns 2-12 and rows B-G using a multichannel pipettor.

4.6.2.1.2 Delivery of drug to microtitre plates

After the appropriate quantity of verapamil was weighed and solubilized in DMEM/FCS, stock solutions of 9 μM and 30 μM were prepared and added to microtitre plates at 30 μL/well immediately after seeding. Dexrazoxane, which was also solubilized in DMEM/FCS as described in Section 4.2.2 was delivered after verapamil at 30 μL/well producing a final volume of 90 μL/well. Into all outer wells was placed 100 μL of PBS for spectrophotometer blanking, and each plate was subsequently wrapped with Saran wrap (Dow Brands Canada Inc., Paris, ON) before placing in the incubator at 37°C with 5% (v/v) CO_2.

4.6.2.1.3 Measurement of cytotoxic effects

After 72 hr of growth the MTS one solution reagent (Promega Corp., Madison, WI, U.S.A.) was thawed for 15 min in a 37°C water bath, and aseptically placed into a sterile boat. Into the appropriate wells of each microtitre plate was added 10 μL of MTS reagent to a final volume of 100 μL/well. Plates were then incubated for 3 hr at 37°C with 5% (v/v) CO_2 after which time a Thermomax 96-well plate reader (Molecular Devices, Menlo Park, CA, U.S.A.) was used to measure absorbances at 490-650 nm in all wells. Dose-response curves were subsequently constructed, and median inhibitory concentrations (IC_{50}) were determined as before, upon non-linear least squares fitting to a four-parameter logistic equation, $Abs_{490/650} = (a - d) / (1 + (x / c)^b) + d$ explicitly described in Section 3.2.2.4.4.

4.6.3 Results

The cytotoxicity of dexrazoxane towards both K562 and K562/DZ1 cells grown in the presence of 0, 3, or 10 μM of verapamil are compared in Fig. 4.7a, b, and c respectively. The unaltered nature of these cytotoxicity profiles suggests at first that verapamil was not able to sensitize K562/DZ1 cells to dexrazoxane. This was further confirmed upon the determination of the median inhibitory concentrations (IC_{50}) of dexrazoxane in the presence of 0, 3, and 10 μm verapamil (Table 4.5). Despite the concentration of verapamil used, there appeared to be no significant effect on the IC_{50} values for either cell line. Although an IC_{50} value slightly lower than normal was determined for K562 cells in the presence of 3 μM verapamil, this was seen as not being an

attributable effect of verapamil given its reasonable proximity to the other IC_{50} vlaues and that 10 μM verapamil did not induce a similar effect. Overall, these results suggest that the K562/DZ1 cell line does not acquire its resistance through an over-expression of P-glycoprotein.

Table 4.5. Cytotoxicity of dexrazoxane towards K562 and K562/DZ1 cells in the presence of verapamil as measured by MTS analysis.

[Verapamil] (μM)	Cell line	IC_{50}[a] (μM)	S.E. (μM)	C.V. (%)	Resistance factor[b]
0	K562	20.3	1.9	9.5	-
	K562/DZ1	2804.0	243.6	8.7	138.0
3	K562	10.3	3.7	36.2	-
	K562/DZ1	2772.0	131.0	4.7	269.4
10	K562	17.8	1.1	6.3	-
	K562/DZ1	2762.0	93.8	3.4	155.2

[a] Cytotoxicity was measured by MTS analysis with a 72 hr exposure to dexrazoxane. The IC_{50} value is the concentration of dexrazoxane at which cell growth is 50% of the maximum observed inhibition. These values were obtained by fitting absorbance measurements to a four-parameter logistic equation.

[b] The resistance factor was calculated from the ratio of the IC_{50} for K562/DZ1 to the IC_{50} of K562 cells at each concentration of verapamil analyzed.

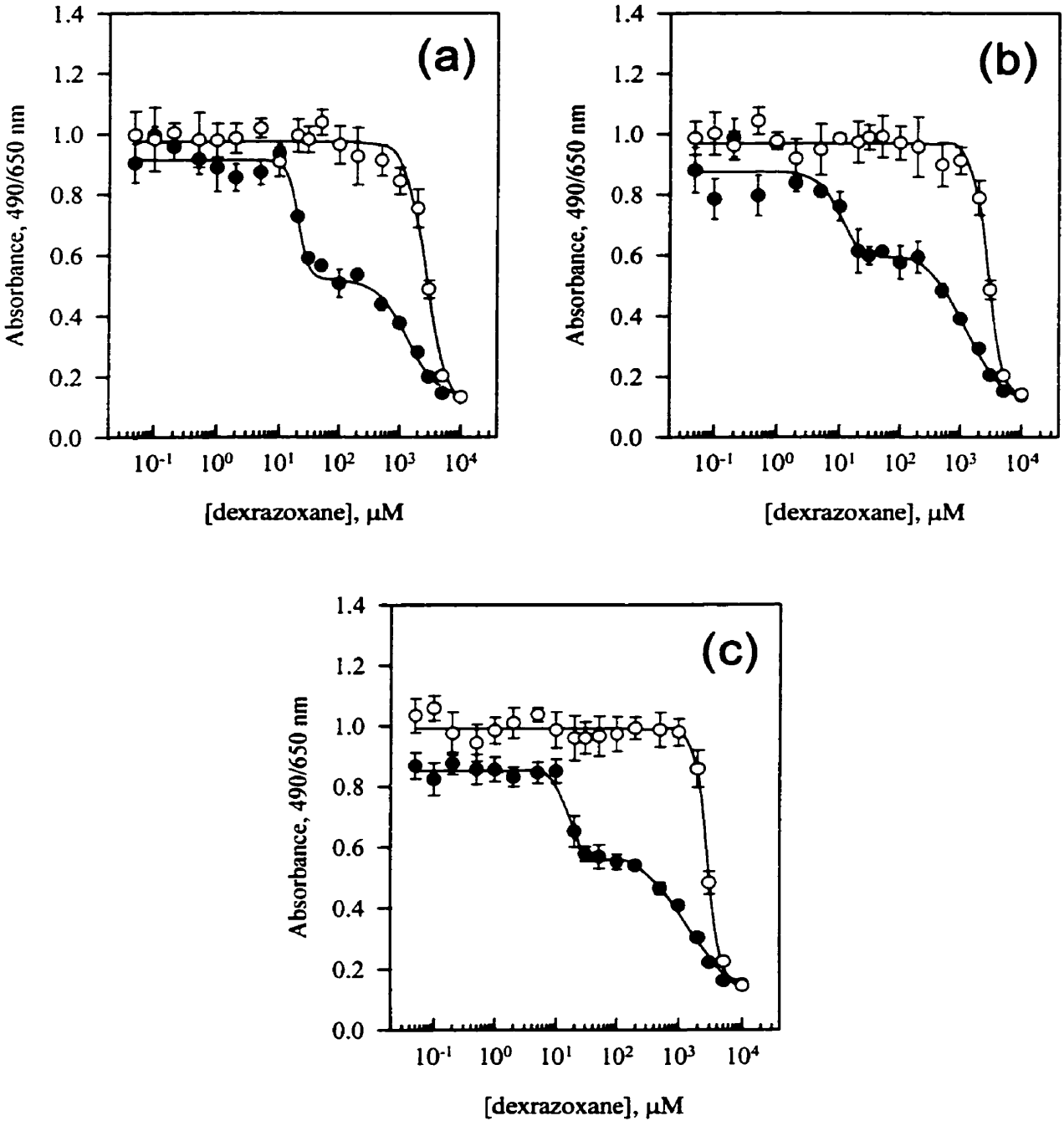

Fig. 4.7. MTS analysis of dexrazoxane-mediated growth inhibition towards K562 and K562/DZ1 cells in the presence of verapamil. K562 (●) and K562/DZ1 (○) cells were treated with (a) 0 μM, (b) 3 μM, or (c) 10 μM of verapamil and then incubated for 72 hr in the presence of dexrazoxane. Absorbances at 490/650 nm were determined after a 3 hr incubation with MTS reagent. The curves represent the results of least squares non-linear regression fits of measured values to a four-parameter logistic equation. The error bars represent standard deviations. The lowest concentrations are the zero values, plotted for convenience on a logarithmic scale with arbitrary values.

4.7 Examination of erythroid-like differentiation and apoptosis in K562/DZ1 cells upon exposure to dexrazoxane

4.7.1 Introduction

In Chapter 3 it was shown that the bisdioxopiperazines dexrazoxane, ICRF-154 and ICRF-193 were all able to induce differentiation of K562 cells towards an erythroid lineage and cause delayed apoptosis. These results were inferred to be a consequence of the catalytic inhibition of topoisomerase II. Although the exact mechanism of drug resistance exhibited by K562/DZ1 cells is not yet known, it was important, as described in the following section to examine whether these cells were able to undergo the process of differentiation or apoptosis in the presence of dexrazoxane. A negative result towards the induction of either of these processes would suggest that topoisomerase II is not readily capable of being inhibited in K562/DZ1 cells. This result would thus lead to the speculation that a mutation in topoisomerase II or an alteration in its activity may be responsible for the enhanced cross-resistance observed in these cells.

4.7.2 Methods

4.7.2.1 Assessment of growth characteristics and hemoglobin production in K562/DZ1 cells exposed to dexrazoxane

Exponentially growing K562 and K562/DZ1 cells were diluted with DMEM/FCS to starting cell densities of $8x10^5$ cells/mL and $2.1x10^5$ cells/mL, repsectively in T-75 flasks. This was followed by the administration of a requiste concentration of dexrazoxane at <10% (v/v), prepared as described in Section 4.2.2 such that the final concentration in

culture was 100 μM. Cells were aseptically removed daily, centrifuged at 250 *g* for 12 min, and resuspended in ~80% (v/v) fresh DMEM/FCS to total volumes that allowed for the attainment of cell densities approximately equivalent to that of before centrifugation. This was followed by a subsequent exposure to 100 μM of dexrazoxane, administered in the same fashion as before. Cell densities were determined at indicated times from removed sample aliquots on a model Z_f Coulter counter using a threshold setting of 7 (100 μm aperture tube, 1/amp. = 2, 1/ap.current = 8, diameter cutoff ≅ 8.7 μm), as explained in Appendix A.2. The growth rate and doubling time of K562/DZ1 cells were determined upon the normalization of cell counts (Section 4.2.5.3) using the single exponential rise equation, $C_t = C_o e^{kt}$ as previously described (Section 4.2.5.4). Viability and the relative percentage of benzidine-positive cells staining for hemoglobin expression were assessed as previously described (Section 4.2.5.1 and 4.2.5.2).

4.7.2.2 DNA fragmentation analysis of dexrazoxane-treated K562/DZ1 cells

Concurrent with the analysis of growth characteristics of K562/DZ1 cells exposed daily to dexrazoxane, agarose gel electrophoresis was used in an attempt to identify the presence of apoptotic K562/DZ1 cells by allowing for visualization of endonuclease-mediated cleaved DNA. Genomic DNA was isolated from K562/DZ1 cells at 0, 48, and 96 hr of dexrazoxane exposure and analyzed by agarose gel electrophoresis as explicitly described in Section 3.5.2.4. In brief, at specified intervals approximately $6x10^6$ cells were collected, washed twice with PBS, then lyzed in 400 μL of lysis buffer (10 mM EDTA, 50 mM Tris-base, pH 8, 0.5% (w/v) sodium lauryl sarcosine, 0.5 mg/mL proteinase K) for 1 hr at 50°C, and then treated with 200 μL of DNase-free RNase A (0.5 mg/mL) for an

additional 1 hr at 50°C. Next, genomic DNA was extracted with phenol/chloroform/ isoamyl alcohol (25/24/1), and precipitated with 3 M sodium acetate (pH 5.2) and 2 volumes of ice-cold 100% ethanol before loading. Loading buffer (0.1 M Na_2EDTA, 0.25% (w/v) bromophenol blue, 40% (w/v) sucrose, pH 8.0) and DNA samples (4 μg) were loaded onto a presolidified, 2% (w/v) agarose gel containing 0.2 μg/mL ethidium bromide. Agarose gels were run at 50 V for 2 hr in TBE buffer (0.1 M Tris-base, 0.1 M boric acid, 2 mM Na_2EDTA), then visualized under UV trans-illumination, and photographed with a Polaroid direct screen instant camera DS34, with ISO3000 type 667 Polaroid film (1/8 s exposure, 5.6 f-stop, 30 s development time).

4.7.3 Results

Consistent with their inherent stable resistance, K562/DZ1 cells exposed to dexrazoxane continued to proliferate at an exponential rate of $3.7x10^{-2}$ hr^{-1} with a doubling time of 19 hr (Fig. 4.8a). This result compares highly with the 21 hr doubling time of unexposed control K562/DZ1 cells (Fig. 4.5) suggesting that dexrazoxane does not retard the growth of K562/DZ1 cells in the same manner as it does with parental K562 cells. Additionally, after 96 hr of dexrazoxane exposure K562/DZ1 cells were ~100% viable as assessed by trypan blue dye exclusion analysis, and cell morhpology remained indistinguishable from control unexposed cells.

Previously it was shown that prior to their cloning, the relative percentage of dexrazoxane-resistant K562RB cells expressing hemoglobin gradually diminished (Fig. 4.1b). At the time of their isolation into K562/DZ clones 1-10, K562RB cells exhibited a pre-cloning hemoglobin expression level of ~6%, as assessed by benzidine staining (data not shown). It was therefore interesting to identify first what was the average level of hemoglobin expression in K562/DZ1 cells, and second what would be the effect of dexrazoxane on this expression level. Three months after cloning and growth in drug-free medium K562/DZ1 cells were shown to exhibit a level of benzidine-positivity of ~1.1-1.4%. This result, which is twice the level expressed in parent K562 cells (~0.3-0.5%, Section 3.4.3.1) suggests that although hemoglobin containing cells were not maintained as a representative proportion of the population after cloning, control K562/DZ1 cells do in fact exhibit the appearance of a partially differentiated state. After 144 hr of daily exposure to dexrazoxane the percentage of benzidine-stained K562/DZ1 cells marginally increased to ~2.5% (Fig. 4.8b). However, this apparent increasing trend was subsequently

deemed non-significant, by statistical linear regression analysis. Dexrazoxane-treated K562/DZ1 cells appeared identical to control cells in terms of size (~14 μm diameter), and shape (circular). This result clearly differs from that of parent K562 cells exposed to dexrazoxane for the same period of time. Dexrazoxane-treated K562 cells were not only shown to exhibit a distinct morphology, and enlarged cell size (Section 3.4.3), but also significantly ($p<0.001$) increased in hemoglobin expression relative to the duration of exposure (Fig. 3.16 and 4.8). Agarose gel electrophoresis of dexrazoxane-treated chromosomal K562/DZ1 DNA is displayed in Fig. 4.9. After 48 and 96 hr of dexrazoxane exposure, electrophoretic migration of DNA was identical to that of the control with no observable apperance of a ladder-like pattern of DNA fragments, as previously seen in parent K562 cells (Fig. 3.24). Although this technique alone does not give conclusive proof of apoptosis, it is reasonable to assume, based also in part on the lack of a decline in viability, that apoptosis was not induced in K562/DZ1 cells upon dexrazoxane exposure.

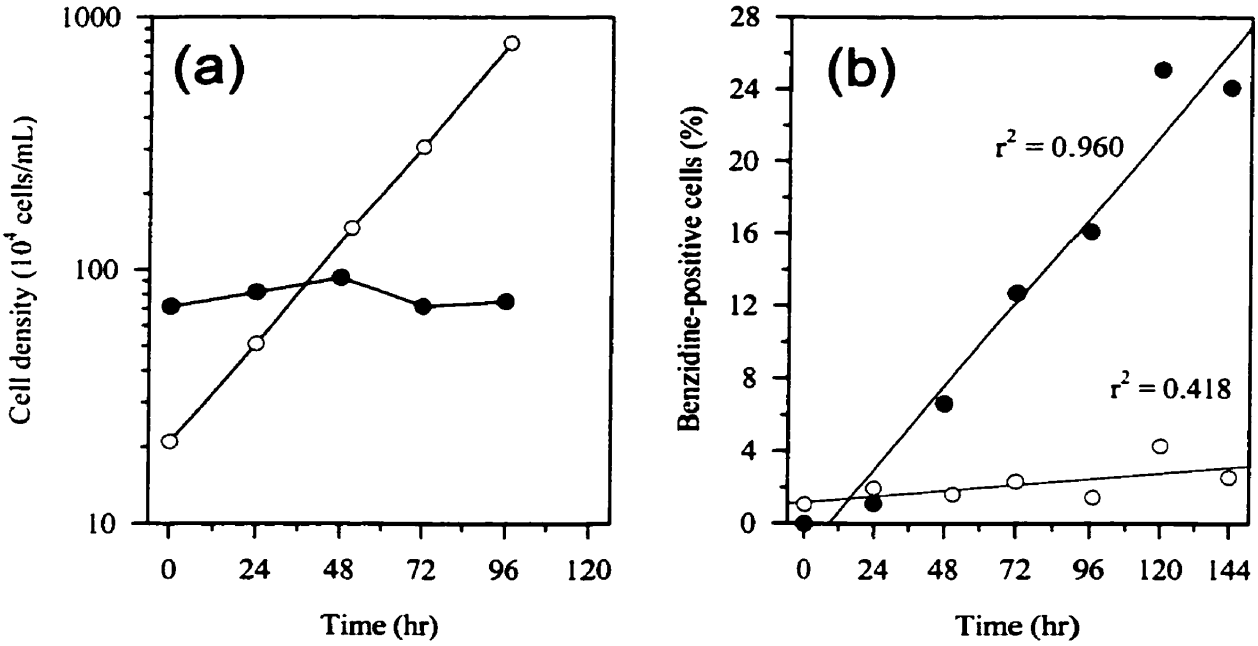

Fig. 4.8. Effects of dexrazoxane on the growth and production of hemoglobin in K562 and K562/DZ1 cells. K562 (●) and K562/DZ1 (○) cells were seeded at $8x10^5$ and $2.1x10^5$ cells/mL, respectively and treated daily with 100 μM dexrazoxane with media replacement. At indicated times, samples were removed and (a) cell densities were determined using a Coulter counter (threshold 7, 100 μm aperture, diameter cutoff ≅ 8.7 μm) followed by normalization; and (b) hemoglobin expression was measured by benzidine staining. Over a period of 96 hr of dexrazoxane exposure, viability was not compromised in K562/DZ1 cells and was maintained at a level of ~100% (data not shown). K562/DZ1 doubling time in the presence of dexrazoxane was found to be 19 hr. A highly significant relationship ($p<0.001$) between hemoglobin production and dexrazoxane exposure was identified only in K562 cells by statistical linear regression analysis. All K562 data presented here is re-plotted from from Fig. 3.13.

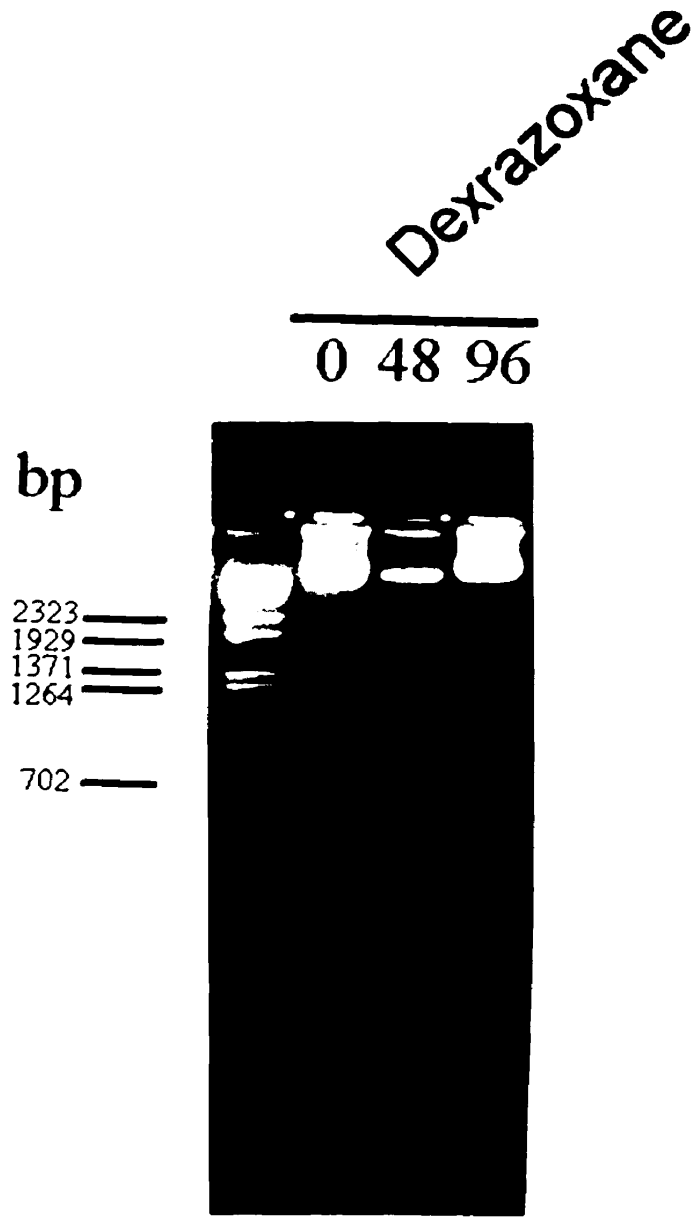

Fig. 4.9. Agarose gel electrophoresis of DNA extracted from K562/DZ1 cells exposed to dexrazoxane. K562/DZ1 cells were seeded at $21x10^5$ cells/mL and treated daily with 100 μM dexrazoxane with media replacement. At indicated times of dexrazoxane exposure (0 hr: *lane 2*, 48 hr: *lane 3*, 96 hr: *lane 4*) DNA was extracted from removed cell samples as described in Section 3.5.2.4 and analyzed on a 2% (w/v) agarose gel containing 0.2 μg/mL ethidium bromide, run at 50 V for 2 hr. The lowest bands on the Lambda BstE II digest molecular weight marker lane (*lane 1*) represent DNA with a molecular weight equivalent of 2323, 1929, 1371, 1264, and 702 base pairs, respectively.

4.8 Discussion

In the present study a human erythroleukemic K562 cell line was selected for resistance by continuous daily exposure to a relatively high concentration of dexrazoxane. Cells were exposed to dexrazoxane for the total duration of two months with a two week intermittent period of cell recovery after the first two weeks of treatment. As reviewed earlier in Section 3.6, K562 cells are predisposed to a greater survival capacity in the presence of cytotoxic drugs than other leukemic cell lines due in part to the expression of the BCR-ABL tyrosine kinase [26,27]. The constitutive action of this enzyme is to transduce signals downstream to maintain relatively high levels of the presumed channel protein *bcl-X_L* thereby suppressing the transport of apoptotic related signals [27-29]. The refractoriness of K562 cells towards drug-induced cell cycle arrest was sufficiently overcome by utlizing a regimen of continuous exposure to a concentration of dexrazoxane 5-fold greater than the median growth inhibitory concentration of 20.3 μM (Table 4.3). It is possible that by using such an intense drugging protocol rather than gradually increasing the concentration of dexrazoxane, that resistant cells became a predominant representative proportion of the cell population after only a short period of time.

Upon the establishment of a dexrazoxane-resistant K562 cell population ten sublines were subsequently cloned and named K562/DZ1-10. Although three distinct groups of K562/DZ clones were classified based on their respective doubling times (Table 4.2), all clones exhibited the same degree of resistance towards dexrazoxane within experimental error (Table 4.3). Overall, these K562/DZ clones were shown to be ~84-110-fold resistant to dexrazoxane, as compared to parental K562 cells. Despite the fact that only the K562/DZ1 cell line was chosen for use in all future experiments it is interesting to

speculate whether a difference truly exists between all of the dexrazoxane-resistant clones isolated. If different and possibly concurrent biochemical mechanisms of drug resistance exist in these cells would this result in such similar degrees of resistance towards dexrazoxane? In particular, as discussed below in further detail, resistance may have developed as a result of the expression of an altered, possibly mutated form of topoisomerase II. It remains to be seen whether all of these K562/DZ clones possess the same or different functional mutations which confer an equal degree of resistance. The existence of different mutations in topoisomerase II would provide some explanation of the various doubling times observed. Cell cycling may have been seen to prolong to various degrees by topoisomerase II enzymes with different functional abilities. The essential roles of topoisomerase II during mitosis in the segregation and condensation of chromosomes are of particular concern with respect to such possible differences. Furthermore, the establishment of several dexrazoxane-resistant cell lines with different functional mutations may prove extremely useful in further characterizing the biochemical and molecular interactions between the bisdioxopiperazines and topoisomerase II.

The cloned K562/DZ1 cell line chosen for all future studies exhibited one of the fastest doubling times and highest levels of dexrazoxane-resistance of all K562/DZ clones (Table 4.2 and 4.3). After a two month period of growth in drug-free media, K562/DZ1 cells exhibited a doubling time of 21 hr (Fig. 4.5), which was relatively close to the original assessment of 23 hr (Table 4.2) and to that of parental K562 cells, ~19 hr (Table 3.4). The cloned K562/DZ1 cell line was initially, 105-fold resistant to dexrazoxane exhibiting an IC_{50} value of 2125 ± 250 μM as compared to parental K562 cells, 20.3 ± 1.9 μM (Table 4.3). After two and three months of growth in drug-free media K562/DZ1 cells

were re-determined to be 126-fold and 138-fold resistant to dexrazoxane, respectively (Table 4.4 and 4.5). Given the range of standard error in these subsequent determinations of dexrazoxane IC_{50}, 2568 ± 174 μM and 2804 ± 244 μM respectively dexrazoxane-resistance appeared to remain competently stable. Although it is common practice to return to the original stock cell population from cryogenic storage every 2-3 months, it remains to be seen whether the K562/DZ1 cell line retains its resistance towards dexrazoxane for a much longer period of time when grown in drug-free media.

The K562/DZ1 cell line was also shown to display a high degree of cross-resistance towards other structurally similar bisdioxopiperazine analogs (Fig. 4.6 and Table 4.4). In particular, K562/DZ1 cells were immeasurably greater than 93-fold and 4.5-fold resistant to ICRF-193 and ICRF-154, respectively (Table 4.4). Furthermore, K562/DZ1 cells were moderately cross-resistant towards the cleavable complex-forming topoisomerase II inhibitors etoposide and doxorubicin [19], exhibiting resistance factors of 4-fold and 2.4-fold, respectively (Table 4.4). Although future studies may or may not identify the presence of point mutations in the genes encoding the topoisomerase II isoforms, it is reasonable to speculate that the higher level of resistance exhibited towards the bisdioxopiperazines could be due to a site-specific point mutation which alters the conformation of topoisomerase II. As a result, it may be possible that cleavable complex-forming inhibitors are only partially hindered in their ability to stably interact with K562/DZ1 topoisomerase II, thus leading to a more moderate degree of resistance when compared to parental K562 cells.

Acquired resistance to various topoisomerase II inhibitors is often correlated with a reduced expression of topoisomerase II protein levels [30-32], a change in the

phosphorylation status of topoisomerase II [33-35], altered localization of topoisomerase II [36], a decrease in drug accumulation through the expression of the MDR phenotype [1,37-39], and/or mutation(s) resulting in a change in the biochemical activities of topoisomerase II [30,39,40]. A dexrazoxane-resistant (1500-fold) CHO cell line (DZR) previously established in our laboratory [18], was later shown to be truly 500-fold resistant to dexrazoxane (Table 2.1) [41]. In contrast to K562/DZ1 cells, cross-resistance towards ICRF-193, a stronger catalytic topoisomerase II inhibitor [15,42] was much less in DZR cells thus suggesting two possible differing mechanisms of resistance, or different titers of the topoisomerase II enzyme present. Although DZR cells possessed reduced levels of topoisomerase II as compared to parental CHO cells [18], acquired drug resistance was subsequently attributed to a Thr48Ile point mutation in topoisomerase II and decreased drug-induced DNA-enzyme complexes [43]. At this time the exact mechanism of drug resistance present in K562/DZ1 cells has not been elucidated although some efforts have been made to confirm, or rule out the above mentioned mechanisms of acquired drug resistance. The possibility that K562/DZ1 cells express the MDR phenotype has all but been eliminated. Verapamil was shown to have no significant effect on dexrazoxane-mediated cytotoxicity in either K562/DZ1 cells or parental K562 cells (Fig. 4.7 and Table 4.5). Although this result suggests that K562/DZ1 cells did not acquire dexrazoxane resistance through the over-expression of P-glycoprotein the possibility of cross-resistance towards other classic MDR-related cytotoxic agents necessitates further exploration. Moreover, K562/DZ1 cells may be mediated by other atypical mechanisms of MDR. Currently, the expression of other drug transport protein pumps such as the MDR-associated protein (MRP) [12,37] and lung resistance protein (LRP) [44] are emerging as

clinically relevant mechanisms of MDR [10]. These efflux transporter pumps mediate resistance against a broad spectrum of drugs, similar but not identical to those of P-glycoprotein [12,44,45] and have been found to be over-expressed in normal and tumor tissue cells concurrent with or in the absence of P-glycoprotein expression [12,44].

Assuming that the same amount of drug reaches the topoisomerase II target, cells with higher expression levels of topoisomerase II are typically more drug-sensitive [12,46-48]. Although this may be true of a number of different drug-resistant cell lines, decreased topoisomerase II levels has been observed to lead to an increased drug-sensitivity, at least with respect to the bisdioxopiperazines [48]. In particular, an etoposide-resistant K562 cell line (K/VP.5) with reduced topoisomerase II expression levels has been shown to be more sensitive to dexrazoxane than parental K562 cells [46]. Through collaboration with Dr. J.C. Yalowich (Dept. Pharmacology, University of Pittsburgh School of Medicine and Cancer Institute), K562/DZ1 cells and a similarly established dexrazoxane-resistant K562/I1 cell line have recently been further characterized. Although K562/I1 cells were established by exposure to 1000 μM dexrazoxane, as opposed to 100 μM in the case of K562/DZ1 cells these cells were only 30-fold resistant to dexrazoxane [49]. Recent findings have revealed that both K562/DZ1 and K562/I1 cell lines exhibit topoisomerase II α and β levels unchanged from that of parental K562 cells [49]. This result therefore suggests that either dexrazoxane-resistant K562 cell line did not acquire resistance through the expression of altered topoisomerase II protein levels.

To date, only a limited number of cell lines have been selected for resistance towards bisdioxopiperazine analogs [50-52]. Although there exist inherent differences between these cell lines they all similarly exhibit a high level of cross-resistance towards

other bisdioxopiperazines and moderate levels of cross-resistance towards cleavable complex-forming topoisomerase II inhibitors. Exhibiting similar attributes to our previously established DZR cells [18], a CHO-derived ICRF-159 resistant (300-fold) cell line (CHO/159-1) has also been described as possessing 50% reduced topoisomerase IIα content [18]. A human small lung cancer NYH cell line selected for resistance towards dexrazoxane (5.5-fold) were on the other hand slightly hypersensitive to the topoisomerase II poisons doxorubicin and etoposide due in part to a 25% increase in topoisomerase IIα level [51].

Mutations acquired in cells exposed to the bisdioxopiperazines have not yet been extensively described. Upon inhibition, topoisomerase II may mediate mutagenicity through illegitimate recombination of non-specific and non-homologous DNA sequences. This may consequently generate deletions, insertions, duplications, substitutions, and/or inversions in the normal genetic structure of cells [53]. Some cell lines selected for resistance towards the bisdioxopiperazines have been shown to possess functional mutations in the proximal NH_2-terminal clamp part of topoisomerase II [43,50] as well as in the Walker A consensus ATP binding region [51]. In particular, aside from the Thr48Ile point mutation previously identified in DZR cells [43], CHO/159-1 cells have been described as possessing a Tyr49Phe point mutation and a sequence deletion in highly conserved regions of topoisomerase II [50]. Although such mutations maintain normal topoisomerase II functions in the presence of bisdioxopiperazines, resistance may directly be the result of a sustained open-clamp topoisomerase II state due to decreased ATP binding [51], and/or destabilized monomer-monomer interaction during the closed clamp formation [50,54,55]. Finally, these mutations may be specific to bisdioxopiperazine

resistance [50] in that they lie distal to the Walker B/dinucleotide binding domain or the catalytic active site Tyr804 residue where other cell lines, selected for resistance towards topoisomerase II poisons commonly possess mutations [56,57].

The catalytic inhibitors of topoisomerase II known as the bisdioxopiperazines (dexrazoxane, ICRF-193, and ICRF-154) as well as etoposide, a topoisomerase II poison have all been previously demonstrated to induce erythroid-like differentiation and delayed apoptosis in K562 cells (Chapter 3). After 96 hr of dexrazoxane treatment, agarose gel electrophoresis of isolated genomic K562/DZ1 DNA revealed an absence of any laddering pattern representative of endonuclease-mediated DNA fragmentation. These results suggested that K562/DZ1 cells were extremely resistant to the induction of apoptosis. In contrast though, a dexrazoxane-resistant CEM cell line which possesses increased expression levels of topoisomerase IIα has been shown to exhibit altered apoptotic responses to dexrazoxane, prominent 48-72 hr later than parental K562 cells [58]. Furthermore, it would be interesting to study in K562/DZ1 cells the effect of various topoisomerase II inhibitors on the expression of such apoptotic-related genes as *bcr-abl*, *bcl-X*, and c-*myb*. Laroche-Clary *et al.* [59] has shown by quantifying the expression of amplified apoptotic genes that the topoisomerase II poison amsacrine is able to induce apoptosis in an MDR-K562 variant, selected with doxorubicin but not in wild-type K562 cells. Although studies are currently underway world-wide to further understand the interactions between different topoisomerase II inhibitors and this target enzyme, the question may still remain: how is the mechanism/degree of resistance, or topoisomerase II inhibition related to the cell-line specific induced expression of apoptotic and/or differentiation related genes?

In the following study dexrazoxane-resistant K562/DZ1 cells were also shown to exhibit, in their natural state a relative hemoglobin expression level greater than that of parental K562 cells (Fig. 4.8b). Upon exposure to dexrazoxane, hemoglobin expression increased marginally without statistical significance (Fig. 4.8b) as cells continued to proliferate unaltered (Fig. 4.8a). An etoposide-resistant K562 cell line (K/VP.5) has been previously described as expressing a level of hemoglobin content 5-fold greater than parental K562 cells [60]. After a 24 hr exposure to 50 μM of hemin, hemoglobin content in K/VP.5 and K562 cells increased 5-fold from control levels [60]. Although K/VP.5 cells differ from K562/DZ1 cells in that the former contains reduced levels of topoisomerase II mRNA [40], these results raise the question of whether erythroid-like differentiation can truly be induced in cell lines selected for resistance towards topoisomerase II inhibitory agents. In particular, future studies may explore the susceptibility of K562/DZ1 cells to the induction of megakaryocyte, granulocytic, and/or erythroid-like differentiation by various topoisomerase II inhibitors and other inducers.

Overall, the results of the present study have indicated the successful establishment of a dexrazoxane-resistant human erythroleukemic K562 cell line with acquired cross-resistance towards other types of topoisomerase II inhibitors. Future studies are planned to address some of the many questions mentioned above, with the initial interest of characterizing the exact mechanism of drug resistance in K562/DZ1 cells. The usefulness of this particular dexrazoxane-resistant cell line may yet serve to complement the studies of others towards not only understanding topoisomerase II-targeted drug interactions but also acquiring insight into the drug-induced function and activity of topoisomerase II during apoptosis and differentiation.

4.9 References

1. Ma, D.F.D. and Bell, D.R. Multidrug resistance and p-glycoprotein in human cancer. *Aust NZ J Med.*, **19**: 736-743, 1989.

2. Arceci, R. Clinical significance of p-glycoprotein in multidrug resistance malignancies. *Blood*, **81**: 2215-2222, 1993.

3. Goldie, J.H. and Coldman, A.J. Quantitative model for multiple levels of drug resistance in clinical tumors. *Cancer. Treat. Rep.*, **67**: 923-931, 1983.

4. Kartner, N. and Ling, V. Multidrug resistance in cancer. *Sci. Am.*, **260**: 44-51, 1989.

5. Hayes, J.D. and Wolf, C.R. Molecular mechanisms of drug resistance. *J. Biochem.*, **272**: 281-295, 1990.

6. Hall, A., Cattan, A.R., and Proctor, S.J. Mechanisms of drug resistance in acute leukaemia. *Leuk. Res.*, **13**: 351-356, 1989.

7. Borst, P. Genetic mechanisms of drug resistance. *Reviews in Oncology*, **4**: 87-95, 1991.

8. Ling, V. Multidrug resistance and p-glycoprotein expression. In: P.V. Wooley and K.D. Tew (eds.), Mechanisms of Drug Resistance in Neoplastic Cells., pp. 197-209, San Diego, CA: Academic Press. 1988.

9. Gerlach, J.H., Kartner, N., Bell, D.R., and Ling, V. *Cancer Surveys*, **5**: 26-41, 1986.

10. Trambas, C.M., Muller, H.K., and Woods, G.M. P-glycoprotein mediated multidrug resistance and its implications for pathology. *Pathology*, **29**: 122-130, 1997.

11. Riordan, J.R. and Ling, V. Genetic and biochemical characterization of multidrug resistance. *Pharmacol. Ther.*, **28**: 51-75, 1985.

12. Loe, D.W., Deeley, R.G., and Cole, S.P.C. Biology of the multidrug resistance-associated protein, MRP. *Eur. J. Cancer*, **32A**: 945-957, 1996.

13. Gianni, L. Anthracycline resistance: the problem and its current definition. *Semin. Oncol.*, **24**: S10-11-S10-17, 1997.

14. Gopalakrishnan, T.V. and Anderson, W.F. Mouse erythroleukemia cells. *Methods Enzymol.*, **58:506-11**: 506-511, 1979.

15. Hasinoff, B.B., Kuschak, T.I., Yalowich, J.C., and Creighton, A.M. A QSAR study comparing the cytotoxicity and DNA topoisomerase II inhibitory effects of bisdioxopiperazine analogs of ICRF-187 (dexrazoxane). *Biochem. Pharm.*, **50**: 953-958, 1995.

16. Hasinoff, B.B. Pharmacodynamics of the hydrolysis-activation of the cardioprotective agent (+)-1,2-bis(3,5-dioxopiperazinyl-1-yl)propane. *J. Pharm. Sci.*, **83**: 64-67, 1994.

17. Tanabe, K., Ikebuchi, K., Ishida, R., and Andoh, T. Inhibition of topoiosmerase II by antitumour agents bis(2,6-dioxopiperazine) derivatives. *Cancer Res.*, **51**: 4903-4908, 1991.

18. Hasinoff, B.B., Kuschak, T.I., Creighton, A.M., Fattman, C.L., Allan, W.P., Thampatty, P., and Yalowich, J.C. Characterization of a Chinese hamster ovary cell line with acquired resistance to the bisdioxopiperazine dexrazoxane (ICRF-187) catalytic inhibitor of topoisomerase II. *Biochem. Pharm.*, **53**: 1843-1853, 1997.

19. Corbett, A.H. and Osheroff, N. When good enzymes go bad: conversion of topoisomerase II to a cellular toxin by antineoplastic drugs. *Chem. Res. Toxicol.*, **6**: 585-597, 1993.

20. Juranka, P.F., Zastawny, R.L., and Ling, V. P-glycoprotein: multidrug-resistance and a superfamily of membrane-associated transport proteins. *FASEB*, **3**: 2583-2591, 1989.

21. Hegewisch-Becker, S. MDR1 reversal: criteria for clinical trials designed to overcome the multidrug resistance phenotype. *Leukemia*, **10**: S32-S381996.

22. Roninson, I.B. The role of the mdr1 (p-glycoprotein) gene in multidrug resistance in vitro and in vivo. *Biochem. Pharm.*, **43**: 95-102, 1992.

23. Bradley, G. and Ling, V. P-glycoprotein, multidrug resistance and tumor progression. *Cancer and Metastasis Reviews*, **13**: 223-233, 1994.

24. Salmon, S.E., Dalton, W.S., Grogan, T.M., Plezia, P., Lehnert, M., Roe, D.J., and Miller, T.P. Multidrug-resistant myeloma: laboratory and clinical effects of verapamil as a chemosensitizer. *Blood*, **78**: 44-50, 1991.

25. Dalton, W.S., Grogan, T.M., Meltzer, P.S., Scheper, R.J., Durie, B.G., Taylor, C.W., and Miller, T.P. Drug-resistance in multiple myeloma and non-Hodgkin's lymphoma: detection of P-glycoprotein and potential circumvention by addition of verapamil to chemotherapy. *J. Clin. Oncol.*, **7**: 415-424, 1989.

26. Evans, C.A., Owen-Lynch, P.J., Whetton, A.D., and Dive, C. Activation of the Abelson tyrosine kinase activity is associated with suppression of apoptosis in hemopoietic cells. *Cancer Res.*, **53**: 1735-1738, 1993.

27. McGahon, A., Bissonnette, R., Schmitt, M., Cotter, K.M., Green, D.R., and Cotter, T.G. BCR-ABL maintains resistance of chronic myelogenous leukemia cells to apoptotic cell death [published erratum appears in Blood 1994 Jun 15;83(12):3835]. *Blood*, **83**: 1179-1187, 1994.

28. Cullen, W.C. and McDonald, T.P. Comparison of stereologic techniques for the quantification of megakaryocyte size and number. *Exp. Hematol.*, **14**: 782-788, 1986.

29. McKenna, S.L. and Cotter, T.G. Functional aspects of apoptosis in hematopoiesis and consequences of failure. *Adv. Cancer Res.*, **71:121-64**: 121-164, 1997.

30. Webb, C.D., Latham, M.D., Lock, R.B., and Sullivan, D.M. Attenuated topoisomerase content directly correlates with a low level of drug resistance in a Chinese hamster ovary cell line. *Cancer Res.*, **51**: 6542-6549, 1991.

31. Osheroff, N., Corbett, A.H., and Robinson, M.J. Mechanism of action of topoisomerase II-targeted antineoplastic drugs. *Adv. Pharmacol.*, **29B**: 105-126, 1994.

32. Chen, G.L., Yang, L., Rowe, T.C., Halligan, B.D., Tewey, K.M., and Liu, L.F. Nonintercalative antitumor drugs interfere with the breakage-reunion reaction of mammalian DNA topoisomerase II. *J. Biol. Chem.*, **259**: 13560-13566, 1984.

33. Ritke, M.K., Roberts, D., Allan, W.P., Raymond, J., Bergoltz, V.V., and Yalowich, J.C. Altered stability of etoposide-induced topoisomerase II-DNA complexes in resistant human leukaemia K562 cells. *Br. J. Cancer*, **69**: 687-697, 1994.

34. Ritke, M.K., Allan, W.P., Fattman, C.L., Gunduz, N.N., and Yalowich, J.C. Reduced phosphorylation of topoisomerase II in etoposide-resistant human leukemia K562 cells. *Am. Soc. Pharm. Exp. Ther.*, **46**: 58-66, 1994.

35. Takano, H., Kohno, K., Ono, M., Uchida, Y., and Kuwano, M. Increased phosphorylation of DNA topoisomerase II in etoposide-resistant mutants of human cancer KB cells. *Cancer Res.*, **51**: 3951-3957, 1991.

36. Feldhoff, P.W., Mirski, S.E.L., Cole, S.P.C., and Sullivan, D.M. Altered subcellular distribution of topoisomerase II-alpha in a drug-resistant human small lung cancer cell line. *Cancer Res.*, **54**: 756-762, 1994.

37. Lautier, D., Canitrot, Y., Deeley, R.G., and Cole, S.P.C. Multidrug resistance mediated by the multidrug resistance protein (MRP) gene. *Biochem. Pharm.*, **52**: 967-977, 1996.

38. Matsuo, K., Kohno, K., Takano, H., Sato, S., Kiue, A., and Kuwano, M. Reduction of drug accumulation and DNA topoisomerase II activity in acquired teniposide-resistant human cancer KB cell lines. *Cancer Res.*, **50**: 5819-5824, 1990.

39. Kamath, N., Grabowski, D., Ford, J., Kerrigan, D., Pommier, Y., and Ganapathi, R. Overexpression of P-glycoprotein and alterations in topoisomerase II in P388 mouse leukemia cells selected *in vivo* for resistance to mitoxantrone. *Biochem. Pharm.*, **44**: 937-945, 1992.

40. Ritke, M.K. and Yalowich, J.C. Altered gene expression in human leukemia K562 cells selected for resistance to etoposide. *Biochem. Pharm.*, **46**: 2007-2020, 1993.

41. Hasinoff, B.B., Creighton, A.M., Kozlowska, H., Thampatty, P., Allan, W.P., and Yalowich, J.C. Mitindomide is a catalytic inhibitor of DNA topoisomerase II that acts at the bisdioxopiperazine binding site. *Mol. Pharmacol.*, **52**: 839-845, 1997.

42. Ishida, R., Miki, T., Narita, T., Yui, R., Sato, M., Utsumi, K.R., Tanabe, K., and Andoh, T. Inhibition of intracellular topoisomerase II by antitumor bis(2,6-dioxopiperazine) derivatives: mode of cell growth inhibition distinct from that of cleavable complex-forming type inhibitors. *Cancer Res.*, **51**: 4909-4916, 1991.

43. Yalowich, J.C., Thampatty, P., Allan, W.P., Chee, G.-L., and Hasinoff, B.B. Acquired resistance to ICRF-187 (dexrazoxane) in a CHO cell line is associated with a point mutation in DNA topoisomerase II-alpha (topo II) and decreased drug-induced DNA-enzyme complexes. *Proc Am Assoc Cancer Res*, **39**: 375, 1998.

44. Krishan, A.K., Fitz, C.M., and Andritsch, I. Drug retention, efflux, and resistance in tumor cells. *Cytometry*, **29**: 279-285, 1997.

45. Berger, W., Elbling, L., Hauptmann, E., and Micksche, M. Expression of the multidrug resistance-associated protein (MRP) and chemoresistance of human non-small-cell lung cancer cells. *Int. J. Cancer*, **73**: 84-93, 1997.

46. Fattman, C.L., Allan, W.P., Hasinoff, B.B., and Yalowich, J.C. Collateral sensitivity to the bisdioxopiperazine dexrazoxane (ICRF-187) in etoposide (VP-16)-resistant human leukemia K562 cells. *Biochem. Pharm.*, **52**: 635-642, 1996.

47. Davies, S.L., Bergh, J., Harris, A.L., and Hickson, I.D. Response to ICRF-159 in cell lines resistant to cleavable complex- forming topoisomerase II inhibitors. *Br. J. Cancer*, **75**: 816-821, 1997.

48. Ishida, R., Hamatake, M., Wasserman, R.A., Nitiss, J.L., and Wang, J.C. DNA topoisomerase II is the molecular target of bisdioxopiperazine derivatives ICRF-159 and ICRF-193 in *Saccharomyces cerevisiae. Cancer Res.*, **55**: 2299-2303, 1995.

49. Yalowich, J.C., Khelifa, T., Allan, W.P., Abram, M.E., and Hasinoff, B.B. Characterization of K562 cell lines selected for resistance to the DNA topoisomerase II inhibitor dexrazoxane (ICRF-187). *Proc Am Assoc Cancer Res*, **00**: 00, 2000.

50. Sehested, M., Wessel, I., Jensen, L.H., Holm, B., Oliveri, R.S., Kenwrick, S., Creighton, A.M., Nitiss, J.L., and Jensen, P.B. Chinese hamster ovary cells resistant to the topoisomerase II catalytic inhibitor ICRF-159: a Tyr49Phe mutation confers high-level resistance to bisdioxopiperazines. *Cancer Res.*, **58**: 1460-1468, 1998.

51. Wessel, I., Jensen, L.H., Jensen, P.B., Falck, J., Rose, A., Roerth, M., Nitiss, J.L., and Sehested, M. Human small cell lung cancer NYH cells selected for resistance to the bisdioxopiperazine topoisomerase II catalytic inhibitor ICRF-187 demonstrate a functional R162Q mutation in the walker A consensus ATP binding domain of the alpha isoform. *Cancer Res.*, **59**: 3442-3450, 1999.

52. White, K. and Creighton, A.M. Mechanistic studies with a cell line resistant to ICRF-159. *Br. J. Cancer*, **34**: 1976.

53. Baguley, B.C. and Ferguson, L.R. Mutagenic properties of topoisomerase-targeted drugs. *Biochem. Biophys. Acta.*, **1400**: 213-222, 1998.

54. Roca, J. and Wang, J.C. DNA transport by a type II DNA topoisomerase: evidence in favor of a two-gate mechanism. *Cell*, **77**: 609-616, 1994.

55. Roca, J., Ishida, R., Berger, J.M., Andoh, T., and Wang, J.C. Antitumor bisdioxopiperazines inhibit yeast DNA topoisomerase II by trapping the enzyme in the form of a closed protein clamp. *Proc. Natl. Acad. Sci.U.S.A.*, **91**: 1781-1785, 1994.

56. Chan, V.T., Ng, S.W., Eder, J.P., and Schnipper, L.E. Molecular cloning and identification of a point mutation in the topoisomerase II cDNA from an etoposide-resistant Chinese hamster ovary cell line. *J. Biol. Chem.*, **268**: 2160-2165, 1993.

57. Hinds, M., Diesseroth, K., Mayes, J., Altschuler, E., Jansen, R., Ledley, F.D., and Zwelling, L.A. Identification of a point mutation in the topoisomerase II gene from a human leukemia cell line containing an amsacrine-resistant form of topoisomerase II. *Cancer Res.*, **51**: 4729-4731, 1991.

58. Morgan, S.E., Cadena, R.S., and Beck, W.T. A dexrazoxane (ICRF-187)-resistant CEM cell line expresses enhanced topoisomerase (topo) II [alpha] with altered G2/M checkpoint and apoptotic responses. *Proc Am Assoc Cancer Res*, **40**: 4489, 1999.

59. Laroche-Clary, A., Larrue, A., Vekris, A., and Robert, J. Effect of topoisomerase II inhibitors on the expression of the hybrid gene bcr-abl in doxorubicin-sensitive and resistant K562 cells in relation to the induction of apoptosis. *Proc Am Assoc Cancer Res*, **40**: 4490, 1999.

60. Yalowich, J.C., Gorbunov, N.V., Kozlov, A.V., Allan, W.P., and Kagan, V.E. Mechanisms of nitric oxide protection against tert-butyl hydroperoxide-induced cytotoxicity in iNOS-transduced human erythroleukemia cells. *Biochemistry*, **38**: 10691-10698, 1999.

APPENDIX A:

Calibration, cell counting, and sizing using a model Z_f Coulter counter

A.1 Background information

A.1.1 The Coulter Principle

Electrical sizing, by use of a Coulter counter is a method of flow cytometry. Cells suspended in an electrolyte solution can be counted at a rate of a few thousand cells per second. The main advantages over conventional cell counting methods, such as analysis under a hemacytometer include its ease of use, as well as its high speed and the accuracy of its measurements [1]. The Coulter principle, originally introduced by W.H. Coulter (1953) dictated that each cell that passes through the sizing transducer of the Coulter counter generates an electrical pulse, which contains in its quantity (magnitude) information about the volume (size) of the cell [2]. Displayed in Fig. A.1 is an illustration of a typical Coulter counter. Essentially it consists of a narrow glass tube with an interior grounded electrode and exterior active electrode, all submerged in a diluted solution of cells made from an electrically conducting fluid (an electrolyte such as Isoton II). At the bottom of the glass tube is a small orifice or aperture through which cells flow by suction from the electrolyte suspension into the glass tube. The volume of the electrolyte suspension that enters the orifice and passes between the electrodes is constant, creating an electric current. Each cell passing through the orifice causes a change in the electric resistance of this current from that of the electrolyte alone. Each resistance change is transformed by the current into a pulse-shaped electrical signal, whereby the height of this pulse is representative of the volume of that particular cell. For every pulse generated by a cell

by a cell passing through the orifice a numerical readout is displayed. After the set volume of electrolyte suspended cells passes through the orifice the counting stops revealing a number representative of the number of cells in that set volume. By accounting for the various dilutions made and this set volume, then either the concentration or total number of cells in the original stock solution can be estimated with high statistical relevance [205].

The glass tube of the Coulter counter may be replaced with another one possessing a different aperture or orifice diameter size. Typically the diameter of the orifice can range between 20-200 μm. The choice of a particular orifice diameter depends on the nature of the experiment and the size of the cells or particles being counted. Smaller particles are more difficult to accurately count with a large orifice, just as large particles are hard to count with a small orifice. Upon replacement of an aperture of differing orifice size, the instrument must then be calibrated with standard sized polystyrene latex bead (see Section A.3).

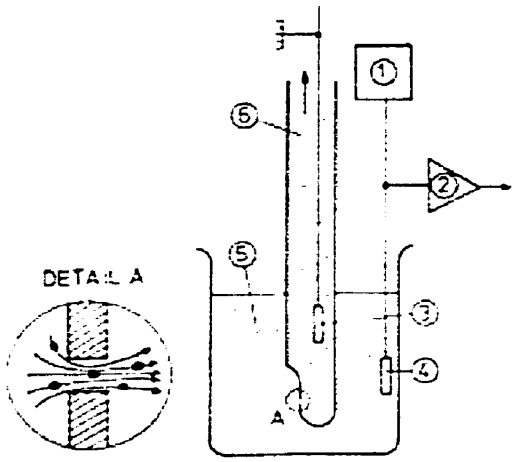

Fig. A.1. A basic illustration of a Coulter flow principle. (1) Current source; (2) amplifier; (3) grounded electrode; (4) active electrode; (5) highly diluted cell suspension; (6) tube where suction is applied. "Detail A" shows the orifice itself with random particle paths.

A.2 General operating procedure

A.2.1 System controls

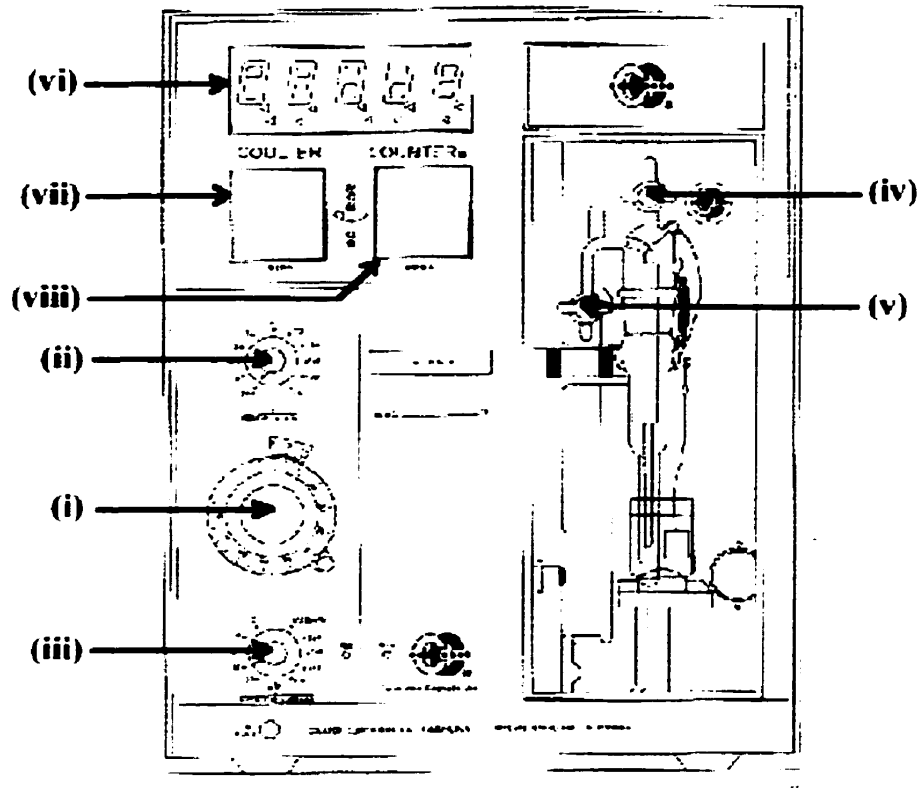

Fig. A.2. The model Z_f Coulter counter.

Table A.1. Description of Coulter counter controls.

	Control / switch	Description of function
(i)	threshold control	-determines the lower size limit of the count
(ii)	1/amplification switch	-adjusts the gain on the amplifier
(iii)	1/aperture current switch	-regulates the amount of current flow through the aperture
(iv)	auxiliary stopcock	-used to flush the aperture tube

(v)	vacuum control stopcock	-used to initiate counting -in vertical "open" position electronic counter is reset -in horizontal "closed" position counting is initiated
(vi)	numeric readout	-displays number of counts for the selected threshold division
(vii)	oscilloscope screen	-provides operator with visual indication of the noise level, clogged aperture, and a pulse pattern representation of cells passing through the orifice
(viii)	debris monitor	-a projection screen to view aperture orifice for possible blockage by debris

A.2.2 Charts and equations for coincidence correction

A common problem experienced with the use of the Coulter counter is the concept of count loss. This dilemma occurs as a result of a coincident passage of cells, or rather more than one cell simultaneously entering the aperture at once and consequently registering as a single pulse and count. With aperture tubes of larger orifice diameters the chance of more than one cell being registered as a single count is much greater, as is the coincidence correction which need to be applied to the registered numeric readout count. This phenomena will also occur in highly concentrated electrolyte cell suspensions and in circumstances when cells have not been well resuspended and exist in the form of aggregated clumps.

The simplest solution to the aforementioned problem is to simply dilute the sample concentration. However, in cases when this is not applicable a correction factor must be employed. These correction factors are justified when dealing with normal distributions of cell populations. Outlined in the following subsections are a series of charts and coincidence correction equations that can be used to correct cell count values for either the 100 μm or 140 μm aperture tubes.

When applying a coincidence correction to cell counts there are first a few points to consider. First, coincidence correction on a count of 10,000 cells per 0.5 mL sample is negligible, whereupon the error is only 3%. Second, counts should be maintained above 1,000 cells per 0.5 mL due the increased accuracy of the Coulter counter in this range. Finally, for counts obtained above 90,000 cells per 0.5 mL of sample then a higher dilution should be used. Counts above such values are less accurate due to the fact that the number of cells passing through the aperture exceeds the maximum speed at which the counting mechanism operates in the Coulter counter.

A.2.2.1 Applying a coincidence correction to a displayed Coulter count

In the following section is outlined the appropriate equations to be used when correcting for the coincident passage of cells through either a 100 μm or 140 μm aperture tube and a 0.5 mL sampling volume. Fig. A.3 depicts the appropriate coincidence correction chart provided by Coulter Electronics (Burlington, ON) for a 0.5 mL sampling volume and a range of aperture tube with different orifice diameters.

Fig. A.3. Coulter counter coincidence correction chart for a 0.5 mL sample volume.

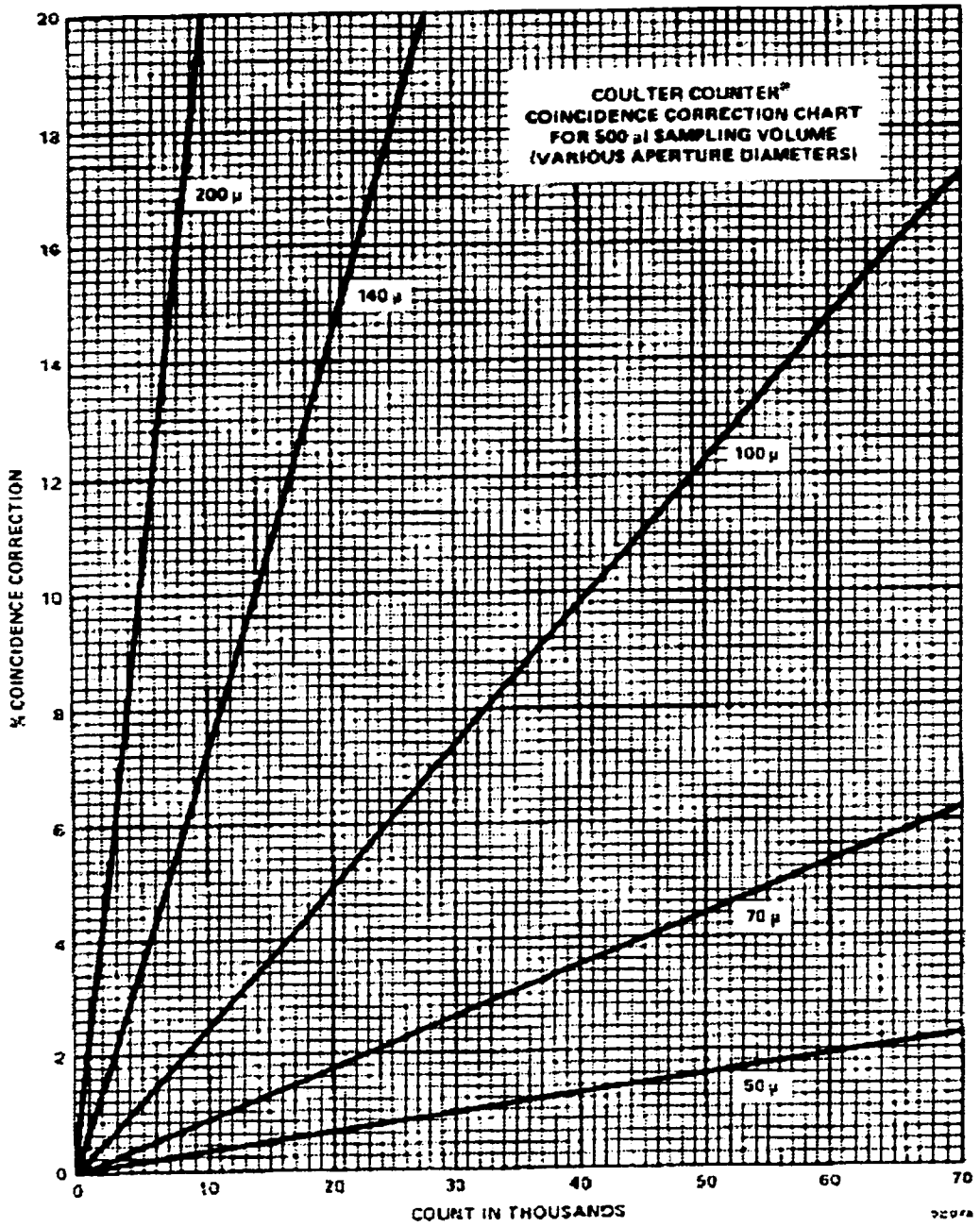

The relevant equations for coincidence correction of counts from 100 μm and 140 μm aperture tubes were determined empirically from Fig. A.3 as follows:

For 100 μm aperture tube:

correction of:

2.43% at 10,000 cells	→	slope = 2.43%/10,000cells	=	2.43E-04%/cell
7.38% at 30,000 cells	→	slope = 7.38%/30,000cells	=	2.46E-04%/cell
12.22% at 50,000 cells	→	slope = 12.22%/50,000cells	=	2.44E-04%/cell
17.18% at 70,000 cells	→	slope = 17.18%/70,000cells	=	2.45E-04%/cell
			AVERAGE =	2.44E-04%/cell
			FACTORIAL AVERAGE =	2.44E-06/cell

Example: Correction at 50,000 cells:
Correction Factor = 2.44E-06/cell x 50,000 cells = 0.122 (i.e. 12.22%)
True Number = (50,000 x 0.122) + 50,000
= 6,100 + 50,000
= 56,100 cells

∴ Equation for coincidence correction for a 100 μm aperture tube (where n = numeric readout count) is:

$$\textit{true number} = n\,(n \times 2.44E\text{-}06) + n$$
$$= n^2\,(2.44E\text{-}06) + n$$

For 140 μm aperture tube:

correction of:

14.37% at 20,000 cells	→	slope = 14.37%/20,000cells	=	7.185E-04%/cell
			=	7.185E-06/cell

Example: Correction at 20,000 cells:
Correction Factor = 7.185E-06/cell x 20,000 cells = 0.1437 (i.e. 14.37%)
True Number = (20,000 x 0.1437) + 20,000
= 2874 + 20,000
= 22,874 cells

∴ Equation for coincidence correction for a 140 μm aperture tube (where n = numeric readout count) is:

$$\textit{true number} = n\,(n \times 7.185E\text{-}06) + n$$
$$= n^2\,(7.185E\text{-}06) + n$$

The above mentioned equations for coincidence correction can easily be inputted directly into an EXCEL worksheet as a formula for a single spreadsheet cell. The following EXCEL formula will correct a count from one cell and places it in another in its fully corrected form, with respect to the true number determination

i.e. F60 = ((POWER(F59,2))*(0.000007185))+F59

A.2.3 Performing a Basic Cell Count: Start to Finish

Before using the Coulter counter for determining cell concentration it is important to make sure that the proper aperture tube is in place. The full range of detection for an aperture tube is between 2% and 40% of its orifice diameter. Whenever a new aperture tube is installed it must first be calibrated with standard sized latex particles which fall within 5% to 20% of its orifice diameter (see Section A.3).

The optimal settings to use for counting with a 100 μm aperture tube in place are a 1/amp. = 2, 1/ap.current = 8, and a threshold division = 7. As explained explicitly in a later section with respect to actual sizing of cell populations a threshold setting of 7 provides a cutoff during the counting process such that only cells with a diameter of 8.7 μm and above will be counted. In some cases it may be more pertinent to use a higher threshold setting for a more accurate counting especially if there are a range of cell sizes present. A threshold setting = 20 with a 1/amp. = 2, and 1/ap.current = 8, produces a cutoff of 11.9 μm. Although this setting is a little closer to mean cell diameters of such cells like CHO and K562, in control populations the determined cell count using either a threshold of 7 or 20 usually produces the same result.

A.2.3.1 Flushing the system before counting

I. Turn on the Coulter counter by pulling on the on/off knob in the bottom left-hand corner and let it warm up for a few minutes in order to build up a vacuum. Also, make sure that the sample volume switch on the right-hand side of the Coulter counter is set to 0.5 mL. Next, place a sample vial 3/4 full of Isoton II onto the platform stand and submerge the aperture tube and external electrode into the Isoton II if this has not already been done. Reposition the sample vial so that the aperture tube orifice is displayed centered on the debris monitor.

II. Fill the system with Isoton II by turning the auxiliary stopcock clockwise to a vertical position, followed by turning the control stopcock to a vertical position in the same fashion. After a few seconds of flushing return both stopcocks to their original horizontal positions in the same order.

III. Next, perform a few trial counts using the Coulter counter on just the Isoton II solution alone to confirm that it is operating adequately and/or that the Isoton II solution is not contaminated with exogenous particles. First, turn the control stopcock clockwise to a vertical position. Then wait until a flatline is observed on the oscilloscope screen before continuing the same motion of the control stopcock to a horizontal position. After a few seconds a count is shown on the numeric readout display. Repeating this procedure a few times provides an average Isoton II background reading, which in some circumstances may be necessary if particles have settled out in the stock Isoton II solution.

A.2.3.2 Preparing and counting a cell suspension sample

I. After cells have been harvested from culture remove a small sample for counting. Into a Coulter counter sample vial tared on a top loading balance add a recordable amount of Isoton II solution. Then, into the same vial place a recordable amount of your cell suspension. Ideally, most any range of cell suspension dilutions will suffice, although the coincidence correction from concentrated samples will be great. A commonly used dilution is usually 1 g or mL of cell suspension in a total weight or volume of 15 g or mL with Isoton II. A total volume of 15 mL will provide between 10-12 separate counts which can later be averaged, before the volume in the vial falls below the external electrode and counts become more ambiguous with repetition.

II. In order to determine the concentration of cells in the prepared sample place it onto the platform stand and submerge the aperture tube and external electrode. Reposition the sample vial so that the aperture tube orifice is displayed centered on the debris monitor. Next, turn the control stopcock clockwise to a vertical position. Then wait until a flatline is observed on the oscilloscope screen before continuing the same motion of the control stopcock to a horizontal position. After a few seconds a count is shown on the numeric readout display. Finally, repeat the above procedure a few times mixing the solution in between gently with a plastic transfer pipet in order to provide an average count for your sample.

A.2.3.3 Calculation of cell concentration from numeric readout count

After a number of counts have been obtained an average value is determined which is followed by a coincidence correction. Finally, the concentration of cells in the original stock cell suspension is determined by accounting for the dilution made in Isoton II and the sampling volume as shown here in the following sample calculation.

Example: For a 1/17 mL dilution of a stock cell suspension, and counting using a 140 μm aperture tube.

Counts: 16088 16350 16202
16404 16385 16282

Average Count = 16285 cells

Corrected Count $= n^2 (7.185E\text{-}06) + n$
$= (16285)^2 (7.185E\text{-}06) + 16285$
$= 1905 + 16285$
$= 18190$ cells

#cells/mL in original cell suspension $= 18190 \text{ cells} \times \frac{17}{1} \times \frac{1}{0.5 \text{ mL}} = 618{,}460 \text{ cells/mL}$

A.3 Aperture calibration

A.3.1 Materials

Coulter counter size standard L15 nominal latex beads and Isoton II electrolyte solution (Coulter Electronics, Burlingtion, ON). Latex beads appropriate for a 100 μm aperture tube calibration are 15.05 μm in mode diameter (PN 6602797), and for a 140 μm aperture tube calibration are 42.80 μm in mode diameter (PN 6602800).

A.3.2 Method

I. First, repeatedly invert the Coulter counter size standard latex beads vial vigorously several times and add ~45 droplets of the beads to 150 mL of Isoton II prepared in a 200 mL beaker. Next, stir the solution with a spatula to obtain a homogenous solution and then pour approximately 50 mL of it into a clean 50 mL beaker.

II. After properly washing and flushing the aperture tube with Isoton II (see Section A.2.3.1) place the 50 mL beaker onto the platform stand with the aperture tube and external electrode submerged in the center of the solution.

III. For the 100 μm aperture tube calibrate using the settings 1/amp = 2 and 1/ap. current = 8 and for the 140 μm aperture tube use the settings 1/amp = 2 and 1/ap. current = 2. Next, change the threshold control setting to 4, such that the corresponding line divisions align directly. Starting at this lower threshold division of 4, initiate the counting by turning the control stopcock as outlined previously in A.2.3.2.II. Record the reading on the numeric readout display and then change the lower threshold by 4 divisions again to a setting of 8. Gently mix the solution a few times with a plastic transfer pipet and repeat the counting procedure. Continue to change the lower threshold division each time by a factor of 4 and record the numerical output until a final lower threshold of 100 is reached.

IV. Once completed, repeat the entire aforementioned process (I and II) at least two more times from the stock 150 mL Isoton II solution containing latex beads.

A.3.3 Data Analysis

A.3.3.1 Terminology

Count = the value displayed on the numerical display after the completion of each operational run
Corrected Count (CC) = is the cell count after coincidence correction

Window Number (WN) = represents the window size
Window Count (WC) = (CC in threshold number 4n) – (CC in threshold number 4(n+2))
WN x WC = Window Number x Window Count
TC = Total Count = sum of all window counts
TV = Total Volume = sum of all (WN x WC)

MCT = Mean Cell Threshold
= the threshold division where the cell count has decreased by half
= TV/TC or determined from a 4 parameter fit curve of Lower Threshold vs. Corrected Average Cell Count
MCV = Mean Cell Volume
= CF x MCT
= $(4/3)(\pi R^3)$ where R = radius of the CC Size Standard spheres

CF = Correction Factor used in the sizing of cell distributions
CF = MCV/MCT = K*I*A = volume per threshold division in μm^3/division
where I = 1/aperture current switch setting
A = 1/amplification switch setting
K = a constant for a particular aperture tube and set of electronics, calculated using a known CC Size Standard spherical latex particles

$$\therefore K = \frac{(MCV/MCT)}{I * A} \quad \text{(no units)}$$

A.3.3.2 Determining the values of T, CF and K for the respective aperture tube

The main objective in the calibration of each newly replaced aperture tube is to obtain values for the variables *T*, *CF* and *K*. Once determined, these values later serve a key importance in the calculation of the mean cell volume of an analyzed cell population (see Section A.4). To that end the following section outlines the necessary procedure

towards computing these values using an EXCEL spreadsheet and the collected counts from the size standard latex beads in Section A.3.3.

Onto an EXCEL spreadsheet similar to Spreadsheat A.1 are entered the respective counts from lower thresholds of 4-100 as recorded from each replicate trial of counted latex beads (see Section A.3.2). Next, the 3 replicate counts at each lower threshold division are averaged together and then correction for coincidence passage of cells using the appropriate correction factor for the particular aperture tube used, as outlined in Section A.2.3.1.

Determining MCT, the threshold division at which particle count decreases by half:

Method 1:

Using SigmaPlot (Jandel Scientific Corp., San Rafael, CA) create a distribution of lower threshold divisions 4-100 vs. the coincidence corrected average counts for each division as shown in Fig. A.4. The data points on this plot are fitted using first a 2-parameter and then a 4-parameter logistical non-linear curve fitting equation,

$$f = (a-d) / (1 + (x/c)^b) + d$$

where a and d were set to the maximum and minimum corrected average counts, respectively. The values exponential value of b and c were substituted into the 4-parameter equation after determination using 2-parameters. The final value of c represents the value of T or threshold division at which the particle count has decreased by half of its original value.

Spreadsheet A.1. Aperture calibration.

Spreadsheet A.1. Calibration datasheet for 100 µm aperature tube																				
Coulter counter settings of:				1/amp = 2	1/ap.curr. = 8															
Lower Thres-hold	Counts:			Avg. Count	Corr. Count	Win. # (WIN)	Win Count (WC)			Avg. Win. Count	S.E.	WIN x WC			Avg. WIN x WC	S.E.
	#1	#2	#3				#1	#2	#3			#1	#2	#3		
4	5371	5650	5134	5385	5456											
8	5301	5549	5244	5365	5435	8	292	0	53	115	90.0	2338	0	426	922	720
12	5086	5684	5082	5284	5352	12	108	0	237	115	68.5	1292	0	2841	1378	822
16	5196	5662	5013	5290	5359	16	0	0	80	27	26.7	0	0	1279	426	427
20	5105	5705	5004	5271	5339	20	117	5	0	41	38.2	2337	103	0	813	763
24	5082	5657	5053	5264	5332	24	34	124	41	66	29.1	812	2984	983	1593	698
28	5072	5584	4964	5207	5273	28	0	163	162	108	54.3	0	4573	4531	3035	1519
32	5124	5498	4895	5172	5238	32	391	283	161	278	66.6	12515	9067	5144	8909	2132
36	4690	5308	4907	4935	4994	36	1822	2132	2011	1988	90.4	65587	76765	72383	71578	3256
40	3339	3411	2922	3224	3249	40	3587	4089	3797	3824	145.5	143497	163549	151865	152970	5822
44	1153	1284	1064	1167	1170	44	3140	3188	2756	3028	137.0	138163	140282	121253	133233	6028
48	226	251	187	221	221	48	952	1048	877	959	49.6	45703	50298	42080	46027	2381
52	204	240	190	211	211	52	31	23	0	18	9.3	1614	1197	0	937	484
56	195	228	217	213	213	56	6	21	21	16	5.0	336	1177	1177	897	281
60	198	219	169	195	195	60	29	12	4	15	7.4	1742	721	240	901	443
64	166	216	213	198	198	64	0	1	0	0	0.3	0	64	0	21	21
68	200	218	188	202	202	68	0	0	50	17	16.7	0	0	3403	1134	1136
72	171	227	163	187	187	72	24	46	22	31	7.7	1730	3315	1585	2210	555
76	176	172	166	171	171	76	34	79	46	53	13.5	2586	6009	3498	4031	1025
80	137	148	117	134	134	80	105	66	60	77	14.1	8405	5284	4803	6164	1130
84	71	106	106	94	94	84	113	106	83	101	9.1	9496	8908	6975	8459	762
88	24	42	34	33	33	88	42	79	68	63	11.0	3697	6954	5986	5546	967
92	29	27	38	31	31	92	0	17	0	6	5.7	0	1564	0	521	522
96	32	25	38	32	32	96	6	4	18	9	4.4	576	384	1728	896	420
100	23	23	20	22	22											
						TC =	10833	11488	10545	10956	TV =	442426	483200	432182	452603	
NOTE: Coincidence correction for 100 µm aperture tube = 2.44×10^{-6}																

Method 2:

Into a separate column on the EXCEL spreadsheet enter in as shown onto Spreadsheet A.1 the respective Window Numbers (*WN*) values. These values simply represent the midpoint lower threshold division value between consecutively measured divisions, such that the separation between windows is 8 threshold divisions. Each *WN* value can be determined by the equation,

WN = (LTD*n) - LTD where n = every number from 3 to 25
and *LTD* = lowest measured threshold division, in this case simply substitute the value of 4 here

In another set of columns is determined the relative size of each window or rather the number of counts or Window Counts (*WC*) falling within each Window Number. The *WC* values simply represent the difference in counts between every other Lower Threshold value. These values are calculated from each set of replicate coincidence corrected counts (*CC*) and the corrected average counts measured for each Lower Threshold using the equation,

WC = (CC in threshold number 4n) - (CC in threshold number 4(n+2))

i.e. The difference between Lower Threshold 4 and 12 is placed next to *WN* = 8
The difference between Lower Threshold 8 and 16 is placed next to *WN* = 12
The difference between Lower Threshold 12 and 20 is placed next to *WN* = 16

When the consecutive values of Window Numbers are plotted vs. the values of there Window Counts a distribution is revealed (Fig. A.5). Increasing *WN* represent a series of discrete steps in volume or windows in which the number of counts, *WC* are determined.

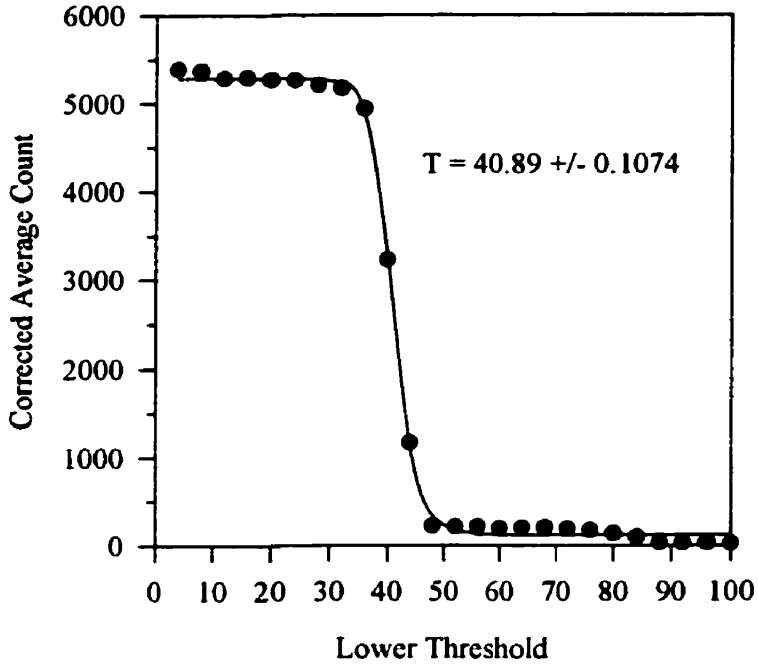

Fig. A.4. Determination of *MCT* or the threshold division at which the particle count has decreased by half by Method 1.

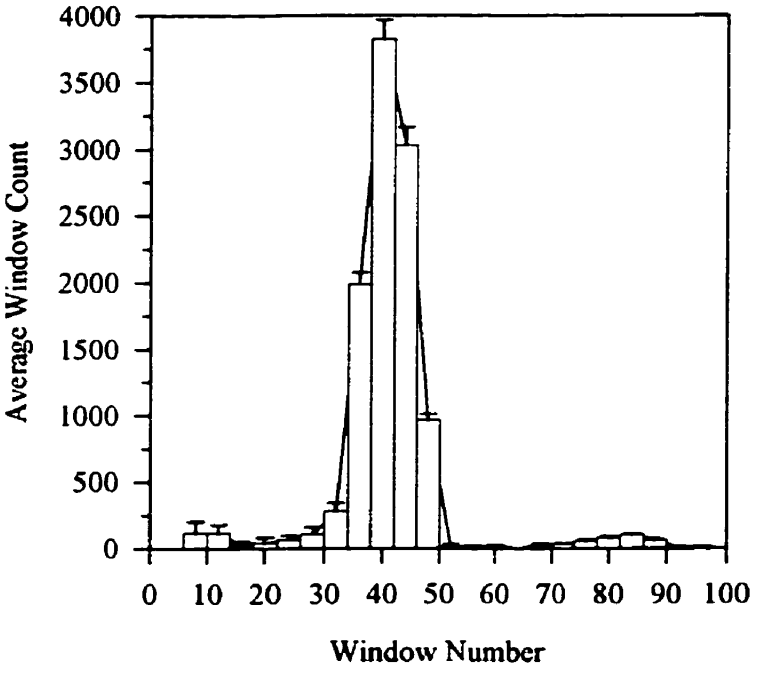

Fig. A.5. Size distribution of 15.05 μm latex beads used for calibrating 100 μm aperture tube.

In a final set of spreadsheet columns calculate the values of ***(WN x WC)*** for each replicate determination by multiplying the *WN* values by their corresponding *WC* values. The *WN x WC* value for each *WN* represents the volume of that particular window. When these values are added up for each replicate determination the overall value is the total measured volume or *TV*. And, when the corresponding counts, *WC* for each window are added up the overall total value is called the total count, *TC*. When the total measured volume, *TV* is divided by the total number of *WC*, *TC* the resultant value is the mean cell threshold, *MCT*.

i.e. ***TV*** = Total Volume of all of the WNxWC values added together for each replicate
TC = Total Count of all of the WC values added together for each replicate
MCT = TV/TC

For a more accurate determination of *MCT* based on Fig. A.4 only those values falling within the actual peak portion of the curve may be included. In other words you can determine *TC* and *TV*, and hence *MCT* based solely on the individual values of *WC* and *WC* x *WN* falling between *WN* 28-50.

Determining the correction factor, CF and empirical constant, K:

The equation for calculating the correction factor, *CF* of an aperture tube is given by,

CF = MCV/MCT

where, MCT is determined by either Method 1 or 2 (see above)
and MCV = mean cell volume (or mean volume of latex beads)
$= (4/3)(\pi R^3)$
where R = radius of the CC size standard latex beads
Since D = 15.05 μm (for 100 μm aperture tube calibration latex beads)
$\therefore R = 7.525$ μm
then $R^3 = 426.10783$ μm^3

$$\therefore MCV = (4/3)\pi R^3$$
$$= (4/3)(3.14)(426.10783)$$
$$= 1784.8763\ \mu m^3$$

Presented here in Table A.2 is a summary of the above calculations for MCT, MCV, and CF as determined from values presented in Table A.2

Table A.2. Summary of empirically determined values of MCT, MCV, and CF.

Replicate number	***MCT = TV/TC***	***MCV***	***CF = MCV/MCT***
1	40.8387	1784.8763	43.7055
2	42.0626	1784.8763	42.4338
3	40.9828	1784.8763	43.5518
From average WC of 1-3	41.3127	1784.8763	43.2040
Overall average:	41.2992	1784.8763	43.2238

Therefore, with the 100 μm aperture tube in place the mean volume per threshold division, or *CF* is 43.2238 μm^3.

Finally, the equation for calculating the empirical constant, *K* for a particular aperture tube is given by the equation,

$$K = \frac{(CF)}{I * A}$$

where, I = 1/aperture current switch setting = 2
A = 1/amplification switch setting = 2

$$K = \frac{(MCV/MCT)}{I * A}$$
$$= \frac{(1784.8763 / 41.2992)}{2 \times 8}$$
$$= 2.728$$

A.4 Cell sizing, volume, and diameter determination

The procedure for sizing a given cell population is very similar in nature to the protocol used for calibrating an aperture tube with size standard latex beads (see Section A.3). The only exception though resides in the fact that the cell population under study may contain a wide range of sizes. Therefore, we may not be able to obtain a full analysis of the size distribution of the population using only one 1/amp and 1/ap.current setting, as was the case with the size standard, normally distributed latex beads. Instead, cells will be counted through a range of lower threshold settings in entirety for each of a series of different 1/amp and 1/ap.current settings. As detailed in the accompanying spreadsheets, each 1/amp and 1/ap.current setting examines a limited portion of the final size distribution curve, or rather counts only cells that fall within a particular volume range. Also, each of these separate portions of the entire size distribution partially overlap with the previously examined portion. In the final step of the sizing procedure the collected Window Count (WC) data is normalized to a single 1/amp and 1/ap.current setting and then averaged together to produce the desired distribution of sizes within the population.

A.4.1 Method

I. Harvest or otherwise remove a sufficient quantity of cells in media from the culture to be analyzed and place them in a 50 mL conical centrifuge tube. The amount of cells removed will depend on the overall number of 1/amp and 1/ap.current settings needed, and the number of replicate determinations from each necessary to cover the entire distribution of sizes. An ideal concentration of cells to use is between 0.3-1x10^6 cells/mL. When diluted 3:55 mL in Isoton II you want the numeric

output of the initially measured lower threshold of 4 to be a high enough value, on the order of 7000-10000 so that the rest of the distribution can adequately be examined. In other words, as you count the number of cells at each subsequent threshold division the displayed count on the numeric readout display will decrease. As this happens you do not want this number to reach or approach a value of 0 before you have had a chance to reach the lower threshold division of 100.

Determining the required number of cells and overall volume of cell suspension needed to size the entire population:

If your stock cell suspension has a concentration of cells of $3x10^5$ cells/mL, and you dilute them in Isoton II by 3:55 mL, and size 3 replicates per 1/amp, 1/ap.current setting for a total of 3 separate settings then,

cells needed = 3×10^5 cells/mL x 3 mL/replicate x 3 replicates/setting x 3 settings
$\cong 8 \times 10^6$ cells

volume of cell suspension needed = 3 mL/replicate x 3 replicates/setting x 3 settings
$\cong$ 27 mL

II. After preparation, invert the tube containing the cell suspension so as to prevent settling. Then, into a clean glass 60 mL beaker dilute the cells 3:55 mL in Isoton II. If a different dilution factor is chosen be sure to maintain consistency for each performed replicate.

III. After properly washing and flushing the aperture tube with Isoton II (see Section A.2.3.1) place the sample beaker onto the platform stand submerging the aperture tube and external electrode into solution. Beginning with a 1/amp = 2, 1/ap.current

= 8 for the 100 μm aperture tube and a threshold division of 4 initiate counting by turning clockwise the control stopcock vertical then horizontal, recording the displayed number afterwards.

IV. Next, repeat the counting process as before, first at thresholds of 8, 12, 16, 20 then 100, 96, 92, 88 before going onto covering the entire range of thresholds from 4-100. First, check the recorded value for the threshold of 4 to see that it is large enough to cover the distribution, and then confirm that the value at the threshold of 100 is still readable and not close to 0. Second, as explained in Section A.3.3.2 determine the number of Window Counts (*WC*) within the first few and last few Window Numbers (*WN*). In other words, for WN = 8, the WC is the count at threshold 12 minus the count at threshold 4, etc.

Ideally, we do not want the WC to decrease from WN = 8 to 96 too fast or too slow. Instead much like Fig. A.4 we want the WC to decrease by half by the time a lower threshold of 50 is counted. A consistent WC of around 200 for the first few WN is best. If the first few WC values are large, around 1000 then a WC value of 0 will be achieved before a lower threshold of 100 is reached. Consequently, with the current 1/amp, 1/ap.current settings a portion of size distribution beyond the peak is being analyzed. The solution to this problem is to lower only the 1/ap. current setting by one notch and repeat the counting process again for the first few threshold divisions. If the first few WC values are small, less than 100 then we are examining the low end of the size distribution curve and accordingly nothing of significance by the point a threshold of 100 is counted. The solution to this problem is to raise only the 1/ap.current setting by one notch and repeat the counting process again for the first few threshold divisions.

V. Once the proper initial 1/amp, 1/ap.current settings have been established start again at a threshold of 4, take a reading and then change the threshold by 4 divisions to the next setting and repeat until a threshold of 100 is reached. In between measurements gently mix the solution a few times with a plastic transfer pipet.

VI. Next, repeat the aforementioned procedure in replicate, about 2-3 times for each set of new 1/amp, 1/ap.current settings. It is best to keep 1/amp setting constant and change only the 1/ap.current switch 1-2 notches above/below the initial setting so that essentially the entire size distribution will eventually be covered.

A.4.2 Data analysis

A.4.2.1 Calculating coincidence corrected counts, *WN*, and *WC*

As explained earlier in Section A.3.3.2 the counts obtained from lower thresholds of 4-100 are entered onto EXCEL spreadsheets similar to Spreadsheet A.2, one for each separate set of 1/amp, 1/ap.current setting analyzed. At the end of this Appendix is provided a series of these example spreadsheets used is the sizing of K562 cells after 0, 72 hr of dexrazoxane (ICRF-187) exposure (Spreadsheets A.2-A.7).

The replicate counts at each lower threshold division are averaged together and then correction for coincidence passage of cells is made using the appropriate correction factor for the particular aperture tube used, as outlined in Section A.2.2.1. Into a separate column on the spreadsheet (see Spreadsheet A.2) is entered the respective Window Numbers (*WN*) values. Each *WN* value can be determined by the equation,

$WN = (LTD*n) - LTD$ where n = every number from 3 to 25
and LTD = lowest measured threshold division, in this case simply substitute the value of 4 here

In another set of columns is determined the relative size of each window or rather the number of counts or Window Counts (*WC*) falling within each Window Number. These values are calculated from each set of replicate coincidence corrected counts (*CC*) and the corrected average counts measured for each Lower Threshold using the equation,

$WC = (CC \text{ in threshold number } 4n) - (CC \text{ in threshold number } 4(n+2))$

In a final set of spreadsheet columns the values of $(WN \times WC)$ for each replicate are calculated by multiplying the *WN* values by their corresponding *WC* values.

A.4.2.2 Calculating the volume and diameter sizes corresponding to each *WN*

To ultimately plot a distribution curve of size vs. *WC* from the collected data the volume and diameter sizes corresponding to each Window Number (*WN*) need to be determined.

Determining the corresponding volume (μm^3) for each Window Number:

Remember from Section A.3.3.2.

$$K = \frac{(MCV/MCT)}{I*A}$$

which rearranges to form,

$$MCV/MCT = V/T = K*I*A$$

$$\therefore \quad V = (K*I*A)\,T$$

where T = Window Number
K = Empirical constant (2.728)
I = 1/ap.current setting
A = 1/amp setting

Sample calculation:

For settings of 1/amp = 2 and 1/ap.current = 8
Then the corresponding volume for a Window Number (*WN*) of 8 is:

$$V = (K*I*A)^{T}$$
$$= (2.728 \times 2 \times 8) \times T$$
$$= (43.648) \times T$$
$$= (43.648) \times 8$$
$$= 349.18\ \mu m^3$$

Determining the corresponding diameter (μm) for each Window Number:

Remember from Section A.3.3.2.

$V = 4/3\pi r^3$ where V = same volume as determined above

$$r = \sqrt[3]{(3/4)(V)/\pi}$$
$$r = ((3/4)(V)/\pi)^{1/3}$$

Since $D = 2r$ $\therefore$ $D = 2 \times ((3/4)(V)/\pi)^{1/3}$

Sample calculation:

For settings of 1/amp = 2 and 1/ap.current = 8
Then the corresponding diameter from the above determined volume of 349.18 μm^3 from settings of 1/amp = 2 and 1/ap.current = 2, and WN = 8:

$$D = 2 \times ((3/4)(V)/\pi)^{1/3}$$
$$= 2 \times ((3/4)(349.18)/\pi)^{1/3}$$
$$= 8.74\ \mu m$$

A.4.2.3 Normalization of *WC* and *(WNxWC)* values to one 1/amp. and 1/ap.current setting

When more than one set of 1/amp, 1/ap.current settings are used to plot the size distribution of a cell line we need to normalize all of the calculated Window Counts (*WC*), to one particular setting. In addition, if at a later stage the Mean Cell Volume or Diameter (*MCV* or *MCD*) of the population is to be determined then we must also normalize the *(WNxWC)* values in the same manner. The reasoning for normalization is that when non-

normalized Window Counts are plotted versus Volume for a range of 1/amp, 1/ap.current settings the result is not a continuous curve but rather one that is disjointed at the sections where the windows of view overlap, as shown in Fig. A.6 for 0 hr K562 cells.

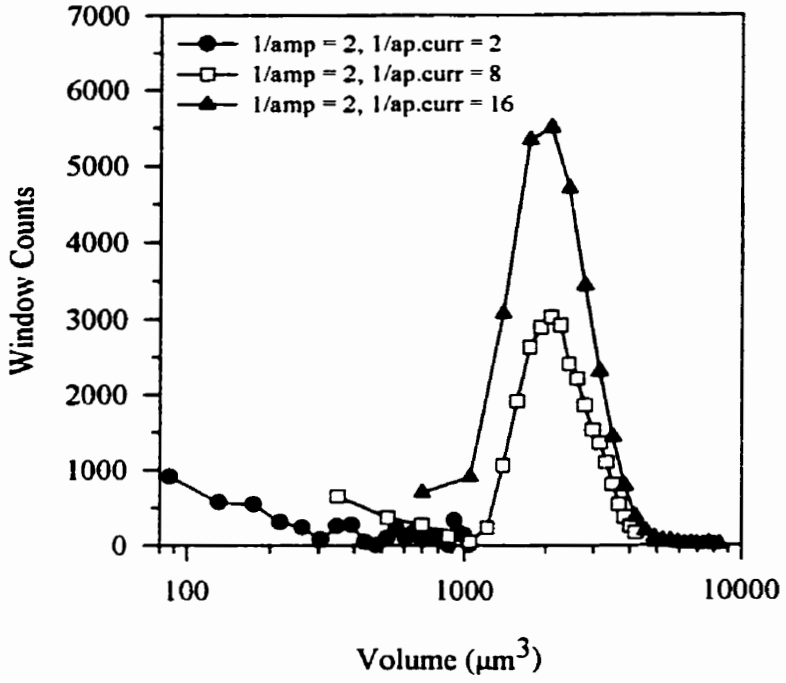

Fig. A.6. Non-normalized size distribution of cells counted at 3 different 1/amp, 1/ap.current settings.

The accompanying EXCEL spreadsheets (Spreadsheets A.5-A.6) at the end of this Appendix help to demonstrate the process of normalization of *WC* and *(WNxWC)* values to the settings of 1/amp = 2 and 1/ap.current = 2. Based on the previous equation V = (K·I·A)·T we can see that volume is proportional to a factor of the product of the 1/amp and 1/ap.current. Therefore if we multiply or divide the *WC* and *(WNxWC)* values obtained from different settings by set factors we can make them proportional to those values obtained from the 1/amp = 2 and 1/ap.current = 2 settings.

Sample Calculation:

Normalizing to 1/Amp = 2, 1/ap.current = 2 → 2 x 2 = 4 **(A)**

WC = 1247 for 1/amp = 2, 1/ap.current = 8 → 2 x 8 = 16 **(B)**

Since the difference between **(A)** and **(B)** is a factor of 4 we divide the WC from **(B)** by 4 to get the new WC, which is proportional to **(A)**:

i.e. WC = 1247 / 4 = 312

WC = 3665 for 1/amp = 2, 1/ap.current = 1 → 2 x 1 = 2 **(C)**

Since the difference between **(A)** and **(C)** is a factor of 2 we multiply the WC from **(C)** by 4 to get the new WC, which is proportional to **(A)**:

i.e. WC = 3665 x 2 = 7331

Once all of the *WC,* and *(WNxWC)* values from each setting have been made proportional to each other, respectively then before the data can be plotted one final step remains. As can be seen in Fig. A.6 there exists some overlapping portions of the distribution between separately analyzed 1/amp, 1/ap.current settings. Therefore the normalized data from each setting used needs to be averaged together at those volume/diameter values where there exists an overlap. These new values are then put into

a separate section on the spreadsheet (labeled "All WC or WNxWC Averaged together") alongside their corresponding volume/diameter values. Subsequently WC (or cell number) vs. volume/diameter may then be plotted.

For example on Spreadsheet A.5:

Comparing the data for 1/amp = 2, 1/ap.current = 2 (referred to as 2/2) and 1/amp = 2, 1/ap.current = 8 (referred to as 2/8) the WC values for a volume of 349 μm^3 need to be averaged together.

Also, comparing the data for settings 2/2, 2/8, 2/16 the WC values for a volume of 698 μm^3 need to be averaged together.

A.4.2.4 Calculating the MCV, and MCD from Coulter counter sizing data

In order to calculate the Mean Cell Volume (MCV) or Mean Cell Diameter (MCD of a cell population using Coulter counter data a few conditions must be satisfied. First, all *WC* and *(WNxWC)* values must be normalized to a single 1/amp, 1/ap.current setting (see Section A.4.2.3). Second, the size distribution when plotted must exhibit Gaussian-like features and be complete in nature. For example, in Fig A.7 are displayed two distribution curves. The first curve (0 hr plot) is complete in nature, and the second curve (72 hr plot) exhibits a pattern of decay with no identifiable midpoint.

Demonstrated on Spreadsheet A.7 are the necessary calculations needed to determine the MCV or MCD of a population. For the purpose of comparison, MCV was calculated for the second curve in Fig. A.7 (72 hr plot). This was done so as to demonstrate the concept that an accurate determination of MCV cannot be achieved due to the high incidence of background electrical noise or a high proportion of particles in such cell populations. On an EXCEL spreadsheet are placed the normalized values of *WC* and

(WNxWC) along side their corresponding window size, expressed in terms of volume or diameter.

Example (see Spreadsheet A.7, Time = 0 hr data):

Determine the total *WC* value or *TC* by adding up all of the *WC* values. Determine total volume, *TV* by doing the same for all of the *(WNxWC)* values. Correspondingly, from Spreadsheet A.7 these values are,

$TC = 10986$ and $TV = 427968$

Next, calculate the mean cell threshold value using the equation,

$$MCT = TV/TC$$
$$= 427968 / 10986$$
$$= 38.9547$$

Remember from Section A.3.3.2 that,

$CF = MCV/MCT$ where CF = 43.238, after 100 μm aperture tube calibration

$$\therefore MCV = MCT*CF$$
$$= (38.9547)(43.238)$$
$$= 1683.77\ \mu m^3$$

$$\therefore MCD = \sqrt[3]{((3/4)(MCV)/\pi)}$$
$$= ((3/4)(MCV)/\pi)^{1/3}$$
$$= ((3/4)(1683.77)/3.14)^{1/3}$$
$$= 14.76\ \mu m$$

A.4.2.5 Curve smoothing to remove noise in the size distribution

Sometimes, due to the number of fine particulates in the cell suspension a evenly smoothed curve is not readily obtained. Therefore, in order to make the data appear alittle more presentable we can smooth out the data such that this noise is somewhat reduced. SigmaPlot contains a function that allows for such curve smoothing. It is known as the "Running Average" function, which can be entered under <Transforms>, then <User-

defined>. What it does is it takes the running average of a set sequence of data, then shifts to the next starting data point and does the same thing. In other words if you want it to average every 3 data points, it will start from the beginning and average the first 3 points, then move to the second data point and average the next 3, then to the third point, and so on. You can allow it to average every 3, 5, 7, etc number of points and display the average of these values. The only shortcoming is that consequently some data is not averaged and will be lost, or should not thusly included in the plot. Finally, plot the new running averaged volumes vs. their corresponding running averaged Window Counts (*WC*) to see the new smoother plot.

Example:

If you want to take the running average of whatever is in column 1 and put it in column 2 with a window or averaging sequence of 3 then the formula would look like this:

col(2) = runavg(col(1), 3)

Further improvements of a distribution plot may be made purely for cosmetic purposes. Many sizing attempts using a 100 μm aperture tube have shown that *WC* become erroneous and exponentially increase logarithmically as cell size decreases [2]. This occurs particularly for *WN* values which count particles within the range of 0-900 μm^3 in volume or 0-12 μm in diameter. This attribute of the Coulter counter may be attributed to electronic noise which becomes more accentuated when utilizing high 1/amp, 1/ap.current settings. Therefore, as shown in Fig. A.7 a cutoff can be applied such that only data collected above volume values of 900 μm^3 will be shown in the final resultant distribution plot.

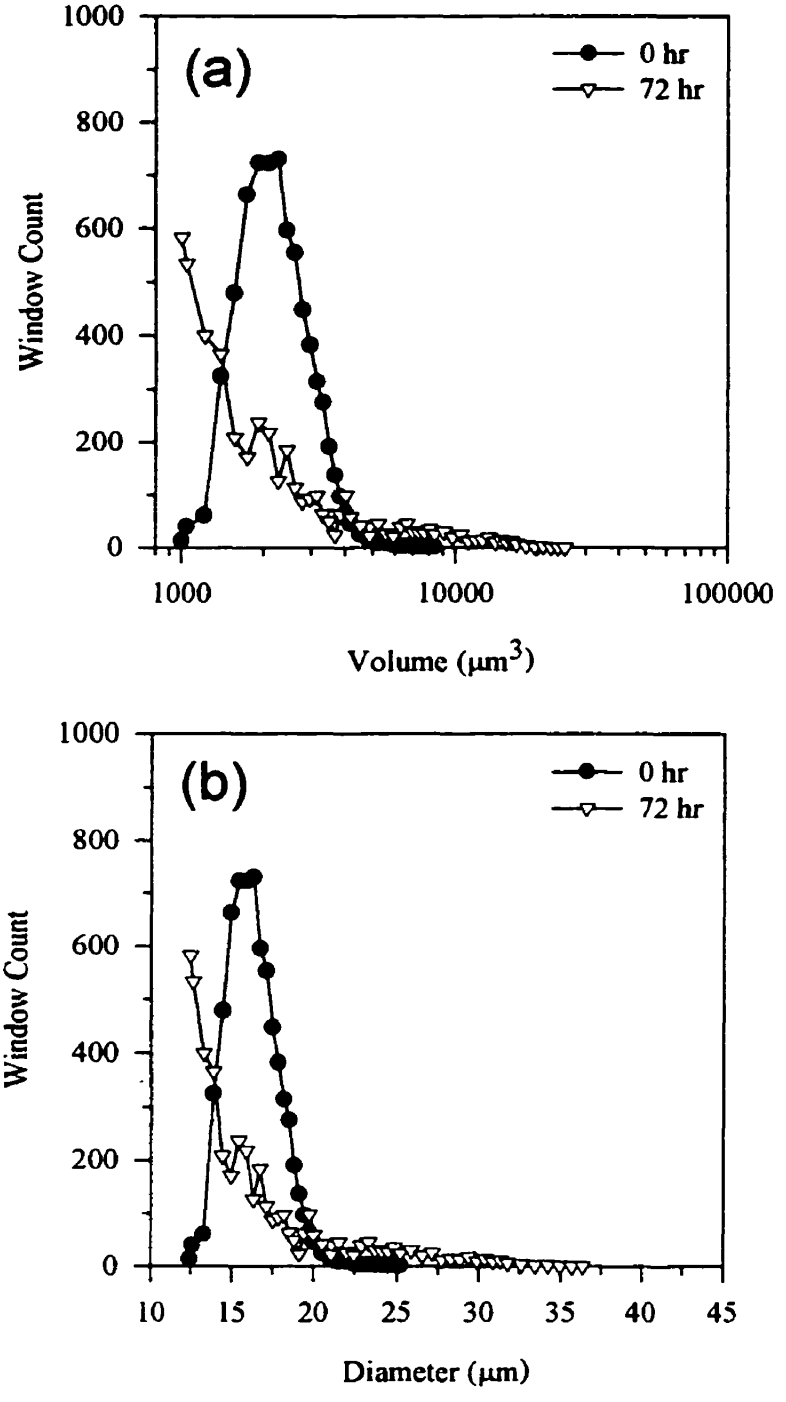

Fig. A.7. Size distribution analysis of K562 cells exposed daily to 100 μM dexrazoxane. At indicated time intervals ~1x10^7 cells were removed and counted utilizing a model Z_f Coulter counter (100 μm aperture tube). Final cell counts were normalized to equal the control settings (1/amp = 2, 1/ap.current = 2), and expressed as a distribution as a function of (a) volume, or (b) diameter.

Drugged K562 Cells				TIME = 0hr									Spreadsheet A.2.		
				1ml cell susp'n / 51ml total w/ Isotonll											
100 μ aperature tube in place															
Cell Volume Distribution from Coulter Counter							1/amp = 2	1/ap.curr. = 2					1st		
Lower	Counts:			Win.	*Win. Count (WC)		Avg.	S.E.	Volume	WN x WC			Avg.	S.E.	Diameter
Thres-	#1	#2		#	(on corr counts)		Win.		(μm^3)	#1	#2		WN x		(μm)
hold				(WN)	#1	#2	Count						WC		
4	15779	15227													
8	14822	14899		8	1180	632	906	274	87	9437	5055		7246	2191	5.50
12	14681	14638		12	664	477	570	94	131	7967	5722		6845	1122	6.30
16	14202	14454		16	271	814	542	271	175	4336	13023		8679	4344	6.94
20	14428	13877		20	0	307	307	154	218	0	6141		3070	3070	7.47
24	14291	14167		24	239	0	239	119	262	5726	0		2863	2863	7.94
28	14205	14120		28	22	130	76	54	306	629	3651		2140	1511	8.36
32	14270	14045		32	189	331	260	71	349	6054	10596		8325	2271	8.74
36	14028	13810		36	427	111	269	158	393	15389	4000		9694	5695	9.09
40	13870	13941		40	80	9	44	36	437	3205	342		1773	1432	9.41
44	13953	13802		44	0	0	0	0	480	0	0		0	0	9.72
48	14058	14077		48	95	0	95	48	524	4562	0		2281	2281	10.00
52	13864	13815		52	152	274	213	61	567	7888	14274		11081	3193	10.27
56	13916	13820		56	188	0	94	94	611	10519	0		5259	5259	10.53
60	13688	13879		60	247	77	162	85	655	14793	4611		9702	5091	10.78
64	13685	13748		64	23	172	98	74	698	1502	10998		6250	4748	11.01
68	13666	13718		68	83	0	83	42	742	5657	0		2829	2829	11.23
72	13607	13784		72	59	173	116	57	786	4224	12440		8332	4108	11.45
76	13611	13556		76	106	0	106	53	829	8022	0		4011	4011	11.66
80	13508	13834		80	0	0	0	0	873	0	0		0	0	11.86
84	13687	13617		84	0	327	327	164	917	0	27510		13755	13755	12.05
88	13549	13527		88	256	62	159	97	960	22518	5442		13980	8538	12.24
92	13447	13559		92	129	0	129	64	1004	11865	0		5932	5932	12.43
96	13428	13623		96	4	0	4	2	1048	409	0		205	205	12.60
100	13443	13619													
K =	2.7282			A =	2	I =	2			CV = CT*CF = (4/3)(πr^3)					
V = T*K*I*A		= T * (2.728167*2*2) =			T *	10.9127	μm^3			r = ^{3}/ ((3/4)(CT*CF)/π)					
CT = WC*WN / WC										d = 2r μm					
CF = 43.2142															

Spreadsheet A.2.

Drugged K562 Cells				TIME = 0hr									Spreadsheet A.3.		
				1ml cell susp'n / 51ml total w/ Isotonll											
100 μ aperature tube in place															
Cell Volume Distribution from Coulter Counter							1/amp = 2	1/ap.curr. = 8				2nd			
Lower	Counts:			Win.	*Win. Count (WC)		Avg.	S.E.	Volume	WN x WC			Avg.	S.E.	Diameter
Thres-	#1	#2		#	(on corr counts)		Win.		(μm^3)	#1	#2		WN x		(μm)
hold				(WN)	#1	#2	Count						WC		
4	13907	14880													
8	13657	14293		8	463	843	653	190	349	3704	6741		5223	1519	8.74
12	13473	14093		12	286	446	366	80	524	3428	5348		4388	960	10.00
16	13389	13876		16	162	383	273	111	698	2591	6134		4363	1772	11.01
20	13321	13734		20	127	101	114	13	873	2535	2028		2282	253	11.86
24	13270	13781		24	55	0	55	28	1048	1329	0		664	664	12.60
28	13269	13856		28	80	398	239	159	1222	2236	11137		6686	4451	13.27
32	13195	13408		32	693	1428	1061	368	1397	22182	45707		33944	11763	13.87
36	12617	12514		36	1516	2306	1911	395	1571	54577	83008		68792	14215	14.43
40	11766	11233		40	2112	3150	2631	519	1746	84493	125989		105241	20748	14.94
44	10618	9525		44	2639	3145	2892	253	1921	116105	138361		127233	11128	15.42
48	9256	8231		48	3013	3040	3027	13	2095	144631	145924		145277	647	15.88
52	7734	6600		52	2926	2917	2921	4	2270	152147	151681		151914	233	16.31
56	6438	5408		56	2467	2352	2410	58	2444	138168	131711		134940	3229	16.72
60	5343	4309		60	2372	2052	2212	160	2619	142296	123130		132713	9583	17.10
64	4126	3399		64	2006	1710	1858	148	2794	128371	109470		118920	9451	17.48
68	3379	2627		68	1552	1501	1527	25	2968	105540	102083		103812	1728	17.83
72	2599	1917		72	1464	1253	1358	105	3143	105389	90227		97808	7581	18.18
76	1934	1386		76	1245	952	1098	147	3317	94615	72326		83470	11144	18.51
80	1366	972		80	957	654	806	151	3492	76541	52350		64445	12096	18.83
84	984	735		84	676	412	544	132	3667	56816	34569		45692	11124	19.14
88	693	562		88	437	309	373	64	3841	38423	27181		32802	5621	19.43
92	549	427		92	285	227	256	29	4016	26198	20930		23564	2634	19.72
96	409	335		96	198	146	172	26	4190	19050	14040		16545	2505	20.01
100	351	281													
K =	2.7282			A =	2	I =	8			CV = CT*CF = (4/3)(πr^3)					
V = T*K*I*A		= T * (2.728167*2*8) =			T *	43.6507	μm^3			r = ^{3}/ ((3/4)(CT*CF)/π)					
CT = WC*WN / WC										d = 2r μm					
CF = 43.2142															

Drugged K562 Cells				TIME = 0hr								Spreadsheet A.4.		
				1ml cell susp'n / 51ml total w/ Isotonll										
100 μ aperature tube in place														
Cell Volume Distribution from Coulter Counter							1/amp = 2	1/ap.curr. = 16				3rd		
Lower Thres-hold	Counts: #1	#2		Win. # (WN)	*Win. Count (WC) (on corr counts) #1	#2	Avg. Win. Count	S.E.	Volume (μm^3)	WN x WC #1	#2	Avg. WN x WC	S.E.	Diameter (μm)
4	13908	14631												
8	13880	14022		8	258	1132	695	437	698	2066	9055	5561	3494	11.01
12	13666	13572		12	938	882	910	28	1048	11253	10583	10918	335	12.60
16	13000	13195		16	2887	3253	3070	183	1397	46184	52056	49120	2936	13.87
20	10943	10499		20	5184	5501	5343	158	1746	103690	110021	106856	3166	14.94
24	8069	7964		24	5547	5463	5505	42	2095	133137	131112	132125	1012	15.88
28	5611	5238		28	4606	4805	4706	99	2444	128980	134551	131765	2786	16.72
32	3590	3287		32	3548	3319	3434	114	2794	113528	106221	109875	3653	17.48
36	2129	1976		36	2421	2189	2305	116	3143	87154	78815	82984	4170	18.18
40	1197	1121		40	1479	1386	1432	47	3492	59160	55426	57293	1867	18.83
44	660	599		44	802	764	783	19	3841	35293	33605	34449	844	19.43
48	398	360		48	385	374	379	6	4190	18474	17940	18207	267	20.01
52	276	226		52	205	185	195	10	4540	10675	9633	10154	521	20.55
56	193	175		56	124	87	106	19	4889	6951	4876	5914	1037	21.06
60	152	139		60	83	52	68	16	5238	4984	3122	4053	931	21.55
64	110	123		64	67	57	62	5	5587	4290	3650	3970	320	22.02
68	85	82		68	28	50	39	11	5936	1905	3402	2653	748	22.47
72	82	73		72	12	34	23	11	6286	864	2449	1657	792	22.90
76	73	48		76	27	24	26	2	6635	2053	1825	1939	114	23.32
80	55	49		80	19	14	17	3	6984	1520	1120	1320	200	23.72
84	54	34		84	18	6	12	6	7333	1512	504	1008	504	24.11
88	37	43		88	28	0	28	14	7683	2464	0	1232	1232	24.49
92	26	39		92	4	24	14	10	8032	368	2208	1288	920	24.85
96	33	19		96	0	18	18	9	8381	0	1728	864	864	25.21
100	32	21												
K =	2.7282			A =	2	I =	16			CV = CT*CF = (4/3)(πr³)				
V = T*K*I*A		= T * (2.728167*2*16) =			T *	87.3013	μm^3			r = ³/ ((3/4)(CT*CF)/π)				
CT = WC*WN / WC										d = 2r μm				
CF = 43.2142														

Spreadsheet A.4.

Spreadsheet A.5.

Normalization of the Window Counts to a 2/2 setting													Spreadsheet A.6.		
Time = 0hrs															
Win. # (WN)	Avg. Win. Count 2/2	Vol. (μm^3)	Avg. Win. Count 2/8	Norm. Win. Count to 2/2	Vol. (μm^3)	Avg. Win. Count 2/16	Norm. Win. Count to 2/2	Vol. (μm^3)	Avg. Win. Count 2/32	Norm. Win. Count to 2/2	Vol. (μm^3)	Avg. Win. Count 4/32	Norm. Win. Count to 2/2	Vol. (μm^3)
8	906	87	653	163	349	695	87	698		0	1397		0	2794
12	570	131	366	91	524	910	114	1048		0	2095		0	4190
16	542	175	273	68	698	3070	384	1397		0	2794		0	5587
20	307	218	114	29	873	5343	668	1746		0	3492		0	6984
24	239	262	55	14	1048	5505	688	2095		0	4190		0	8381
28	76	306	239	60	1222	4706	588	2444		0	4889		0	9778
32	260	349	1061	265	1397	3434	429	2794		0	5587		0	11175
36	269	393	1911	478	1571	2305	288	3143		0	6286		0	12571
40	44	437	2631	658	1746	1432	179	3492		0	6984		0	13968
44	0	480	2892	723	1921	783	98	3841		0	7683		0	15365
48	95	524	3027	757	2095	379	47	4190		0	8381		0	16762
52	213	567	2921	730	2270	195	24	4540		0	9079		0	18159
56	94	611	2410	602	2444	106	13	4889		0	9778		0	19556
60	162	655	2212	553	2619	68	8	5238		0	10476		0	20952
64	98	698	1858	465	2794	62	8	5587		0	11175		0	22349
68	83	742	1527	382	2968	39	5	5936		0	11873		0	23746
72	116	786	1358	340	3143	23	3	6286		0	12571		0	25143
76	106	829	1098	275	3317	26	3	6635		0	13270		0	26540
80	0	873	806	201	3492	17	2	6984		0	13968		0	27936
84	327	917	544	136	3667	12	2	7333		0	14667		0	29333
88	159	960	373	93	3841	28	4	7683		0	15365		0	30730
92	129	1004	256	64	4016	14	2	8032		0	16063		0	32127
96	4	1048	172	43	4190	18	2	8381		0	16762		0	33524
All WC Averaged Together														
Avg. Win. Count 2/2	Vol. (mm3)	Dia. (mm)	Avg. Win. Count 2/2	Vol. (mm3)	Dia. (mm)	Avg. Win. Count 2/2	Vol. (mm3)	Dia. (mm)	Avg. Win. Count 2/2	Vol. (mm3)	Dia. (mm)			
906	87	5.50	60	1222	13.27	1	6286	22.90	0	23746				
570	131	6.30	216	1397	13.87	3	6635	23.32	0	25143				
542	175	6.94	478	1571	14.43	1	6984	23.72	0	26540				
307	218	7.47	663	1746	14.94	2	7333	24.11	0	27936				
239	262	7.94	723	1921	15.42	2	7683	24.49	0	29333				
76	306	8.36	482	2095	15.88	2	8032	24.85	0	30730				
212	349	8.74	730	2270	16.31	1	8381	25.21	0	32127				
269	393	9.09	595	2444	16.72	0	9079	25.89	0	33524				
44	437	9.41	553	2619	17.10	0	9778	26.54						
0	480	9.72	223	2794	17.48	0	10476	27.15						
93	524	10.00	382	2968	17.83	0	11175	27.74						
213	567	10.27	314	3143	18.18	0	11873	28.31						
94	611	10.53	275	3317	18.51	0	12571	28.85						
162	655	10.78	127	3492	18.83	0	13270	29.38						
84	698	11.01	136	3667	19.14	0	13968	29.89						
83	742	11.23	96	3841	19.43	0	14667	30.38						
116	786	11.45	64	4016	19.72	0	15365	30.85						
106	829	11.66	23	4190	20.01	0	16063	31.31						
14	873	11.86	24	4540	20.55	0	16762	31.76						
327	917	12.05	7	4889	21.06	0	18159	32.62						
159	960	12.24	8	5238	21.55	0	19556	33.43						
129	1004	12.43	3	5587	22.02	0	20952	34.21						
44	1048	12.60	5	5936	22.47	0	22349	34.95						

Spreadsheet A.6.

Normalization of the WCxWN to a 2/2 setting														Spreadsheet A.6.	
Time = 0hrs															
Win. # (WN)	Avg. WNxWC 2/2	Vol. (μm^3)	Avg. WNxWC 2/8	Norm. WNxWC to 2/2	Vol. (μm^3)	Avg. WNxWC 2/16	Norm. WNxWC to 2/2	Vol. (μm^3)	Avg. WNxWC 2/32	Norm. WNxWC to 2/2	Vol. (μm^3)	Avg. WNxWC 4/32	Norm. WNxWC to 2/2	Vol. (μm^3)
8	7246	87	5223	1306	349	5561	695	698		0	1397		0	2794
12	6845	131	4388	1097	524	10918	1365	1048		0	2095		0	4190
16	8679	175	4363	1091	698	49120	6140	1397		0	2794		0	5587
20	3070	218	2282	570	873	106856	13357	1746		0	3492		0	6984
24	2863	262	664	166	1048	132125	16516	2095		0	4190		0	8381
28	2140	306	6686	1672	1222	131765	16471	2444		0	4889		0	9778
32	8325	349	33944	8486	1397	109875	13734	2794		0	5587		0	11175
36	9694	393	68792	17198	1571	82984	10373	3143		0	6286		0	12571
40	1773	437	105241	26310	1746	57293	7162	3492		0	6984		0	13968
44	0	480	127233	31808	1921	34449	4306	3841		0	7683		0	15365
48	2281	524	145277	36319	2095	18207	2276	4190		0	8381		0	16762
52	11081	567	151914	37979	2270	10154	1269	4540		0	9079		0	18159
56	5259	611	134940	33735	2444	5914	739	4889		0	9778		0	19556
60	9702	655	132713	33178	2619	4053	507	5238		0	10476		0	20952
64	6250	698	118920	29730	2794	3970	496	5587		0	11175		0	22349
68	2829	742	103812	25953	2968	2653	332	5936		0	11873		0	23746
72	8332	786	97808	24452	3143	1657	207	6286		0	12571		0	25143
76	4011	829	83470	20868	3317	1939	242	6635		0	13270		0	26540
80	0	873	64445	16111	3492	1320	165	6984		0	13968		0	27936
84	13755	917	45692	11423	3667	1008	126	7333		0	14667		0	29333
88	13980	960	32802	8201	3841	1232	154	7683		0	15365		0	30730
92	5932	1004	23564	5891	4016	1288	161	8032		0	16063		0	32127
96	205	1048	16545	4136	4190	864	108	8381		0	16762		0	33524
All WC Averaged Together															
Avg. WNxWC 2/2	Vol. (μm^3)	Dia. (μm)	Avg. WNxWC 2/2	Vol. (μm^3)	Dia. (μm)	Avg. WNxWC 2/2	Vol. (μm^3)	Dia. (μm)	Avg. WNxWC 2/2	Vol. (μm^3)	Dia. (μm)			
7246	87	5.50	1672	1222	13.27	104	6286	22.90	0	23746				
6845	131	6.30	4875	1397	13.87	242	6635	23.32	0	25143				
8679	175	6.94	17198	1571	14.43	55	6984	23.72	0	26540				
3070	218	7.47	19834	1746	14.94	126	7333	24.11	0	27936				
2863	262	7.94	31808	1921	15.42	77	7683	24.49	0	29333				
2140	306	8.36	17612	2095	15.88	161	8032	24.85	0	30730				
4815	349	8.74	37979	2270	16.31	36	8381	25.21	0	32127				
9694	393	9.09	25103	2444	16.72	0	9079	25.89	0	33524				
1773	437	9.41	33178	2619	17.10	0	9778	26.54						
0	480	9.72	10866	2794	17.48	0	10476	27.15						
1689	524	10.00	25953	2968	17.83	0	11175	27.74						
11081	567	10.27	17413	3143	18.18	0	11873	28.31						
5259	611	10.53	20868	3317	18.51	0	12571	28.85						
9702	655	10.78	7758	3492	18.83	0	13270	29.38						
2679	698	11.01	11423	3667	19.14	0	13968	29.89						
2829	742	11.23	6253	3841	19.43	0	14667	30.38						
8332	786	11.45	5891	4016	19.72	0	15365	30.85						
4011	829	11.66	1603	4190	20.01	0	16063	31.31						
285	873	11.86	1269	4540	20.55	0	16762	31.76						
13755	917	12.05	370	4889	21.06	0	18159	32.62						
13980	960	12.24	507	5238	21.55	0	19556	33.43						
5932	1004	12.43	165	5587	22.02	0	20952	34.21						
578	1048	12.60	332	5936	22.47	0	22349	34.95						

Spreadsheet A.7.

Determination of MCV from normalized WC & WNxWC values — **Spreadsheet A.7.**

	TIME = 0hrs					TIME = 72hrs			
	Avg. Win. Count 2/2	Vol. (μm3)	Dia. (μm)	WNxWC		Avg. Win. Count 2/2	Vol. (μm3)	Dia. (μm)	WNxWC
	906	87	5.50	7246		11476	87	5.50	91809
	570	131	6.30	6845		4525	131	6.30	54300
	542	175	6.94	8679		2457	175	6.94	39306
	307	218	7.47	3070		1595	218	7.47	31891
	239	262	7.94	2863		1301	262	7.94	31227
	76	306	8.36	2140		894	306	8.36	25032
	212	349	8.74	4815		831	349	8.74	14921
	269	393	9.09	9694		722	393	9.09	25995
	44	437	9.41	1773		646	437	9.41	25860
	0	480	9.72	0		495	480	9.72	21789
	93	524	10.00	1689		522	524	10.00	16348
	213	567	10.27	11081		566	567	10.27	29422
	94	611	10.53	5259		249	611	10.53	13950
	162	655	10.78	9702		246	655	10.78	14777
	84	698	11.01	2679		375	698	11.01	11627
	83	742	11.23	2829		298	742	11.23	20283
	116	786	11.45	8332		312	786	11.45	22446
	106	829	11.66	4011		275	829	11.66	20903
	14	873	11.86	285		261	873	11.86	13287
	327	917	12.05	13755		232	917	12.05	19499
	159	960	12.24	13980		135	960	12.24	11902
	129	1004	12.43	5932		185	1004	12.43	17003
	44	1048	12.60	578		169	1048	12.60	8228
	60	1222	13.27	1672		127	1222	13.27	3561
	216	1397	13.87	4875		116	1397	13.87	2097
	478	1571	14.43	17198		66	1571	14.43	2378
	663	1746	14.94	19834		54	1746	14.94	1661
	723	1921	15.42	31808		75	1921	15.42	3319
	482	2095	15.88	17612		69	2095	15.88	1960
	730	2270	16.31	37979		40	2270	16.31	2077
	595	2444	16.72	25103		59	2444	16.72	2415
	553	2619	17.10	33178		36	2619	17.10	2145
	223	2794	17.48	10866		28	2794	17.48	800
	382	2968	17.83	25953		29	2968	17.83	1985
	314	3143	18.18	17413		31	3143	18.18	1777
	275	3317	18.51	20868		20	3317	18.51	1529
	127	3492	18.83	7758		21	3492	18.83	688
	136	3667	19.14	11423		8	3667	19.14	634
	96	3841	19.43	6253		20	3841	19.43	1349
	64	4016	19.72	5891		31	4016	19.72	2879
	23	4190	20.01	1603		18	4190	20.01	975
	24	4540	20.55	1269		13	4540	20.55	679
	7	4889	21.06	370		7	4889	21.06	244
	8	5238	21.55	507		14	5238	21.55	863
	3	5587	22.02	165		12	5587	22.02	364
	5	5936	22.47	332		7	5936	22.47	452
	1	6286	22.90	104		12	6286	22.90	673
	3	6635	23.32	242		14	6635	23.32	1078
	1	6984	23.72	55		9	6984	23.72	529
	2	7333	24.11	126		9	7333	24.11	743
	2	7683	24.49	77		9	7683	24.49	549
	2	8032	24.85	161		11	8032	24.85	998
	1	8381	25.21	36		8	8381	25.21	432

TC =	10986	TV =	427968
MCT =	TV/TC		
=	38.95		
CF =	43.2238		
MCV =	MCTxCF		
=	1683.77	μm3	
MCD =	$\sqrt[3]{((3/4)(V)/\pi)}$		
=	14.76	μm	

A.5 References

1. Volker, K. Sizing of cells by the electrical resistance pulse technique. In: Catsimpoolas and Nicholas (eds.), Cell Analysis, pp. 195-199, New York: Plenum Press. 1985.

2. Lines, R.W. The electrical sensing zone method (The Coulter principle). In: J.Z. Knapp, T.A. Barber and A. Lieberman (eds.), Liquid-and-surface-borne particle measurement handbook, pp. 113-140, New York, N.Y.: Marcel Dekker, Inc. 1996.